Soil-Landscape Modelling

in an Andean Mountain Forest Region

in Southern Ecuador

Dissertation

submitted to the

Faculty of Biology, Chemistry and Geosciences

of the

University of Bayreuth

to attain the degree of

Dr. rer. nat.

presented by

Mareike Ließ

born May 2nd 1979, in Salzgitter

Bayreuth, November 2010

This is a full reprint of the dissertation submitted to attain the academic degree of Doctor of Natural Sciences (Dr. rer. nat.) and approved by the Faculty of Biology, Chemistry and Geosciences of the University of Bayreuth.

This doctoral thesis was prepared at the Department of Geosciences (chair of Soil Physics), University of Bayreuth, between September 16th 2007 and November 12th 2010. It was supervised by Prof. Dr. Bernd Huwe and Prof. Dr. Bruno Glaser.

Acting dean: Prof. Dr. Stephan Clemens

Date of submission: November 12th, 2010

Date of scientific colloquium (disputation): July 7th, 2011

Doctoral Committee:

Prof. Dr. Bernd Huwe	1st reviewer
Prof. Dr. Reinhold Jahn	2nd reviewer
Prof. Dr. Ludwig Zöller	Chairman
Prof. Dr. Egbert Matzner	
Prof. Dr. Carl Beierkuhnlein	

Summary

Soil-landscapes are diverse and complex due to the interaction of pedogenetic, geomorphological and hydrological processes. The resulting soil profile reflects the balance of these processes in its properties. Early conceptual models have by now resulted into quantitative soil-landscape models including soil variation and its unpredictability as a key soil attribute. Soils in the Andean mountain rainforest area of southern Ecuador are influenced by hillslope processes and landslides in particular. The lack of knowledge on the distribution of soils and especially physical soil properties to understand slope failure, resulted in the study of this particular soil-landscape by means of statistical models relating soil to terrain attributes, i.e. predictive soil mapping.

A 24 terrain classes comprising sampling design for soil investigation in mountainous areas was developed to obtain a representative dataset for statistical modelling. The soils were investigated by 56 profiles and 315 auger points. The Reference Soil Groups (RSGs) Histosol, Stagnosol, Umbrisol, Cambisol, Leptosol and Regosol were identified according to the World Reference Base for Soil Resources (WRB). Classification tree models and a probability scheme based on WRB hierarchy were applied to include RSG prediction uncertainty in a digital soil map. Histosol probability depended on hydrological parameters; highest Stagnosol probability was found on slopes < 40° and above 2146 m a.s.l.

Poor model performance, probably due to the prediction of complex categories (RSGs) and WRB inconsequence (absolute and relative value criteria), led to the proposal of "incomplete soil classification" by relating the thickness of the WRB's diagnostic horizons as percentage to the upper 100 soil centimetres, including the organic layer. Typical diagnostic horizons histic, humic, umbric, stagnic and cambic were regionalised in their thickness and occurrence probability by classification and regression trees (CART). Prediction uncertainty was addressed with hundredfold model runs based on different random Jackknife partitions of the dataset. Whether the first mineral soil horizon displays stagnic properties or not, likely depends on physical soil properties in addition to terrain parameters. Incomplete soil classification resulted in histic and stagnic soil parts dominating the first 100 cm of the soil volume for most of the research area.

While soil profiles and auger points were described in their horizon composition,

thickness, Munsell colour and soil texture by finger method (FAO, 2006), soil cohesion, bulk density and texture by pipette and laser were analysed in soil profiles only. Texture results by pipette compared to laser method, showed the expected shift to higher silt and lower clay contents. Linear regression equations were adapted. Pedotransfer functions to predict physical soil properties from the bigger auger dataset analysed by field texture method only, could not be developed, because field texture analysis did not provide satisfying results. It was therefore not possible to correct its results with the more precise laboratory data.

Comparing CART and Random Forest (RF) in their model performance to predict topsoil texture and bulk density as well as mineral soil thickness by hundredfold model runs with random Jackknife partitions, RF predictions resulted more powerful. Altitude a.s.l. was the most important predictor for all three soil parameters. Increasing sand/ clay ratios with increasing altitude, on steep slopes and with overland flow distance to the channel network are caused by shallow subsurface flow removing clay particles downslope. Deeper soil layers are not influenced by the same process and therefore showed different texture properties.

Terrain parameters could only explain the spatial distribution of topsoil properties to a limited extent, subsoil properties could not be predicted at all. Other parameters that likely influence soil properties within the investigation area are parent material and landslides. Strong evidence was found that topsoil horizons did not form from the bedrock underlying the soil profile. Parent material changes within short distance and often within one soil profile. Landslides have a strong influence on soil-landscape formation in shifting soil and rock material.

Soil mechanical and hydrological properties in addition to terrain steepness were hypothesized to be the major factors in causing soil slides. Thus, the factor of safety (FS) was calculated as the soil shear ratio that is necessary to maintain the critical state equilibrium on a potential sliding surface. The depth of the failure plane was assumed at the lower boundary of the stagnic soil layer or complete soil depth, depending on soils being stagnic or non-stagnic. The FS was determined in dependence of soil wetness referring to 0.001, 0.01, 0.1 and 3 mm/h net rainfall rate. Sites with a FS ≥ 1 at 3 mm/h (complete saturation) were classified as unconditionally stable, sites with a FS < 1 at 0.001 mm/h as unconditionally unstable. The latter coincided quite well with landslide scars from a recent aerial photograph.

Zusammenfassung

Das Zusammenspiel pedogener, geomorphologischer und hydrologischer Prozesse führt zu facettenreichen und komplexen Bodenlandschaften. Das daraus enstandene Bodenprofil spiegelt das Gleichgewicht dieser Prozesse in seinen Eigenschaften wieder. Frühe konzeptuelle Modelle haben sich mittlerweile zu quantitativen Bodenlandschafts-Modellen entwickelt, die die Bodenvariabilität und ihre Unvorhersagbarkeit als Schlüssel-Bodeneigenschaft beinhalten. Die Böden der südecuadorianischen andinen Bergregenwaldregion sind durch Hangprozesse und vor allem Hangrutsche beeinflusst. Fehlendes Wissen über die Verteilung der Böden und insbesondere ihrer physikalischen Eigenschaften um Hangrutschungen zu verstehen, führte zur Erforschung dieser Bodenlandschaft durch statistische Modelle, die Bodenparameter zu Reliefparametern in Beziehung setzen (prädiktive Bodenkartierung).

Um einen repräsentativen Datensatz für die statistische Modellierung zu erhalten, wurde ein 24 Reliefklassen umfassendes Probenahme-Design für die Bodenuntersuchung in Berglandschaften entwickelt. Die Böden wurden mittels 56 Profilen und 315 Bohrstockeinschlägen beprobt und die Reference Soil Groups (RSG) Histosol, Stagnosol, Umbrisol, Cambisol, Leptosol und Regosol wurden mittels der World Reference Base for Soil Resources (WRB) identifiziert. Klassifikationsbaummodelle und ein Wahrscheinlichkeitsschema, das auf der Hierarchie der WRB basiert, wurden angewandt um die RSG-Vorhersageunschärfe in eine digitale Bodenkarte zu integrieren. In den Modellen hing die Histosol-Wahrscheinlichkeit von hydrologischen Parametern ab, während die höchste Stagnosol-Wahrscheinlichkeit auf Hängen < 40° Neigung und oberhalb von 2146 m a.s.l. vorhergesagt wurde.

Die schlechte Modellgüte, die vermutlich auf die Vorhersage komplexer Kategorien (RSGs) und Inkonsequenzen in der WRB (absolute und relative Werte als Entscheidungskriterien) zurückzuführen ist, mündete im Vorschlag der „unvollständigen Bodenklassifikation", welche die Mächtigkeiten der diagnostischen WRB-Bodenhorizonte zu den oberen hundert Bodenzentimetern – organische Auflage inklusive – prozentual in Bezug setzt. Die typischen diagnostischen Horizonte histic, humic, umbric, stagnic und cambic wurden in ihrer Mächtigkeit und Auftretenswahrscheinlichkeit mittels Klassifikations- und Regressionsbäumen (CART) regionalisiert. Hierbei wurde die Unschärfe der Vorhersage durch hundertfache Modelläufe

basierend auf jeweils unterschiedlichen zufälligen Jackknife-Teildatensätzen abge-schätzt. Das Vorkommen von stagnierenden Bodeneigenschaften im ersten Mineral-bodenhorizont hängt neben Reliefparametern wahrscheinlich auch von physika-lischen Bodeneigenschaften ab. Im Rahmen der „unvollständigen" Klassifikation wurden im überwiegenden Teil des Untersuchungsgebietes die obersten hundert Zentimeter Bodensäule von den Bodenteilen histic und stagnic dominiert.

Während Bodenprofile und Bohrstockeinschläge in ihrer Horizontzusammensetzung, -mächtigkeit, Munsellfarbe und Bodentextur mittels Fingermethode (FAO, 2006) beschrieben wurden, wurden die Bodenkohäsion, Lagerungsdichte und Labor-Textur (Pipett, Laser) nur in Bodenprofilen bestimmt. Der Vergleich der Texturwerte aus Pipett- und Laseranalyse zeigte die erwartete Verschiebung zu höheren Schluff- und niedrigeren Tongehalten; lineare Regressionsgleichungen wurden angepasst. Es konnten jedoch keine Pedotransferfunktionen aufgestellt werden, um physikalische Bodeneigenschaften auf Grundlage des größeren Bohrstockdatensatzes vorher-zusagen, dessen Textur nur mittels Fingermethode bestimmt wurde, weil die Feldmethode keine zufriedenstellenden Ergebnisse lieferte. Es war somit nicht möglich, deren Ergebnisse mittels der präziseren Labordaten zu korrigieren.

Beim Vergleich der Modellgüte von CART- und Random Forest (RF)- Modellen zur Vorhersage der Textur, Lagerungsdichte und Bodentiefe mittels hundertfacher Modellläufe basierend auf Jackknife-Teilmengen, überragten die RF-Modelle. Die Höhe ü. d. M. war der bedeutendste Prädiktor für alle drei Bodenparameter. Das mit der Höhe, der Hangneigung und dem Abstand zum Fließgewässernetz zunehmende Sand/Ton-Verhältnis wird durch oberflächennahen Zwischenabfluss verursacht, der Tonpartikel Hang abwärts transportiert. Tiefere Bodenschichten werden durch diesen Prozess nicht beeinflusst und wiesen daher andere Textureigenschaften auf.

Reliefparameter konnten die räumliche Verteilung der Oberbodeneigenschaften lediglich zu einem Teil erklären; Unterbodeneigenschaften konnten nicht regiona-lisiert werden. Weitere Parameter, die die Bodeneigenschaften im Untersuchungs-gebiet wahrscheinlich beeinflussen, sind Ausgangsmaterial und Hangrutsche. Es zeigten sich starke Anzeichen, dass Oberbodenhorizonte nicht aus dem das Profil unterlagernden Gestein entstanden sind. Das Ausgangsmaterial wechselt über kurze Distanz und oft innerhalb eines Bodenprofils. Hangrutsche haben einen starken Einfluss auf die Genese der Bodenlandschaft durch die Verlagerung von Boden- und Gesteinsmaterial.

Es wurde angenommen, dass bodenmechanische und –hydrologische Eigenschaften sowie die Steilheit des Terrains die Hauptfaktoren im Auslösen von Hangrutschen darstellen. Folglich wurde der Sicherheitsbeiwert (SB) als das Scherverhältnis berechnet, das notwendig ist, um das Grenzgleichgewicht entlang einer potenziellen Abscherfläche aufrechtzuerhalten. Die Position dieser Abscherfläche wurde an der unteren Grenze des stagnierenden Horizontes oder der gesamten Bodentiefe angenommen in Abhängigkeit davon, ob die Böden stagnierende Eigenschaften aufweisen oder nicht. Der SB wurde in Abhängigkeit von der Bodenfeuchte bei 0,001, 0,01, 0,1 und 3 mm/h Netto-Regenfallrate bestimmt. Standorte mit SB ≥ 1 bei 3 mm/h (vollständige Sättigung) wurden als bedingungslos stabil, solche mit SB < 1 bei 0,001 mm/h als bedingungslos instabil angesehen. Die letzteren stimmten gut mit Hangrutschnarben auf einem aktuellen Luftbild überein.

Resumen

Los paisajes de suelo son diversos y complejos debido a la interacción de los procesos pedogénicos, geomorfológicos e hidrológicos. El perfil de suelo que resulta, refleja el equilibrio de estos procesos dentro de sus propiedades. Los primeros modelos conceptuales ahora se han desarollado en modelos cuantitativos del paisaje del suelo, incluyendo, variaciones del suelo y su imprevisibillidad como un atributo clave. Los suelos en las áreas de bosque lluvioso de las montañas andinas del sur ecuatoriano, están influenciados por los procesos de la pendiente de las colinas y particularmente por los deslizamientos. La falta de conocimiento sobre la distribución de los suelos y especialmente de las propiedades físicas de estos, para comprender la falla de las pendientes, resultó en el estudio de este paisaje particular de suelo por medio de modelos estadísticos relacionando los suelos a atributos del terreno, o sea el mapeo predictivo del suelo.

Un diseño de muestreo que engloba 24 clases de terreno, fue desarrollado para la investigación de suelos en àreas montañosas, a fin de obtener una serie respresentativa de datos para la modelización estadistica. Los suelos fueron investigados por medio de 56 perfiles y 315 puntos barrenados. Los Grupos de Suelos de Referencia (GSR) Histosol, Stagnosol, Umbrisol, Cambisol, Leptosol y Regosol fueron identificados de acuerdo con la Base Referencial Mundial de Recurso Suelo (BRM). Modelos de árboles de clasificación y un esquema de probabilidad basado en la jerarquía de la BRM fueron aplicados para incluir la incertidumbre de la predicción de los GSR en un mapa digitál de suelos. La probabilidad de Histosoles dependió de parámetros hidrológicos. La probabilidad más alta de Stagnosoles fue encontrada en pendientes menores a 40 grados y sobre los 2146 msnm.

El bajo rendimiento del modelo, probablemente debido a la predicción de categorías complejas (GSR) y la inconsecuencia de la BRM (criterios de evaluación absolutos y relativos), condujo a la propuesta de la "clasificación incompleta de suelos", que relaciona la extención de horizontes diagnostico de la BRM como percentaje a los primeros 100 cm de suelo incluyendo la capa orgánica. Los patrones tipicos hístico, húmico, úmbrico, stágnico y cámbico fueron regionalizados en su extención y probabilidad de occurencia por medio de arboles de clasificación y regresión (CART). La incertidumbre de la predicción fue incluida atravez de 100 corridas de

modelo en base de differentes subconjuntos "Jackknife" de la base de datos. Si el primer horizonte mineral muestra propiedades stágnicas o no, probablemente depende de características físicas del suelo en adición a los parámetros del terreno. La clasificación incompleta resultó en las partes de suelo hístico y stágnico dominando a lo largo de los primeros 100 cm de la columna de suelo en la mayoría del área de estudio.

La composición y la extensión de los horizontes, su color Munsell y su textura por método de campo (FAO 2006), fueron descritos en los perfiles y puntos barrenados, mientras que la cohesión, la densidad de la masa y la textura por pipeta y laser fueron analisado sólo en los perfiles. Los resultados de textura por pipeta comparados con el método laser mostraron el desfase esperado de contenidos más altos de limo y más bajos de arcilla. Así ecuaciones de regresión linear fueron adaptadas. Las funciones de pedotransferencia para predecir propiedades físicas de suelo de la base más amplia de datos de barreno, de la cual la textura fue analisada sólo por método de campo, no pudieron ser desarollados, debido a que el análisis de la textura por este método no dió resultados satisfactorios. Por lo tanto no fue posible corregir dichos resultados con datos más precisos del laboratorio.

Comparando CART y Random Forest (RF) en su rendimiento como modelos en la predecicción de la textura y densidad de la masa, como tambien la profundidad del suelo atravez de 100 corridas de modelo en base de subconjuntos "Jackknife" y validaciones cruzadas externas, RF resultó màs efectivo. La altitud sobre el nivél del mar fue el predictor más importante para todos los tres parámetros de suelo. El incremento directo de arena/arcilla con relación a la altitud, inclinación de la pendiente y con la distancia a las quebradas está causada por el flujo poco profundo del agua, que transporta particulas de arcilla pendiente abajo. Las capas de suelo más profundas no están influenciadas por el mismo proceso, por lo tanto no muestran las mismas propiedades de textura.

Los parámetros del terreno solo pudieron explicar la distribución espacial de las propiedades de suelos superficiales en menor medida, mientras que las propiedades de las capas más profundas no pudieron ser predecidas de ninguna manera. Otros parámetros que probablemente influencian las propiedades del suelo en el área de investigación son: el material básico y los deslizamientos de tierra. Se encontró fuerte evidencia de que los horizontes superficiales no se formaron de la roca que esta debajo del perfil. El material básico cambia a distancia corta y frecuentemente

dentro de un mismo perfil. Los deslizamientos tienen una influencia intensa sobre la formación del paisaje del suelo, deslocando material de suelo y de roca.

Las propiedades mecánicas e hidrológicas del suelo en adición al empinamiento del terreno, fueron hipotetizadas a ser los factores mayores en causar deslizamientos de suelo. Así el factor de seguridad (FS) fue calculado como proporción de cizallamiento para mantener el equilibrio de estado crítico sobre una superficie potenciál de deslizamiento. La profundidad de esta superficie fue asumida en el límite bajo del patrón stágnico del suelo, ò a la profundidad completa del suelo respectivamente, dependiendo si es suelo stágnico ò no stágnico. El FS fue determinado en dependencia de la humedad del suelo referida a 0.001, 0.01, 0.1 y 3 mm/h de la taza de precipitación. Sitios con un FS ≥ 1 a 3 mm/h (saturados completamente) fueron clasificados como incondicionalmente estables, sitios con un FS < 1 a 0.001 mm/h como incondicionalmente inestables. Los últimos coinciden bien con las huellas de deslizamientos en una fotografía aérea reciente.

TABLE OF CONTENTS

List of figures

List of tables

List of abbreviations

ANN	**A**rtificial **N**eural **N**etwork
a.s.l.	**a**bove **s**ea **l**evel
BS CA	upslope **C**ontributing **A**rea/ specific catchment area calculated with the **B**raun**S**chweiger Relief Model
BScatch	= BS CA
BT	**B**agging **T**rees
c	circa, 'about'
CART	**C**lassification **A**nd **R**egression **T**rees
CT	**C**lassification **T**ree
DEM	**D**igital **E**levation **M**odel
DGPS	**D**ifferential **G**lobal **P**ositioning **S**ystem
FS	**F**actor of **S**afety
GAM	**G**eneralized **A**dditive **M**odel
GIS	**G**eographic **I**nformation **S**ystem
GPS	**G**lobal **P**ositioning **S**ystem
GLM	**G**eneralized **L**inear **M**odel
HOFD	**H**orizontal **O**verland **F**low **D**istance to the channel network
KRA CA	upslope **C**ontributing **A**rea/ specific catchment area calculated with the **K**inematic **R**outing **A**lgorithm
KRAcatch	= KRA CA
K_{sat}	saturated hydraulic conductivity
Lm	statistical model relating **L**aser texture to **m**ean terrain values
Lnn	statistical model relating **L**aser texture to **n**earest **n**eighbour terrain values
mtry	The size of the subset of predictor variables within Random Forest
n. n.	**n**earest **n**eighbour method
OFD	**O**verland **F**low **D**istance to the channel network
pl.curv	**pl**an **curv**ature
Pm	statistical model relating **P**ipette texture to **m**ean terrain values
Pnn	statistical model relating **P**ipette texture to **n**earest **n**eighbour terrain values
pr.curv	**pr**ofile **curv**ature
RF	**R**andom **F**orest
RFm	**R**andom **F**orest model from **m**ean terrain values
RFnn	**R**andom **F**orest model from **n**earest **n**eighbour terrain values
RSG	**R**eference **S**oil **G**roup
RT	**R**egression **T**ree
RTm	**R**egression **T**ree model from **m**ean terrain values
RTnn	**R**egression **T**ree model from **n**earest **n**eighbour terrain values
VOFD	**V**ertical **O**verland **F**low **D**istance to the channel network
WRB	**W**orld **R**eference **B**ase for Soil Resources

Chapter 1

General Introduction

1.1   Soil-landscape modelling

Since long, soils are understood as a function of their genetic factors: parent material, relief, climate, organisms and time, a concept first described by Dokutschajew (1883) and better known from Jenny (1941). The complex interaction of these factors activate particular soil forming processes, which in dependence of their intensity and duration, lead to characteristic soil properties. The pedosphere is understood as a continuum, defined by the gradual changes of these properties in space (Wysocki et al., 2000). Soils on hillslopes are related by hillslope processes, i.e. subsurface water flow, erosion and landslides. Removal of particles from higher slope positions leads to their accumulation in lower positions. Eventually, the term catena (Milne, 1936) refers to the relief determined pattern of soils on hillslopes. It is defined as a sequence of soils of about the same age derived from similar parent material and occurring under similar climatic conditions, but having different characteristics due to variation in relief and drainage (Wysocki et al., 2000). Through these concepts, Dokutschajew (1883) and Milne (1936) established the first conceptual soil-landscape models that are still widely applied. In addition, soil hydrology provided a major advancement in understanding soil systems by investigating how water moves through landscapes (Wysocki et al., 2000); soil development is closely linked to these water flows that provide transport mechanisms for soil particles.

Soil-landscapes are diverse and complex due to the interaction of pedogenetic, geomorphological and hydrological processes, which operate simultaneously in soils. The resulting profile reflects the balance of these processes in its properties (Grunwald, 2006). Traditional soil surveying and mapping groups soil properties into classes to deduce soil groups, units or types. For soil-landscape models two approaches are available. Some models focus on soil attributes, whereas others

aggregate these attributes to form taxa. Organisation in taxa makes sense where it simplifies the soil continuum reality and makes it easier to interpret the soil continuum. Uncertainties in this approach emanate from the establishment and ordering of classes and their ranking according to the importance of soil characteristics in hierarchical levels, which vary widely among different soil systematisations.

The early conceptual models have by now resulted into quantitative soil-landscape models, which do not only make the spatial prediction of continuous soil properties possible, but include model uncertainty. Pedometrics, "the application of mathematical and statistical methods for the study of the distribution and genesis of soils" (McBratney, 1986), or also termed "soil science under uncertainty" (De Gruijter et al., 1994) together with computers capable of processing huge multidimensional datasets and geographical information systems provide the basis for these new soil-landscape models. Their development is described by the term "digital soil mapping" or "predictive soil mapping" (McBratney et al., 2003; Rossiter, 2004). Being at first an unwelcome nuisance that reduced map reliability, gradually soil variation and its unpredictability was seen as a key soil attribute by itself (Burrough et al., 1994).

To develop a soil map, information from discrete sampling points can be interpolated, whenever data distribution is sufficiently dense, and terrain forms, parent material and vegetation do not show any abrupt changes between any two sampling points, i.e. there has to be spatial correlation between the observations to allow for interpolation (Goovaerts, 1999). In mapping big areas and particularly mountainous landscapes, data density is usually not enough. Furthermore, soil data is often collected along transects, and any transect is one-dimensional, whereas the application, a map, is two-dimensional. Hence, it is not sufficient to interpolate only along transects (Myers, 1994).

Another option to receive continuous maps from discrete sampling points is based on the conceptual model of soil formation. Environmental factors serve as explanatory variables to predict soil properties. Statistical models are used to relate soil properties to variables, which are continuously available for the area under investigation, e.g. terrain, vegetation or parent material. General relationships between soil attributes and environmental factors were identified by conceptual models, their quantification is domain dependent (Grunwald, 2006; Bishop and Minasny, 2006). Hence, the relationship between e.g. slope and soil in one

environmental setting might be strong, but weak in another. In conclusion, no universal equation exists that fits all soil-landscapes (Grunwald, 2006).

1.2   Statistical models

There are several statistical models available to relate soils to environmental predictors. Bishop and Minasny (2006) compared some statistical prediction models: Linear, generalized linear (GLM) and generalized additive (GAM) models, classification and regression trees (CART) and artificial neural networks (ANN). Among the considered model types, only ANN were assigned a better predictive power than CART, but lack the ease of use, parsimony, interpretability and computational efficiency that applies for CART. Furthermore, ANN cannot handle mixed data type (qualitative and quantitative). GLM and GAM, which according to Bishop and Minasny (2006) have an equally good predictive power as CART, lack its good interpretability, ease of use and parsimony. Bagging trees (BT) and Random Forest (RF), according to Prasad et al. (2006), perform even better than regression trees (RT), but lack the open model structure and interpretability, that RT provides. Hence, Prasad et al. (2006) would still recommend the application of all three methods, especially when used in combination, taking advantage of their individual strengths.

CART and RF were chosen for their many advantages over other statistical modelling approaches. In addition to the already mentioned advantages, interactions and nonlinearities among predictor and response variables are permitted. Both models have a good predictive power and are interpretable. While RF is expected to be superior in its predictive power, interpretability is better with CART.

However, both methods are similar as they are both based on CART methodology first described by Breiman et al. (1984). The dataset is subdivided most efficiently by a set of decision rules applied on the predictor variables to gain preferably homogeneous subgroups regarding the response variable. The rules are constructed partitioning the dataset into successively smaller groups (nodes) with binary splits based on a single predictor variable. Predictor variables are examined to choose the one, which best splits up the dataset regarding the response variable. Finally, the subdivision rules form a tree diagram. The optimal split is chosen in minimising the mean square error in case of a continuous response variable and by creating preferably pure end nodes in case of a categorical response variable. The former

results in regression trees (RT), the latter in classification trees (CT).

In RT, the optimal split is found when the difference in mean square error R between the mother node t and the left and right child node t_l and t_r

$$R(t) - \left[R(t_l) + R(t_r)\right] \tag{1}$$

is maximised. The mean square error R in any node t with the number of observations n and the predicted mean value $\square y$, is calculated by:

$$R(t) = 1/n(t) \cdot \sum_{i=1}^{n} \left[y_i(t) - \overline{y}(t)\right]^2 \tag{2}$$

The mean of all data within each node is used for prediction purpose.

As purity measure for CT the Gini criterion (equation 3) is used (Breiman et al., 1984). It therefore serves as a decision criterion to determine, which terrain parameter best separates the dataset continuously in always two subsets to create the purest end nodes.

$$gini(t) = 1 - \sum_{i=1}^{k} P_i^2 \tag{3}$$

The Gini-Index reaches its maximum in a particular node t if all categories k within that node are equally represented. Is the probability P_i equal to zero for all but one category within one node, the Gini-Index reaches its minimal value. For prediction purpose there are two choices: (a) the categorical value accounting for the majority within each end node is used or (b) the percentage of each categorical value within an end node is assigned as occurrence probability.

The other statistical model, Random Forest, constructs a group (forest) of CT or RT. Prediction is made by aggregating the predictions of the forest. The number of trees needs to be set sufficiently high to allow for the convergence of the generalization error (Breiman, 2001). Consequently, RFs do not overfit when more trees are added, but produce a limited generalization error (Breiman, 2001; Prasad et al., 2006; Peters et al., 2007).

All trees are grown without pruning (Breiman, 2001). However, model stability is guaranteed through tree diversity. This is achieved by two means: (1) Choosing at random a subset of predictor variables to grow each tree and (2) sampling with replacement (bootstrapping) and thereby varying the input dataset. The size of the subset of variables (mtry) used to grow each tree, has to be selected by the user. It is a sensitive parameter determining model strength, for it defines the strength of each individual tree in the forest and the correlation between any two trees in the forest.

Increasing mtry, the strength of each tree is growing, but at the same time correlation between trees increases, too (Peters et al., 2007). Tree strength improves model performance, whereas correlation among trees weakens it. In RF, model structure is not accessible. Nevertheless it is interpretable, because the relative importance of the predictor variables is estimated based on how much worse the prediction would be if the data for that predictor was permuted randomly (Prasad et al., 2006).

Both statistical models are performed within the open-source data analysis environment R (R Development Core Team). CART is implemented with the software package rpart; RF, based on Breiman and Cutler's Fortran code, is implemented with the package randomForest.

Model performance is estimated by cross validation. Within CART the dataset is subdivided into k subgroups, and CART is then performed k-1-fold, always leaving one group out, which is used for error estimation. Another option is to construct manifold tree models based on different random subsamples. The data not used for tree construction can range from one observation to half the sample size (Good, 1999) and is used for cross validation. This resampling method estimating the random error of a statistical model is called Jackknifing (Efron, 1982).

The Bootstrap methodology (Efron, 1979), which is implemented in RF, was developed on the Jackknife procedure (Shikano, 2006). Again, random samples are drawn, but in contrast to the latter, by sampling with replacement. Bagging, i.e. bootstrap aggregation, averages the models developed from many random subsamples drawn with replacement. These approaches are also applicable in case of a small dataset without any assumption regarding the distribution function.

1.3   GIS Methodology

Soil mapping by statistical models needs spatially continuous predictor variables. Within the San Francisco catchment in southern Ecuador, only terrain factors are available through a digital elevation model (DEM). This was provided by the research unit's database (Nauss et al., 2007) in the form of a 2 m interval contour line shape-file, which was originally generated from stereo aerial photos by aero-triangulation (Jordan et al., 2005). This shapefile was then transferred into a raster grid by interpolation of points introduced along the contour lines at 2 m interval.

Terrain attributes, calculated from the DEM and used to predict soils within the covered area, include altitude above sea level, slope, aspect, profile and plan terrain

curvature, upslope contributing area (specific catchment area) and overland flow distance to the channel network. Altitude, slope and aspect have been used in many studies to predict soil types, soil depth, horizon thickness and soil properties (McKenzie and Ryan, 1999; Thomas et al., 1999; Ryan et al., 2000). Terrain curvature was used to predict hydromorphic features (Thompson et al., 1997), water content (Lark, 1999) and soil horizon thickness (Park et al., 2001). Upslope contributing area was employed by McBratney et al. (2000) to predict clay content and by Odeh et al. (1991) to predict chemical and physical soil properties, whereas Moran and Bui (2002) used it to predict soil classes. Furthermore, Gessler et al. (1995) found elevation above local stream, distance to local stream and distance to local drainage way to be good predictors of soil attributes. Moran and Bui (2002) described distance downhill to channels and distance downhill from hilltops as good predictor variables of soil classes. Bell et al. (1992) and Lagacherie and Holmes (1997) used the distance to the channel network as parameter to predict soil drainage classes and soil units.

The above mentioned terrain parameters were calculated as raster grids of 2 x 2 m, 10 x 10 m and 20 x 20 m cell size. While the 2 x 2 m grid was used for model development, the bigger cell size reduced the number of grid cells from $7.6 * 10^6$ to $7.6 * 10^4$ and $3.0 * 10^5$ for model application. This was necessary for the reason of limited storage capacities within the open-source data analysis environment software R (R Development Core Team). Slope, aspect and curvature were calculated from the DEM with a 2nd degree polynomial fit (Zevenbergen and Thorne, 1987; Cimmery, 2007). The channel network was allocated using the Strahler stream order ≥ 5 (Strahler, 1957) as initiation threshold, selected based on expert knowledge of the research area.

Two principle flow mechanisms are available for calculating the specific catchment area, i.e. the area contributing flow to each grid cell: (1) flow is permitted to move between grid cell centres only, and (2) flow moves freely. The latter is referred to as flow tracing mechanism. In both mechanisms, linear and flow distribution with divergence is possible and therefore single or multiple flow direction. Among the vast amount of different calculation methods available, the following two were selected: From mechanism (1) the Braunschweiger Digital Relief Model (BS CA) (Bauer et al., 1985), a multiple flow mechanism, and from (2) the Kinematic Routing Algorithm (KRA CA) (Lea, 1992), a one-dimensional flow tracing algorithm, was chosen.

All GIS operations were carried out in SAGA, a free open source GIS software, developed by the working–group Geosystem Analysis (Olaya, 2004; Böhner et al., 2006; Cimmery, 2007). Maps were designed with ArcGIS 9.3 from ESRI.

1.4 Research area

The investigation area is situated in the Southern Ecuadorian Andes between the provincial capitals Loja and Zamora within the Podocarpus – El Condor Biosphere Reserve. Extending on either side from the San Francisco River, it comprises an area of c 26 km².

Average annual total rainfall increases from 2050 mm at 1960 m a.s.l. to c 4400 mm at 3100 m a.s.l. (Rollenbeck, 2006). The rainfall gradient increases by 250 mm per 100 m altitude up to 2600 m a.s.l. and decreases above 2600 m a.s.l. to 100 mm per 100 m altitude a.s.l. (Rollenbeck, 2006). The average air temperature ranges from 19.4 °C at the valley bottom to 9.4 °C at the upper parts (Fries et al., 2009).

Lithologically, the area is part of the Chiguinda unit. Metasiltstones, siltstones and quartzites are intermixed with layers of phyllite and clay schists (Litherland et al., 1994). Furthermore, it is influenced by regular occurrences of landslides. Soil investigation within the area describes stagnic soils (Yasin, 2001; Schrumpf et al., 2001; Kreutzer and Martini, 2002; Bahr, 2007), Histosols (Yasin, 2001; Schrumpf et al., 2001), Cambisols (Yasin, 2001; Kreutzer and Martini, 2002; Wilcke et al., 2002/ 2003; Bahr, 2007) and Umbrisols (Bahr, 2007) (FAO, IUSS Working Group, 2007).

Vegetation includes tropical mountain rainforest, secondary forest, páramo vegetation above the tree line and pastures induced by human activity. Forest slopes are mainly situated on the northwards facing slopes south of the San Francisco River, whereas pasture and secondary forest are found on its northern side. The area exhibits high tree species diversity with very different vegetation at a small scale. Rubiaceae, Lauraceae, Euphorbiaceae and Melastomataceae families account for many species (Homeier et al., 2002). Homeier et al. (2002) differentiated different natural forest types according to their altitude and position on ridge or in the valley respectively.

1.5   Synopsis

1.5.1   Objective of the thesis

Soil investigation has been carried out within the research area for more than 10 years. However, no soil maps are available, unless for a small subcatchment. The plan to develop hydrological as well as landslide models made the regionalisation of soil properties on a landscape level an urgent matter of interest. Hence, the objective of this thesis is to produce digital soil maps of reference soil groups (RSG) (FAO, IUSS Working Group WRB, 2007), typical soil horizons and physical soil properties by means of statistical models including prediction uncertainty. The regionalised physical soil properties are then used to estimate landslide risk and explain the occurrence pattern of landslides. It was hypothesized, that

(1)   it is possible to statistically model the spatial distribution of soil units and properties from terrain parameters and develop digital soil maps.

(2)   CART and RF are adequate models for this purpose.

(3)   slope stability and landslide risk can be estimated based on a DEM and regionalised information from soil investigation.

RSGs, typical soil horizons and their properties have to be predicted solely from terrain parameters calculated from a DEM, because other factors influencing soil formation, e.g. parent material, are not available spatially localised and continuously throughout the landscape, and their investigation would cost too high input. Due to a limited time frame, only soils under natural vegetation (forest and páramo) were sampled; hence, the presented models refer to soils under natural vegetation only.

A sampling design was developed to provide a dataset, which is representative for the area under study. 24 terrain classes were sampled by 56 soil profiles and 315 auger points along transects. Soil texture (pipette, laser), soil cohesion and soil bulk density were measured in soil profiles only, whereas profiles and auger samples were described in their soil horizons, organic layer thickness, Munsell colour and soil texture by finger method (FAO, 2006). Correcting field texture with laboratory texture results would then serve to establish pedotransfer functions to predict e.g. soil bulk density and saturated hydraulic conductivity (K_{sat}) from the bigger auger dataset.

1.5.2 Manuscript 1: Digital soil mapping in southern Ecuador

Manuscript 1 describes the development of the above mentioned sampling design. The 24 terrain classes were formed by an overlay of 4 altitude, 3 slope and 2 aspect classes which were mainly graded based on climatic information. Auger sampling transects were laid according to the catena concept from ridges to side valley creeks covering these 24 classes. The six typical soil types of the research area were identified and classified according to the World Reference Base for Soil Resources (WRB) (FAO, IUSS Working Group WRB, 2007). Histosols are dominating the dataset in all altitudinal and slope classes. They are associated with Stagnosols, Cambisols and Regosols. Umbrisols and Leptosols only occur to a lesser extent.

A first simple CT model was established to predict soil type distribution from terrain parameters. Terrain parameter raster grids, calculated from a 2 m DEM, include altitude, slope, aspect, profile and plan curvature, specific catchment area and overland flow distance to the channel network (OFD). According to the model, Histosols and Stagnosols were identified as dominant soil types. Stagnosols gain importance with increasing altitude and with decreasing slope angle. Model prediction neglected Cambisols and overestimated Umbrisols, but showed a reasonable prediction for Histosols, Stagnosols and Leptosols. The reason that Cambisols are not represented by a model based on terrain parameters might be the possible dependence of their development on landslide influence. The overestimation of Umbrisols might be caused by the lack of a Cambisol prediction scheme.

1.5.3 Manuscript 2: Reference soil group probability prediction

Adapting a single CT model while including all Reference Soil Groups (RSGs) (manuscript 1), organises the tree model by preferring the category dominating the soil dataset (Histosol). Furthermore, predicting only the category forming the majority in any end node for the related landscape position, neglects the fact that other RSGs were assigned to that end node also.

In this manuscript, the problem was overcome by establishing several tree models to predict each RSG individually. Prediction uncertainty was included via occurrence probability of the soil units. Each sampled site was assigned a Boolean value of 1 or 0, indicating whether the soil was classified as a particular RSG, or not. Terrain parameters were assigned from the raster grids as nearest neighbour and mean

value within GPS accuracy radius. Probabilities of all RSGs were readjusted in order to not exceed a combined probability of 1 by two means: (1) by standardizing the probabilities by relating each RSG to the total probability sum and (2) by applying a hierarchical scheme based on WRB hierarchy.

Histosols and Stagnosols showed an occurrence probability > 0 throughout the whole area: Histosols accounted for a probability of 0.2 – 0.4 depending on hydrological parameters; sites with soils displaying sufficient stagnic properties to qualify as Stagnosols, accounted for 0.25 – 0.64. Highest Stagnosol probability was assigned to slopes < 40° and altitudes > 2146 m a.s.l. Leptosols only occurred close to the creeks and on steep slopes.

Probabilities of multiple RSGs at the same landscape position can be understood as competing RSGs, but also as a soil composed of several diagnostic horizons with different soil processes running simultaneously as has been part of soil genesis theory for a long time. Thereby, this provides a good means to acknowledge inter-relations between RSGs.

Poor model performance (R^2 = 0.2), might be improved by choosing a lower resolution to exclude small scale soil diversity, applying a different statistical model or predicting soil properties instead of the complex RSG entities.

1.5.4   Manuscript 3: Incomplete soil classification to benefit the soil continuum – Prediction of diagnostic horizons of Andean mountain forest soils

RSG model adaptation problems (complex entities) are confronted by the prediction of the diagnostic horizons necessary for RSG assignation themselves. WRB incon-sequences causing the problem are identified, and "incomplete soil classification" is proposed to overcome them and acknowledge the soil continuum.

Within this new classification system, soils are only considered until a depth of 100 cm including the organic layer. Diagnostic horizon thickness is then related to these 100 cm. The soil's name refers to the several diagnostic parts as % histic, humic, umbric, stagnic, cambic, leptic and regic. The horizons leptic and regic were introduced for the parts within the 100 cm that refer to continuous rock or weathered material not classifying for any other diagnostic horizon.

Again terrain parameters were used to predict the diagnostic horizons. They were assigned from the raster grids as nearest neighbour and mean value within GPS accuracy radius. The horizons' thickness was predicted by regression trees (RTs),

their occurrence probability with CTs. Disadvantages of tree models – (1) mean values are assigned to large areas with abrupt changes at their boundaries and (2) small changes in the dataset may lead to quite different tree structures – were overcome by hundredfold model runs. The dataset was Jackknifed to construct 100 models by always using a different random ⅔ subsample. The other ⅓ was then used for hundredfold external cross validation with Pearson's r_{xy}.

Incomplete soil classification resulted in histic and stagnic soil parts dominating the first 100 cm of the soil column for most of the research area. Whether the soils, generally their first mineral soil horizon, display stagnic properties or not, might depend on physical soil properties in addition to terrain parameters. Leaving soil classification incomplete to acknowledge the soil continuum seems a good alternative to combat the problems resulting from conventional WRB classification. After all, the extent of diagnostic soil horizons makes the results of soil genetic processes measurable. Furthermore, the horizons are given equal importance. Accordingly, each soil is dominated by a different soil process, simply because it forms the major part of the first 100 soil centimetres. Besides, the system can be easily applied on soils not represented within the research area.

1.5.5 Manuscript 4: Uncertainty in the spatial prediction of soil texture – Comparison of regression tree and Random Forest models

Statistical models were applied to predict the spatial distribution of soil texture from terrain parameters (nearest neighbour and mean values, see manuscript 2). Random Forest (RF) methodology was compared with simple tree models (RT) via hundredfold external cross validation. A RF model is composed of several tree models grown from different random bootstrap subsamples.

In the soil profiles soil texture was analysed horizon-wise by pipette, laser and field method (FAO, 2006). Results by pipette compared to laser method showed the expected shift to higher silt and lower clay contents. Linear regression equations were adapted. Pedotransfer functions to predict physical soil properties (bulk density, K_{sat}) from the bigger auger dataset analysed by field texture method only, could not be developed, because field texture analysis did not provide satisfying results. It was therefore not possible to correct its results with the more precise laboratory data. Comparing soil texture horizon-wise (Ah, E, Bg and Bw), showed no clear differences unless for sand contents. Hence, soil texture was modelled in the first and last soil

horizon to decide whether the soil texture's spatial distribution was influenced by geomorphologic processes or bedrock only.

From the 8 models to predict sand, silt and clay content each, according to the combinations of (1) pipette or laser texture with (2) nearest neighbour or mean terrain parameter values related by (3) a RT or RF statistical model, the model predicting pipette texture by mean terrain values with RF resulted best. Altitude was the most important predictor parameter. However, all terrain factors considered in the analysis influenced the soil texture of the surface horizon. Maps of sand, silt and clay mean values with standard deviation, display the uncertainty of the texture regionalisation according to 100 model runs. Shallow subsurface flow leads to increasing sand/clay ratios with increasing altitude, on steep slopes and with OFD, by removing finer particles downslope directly underneath the soil surface. The deeper soil layers are not influenced by this shallow subsurface flow and therefore did not show the same texture properties. The influence of terrain curvature had the opposite effect on soil texture, compared to that predicted by other authors and cannot be explained by subsurface flow. This finding might be related to the small scale curvature used in our calculations.

1.5.6   Manuscript 5: Estimating slope stability in a steep Andean mountain forest region

Landslides have a strong soil-landscape forming effect within the research area. To investigate their impact, slope stability was determined in dependence on net rainfall rate. Soil mechanical and hydrological properties in addition to terrain steepness were hypothesized to be the major factors in causing landslides. Hence, the factor of safety (FS) was calculated as the soil shear ratio that is necessary to maintain critical state equilibrium on a potential sliding surface.

Regression tree (RT) and Random Forest (RF) models were compared in their predictive power to regionalise the depth of the failure plane and soil bulk density based on terrain parameters. Deduced from manuscript 3 and hydrological flow pattern analysis (Bauer et al.[1]), the depth of the failure plane was assumed at the lower boundary of the stagnic soil layer or soil depth respectively, depending on soils being stagnic or non-stagnic. RF model performance was better than that of RT. The FS was determined in dependence of soil wetness referring to 0.001, 0.01, 0.1 and 3

---

[1] Personal communication. The manuscript was submitted to Journal of Hydrology.

mm/h net rainfall rate. Sites with a FS < 1 at 0.001 mm/h were classified as unconditionally unstable, sites with a FS ≥ 1 at 3 mm/h (complete saturation) as unconditionally stable.

It was hypothesized that the whole area would be covered by stagnic soils without the influence of landslides that lead to lower bulk densities in their accumulation zones. The lower boundary of the stagnic soil layer and soil depth were regionalised and proved to be a good estimation of the depth of the failure plane. However, terrain parameters explained the spatial distribution of soil bulk density and the depth of the failure plane only to a relatively small percentage. Nevertheless, despite their prediction uncertainty a reasonable prediction of unconditionally unstable sites was achieved. Though, for the FS prediction, φ seemed to be more important than a precise prediction of bulk density and the depth of the failure plane. Setting them at random within the detected ranges might still predict landslide scars as unconditionally unstable sites. This assumption as well as the influence of soil cohesion needs further investigation.

1.5.7　Further investigation plans

The five manuscripts included within this cumulative dissertation represent only the beginning of the planned research on soil-landscape modelling. The gained dataset still has to be used in all its capacity. Further investigation plans include:

(1)　the comparison of the performance of CART and RF to further non-tree-algorithm based statistical models in predicting RSGs and soil properties from terrain attributes. Viscarra Rossel and Behrens (2010) recently compared several statistical models and found Random Forest and boosted regression trees outperformed by all other approaches, e.g. support vector machines and artificial neural networks (ANN). The better prediction force of ANN compared to CART was expected according to Bishop and Minasny (2006) and Selle et al. (2008). CART had been used instead of ANN for its earlier mentioned advantages and the required experience in working with ANN. However, the outperformance of RF by ANN was not expected and has to be further investigated.

(2)　the use of additional terrain parameters to predict soil properties. Some models might be improved by the use of further parameters, e.g. slope length, distance to ridge or topographic wetness index.

(3)   using a different subdivision in Jackknifing the dataset to improve model performance, leaving most of the dataset for model development and only a small amount for model evaluation.

(4)   research regarding the influence of GIS raster grid cell size on the models. In manuscript 2 it was assumed that resolution has an impact on model precision so that the used data set might not be enough to represent the investigated landscape to a high precision of 10 m cell size. Furthermore, the influence of some terrain parameters might change in dependence on scale, e.g. terrain curvature (manuscript 4). Accordingly, calculations of the FS showed some dependence on grid cell size (not included within manuscript 5).

(5)   the regionalisation of K_{sat} through the adaptation of a pedotransfer function, relating it to soil texture and bulk density to improve the prediction of the FS.

(6)   the regionalisation of the water storage capacity and weight of the organic layer to improve the prediction of the FS.

(7)   the regionalisation of the vegetation weight to include it within the prediction of the FS.

(1)   the adaptation of a model to regionalise soil cohesion at critical state equilibrium. Soil cohesion depends on other soil parameters, i.e. water and organic carbon content, and soil texture. Simple model adaptations by linear regression were unsatisfying.

(8)   performing an uncertainty analysis of the FS. Capacities of the R software did not allow for a hundredfold FS calculation based on model uncertainties to predict the bulk density and the depth of the failure plane.

(9)   analysing the importance of regionalised soil parameters to predict the FS. Varying parameters at random within the determined ranges might still predict landslide scars on unconditionally unstable sites.

(10)   estimating soil organic carbon stocks on a landscape level.

(11)   the comparison of statistical soil-landscape models developed for different tropical mountain areas.

1.6   List of manuscripts and specification of contribution

This thesis includes five manuscripts. One is published, two are in review with the European Journal of Soil Science, one was submitted to Geoderma and one to Geomorphology. The list below details the contributions of all co-authors.

Manuscript 1

Title: Digital Soil Mapping in Southern Ecuador

Authors: Mareike Ließ, Bruno Glaser & Bernd Huwe

Status: published

Journal: Erdkunde – Archive for Scientific Geography (2009), 63(4), 309 – 319, special edition, ISSN 0014-0015

Contributions:

Ließ	80%	idea, sampling design, data collection, data analysis, manuscript writing, figures, discussion, editing, corresponding author
Glaser	10%	idea, discussion, editing
Huwe	10%	idea, discussion, editing

Manuscript 2

Title: Reference Soil Group Probability Prediction

Authors: Mareike Ließ, Bruno Glaser & Bernd Huwe

Status: revised version in review

Journal: European Journal of Soil Science

Contributions:

Ließ	80%	idea, methods, data collection, data analysis, manuscript writing, figures, discussion, editing, corresponding author
Glaser	10%	idea, discussion, editing
Huwe	10%	idea, discussion, editing

Manuscript 3

Title: Incomplete Soil Classification to Benefit the Soil Continuum
- Prediction of Diagnostic Horizons of Andean Mountain Forest Soils

Authors: Mareike Ließ, Bruno Glaser & Bernd Huwe

Status: revised version in review

Journal: European Journal of Soil Science

Contributions:

Ließ	80%	idea, methods, data collection, data analysis,

manuscript writing, figures, discussion, editing,

corresponding author

Glaser	10%	idea, discussion, editing
Huwe	10%	idea, discussion, editing

Manuscript 4

Title: Spatial Prediction of Soil Texture Variability in a Steep Mountain Forest Area in Ecuador - Comparison of Regression Tree and Random Forest Models

Authors: Mareike Ließ, Bruno Glaser & Bernd Huwe

Status: submitted

Journal: Geoderma

Contributions:

Ließ	80%	idea, methods, data collection, data analysis,
		manuscript writing, figures, discussion, editing,
		corresponding author
Glaser	10%	idea, discussion, editing
Huwe	10%	idea, discussion, editing

Manuscript 5

Title: Estimating Slope Stability in a Steep Andean Mountain Forest Region

Authors: Mareike Ließ, Bruno Glaser & Bernd Huwe

Status: published with a similar content

Journal: Geomorphology. "Functional soil-landscape modelling to estimate slope stability in a steep Andean mountain forest region", 132 (3-4), 287-299. ISSN: 0169-555X

Contributions:

Ließ	80%	idea, methods, data collection, data analysis,
		manuscript writing, figures, discussion, editing,
		corresponding author
Glaser	10%	idea, discussion, editing
Huwe	10%	idea, discussion, editing

1.7 References

Bahr, E., 2007. Verteilung und Charakteristika der Böden der tropischen Bergregenwaldregion Südecuadors in Abhängigkeit der Landnutzung. Diplomarbeit Technische Universität Dresden, Fakultät für Geo-, Hydro- und Forstwissenschaften. Project database: http://www.tropicalmountain forest.org/

Bauer, J., Rohdenburg, H., Bork, H.-R., 1985. Ein digitales Reliefmodell als Vorraussetzung für ein deterministisches Modell der Wasser- und Stoff-Flüsse. In: Bork, H.- R., Rohdenburg, H. (Eds.). Landschaftsgenese und Landschaftsökologie H. 10, Parameteraufbereitung für deterministische Gebiets-Wassermodelle, Grundlagenarbeiten zur Analyse von Agrar-Ökosystemen, p. 1 – 15.

Bishop, T. F. A., Minasny, B., 2006. Digital Soil-Terrain Modeling: The Predictive Potential and Uncertainty. In: Grunwald, S. (Ed.) Environmental Soil-Landscape Modeling. CRC Press, Boca Raton.

Böhner, J., McCloy, K. R., Strobl, J., 2006. SAGA – Analysis and Modelling Application. Göttinger Geographische Abhandlungen 115. Geographische sInstitut der Universität Göttingen.

Breimann, L., Friedmann, J. H., Olshen, R. A., Stone, C. J., 1984. Classification and regression trees, CRC press, Wadsworth.

Breiman, L., 2001. Technical Report for Version 3. http://oz.berkeley.edu/users/ breiman/randomforest2001.pdf (Access: 28/04/2010).

Burrough, P. A., Bouma, J., Yates, S. R., 1994. The state of the art in pedometrics. Geoderma 62: 311 – 326.

Bussmann, R. W., Wilcke, W., Richter, M., 2008. Landslides as Important Disturbance Regimes – Causes and Regeneration. Beck, E., Bendic, J., Kottke, I., Makeschin, F. Mosandl, R. (Eds.). Gradients in a Tropical Mountain Ecosystem of Ecuador. Ecological Studies 198: 319 – 330.

Cimmery, V. (2007): User guide for SAGA (version 2.0), http://sourceforge.net/ projects/saga-gis/files/ (25.11.2009)

De Gruijter, J.J., Webster, R., Myers, D. E., 1994. Preface to Special Issue: Developments in Spatial Statistics for Soil Science. Geoderma 62 NOS. 1-3: vii – viii.

Dokutschajew, W. W., 1883. Russkij Cernozem, St. Petersburg.

Efron, B., 1979. Bootstrap Methods: Another Look at the Jackknife. In: The Annals of Statistics. 7, Nr. 1, S. 1 – 26.

Efron, B., 1982.The Jackknife, the Bootstrap and Other Resampling Plans.CBMS-NSF Regional Conference Series in Applied Mathematics. Society for Industrial and Applied Mathematics. J. W. Arrowsmith Ltd., Bristol, England.

FAO, IUSS Working Group WRB, 2007. World Reference Base for Soil Resources 2006, first update 2007. World Soil Resources Reports No. 103.

FAO, 2006. Guidelines for soil description. Fourth Edition. Food and Acriculture Organization of the United Nations, Rome.

Fries, A., Rollenbeck, R., Göttlicher, D., Nauss, T., Homeier, J., Peters, T., Bendix, J., 2009. Thermal structure of a megadiverse Andean mountain ecosystem in southern Ecuador, and its regionalization. In: Erdkunde 63, 321 – 335.

Gessler, P., Moore, I., McKenzie, N., Ryan, P., 1995. Soil-landscape modelling and spatial prediction of soil attributes. International Journal of Geographical Information Systems, 9/ 4: 421– 432.

Gessler, P., Chadwick, O. A., Chamron, F. Holmes, K. Althouse, L., 2000. Modeling soil-landscape and ecosystem properties using terrain attributes. Soil Science Society of America Journal 64: 2046 – 2056.

Goovaerts, P., 1999. Geostatistics in soil science: state-of-the-art and perspectives. Geoderma 89: 1 – 45.

Good, P. I., 1999. Resampling Methods – A Practical Guide to Data Analysis. Birkhäuser, Boston.

Grunwald, S., 2006. What Do We Really Know about the Space-Time Continuum of Soil Landacapes? In: Grunwald, S. (Ed.), Environmental Soil-Landscape Modeling, CRC Press, Boca Raton. pp. 3 – 36.

Jenny, H., 1941. Factors of Soil Formation. A System of Quantitative Pedology. New York.

Jordan, E., Ungerechts, L., Cáceres, B., Penafiel, A., Francou, B., 2005. Estimation by photogrammetry of the glacier recession on the Cotopaxi Volcano (Ecuador) between 1956 and 1997. In: Hydrological Sciences 50, 949–961.

Kreutzer, D. Martini, J., 2002. Bestimmung und Regionalisierung der gesättigten hydraulischen Leitfähigkeiten in Böden unter tropischem Bergregenwald in Ecuador mit verschiedenen Methoden. Diplomarbeit Justus-Liebig-Universität Gießen, Institut für Angewandte Geowissenschaften. Project database: http://www.tropicalmountain forest.org/

Lark, R. M., 1999. Soil-landform relationships at within-field scales: an investigation using continuous classification. Geoderma 92: 141 – 165.

Lea, N. L., 1992. An aspect driven kinematic routing algorithm. In: Parsons, A. J. and Abrahams, A. D. (eds.) Overland Flow Hydraulics and Erosion Mechanics. London, 393 – 407.

Litherland, M., Aspen, J. A., Jemielita, R. A., 1994. The metamorphic belts of Ecuador. Overseas Mem. Br. Geol Surv 11: 1–147.

McBratney, A. B., 1986. Introduction to Pedometrics: A course of lectures. CSIRO Australia. Devisons of Soils Technical Memorandum 53/ 1986.

McBratney, A. B., Odeh, I. O. A., Bishop, T. F. A., Dunbar, M. D., Shatar, T. M., 2000. An overview of pedometrics techniques for use in soil survey. Geoderma 97: 293 – 327.

McBratney, A. B., Mendonça Santos, M. L., Minasny, B., 2003. On digital soil mapping. Geoderma 117: 3 – 52.

McKenzie, N. J., Ryan, P. J., 1999. Spatial prediction of soil properties using environmental correlation. Geoderma 89: 67 – 94.

Milne, G., 1936. Normal erosion as a factor in soil profile development. Nature 138: 541 – 548.

Meyers, D. E., 1994. Spatial interpolation: an overview. Geoderma 62: 17 – 28.

Moran, C. J., Bui, E. N., 2002. Spatial data mining for enhanced soil map modelling. International Journal of Geographic Information Science 16: 533 – 549.

Nauss, T., Göttlicher, D., Dobbermann, M., Bendix, J., 2007. Central data services in multidisciplinary environmental research projects. In: e-Zeitschrift für Agrarinformatik 2. http://www.preagro.de/ezai/index.php/eZAI/ article/view/28/28 (access: 13.12.2009)

Odeh, I. O. A., Chittleborough, D. J., McBratney, A. B., 1991. Elucidation of soil-landform interrelationships by canonical ordination analysis. Geoderma 49: 1 – 32.

Olaya, V., 2004. A gentle introduction to SAGA GIS. Edition 1.1. http://sourceforge. net/ projects/saga-gis/files/ (25.11.2009)

Park, S. J., McSweeney, K., Lowery, B., 2001. Identification of the spatial distribution of soils using a process-based terrain charcterization. Geoderma 103: 249 – 272.

Peters, J., de Baets, B., Verhoest, N. E. C., Samson, R., Degroeve, S., de Becker, P., Huybrechts, W., 2007. Random Forests as a tool for ecohydrological distribution modelling. Ecological Modelling 207: 304 – 318.

Prasad, A. M., Iverson, L.R., Liaw, A., 2006. Newer classification and regression tree techniques: Bagging and random forest for ecological prediction. Ecosystems 9: 181 – 199.

Rossiter, D. G. (2004). Global Workshop on Digital Soil Mapping, September 14 – 17th 2004, Montpellier. International Union of Soil Sciences. http://www.iuss.org/ Reports/France%202004.htm. (access: 20.08.2010)

Ryan, P. J., McKenzie, N. J., O'Connell, D., Loughhead, A. N., Leppert, P. M., Jacquier, D., Ashton, L., 2000. Integrating forest soils information across scales: spatial prediction of soil properties under Australian forests. Forest Ecology and Management 138: 139 – 157.

Rollenbeck, R., 2006. Variability of precipitation in the Reserva Biólogica San Francisco / Southern Ecuador. In: Lyonia, A Journal of Ecology and Application 9 (1), 43 – 51.

Schrumpf, M., Guggenberger, G., Valarezo, C., Zech, W., 2001. Tropical montane rainforest soils. Development and nutrient status along an altitudinal gradient in the South Ecuadorian Andes. Die Erde, 132; 43–59.

Selle, B., Lischeid, G., Huwe, B., 2008. Effective modelling of percolation at the landscape scale using data-based approaches. Computers & Geosciences 34: 699 – 713.

Shikano, S., 2005. Bootstrap und Jackknife. In: Behnke, J., Gschwend, T., Schindler, D., Schnapp, K.-U., 2006. Methoden der Politikwissenschaft: neuere qualitative und quantitative Analyseverfahren, Baden-Baden: Nomos Verl.-Ges. Online: http://webrum.uni-mannheim.de/sowi/shikanos/ Publikation/BootstrapMethodenbuch-20-12-05.pdf (accessed: 14.09.2010).

Strahler, A. N., 1957. Quantitative analysis of watershed geomorphology. In: Transactions of the American Geophysical Union 38 (6), 913–920.

Thomas, A. L.,King, D., Dambrine, E., Couturier, A., Roque, A., 1999. Predicting soil classes with parameters derived from relief geologic materials in a sandstone region of the Vosges mountains (northeastern France). Geoderma 90: 291 – 305.

Thompson, J. A., Bell, J. C., Butler, C. A., 1997. Quantitative soil-landscape modelling for estimating the areal extent of hydromorphic soils. Soil Science Society of America Journal 61: 971 – 980.

Wilcke, W. ,Yasin, S., Abramowski, U., Valarezo, C., Zech, W., 2002. Nutrient storage and turnover in organic layers under tropical montane rainforest in Ecuador. European Journal of Soil Science, 53: 15–27.

Wilcke, W., Valladarez, H., Stoyan, R., Yasin, S., Valarez, C., Zech, W., 2003. Soil properties on a chronosequence of landslides in montane rainforest, Ecuador. Catena, 53: 79–95.

Wysocki, D. A., Schoeneberger, P. J., LaGarry, H. E., 2000. Geomorphology of soil landscapes. In: Sumner, M. (Ed.), Handbook of soil science. CRC Press, Boca Raton, pp. E1– E39.

Yasin, S., 2001. Water and Nutrient Dynamics in Microcatchments under Montane Forest in the South Ecuadorian Andes. Bayreuther Bodenkundliche Berichte, Band 73.

Zevenbergen L. W., Thorne C. R., 1987. Quantitative Analysis of Land Surface Topography. Earth Surface Processes Landforms 12: 47 – 56.

Chapter 2

Digital Soil Mapping in Southern Ecuador

Mareike Liess, Bruno Glaser and Bernd Huwe
University of Bayreuth, Department of Geosciences, Soil Physics Group
Universitätsstrasse 30, 95447 Bayreuth, Germany

Correspondence: Mareike Ließ; E-mail: Mareike.liess@uni-bayreuth.de

Summary

Soil-landscape modelling is based on understanding the spatial distribution patterns of soil characteristics. A model relating the soil's properties to its position within the landscape is used to predict soil properties in other similar landscape positions. To develop soil-landscape models, the interaction of geographic information technology, advanced statistics and soil science is needed. The focus of this work is to predict the distribution of the different soil types in a tropical mountain forest area in southern Ecuador from relief and hydrological parameters, using a classification tree model (CART) for soil regionalisation. Soils were sampled along transects from ridges towards side valley creeks, using a sampling design with 24 relief units. Major soil types of the research area are Histosols associated with Stagnosols, Cambisols and Regosols. Umbrisols and Leptosols are present to a lesser degree. Stagnosols gain importance with increasing altitude and with decreasing slope angle. Umbrisols are to be found only on slopes <30°. Cambisols occurrence might be related to landslides. The CART model was established by a dataset of 315 auger sampling points. Bedrock and relief curvature had no influence on model development. Applying the CART model to the research area, Histosols and Stagnosols were identified as dominant soil types. Model prediction left out Cambisols and overestimated Umbrisols, but showed a realistic prediction for Histosols, Stagnosols and Leptosols.

Zusammenfassung

Bodenlandschaftsmodellierung basiert auf dem Verständnis der räumlichen Verteilungsmuster von Bodeneigenschaften. Das Modell, das die Beziehung zwischen Bodeneigenschaften und der Lage des Bodens in der Landschaft herstellt, dient dazu, Vorhersagen über Böden in ähnlichen Landschaftspositionen zu treffen. Für die Entwicklung von Bodenlandschaftsmodellen ist eine Interaktion von geographischer Informationstechnologie, höherer Statistik und Bodenkunde notwendig. Ziel dieser Arbeit ist die Vorhersage der Verteilung der Bodentypen in einem tropischen Bergregenwaldgebiet im südlichen Ecuador auf Grundlage von Relief- und hydrologischen Parametern mittels eines Klassifikationsbaum-Modells (CART). Die Böden wurden entlang von Transekten, die von den Hangrücken zu den jeweiligen Seitentalbächen abfallen, mittels eines 24 Reliefeinheiten umfassenden

Sampling-Designs beprobt. Die Hauptbodentypen des Untersuchungsgebietes sind Histosole, die mit Stagnosolen, Cambisolen und Regosolen vergesellschaftet sind. Umbrisole und Leptosole kommen zu einem geringeren Teil vor. Die Bedeutung der Stagnosole nimmt mit der Höhe und abnehmender Hangneigung zu. Umbrisole kommen nur auf Hangneigungen < 30° vor; das Vorkommen der Cambisole könnte mit Hangrutschungen in Zusammenhang stehen. Das CART-Modell wurde auf Grundlage eines 315 Bohrstockeinschläge umfassenden Datensatzes erstellt. Ausgangsgestein und Geländekrümmung hatten keinen Einfluss auf die Modellentwicklung. Das auf das Untersuchungsgebiet angewandte CART-Modell hat Histosole und Stagnosole als Hauptbodentypen identifiziert. Die Modellvorhersage hat Cambisole vernachlässigt und Umbrisole überschätzt. Es leistet aber eine realistische Vorhersage für Histosole, Stagnosole und Leptosole

Keywords: Soil-landscape modelling, CART, GIS, Ecuador, tropical mountain rainforest

2.1 Introduction

Soil-landscapes develop as results of pedo-geomorphological and hydrological processes. Soil-landscape modelling focuses on understanding the spatial distribution of soil characteristics and soil parameters. To develop soil-landscape models, the interaction of geographic information technology, advanced statistics and soil science is needed. As we discovered during long-term field work in southern Ecuador, tropical mountain forest areas pose severe problems to traditional soil mapping approaches, due to their heterogeneity and complex lithological composition. The limited terrain accessibility makes complete area sampling impossible. Therefore, soil-landscape modelling is a challenge in such areas. With our study we will show, that CART-modelling based on digital elevation models (DEMs) and the application of geographic information technology has potential to address this challenge: A model relating the soil's properties to its position within the landscape is used to predict soil properties in other similar landscape positions. Relief and hydrological parameters are used to predict the distribution of the different soil types in a tropical mountain forest area. Möller et al. (2008) used a hierarchical terrain-classification procedure in Saxony-Anhalt, Germany, in order to use topography for digital soil mapping. Barthold et al. (2008) used a design-based

stratified sampling plan in a tropical lowland forest including lithology, vegetation and topography. We developed a sampling design appropriate for soil-landscape mapping in tropical mountaneous forest areas based on relief classes and the catena concept.

Soil data is usually gained in discrete sampling points. To produce a continuous soil map, two general approaches are available: Spatial interpolation between sampling locations and environmental correlation relating spatial patterns of observable landscape parameters to spatial patterns of soil variability. Since we predict soil type, which is a non-continuous variable, geostatistic methods such as kriging are not applicable. Thus, we apply the second approach by focusing on the intensively investigated theory of soils being determined by their position within the landscape, therefore on relief factors, geology, climate and vegetation (Jenny, 1941; Amundson, 2004). There are several methods available to regionalize point observations by investigating the relationship between landscape parameters and soil properties of interest. In many studies, terrain attributes have been used to predict soil properties. The most commonly applied technique to predict soil properties or soil types is linear regression (Troeh, 1964; Walker et al., 1986; Pennock et al., 1987; Odeh et al., 1991/ 1994; Park et al., 2001; Romano and Palladino, 2002; Dercon et al., 2003). Methods like classification and regression trees, artificial neural networks and fuzzy logic have more recently been used in predicting soil properties. Cialella et al. (1997) predict soil drainage classes and Lagacherie and Holmes (1997) soil classes with a classification tree, Bui et al. (1999) predict them with a decision tree and a Bayesian model. Park and Vlek (2002) used artificial neural networks to model soil parameters; De Bruin and Stein (1998) use fuzzy c-means. A more complete overview can be obtained in McBratney et al. (2003) and Bishop and Minasny (2006).

Among the regionalization methods to produce continuous soil property maps from sampled point information based on the DEM, in our study classification and regression trees (CART) are being applied. Comparing several statistical prediction methods, Bishop and Minasny (2006) found, that CART has the most advantages: In contrast to artificial neural networks (ANN), linear models and generalized additive models, CART is easy to use and interpretable. Linear models cannot predict qualitative data and their predictive power is small. Bishop and Minasny (2006) assign a better predictive power to ANN, but Selle et al. (2006) find best model performance in CART when comparing it with Kriging and ANN. Decision trees can

handle data of different types: Continuous, categorical, ordinal and binary. The method can also cope with missing data.

2.2 Approach for soil-landscape modelling

Soil data is usually gained in discrete sampling points. To produce a continuous soil map, two general approaches are available: The spatial interpolation between sampling locations, and environmental correlation relating spatial patterns of observable landscape parameters to spatial patterns of soil variability. Since we predict soil type, which is a non-continuous variable, geostatistic methods such as kriging are not applicable. Thus, we apply the second approach by focusing on the intensively investigated theory of soils being determined by their position within the landscape, therefore on relief factors, geology, climate and vegetation (Jenny, 1941; Admundson, 1994).

There are several methods to regionalize from point observations by investigating the relationship between landscape parameters and soil properties of interest. In many studies, terrain attributes have been used to predict soil properties. The most commonly applied technique to predict soil properties is linear regression (Troeh, 1964; Walker et al., 1986; Pennock et al., 1987; Odeh et al., 1991/ 1994; Park et al., 2001; Romano and Palladino, 2002; Dercon et al., 2003). Methods like CART, ANN and fuzzy logic have more recently been used in predicting soil properties. Cialella et al. (1997) predict soil drainage classes and Lagacherie a. Holmes (1997) soil classes by a classification tree, Bui et al. (1999) predict them with a decision tree and a Bayesian model. Park and Vlek (2002) used ANN to model several soil variables; De Bruin a. Stein (1998) use fuzzy c-means. A more complete overview can be obtained in McBratney et al. (2003) and Bishop and Minasny (2005).

2.2.1 GIS methodology

The System for Automated Geoscientific Analyses (SAGA) was used to obtain the DEM and calculate the necessary terrain and hydrological attributes for model development as well as for model application. SAGA is a free Geographical Information System (GIS) that was developed by the working-group Geosystem Analysis, a close-knit group of scientists from the Göttingen University and scilands GmbH Göttingen.

Since all variables used to predict the soil type are calculated from a DEM, the area to be modelled is determined by the availability of such a DEM. This was provided by the research unit's database (Nauss et al., 2007) in the form of a two meter interval contour line shapefile, which was originally generated from stereo aerial photos by aero-triangulation (Jordan et al., 2005). The area represented by the DEM will from now on be referred to as the investigation area.

As a first step, a DEM had to be calculated from the available polylines' shapefile. A point shapefile was created by introducing points of 2 m distance along the polylines. Then via kriging, a continuous grid of 2 m cell size was calculated with each cell containing the so calculated altitude. Parameters that were calculated from this DEM include altitude, slope, aspect, curvature, catchment size, channel network, and overland flow distance (OFD) to channel network. For model development, slope, aspect and curvature as measured in the field were used, whereas hydrological parameters such as catchment size and OFD were taken from the DEM. Altitude was also taken from the DEM since barometric altitude measurements resulted in high errors due to changing air pressure within few hours. To relate the grid data calculated from the DEM to the sampled soil data, GPS measurements of the auger point position were used. Circling the auger point with the GPS accuracy as radius, the medium value of the responding grid cells within the circle was assigned to the auger point.

The 2 x 2 m precision grid was used for model development, whereas model application was performed on a less precise grid with 10 x 10 m cell size. The precision of the digital terrain attributes calculated from the DEM depends on the algorithm used to calculate the terrain attributes and of course the uncertainty of the DEM. Unfortunately, no information on DEM uncertainty is available and our attempt to gain further information via precise altitude measurements failed due to the already mentioned problems. An estimation of the accuracy might be possible in future by more precise DGPS altitude measurements, since a DGPS is now available within the research area. To calculate slope, aspect and curvature, the Fit 2nd Degree Polynom from Zevenbergen & Thorne (Cimmery, 2007; Behrens, 2003) with SAGA's local morphometry module was applied. Two channel networks were calculated according to the Strahler stream order from the DEM (Strahler, 1957) using the initiation thresholds 6 and 7. The latter represents a smaller precision in channel network than the former. OFD as well as vertical (VOFD) and horizontal overland

flow distance (HOFD) were calculated with respect to these two channel networks. The catchment area of a cell indicates the area upslope of that cell whose flow will eventually reach it. Since choosing one flow algorithm to calculate catchment size is rather difficult, two methods were chosen to allow for flow direction as well as flow tracing algorithms. The first method applied is the "Braunschweiger Digitales Reliefmodell" (Bauer et al., 1985). It is based on a multiple flow direction algorithm. Flow is split between the surrounding cell whose orientation is nearest to the aspect of the centre cell and its two adjacent cells. The other method used for catchment size calculation is based on the Kinematic Routing Algorithm (Lea, 1992), a unidimensional flow tracing algorithm. Here flow behaves like a ball rolling down the DEM, without restricting its position to the centre of cells.

2.2.2   Regionalisation method CART

CART shows a tree structure where the dataset is subdivided regarding the input parameters step by step into subclasses by minimizing the misclassification error or in predicting the assumed class mean of the variable value and its sum of squares. Based on the obtained classification or regression rule obtained by the dataset, CART assigns the respective soil property to every point in the landscape, for which digital elevation information is available. We implemented CART with the rpart library of the R-Project for Statistical Computing developed by Beth Atkinson and Terry Therneau. A complete description of the methodology can be obtained from Breimann et al. (1984). Starting from the parent node, which contains the complete dataset, the set is subdivided until only one auger point is found in each end node of the tree. The branches emanating from each node define the splitting criterion, a logical statement comprised of one of the input variables and the variable value indicating the split location. The subdivision for classification trees, i.e. datasets that are classified based on a categorical variable such as soil type in rpart, is done based on the Gini index as decision criterion for which variable best separates the dataset in each node into two subsets. The Gini index can be interpreted as the decrease of the misclassification probability. In a classification tree, a categorical value is assigned to each end node, usually the value that forms the majority within the node. The subdivision of the dataset in a regression tree, i.e. datasets that are organized based on a continuous variable such as the clay content or thickness of a soil horizon, is also based on minimizing the impurity of the end nodes. The tree

model minimizes the residual sums of squares for each node. A mean is calculated for each end node. Once the complete tree is produced, it is important to prune the tree to avoid overfitting. This is done to avoid putting random variation into predictions. A method to check model performance is the cross validation error. To calculate it, the R-package rpart automatically subdivides the dataset into ten subsets. CART is then performed ten times always using nine parts for model training and the tenth part as evaluation dataset. Among all the trees considered for the final model, the tree with the lowest cross-validated error rate is chosen. The corresponding complexity parameter for that tree helps in pruning the tree to the selected optimal size.

2.2.3 Research area

The study area is situated in the Southern Ecuadorian Andes between Loja and Zamora, at the northern border of the National Park Podocarpus extending from the San Francisco River to either side (Fig. 2.1). Vegetation includes tropical mountain rainforest, páramo vegetation above the tree limit and pastures induced by human activity. Forest slopes are mainly situated on the northwards facing slopes that reach from 1720 m above sea level (a.s.l.) up to the highest peak, the Cerro de Consuelo with c 3160 m a.s.l., whereas the pasture sites are on the other side of the San Francisco River. The area is influenced by regular occurrences of landslides. These have mostly been observed within the forest, but also occur on pastures. Homeier et al. (2002) differentiated different forest types according to their altitude and position on ridge or in the valley respectively. The area exhibits high tree species diversity with very different vegetation at a small scale. Rubiaceae, Lauraceae, Euphorbiaceae and Melastomataceae families account for many species (Homeier et al., 2002). Average annual total rainfall increases from 2050 mm at an altitude of 1960 m a.s.l. to c 4400 mm at the Cerro de Consuelo (Rollenbeck, 2006). The rainfall gradient increases by 250 mm per 100 m altitude up to 2600 m a.s.l. and decreases above 2600 m a.s.l. to 100 mm per 100 m altitude a.s.l. (Rollenbeck, 2006). The average air temperature ranges from 19.4 °C at the valley bottom to 9.4 °C at the upper parts (Fries et al., 2009). Regarding geology, the research area is part of the Chiguinda unit. Metasiltstones, siltstones and quartzites are intermixed with layers of phyllite and clay schists (Litherland et al., 1994).
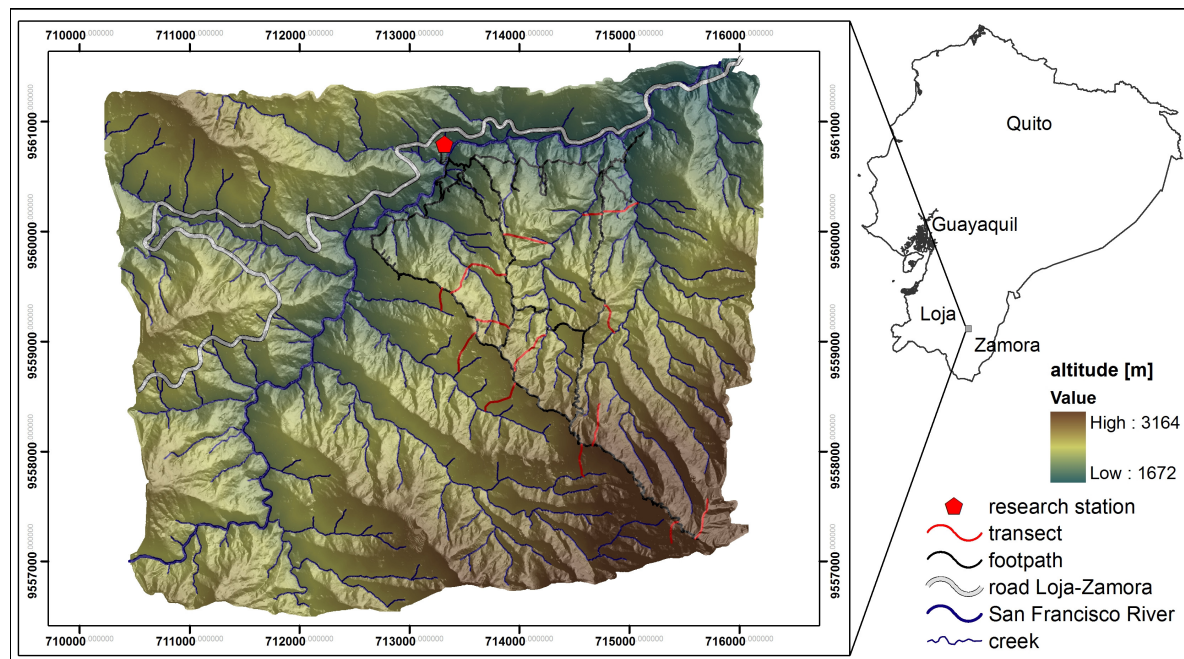
Figure 2.1: Research area (light source for analytical hillshading from north-east)

2.2.4 Sampling scheme

To gain continuous data maps, first of all soil point data has to be assessed. Since available soil data from former studies in the area proved to be rather insufficient for modelling purposes, especially in terms of sampling depth and distribution, we decided to gain our own soil dataset. Due to the complex and hardly accessible terrain of the tropical mountain forest, conventional sampling designs such as random sampling or a systematic sampling by structurizing the whole area with a grid sampling scheme are not applicable. A new sampling strategy representing the whole investigation area with respect to soil distribution and being applicable within a reasonable time period was designed as explained in the following.

The investigation area was divided into 24 relief units according to an overlay of a four-class elevation map, a three-class slope map and a two-class aspect map (Fig. 2.2). Since climate and vegetation have an important influence on soil formation, elevation classes were formed according to forest types as investigated by Homeier et al. (2002) and the rainfall gradient (Rollenbeck, 2006). The forest types were assigned according to different species composition, tree density and tree height. Aspect was divided into the main wind directions, east and west. September to April, heavy convective rainfall is received at western slopes, and from May to September at rather eastern slopes (Rollenbeck, 2006). Since the research area is heavily affected by landslides, they also have an important influence on soil formation.

Earlier studies on landslides in the area (Wilcke et al., 2003) showed, that landslides mostly occur on slopes with angles higher than 35 degrees, Gao (1993) found, that landslide risk increases above 31° slope angle, Zhou et al. (2002) found most landslides on slope angles with 25 to 35 degrees. We designated three slope classes: < 31°, 31–41° and > 41° according to the histogram of the investigation area.
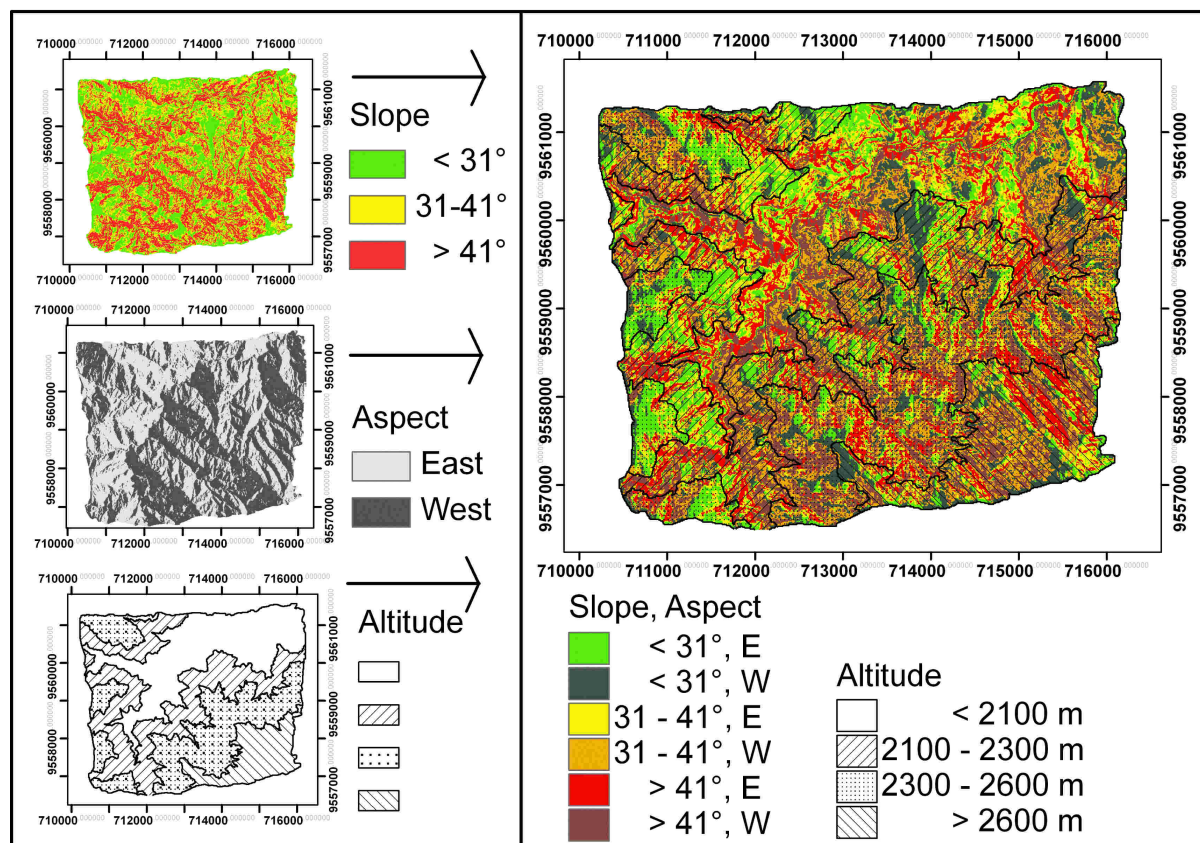
Figure 2.2: Sampling Design: Combining 3 slope, 2 aspect and 4 altitudinal classes to 24 relief units.

These 24 relief units were then sampled on different slopes via auger sampling with a Pürckhauer up to two meters in depth or C horizon respectively. According to the catena concept, transects from the ridges towards the side valley creeks were investigated (Fig. 2.1). In this way, sampling was ensured on different slope angles, altitude, aspect and curvature as well as sampling spots of different vegetation. As a result of the high slope angles – according to the DEM, at least 9% of the area has slope angles of 50° and higher – transects also had to be chosen due to accessibility. During field work, we usually found, that slope angles were underestimated by the DEM. This is why a much higher percentage of gradients steeper than 50° was found during our investigation. Parameters necessary for soil classification in accordance with the World Reference Base for Soil Resources (FAO, IUSS Working Group WRB,

2007), i.e. bedrock, tree height and canopy density as well as geographic position via GPS, altitude, slope, curvature and aspect were assessed.

In applying Jenny's (1941) concept of predicting soil properties, the dependence of soil properties had to be reduced to relief properties since other parameters are not available for the research area or are not available with a sufficient accuracy. No detailed geological map of the research area is available and would cost a too high input to produce, since bedding of the parent material changes on a micro scale (decimetres to meters). Bedrock is therefore considered to be a uniform mass in establishing a model to be applied to the study area, but checked regarding its predicting force for the model, i.e. if it was possible to calculate a better model in case geological data would be available for the whole area. Vegetation data is also not available to a sufficient extent for the area, its importance for the soil-landscape model will be checked in a similar way. Climate data is available for the study area provided by an X-band local area weather radar with a 60 km radius and 500 x 500 m resolution covering the study area by about 50 radar pixels (Rollenbeck, 2006). This of course is not comparable to the much higher resolution of the DEM with 2 m. Hence, climate data is furthermore assumed to be represented to some extent by altitude and aspect.

2.3   Results

Up to now, 315 auger points have been investigated. Major soil types as well as an occurrence pattern are already obvious from these data. As soil forming material we found schists, claystones, phyllites, sandstones, siltstones and quartz crystals in the investigation area. The bedding of the parent material varies on a micro scale, mostly highly weathered rocks are found unless close to major creeks.

2.3.1   Major soil types and their abundance

Investigated soils were classified as Histosols, Stagnosols, Cambisols, Umbrisols, Leptosols and Regosols (Fig. 2.3) according to World Reference Base for Soil Resources (FAO, IUSS Working Group WRB, 2007).

As shown in Figure 2.4a, Histosols form the majority in all altitudinal classes with 39 to 56%. The occurrence of Stagnosols increases with altitude. Many soils that we classified as Histosols, also show a stagnic colour pattern. The percentage of

Regosols decreases with increasing altitude.

Regarding slope classes (Fig. 2.4b), Histosols have an even higher contribution with 47 to 59% to the overall soil types. The coverage of Stagnosols decreased with increasing slope angle. The abundance of Cambisols increased with increasing slope angle. Umbrisols are only found on slopes < 30°.
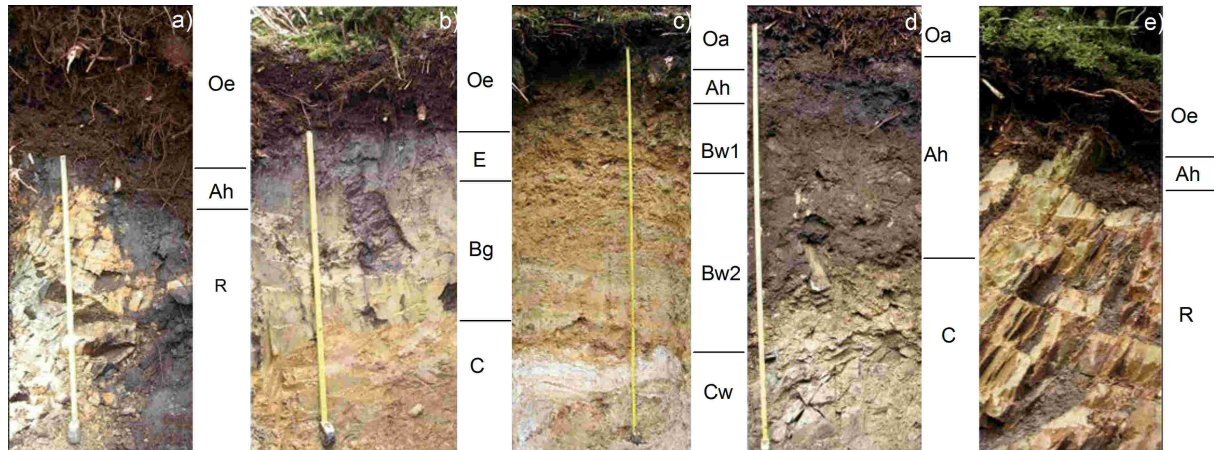
Figure 2.3: Major soil types of the area: a) Histosol, b) Stagnosol, c) Cambisol, d) Umbrisol, e) Leptosol
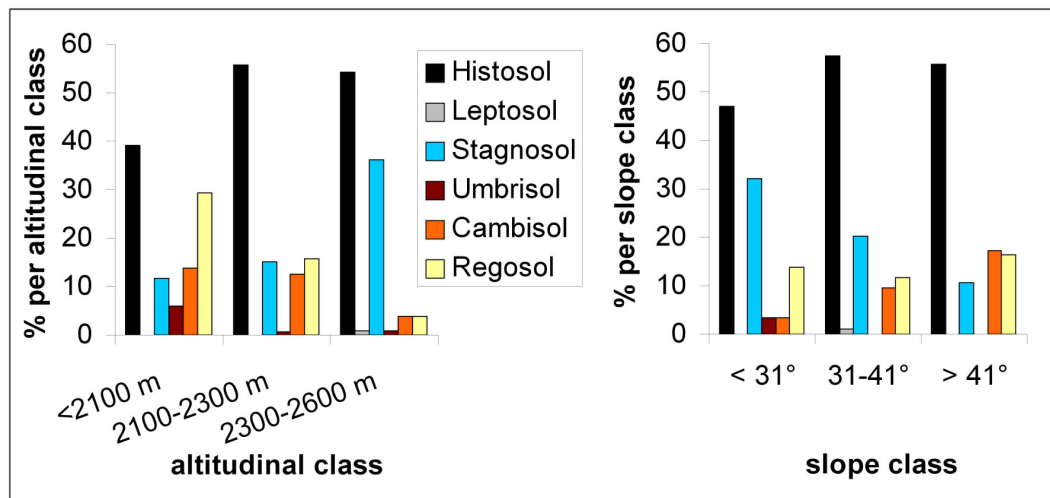
Figure 2.4 a, b: Soil types distribution according to altitudinal (a) and slope classes (b). Data from 315 auger points.

2.3.2 Soil type model with CART

Figure 2.5 shows the pruned classification tree with soil type as the classifying variable and several relief and hydrological parameters as input variables. The small pie charts display the percentages of auger points with a specific soil type assigned to the end node. The soil type that forms the majority within the end node is the classifying category for that end node. This soil type is assigned to the corresponding combination of relief and hydrological categories if it comes to model application.

Those auger points that fall into the same category of the classifying variables, but were classified with a different soil type, display the impurity of each end node and therefore the model imprecision. Five end nodes were assigned to Histosols, six to Stagnosols, one to Regosols, one to Leptosols and one to Umbrisols. The blue numbers beneath the circle diagrams display the number of auger points used to form the end node.
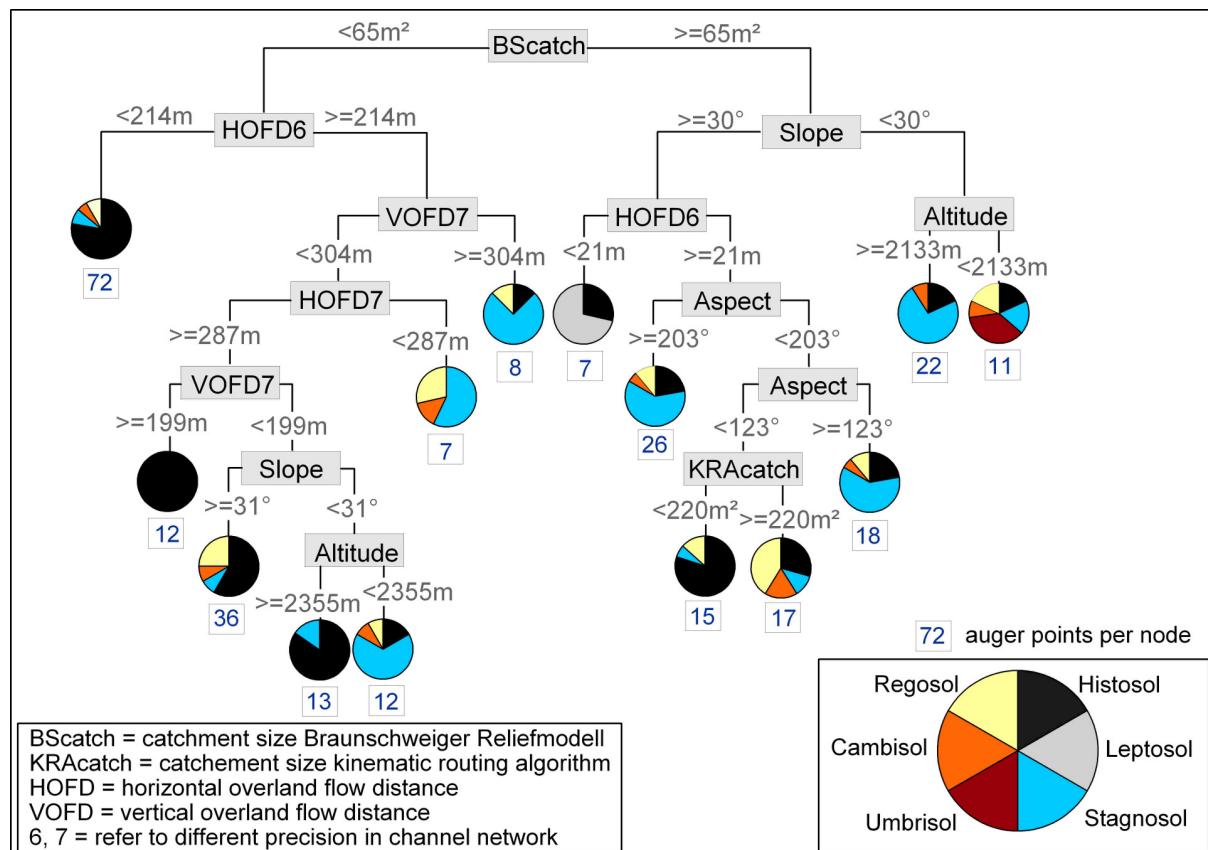
Figure 2.5: Pruned classification tree to predict soil types' distribution within the research area. Pie charts indicate the probability of each soil type per end node.

Table 2.1 gives an overview of the several relief and hydrological parameters of importance for model development. Bedrock and curvature showed no influence on model development, whereas all other parameters had an influence on the prediction of at least three soil types.

Figure 2.6 shows model application to the research area. According to the classification tree (Fig. 2.5) Leptosols are only assigned to sites close to the creeks (HOFD6 < 21m) where slopes ≥ 30°and catchment areas ≥ 65 m² prevail. According to the model, Umbrisols are only found at altitudes < 2133 m a.s.l. and on slopes < 30°. Although Regosols are assigned to several end nodes (Fig. 2.5), there is only one end node where they form the majority and therefore gain importance in model prediction. Slope, aspect, catchment area and OFD are used as classifying variables.

In the same way, Cambisols are also distributed among several end nodes. Unfortunately, they are divided to such an extent, that they do not gain the majority in any of the end nodes and therefore do not play a role in model prediction. The only pure end node is assigned to Histosols and only depends on distance to the creek network as well as catchment size. Furthermore, there is only one end node in which Histosols are not present. The same is true for Stagnosols.

Table 2.1: Influence of relief and hydrological parameters on model development

soiltype	influence on model development						
	altitude	slope	aspect	curvature	OFD	catchment size	bedrock
Histosol	☑	☑	☑	☒	☑	☑	☒
Leptosol	☒	☑	☒	☒	☑	☑	☒
Stagnosol	☑	☑	☑	☒	☑	☑	☒
Umbrisol	☑	☑	☒	☒	☒	☑	☒
Cambisol	☑	☑	☑	☒	☑	☑	☒
Regosol	☑	☑	☑	☒	☑	☑	☒

☒ no influence   ☑ influence   ☑ influence of minor importance

Figure 2.7 gives an overview of the distribution of the soil types within the research area after model application. Their distribution was calculated for each sampling unit. This shows, that Histosols form the majority in all four altitudinal classes for slope angles higher than 31°. Their abundance increases with slope. For slope angles higher than 31°, aspect also seems to have an influence since western slopes always show higher Histosol percentages. Stagnosols are the most important soils for slope angles smaller than 31° with exception of altitudes smaller than 2100 m a.s.l. For altitudes smaller than 2100 m a.s.l. and slope angles smaller 31° Umbrisols contribute the major percentage. Regosols only contribute a significant part to slope classes ≥ 31°.
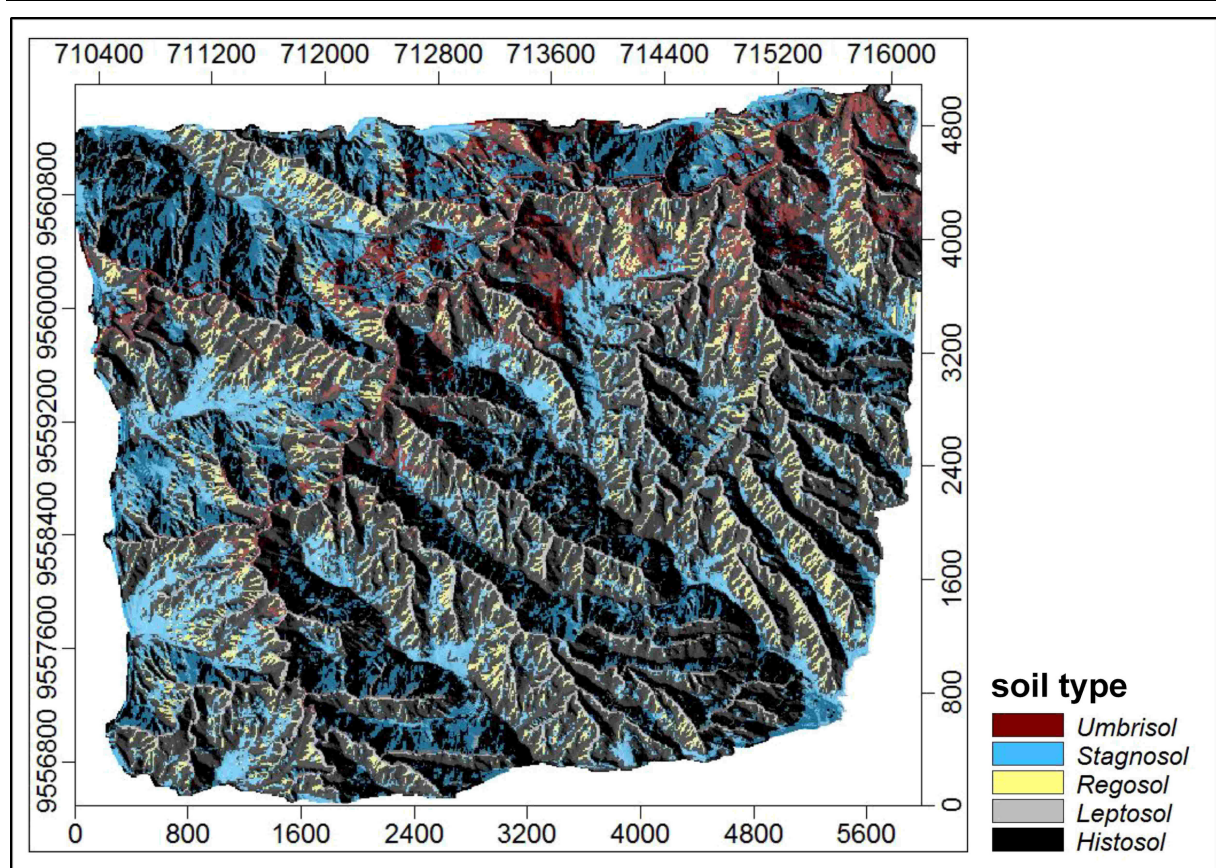
Figure 2.6: Soil types distribution: Classification tree for soil types applied to the research area, overlaid hillshading with light source from north-east
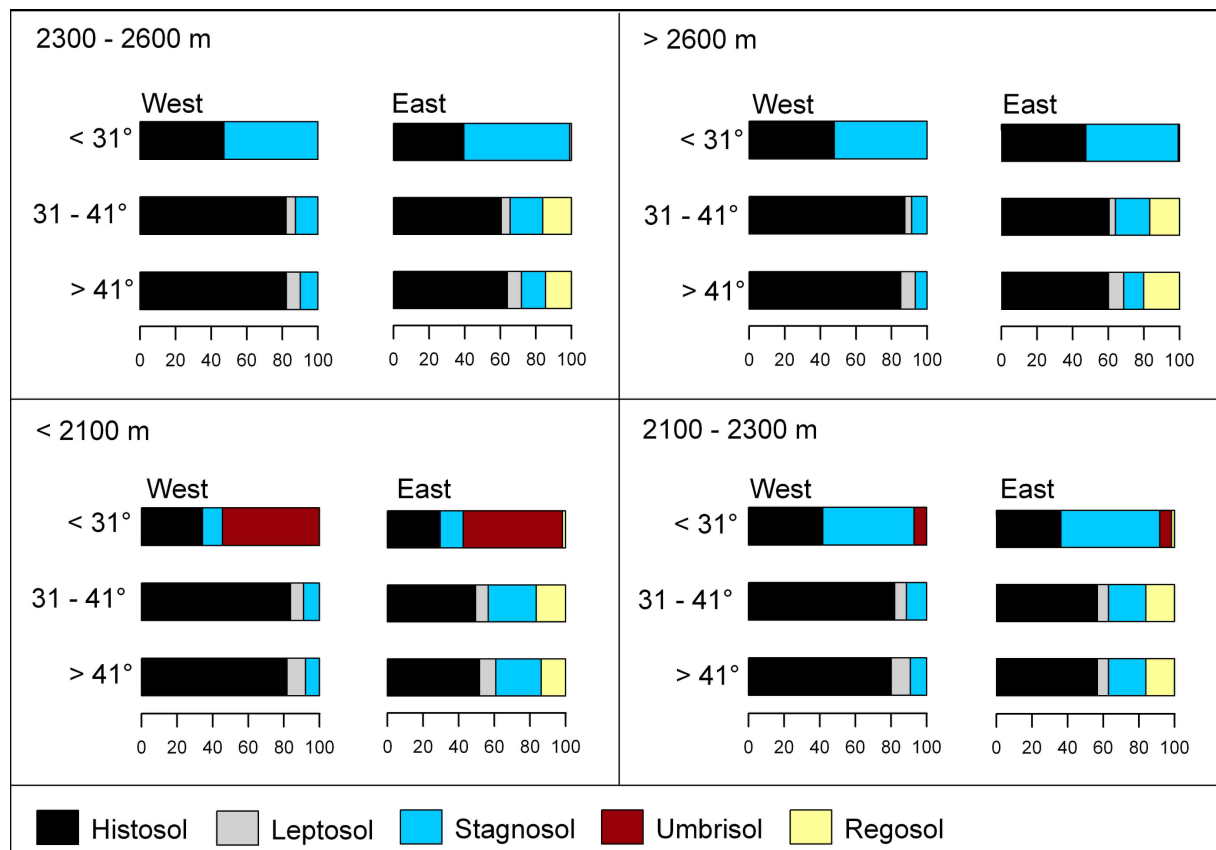
Figure 2.7: Soil types distribution per sampling unit after model application

2.4   Discussion

Our results clearly demonstrated that Histosol is the main soil type of the investigation area, followed by Stagnosol and Regosol. Cambisols, Umbrisols and Leptosols only occur to a much lesser extent.

Stagnosol occurrence increases with altitude (Fig. 2.4a), as was also found by Schrumpf et al. (2001) who diagnosed an increase in hydromorphic properties and designated soils as Humaquepts. Frei (1958) already emphasized the importance of moisture regime and water percolation. The coverage of Stagnosols decreased with increasing slope angle as water storage gets less frequent (Fig. 2.4b).

The abundance of Cambisols (Fig. 2.4b) increases with increasing slope angle, probably due to more frequent occurrence of landslides leading to disturbed soil profiles and shallower organic layers. Wilcke et al. (2003) and Schrumpf et al. (2001) also mainly found Cambisols on landslide affected sites. Umbrisols are only found on slope angles < 31°, where landslides are less likely and therefore dark coloured A-Horizons have enough time to develop. Another explanation might be, that they occur within the accumulation zone of former landslides.

The applied CART model identified Histosols and Stagnosols as the dominant soil types. As Histosols and Stagnosols are normally found in close association, this finding is most probably not an artefact of our method. However, the occurrence of Umbrisols is clearly overestimated by our model. This might be due to the lack of a good prediction scheme for Cambisols. Cambisols occur to a much higher percentage within our dataset than Umbrisols (Fig. 2.4). Their distribution on several end nodes with no clear prediction scheme might be the reason for Umbrisols to be considered on a relatively short branch of the classification tree (Fig. 2.5). Leptosols are found close to the creeks. They seem to be overestimated by the model according to the soil dataset displayed in Figure 2.4. In this context, it has to be taken into account, that sampling was performed on transects, which only sampled sites close to the creeks with a few auger points, whereas slopes were sampled with a much higher number. Since we always found Leptosols close to the creeks, we used this expert knowledge to give Leptosols their respective importance within the model. We also classified Leptosols on very steep slopes, but since we also classified other soil types in similar positions, this information cannot be generalised and therefore did not enter into the model development.

The classification tree model developed with rpart represents the area to some

extent. As is especially shown by the lack of Cambisols in predicting the soil type distribution within the investigation area, some dependencies of the soils have not been assessed. An important variable in Cambisols prediction might have been overseen. Another possible explanation is the already mentioned possible dependence of Cambisol occurrence on sites influenced by landslides.

It is of course always difficult to relate a rather abstract variable such as soil type, which is based on a complex systematisation system, directly to the landscape. More complex modelling approaches including probability models for soil type occurrence are currently in progress to represent the area to a much better extent. Soil-landscape models based on different soil parameters can be combined to create a soil type distribution map by combining these various models. Model performance can be further improved by excluding model impurity via an approach to predict soil probability. Other regression approaches such as artificial neural networks and random forest will be considered in the future.

2.5   Acknowledgements

2.6   References

Amundson, R. (2004): Soil formation. In: Holland, H. D. and Turekian, K. K. (eds.): Treatise on geochemistry. Amsterdam, 1–35.

Barthold, F. K.; Stallard, R. F. and Elsenbeer, H. (2008): Soil nutrient-landscape relationships in a lowland tropical rainforest in Panama. In: Forest Ecology and Management 255, 1135–1148. Doi:10.1016/j.foreco.2007.09.089

Bauer, J.; Rohdenburg, H. and Bork, H.-R. (1985): Ein Digitales Reliefmodell als Voraussetzung für ein deterministisches Modell der Wasser- und Stoff-Flüsse. In: Landschaftsgenese und Landschaftsökologie 10, 1 – 15.

Behrens, T. (2003): Digitale Reliefanalyse als Basis von Boden-Landschafts-Modellen – Am Beispiel der Modellierung periglazialer Lagen im Ostharz. Boden und Landschaft 42. Gießen.

Bishop, T. F. A. and Minasny, B. (2006): Digital soil-terrain modeling: the predictive potential and uncertainty. In: Grunwald, S. (ed.): Environmental soil-landscape modeling – geographic information technologies and pedometrics. Boca Raton.

Breimann, L.; Friedmann, J. H.; Olshen, R. A. and Stone, C. J. (1984): Classification and regression trees. Wadsworth.

Bui, E. N.; Loughead, A. and Corner, R. (1999): Extracting soil-landscape rules from previous soil surveys. In: Australian Journal of Soil Research 37, 495–508. Doi:10.1071/S98047

Cialella, A. T.; Dubayah, R.; Lawrence, W. and Levine, E. (1997): Predicting soil drainage class using remotely sensed and digital elevation data. In: Photogrammetric Engineering & Remote Sensing 63 (2), 171–178.

Cimmery, V. (2007): User guide for SAGA (version 2.0), http://sourceforge.net/projects/saga-gis/files/ (25.11.2009)

de Bruin, S. and Stein, A. (1998): Soil-landscape modelling using fuzzy *c*-means clustering of attribute data derived from a Digital Elevation Model (DEM). In: Geoderma 83, 17–33. Doi:10.1016/S0016-7061(97)00143-2

Dercon, G.; Deckers, J.; Govers, G.; Poesen, J.; Sánchez, H.; Vanegas, R.; Ramírez, M. and Loaiza, G. (2003): Spatial variability in soil properties on slow-forming terraces in the Andes region of Ecuador. In: Soil & Tillage Research 72, 31–41. Doi:10.1016/S0167- 1987(03)00049-7

FAO, IUSS WORKING GROUP WRB (2007): World Reference Base for Soil Resources 2006, first update 2007. World Soil Resources Reports 103.

Frei, E. (1958): Eine Studie über den Zusammenhang zwischen Bodentyp, Klima und Vegetation in Ecuador. In: Plant and Soil 9, 215–236. Doi:10.1007/BF01394152

Fries, A.; Rollenbeck, R.; Göttlicher, D.; Nauss, T.; Homeier, J.; Peters, T. and Bendix, J. (2009): Thermal structure of a megadiverse Andean mountain ecosystem

in southern Ecuador, and its regionalization. In: Erdkunde 63, 321–335. Doi: 103112/erdkunde.2009.04.03

Gao, J. (1993): Identification of topographic settings conducive to landsliding from DEM in Nelson County, VA, USA. In: Earth Surface Processes and Landforms 18, 579–591. Doi:10.1002/esp.3290180702

Homeier, J.; Dalitz, H. and Breckle, S.-W. (2002): Waldstruktur und Baumartendiversität im montanen Regenwald der Estacón Científica San Franscisco. In: Südecuador. Ber. d. Reinh. Tüxen-Ges. 14, 109–118.

Jenny, H. (1941): Factors of soil formation. A system of quantitative pedology. New York.

Jordan, E.; Ungerechts, L.; Cáceres, B.; Penafiel, A. and Francou, B. (2005): Estimation by photogrammetry of the glacier recession on the Cotopaxi Volcano (Ecuador) between 1956 and 1997. In: Hydrological Sciences 50, 949–961.

Lagacherie, P. and Holmes, S. (1997): Addressing geographical data errors in a classification tree soil unit prediction. In: International Journal of Geographical Information Science 11, 183–198. Doi:10.1080/136588197242455

Lea, N. L. (1992): An aspect driven kinematic routing algorithm. In: Parsons, A. J. and Abrahams, A. D. (eds.) Overland Flow Hydraulics and Erosion Mechanics. London, 393 – 407.

Litherland, M.; Aspen, J. A. and Jemielita R. A. (1994): The metamorphic belts of Ecuador. In: Overseas Mem. Br. Geol Surv 11, 1–147.

McBratney, A. B.; Mendonça Santos, M. L. and Minasny, B. (2003): On digital soil mapping. In: Geoderma 117, 3–52. Doi:10.1016/S0016-7061(03)00223-4

Möller, M.; Volk, M.; Friedrich, K. and Lymburner, L. (2008): Placing soil-genesis and transport processes into a landscape context: a multiscale terrain-analysis approach. In: Journal of Plant Nutrition and Soil Science 171, 419– 430. Doi:10.1002/jpln.200625039

Nauss, T.; Göttlicher, D.; Dobbermann, M. and Bendix, J. (2007): Central data services in multidisciplinary environmental research projects. In: e-Zeitschrift für

Agrarinformatik 2. http://www.preagro.de/ezai/index.php/eZAI/ article/view/28/28 (13.12.2009)

Odeh, I. O. A.; Chittleborough, D. J. and McBratney, A. B. (1991): Elucidation of soil-landform interrelationships by canonical ordination analysis. In: Geoderma 49, 1–32. Doi:10.1016/0016-7061(91)90089-C

Odeh, I. O. A; McBratney, A. B. and Chittleborough, D. J. (1994): Spatial prediction of soil properties from landform attributes derived from a digital elevation model. In: Geoderma 63, 197-214. Doi:10.1016/0016-7061(94)90063-9

Park, S. J. and Vlek, L. G. (2002): Prediction of three-dimensional soil spatial variability: a comparison of three environmental correlation techniques. In: Geoderma 109, 117–140. Doi:10.1016/S0016-7061(02)00146-5

Park, S. J.; McSweetney, K. and Lowery, B. (2001): Identification of spatial distribution of soils using a process-based terrain characterization. In: Geoderma 103, 249– 272. Doi:10.1016/S0016-7061(01)00042-8

Pennock, D. J.; Zebarth, B. J. and De Jong, E. (1987): Landform classification and soil distribution in hummocky terrain, Saskatchewan, Canada. In: Geoderma 40, 297–315. Doi:10.1016/0016-7061(87)90040-1

Rollenbeck, R. (2006): Variability of precipitation in the Reserva Biólogica San Francisco / Southern Ecuador. In: Lyonia, A Journal of Ecology and Application 9 (1), 43 – 51.

Romano, N. and Palladino, M. (2002): Prediction of soil water retention using soil physical data and terrain attributes. In: Journal of Hydrology 265, 56–75. Doi:10.1016/ S0022-1694(02)00094-X

Schrumpf, M.; Guggenberger, G.; Valarezo, C. and Zech, W. (2001): Tropical montane rainforest soils. Development and nutrient status along an altitudinal gradient in the South Ecuadorian Andes. In: Die Erde 132, 43–59.

Selle, B.; Morgen, R. and Huwe, B.: (2006): Regionalising the available water capacity from readily available data. In: Geoderma 132, 391–405. Doi:10.1016/j.geoderma.2005.05.015

Stoyan, R. (2000): Aktivität, Ursachen und Klassifikation der Rutschungen in San Francisco/Südecuador. Diploma thesis. Erlangen.

Strahler, A. N. (1957): Quantitative analysis of watershed geomorphology. In: Transactions of the American Geophysical Union 38 (6), 913–920.

Troeh, F. R. (1964): Landform parameters correlated to soil drainage. In: Soil Science Society of America Journal 28, 808–812.

Walker, P. H.; Hall, G. F. and Protz, R. (1968): Relation between landform parameters and soil properties. In: Soil Science Society of America Journal 32, 101–104.

Wilcke, W.; Valladarez, H.; Stoyan, R.; Yasin, S.; Valarez, C. and Zech, W. (2003): Soil properties on a chronosequence of landslides in montane rainforest, Ecuador. In: Catena 53, 79–95. Doi:10.1016/S0341- 8162(02)00196-0

Zhou, C. H.; Lee, C. F.; Li, J. and Xu, Z. W. (2002): On the spatial relationship between landslides and causative factors on Lantau Island, Hong Kong. In: Geomorphology 43, 197–207. Doi:10.1016/S0169-555X(01)00130-1

Chapter 3

Reference Soil Group Probability Prediction

MAREIKE LIEß [a], BRUNO GLASER [b], BERND HUWE [a]

a University of Bayreuth, Department of Geosciences, Soil Physics Group
  Universitätsstrasse 30, 95447 Bayreuth, Germany

b Martin-Luther University Halle-Wittenberg, Soil Biogeochemistry, von-Seckendorff-
  Platz 3, 06120 Halle, Germany

Correspondence: Mareike Ließ, E-mail: mareike.liess@uni-bayreuth.de

Summary

Digital soil maps of the distribution of typical Reference Soil Groups (RSGs) (FAO, IUSS Working Group WRB, 2007) in the southern Ecuadorian Andes were developed via classification tree (CT) models. Their spatial prediction was based on various relief and hydrological parameters calculated from a digital elevation model. Prediction uncertainty was included via occurrence probability of the soil units. Thereby, each RSG was predicted independently from the others by a CT. Finally, the RSG probability was adapted according to a calculation scheme based on World Reference Base for Soil Resources (WRB) (FAO, IUSS Working Group WRB, 2007) hierarchy. Probabilities can be interpreted as competing RSGs in similar landscape positions, but may also account for soils that could be assigned to various RSGs simultaneously according to their probabilities.

Histosols and Stagnosols displayed a specific occurrence probability throughout the whole area, whereas Leptosols occur only in limited landscape positions. Model development to predict the occurrence probability of Umbrisols, Cambisols and Regosols was impossible. Histosols accounted for a probability of 0.2 – 0.4 depending on hydrological parameters. Sites with soils having sufficient stagnic properties to qualify as Stagnosols accounted for 0.25 – 0.64 with sites on slopes < 40° and altitudes > 2146 m a.s.l. revealing the highest Stagnosol probability.

Terrain attributes could only explain RSG distribution to some extent within this mountainous tropical landscape influenced by landslides. The size of the used dataset was probably not large enough to represent the investigated soil-landscape with high precision. What typically makes WRB RSG prediction problematic, is the complex character of the RSG entities.

Keywords: classification tree, Reference Soil Group, spatial prediction

3.1   Introduction

Soil research within the area of the scientific research station San Francisco in the southern Ecuadorian Andes has been carried out for many years, but until now no detailed soil map exists apart from Liess et al. (2009). Their soil map, based on Reference Soil Groups (RSGs) from the World Reference Base for Soil Resources

(WRB) (FAO, IUSS Working Group WRB, 2007), was a first trial. It says nothing about prediction uncertainty and excludes Cambisols. However, Cambisols are part of their dataset and have also been described by Yasin (2001) and Wilcke et al. (2002/ 2003). Other soils that occur under natural vegetation within the research area are Histosols, Stagnosols, Umbrisols and Regosols (FAO, IUSS Working Group WRB, 2007). Histosols were described by Yasin (2001) and Schrumpf et al. (2001) as Haplosaprists according to Soil Taxonomy classification (Soil Survey Staff, 2006). Yasin (2001) investigated forest soils only between 1900 – 2240 m a.s.l., whereas Schrumpf et al. (2001) explored soils along an altitudinal gradient from 1850 – 3050 m a.s.l. Thus, Histosols were found on slope angles varying from 10 – 50° at 1850 – 2700 m a.s.l.; Stagnosols were described between 2080 – 2850 m a.s.l. (Yasin, 2001; Schrumpf et al., 2001; Liess et al., 2009). Umbrisols were assigned by Schrumpf et al. (2001) and Liess et al. (2009).

By extending the dataset of Liess et al. (2009) and constructing various CTs, we expect to develop a more precise RSG map and include prediction uncertainty by displaying the RSG probability. The investigated soils will be related to terrain parameters by a classification tree (CT) (Breimann et al., 1984) that organises the dataset according to the respective RSG. The tree model can then be used to assign the RSG probabilities to the whole area covered by a digital elevation model (DEM).

Prediction of soil types from terrain factors by statistical models, is based on Jenny's concept of soil formation (Jenny, 1941). It is a standard approach within the field of soil-landscape modelling. Lagacherie and Holmes (1997) as well as Moran and Bui (2002) assigned soil classes by CTs based on parameters calculated from a DEM. Skidmore et al. (1996), Thomas et al. (1999) and Dobos et al. (2000) spatially predicted soil types from terrain analysis. Furthermore, Gessler et al. (1995), Moore et al. (1993) and Odeh et al. (1994) predicted soil attributes from the terrain parameters. Bourennane et al. (2000) and Hengl et al. (2004) regionalised soil horizon and topsoil thickness from a DEM.

3.2 Material and methods

3.2.1 Research area

The research area is situated between the provincial capitals Loja and Zamora (Figure 3.1) in the southern Ecuadorian Andes from 1670 to 3160 m a.s.l. It extends

in UTM-Zone 17M from west to east between 710500 and 716000, and from north to south between 9561500 and 9557000 (Figure 3.1). The San Francisco River divides the area into two parts: The north-west facing slopes south of the river are covered by montane rainforest and subpáramo vegetation above the tree line. Within this area, Homeier et al. (2002) differentiated different forest types according to their altitude and position on the ridge or in the valley. The south-eastern facing slopes north of the river are mainly covered by pastures and succession vegetation after fire clearance when sites are left unused. For soil model development, we only regarded sites under natural vegetation.
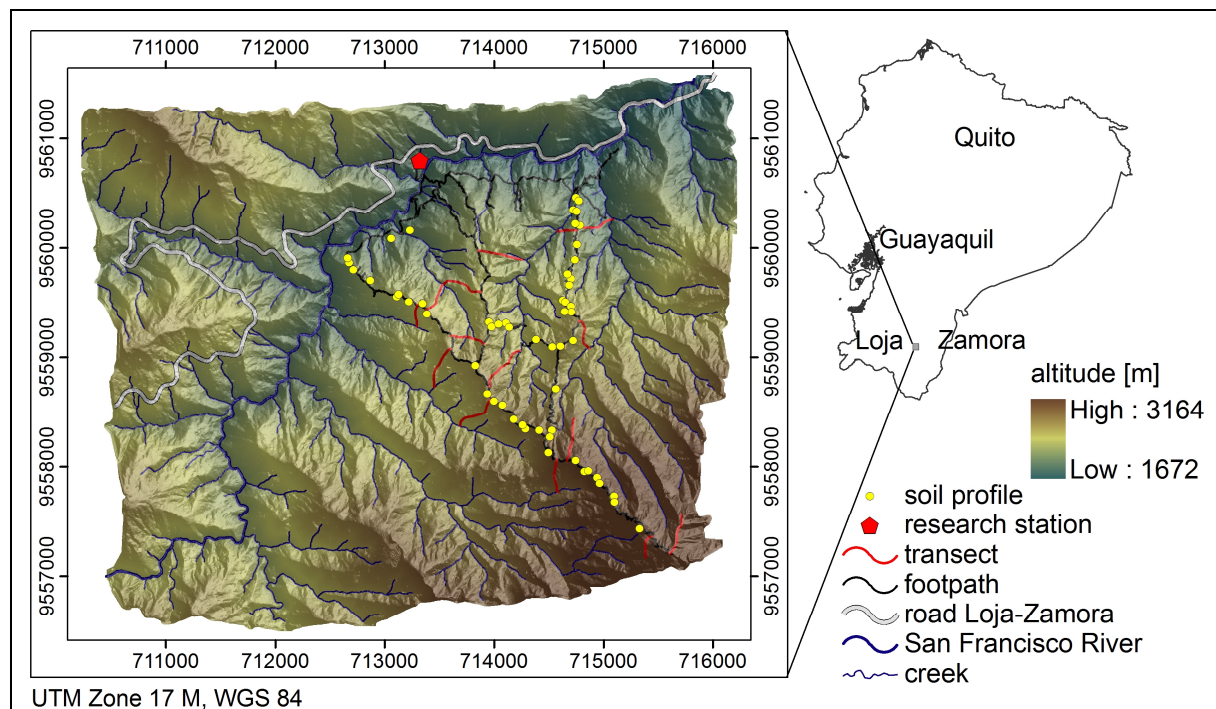
Figure 3.1: Research area. Overlaid hillshading with light source from north-east (adapted from Liess et al. 2009).

As part of the Chiguinda unit, the research area is lithologically covered by metasiltstones, siltstones and quartzites which are intermixed with layers of phyllite and clay schists (Litherland et al., 1994). Furthermore, it is influenced by the regular occurrence of landslides. Average total annual rainfall increases from 2050 mm at an altitude of 1960 m a.s.l. to approximately 4400 mm at 3100 m a.s.l. (Rollenbeck, 2006). Average air temperature decreases with increasing altitude from 19.4 to 9.4 °C (Fries et al., 2009).

3.2.2 Classification trees

We used classification trees (CTs), a method first described by Breimann et al. (1984), to relate the RSGs to terrain parameters. It was conducted with the rpart library of the R-Project for Statistical Computing (Therneau and Atkinson, 2003).

In CTs subdivision is based on a categorical response variable, i. e. RSG. The final subsets, also called end nodes, should be as pure as possible. This is done by trying to assign them to only one category in the response variable, e.g. to Histosol. The Gini criterion (Equation 1) is applied as a measure of purity (Breiman et al., 1984). It serves as a decision criterion, to determine which terrain parameter best separates the dataset continuously into always two subsets to create the purest end nodes.

$$gini(t) = 1 - \sum_{i=1}^{k} P_i^2 \qquad (1)$$

The Gini-Index reaches its maximum in a particular node t if all categories k within this node are equally represented. On the other hand, when the probability P_i is equal to zero for all but one category within any node, the Gini-Index reaches its minimal value. The categorical value accounting for the majority within each end node is then assigned to the corresponding parameter values, indicating the typical position within the landscape (e.g. Liess et al., 2009). However, another option is to assign the percentage of each categorical value within an end node as occurrence probability to the corresponding landscape position.

The CT is pruned to avoid overfitting and obviate random variation. To assess model performance, the cross validation error (CV) is calculated. The dataset is subdivided into 10 subsets, and the process is repeated 10 times with 9 parts for model training and the 10th part as the evaluation dataset. Eventually, among all trees considered for the final model, the tree with the lowest cross validated error rate is chosen. CV and model pseudo R² are calculated. Pseudo stability indices are constructed to satisfy the different interpretations, e.g. explained variance or square of correlation. They are similar to R² in that they also range between 0 and 1 and a higher value represents a better adaptation to the data.

3.2.3 Dataset and GIS methodology to gain terrain data

Topographic data for the research area is available on a continuous landscape level. The DEM used to obtain terrain parameters for the establishment of a prediction

model of RSG occurrence has 2 m cell size (Liess et al., 2009). For model application, this accuracy was reduced to 10 m to decrease calculation time. The terrain parameters used included altitude a.s.l., aspect, slope angle, terrain curvature, upslope contributing catchment area and overland flow distance to the channel network (OFD).

Slope angle, aspect and curvature were calculated with a 2nd degree polynomial fit from Zevenbergen and Thorne (Zevenbergen and Thorne, 1987; Cimmery, 2007). The contributing area was calculated with two methods; (1) based on the Kinematic Routing Algorithm (KRA CA) (Lea, 1992) and (2) based on the Braunschweiger Digital Relief Model (BS CA) (Bauer et al., 1985). We did not only use the OFD, but also calculated the horizontal (HOFD) and vertical (VOFD) overland flow distances. The channel network itself was calculated applying the Strahler stream order 6 as initiation threshold (Strahler, 1957). Terrain curvature was calculated using directly adjacent cells. Finally, the terrain parameters were calculated and the RSGs were predicted for each individual raster grid cell. The free and open source GIS software, SAGA, was used (Böhner et al., 2006).

The research area was sampled at 367 sites, including 311 auger points and 56 soil profiles. Soil sampling covered 24 sampling classes and produced by an overlay of four altitudinal, three slope angle and two aspect classes (Liess et al., 2009). Transects for auger sampling (Figure 3.1) were laid according to the catena concept (Milne, 1935) from hilltop to valley bottom.

Two methods were used to assign terrain parameters to the soil dataset. On the one hand, the nearest neighbour (n. n.) value was allocated to each soil profile or auger point. On the other hand, a buffer representing the radius of GPS accuracy was placed around the sampled location, and the calculated mean value of the corresponding area was assigned. This assignment was completed for each of the described parameters apart from the slope angle and aspect. These were directly measured in the field. Slope angle and aspect as calculated from the DEM were solely used for model application.

3.2.4 Probability calculation

The probability of each RSG was predicted via a CT which grouped the soil sampling points regarding the existence or absence of that RSG. Thus, the percentage of sampling points assigned to the corresponding RSG in each end node of the tree

was used to predict the probability of that RSG. Thereby, the diagnostic properties necessary for assigning the particular RSG were used, whereas the necessary absence of other properties was neglected. This was done in particular to establish a good prediction scheme for Stagnosols. We decided that the occurrence and thickness of a sufficient stagnic colour pattern and/ or albic horizon is more important than the limitation in organic layer thickness. As a consequence, soils with a 40 cm organic layer displaying also a thick stagnic horizon were classified as Histosols and Stagnosols. Any other proceeding would have made the development of a Stagnosol prediction scheme incomplete and complex.

To sum the individual probabilities and standardize them by relating each RSG to the total probability sum, is one option. This option neglects WRB (FAO, IUSS Working Group WRB, 2007) hierarchy, because all RSGs are competing on an equal level and no soil process is given dominance over another. As a consequence, the probabilities refer to the probability of the diagnostic property necessary for RSG assignation. Later we will refer to these as WRB independent probabilities.

Figure 3.2 shows the probability calculation scheme based on WRB (FAO, IUSS Working Group WRB, 2007) hierarchy.

$$1-P_H = P_{L(max)}$$
$$P_{L(max)} - P_L = P_{S(max)}$$
$$P_{S(max)} - P_S = P_{U(max)}$$
$$P_{U(max)} - P_U = P_{C(max)}$$
$$P_{C(max)} - P_C = P_R$$
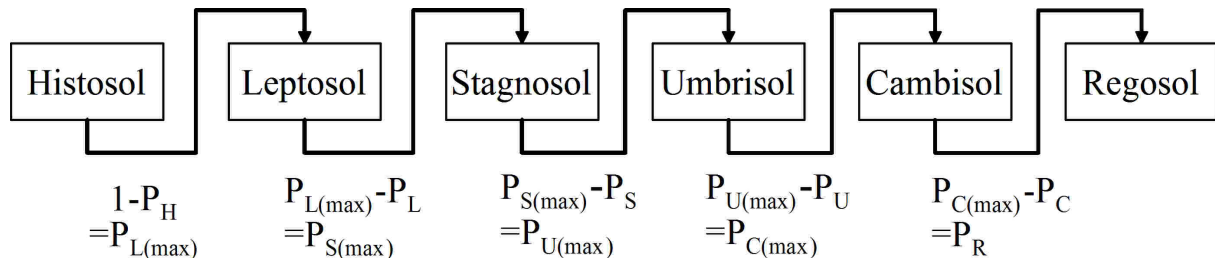
Figure 3.2: Hierarchical calculation scheme for the maximum possible probability of each RSG according to WRB hierarchy. P_X is the actual probability of the respective RSG: H Histosol, L Leptosol, S Stagnosol, U Umbrisol, C Cambisol, R Regosol. $P_{X(max)}$ is the maximum possible probability of RSG.

It is used to calculate the maximal possible probability for each RSG from the probability predicted by the CTs. Maximal Leptosol probability is left after subtracting Histosol probability from 1. Maximal Stagnosol probability is left after also subtracting the actual Leptosol probability and so on. Equation 2 shows the calculation of the actual probability, P_X, according to the CT probability, $P_{X(tree)}$, and the maximal possible probability, $P_{X(max)}$.

$$P_{x(max)} \cdot P_{x(tree)} = P_x \qquad\qquad (2)$$

3.3 Results and discussion

3.3.1 Classification tree models and digital soil maps

Figure 3.3 presents the CT models to predict Histosol, Leptosol and Stagnosol occurrence probability from nearest neighbour (n. n.) and mean terrain values.
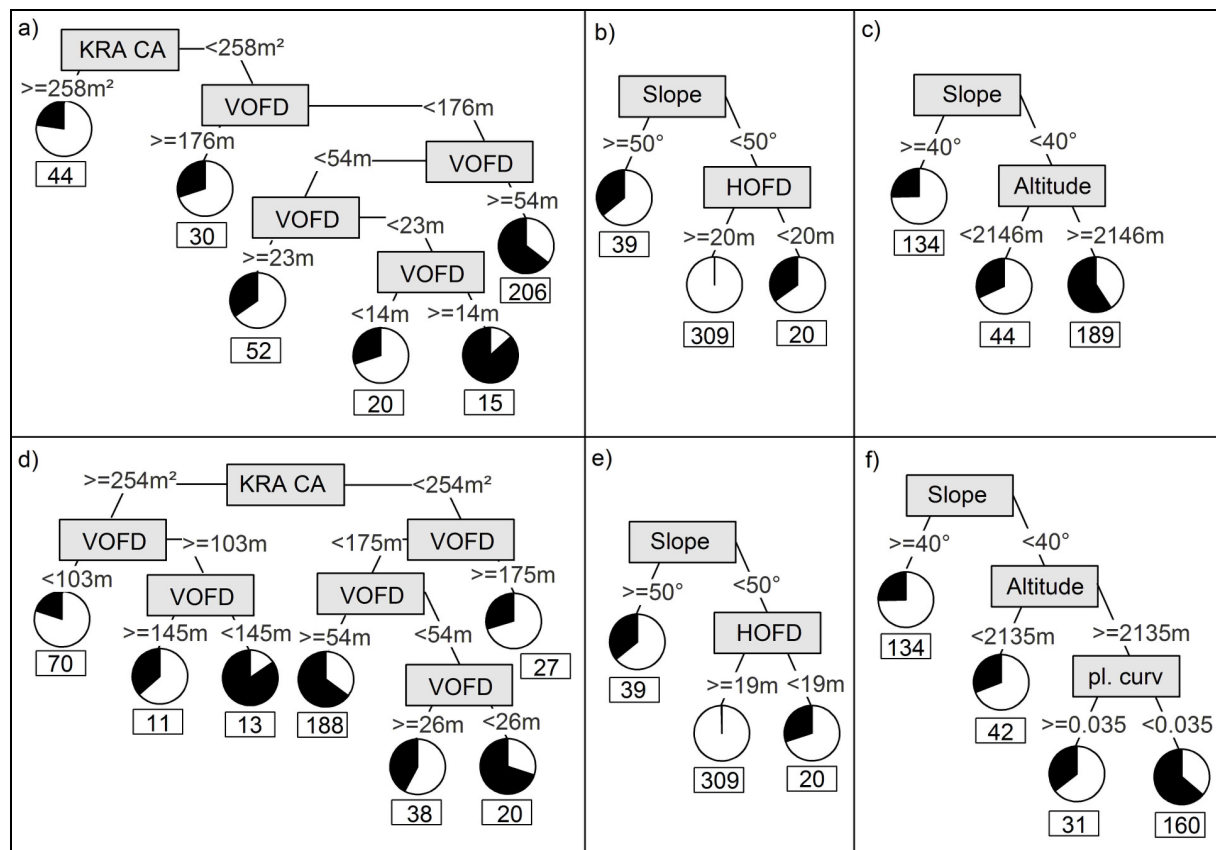
Figure 3.3: Classification trees predicting RSG probability. The pie charts' black parts represent the occurrence probability in the corresponding landscape positions. The numbers in the boxes underneath the charts refer to the number of sampling sites used for the probability prediction in each end node. Prediction by n. n. terrain values: a) Histosol probability, b) Leptosol probability and c) Stagnosol probability. Prediction by mean terrain values: d) Histosol probability, e) Leptosol probability and f) Stagnosol probability. (KRA CA = upslope contributing catchment area according to the Kinematic Routing Algorithm, VOFD = vertical overland flow distance, HOFD = horizontal overland flow distance, pl. curv = plan curvature).

The RSG Histosol is assigned to soils with an organic layer ≥ 40 cm (FAO, IUSS Working Group WRB, 2007). Its probability within the research area was found to depend on two hydrological parameters (Figures 3.3a and 3.3d): KRA CA and VOFD. Probability is predicted with at least 0.2 (Figure 3.3a, d) throughout the research area. The highest probability (0.87) as predicted by n. n. relief values (Figure 3.3a) was obtained for small catchments (KRA CA < 258 m²) within a distance of 14 – 23 m from the channel network. Though, probabilities are also high, 0.65, for small

catchments (KRA CA < 258 m²) within a VOFD of 54 – 176 m. The latter is a more conservative prediction, since it is based on 206 sampled sites and not only 15 as for the first differentiation criteria (Figure 3.3a). Sites seem to coincide in some parts with upper slope areas and ridges (Figure 3.4a).

Prediction by mean terrain values (Figure 3.3d) again shows high probabilities in similar landscape positions, i.e. for small catchments < 254 m² from 54 – 175 m VOFD (0.65) and < 26 m VOFD (0.70). The former is the safest prediction similar to the Histosol prediction from n. n. terrain values (188 sampled sites). Areas likely to be covered by Histosols with this 0.65 probability are again found along ridges. In contrast to the CT from n. n. terrain values, the highest probabilities, 0.85, by mean relief values (Figure 3.3d) are assigned to large catchments (≥ 254 m²) with a VOFD from 103 – 145 m, dominating in dark colours as broad belts at 103 m distance around the creeks (Figure 3.4b). This also accounts for the major difference between the two models (Figure 3.4c). But since the corresponding end node in the tree model (Figure 3.3d) is only supported by 13 sampled sites, this finding is not representative for the research area.
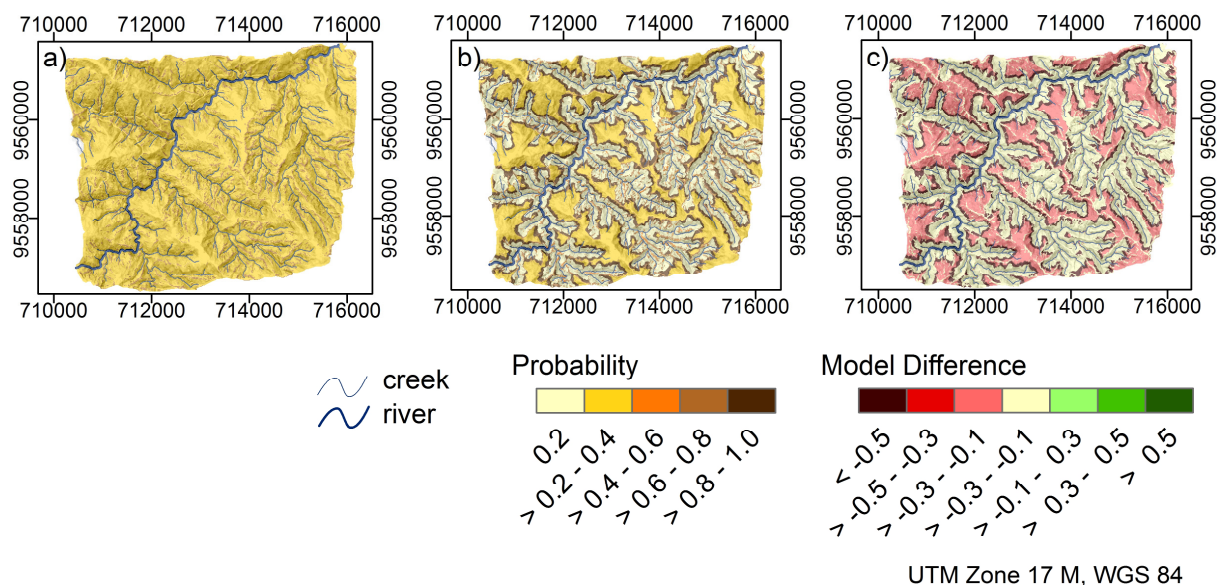
Figure 3.4: Maps of Histosol occurrence probability (Overlaid hillshading with light source from north-east): a) Prediction by n. n. terrain values, b) prediction by mean terrain values and c) model difference.

The lighter colours in Figure 3.4b compared to Figure 3.4a are due to the fact that a probability of 0.20 (< 103 m VOFD, Figure 3.3d) falls into a smaller mapping class than 0.23 (Figure 3.3a) in the map layout. The similarity between the two models for the mentioned sites is indicated by yellow colours in Figure 3.4c. The sites mapped in red colours refer to a 0.1 – 0.3 higher probability as predicted by mean relief values.

Comparison of the two tree models (Figures 3.3a and 3.3d) shows that differences are not higher than 0.13. The models differ only by a probability of 0.03 – 0.13, neglecting the mentioned 13 sites.

Leptosols refer to soils limited to 25 cm depth by continuous rock (FAO, IUSS Working Group WRB, 2007). During soil sampling we rarely attained continuous rock, and refusal typically occured at the C horizon. This made the establishment of a model predicting soil depth to continuous rock impossible. Therefore, to calculate Leptosol occurrence probability we had to apply expert knowledge in addition to the CT methodology. We knew from field work and data review that Leptosols are found on steep slopes >= 50° and close to the creeks at approximately < 20 m HOFD. But since other soils occurred at the same landscape positions and even with a much higher probability, we excluded those for model development. Afterwards, we included them again to calculate the probabilities of the tree end nodes. This explains the rather untypical appearance of the Leptosol CTs (Figures 3.3b and 3.3e). Usually for any final subdivision into two end nodes, one of them would always display a probability > 0.5 and the other < 0.5. However, for the reason of adding more datasets after tree development this is not the case. This was necessary in order to develop a reasonable model and account for true probabilities. Leptosol CTs established with n. n. and mean terrain values are very similar. In the already mentioned positions, Leptosol probability was assumed 0.30 – 0.36 (Figure 3.3b and 3.3e).

Figures 3.5a and 3.5b show the Leptosol probability distribution within the research area after model application. With the inclusion of WRB (FAO, IUSS Working Group WRB, 2007) hierarchy, Leptosol probability also depends on Histosol probability. But since Histosol probability close to the creeks (< 103 m VOFD) is predicted with only 0.2, model from mean relief values (Figure 3.3d), and 0.3, model from n. n. relief values (Figure 3.3a), it does not influence Leptosol probability much for those sites. Model difference regarding prediction by n. n. and mean terrain values (Figure 3.5c) is always ≤ ± 0.1 (0.05); including WRB hierarchy (FAO, IUSS Working Group WRB, 2007), model difference (Figure 3.5f) is increasing (hardly recognisable in the map). Model difference regarding probability predicted directly by the CTs and probability being calculated based on WRB hierarchy (Figures 3.5g and 3.5h) shows a similar picture. The difference between the WRB independent and dependent prediction by n. n. values (Figure 3.5g) is ≤ ± 0.1, but higher regarding the prediction difference by

mean terrain values (Figure 3.5h).
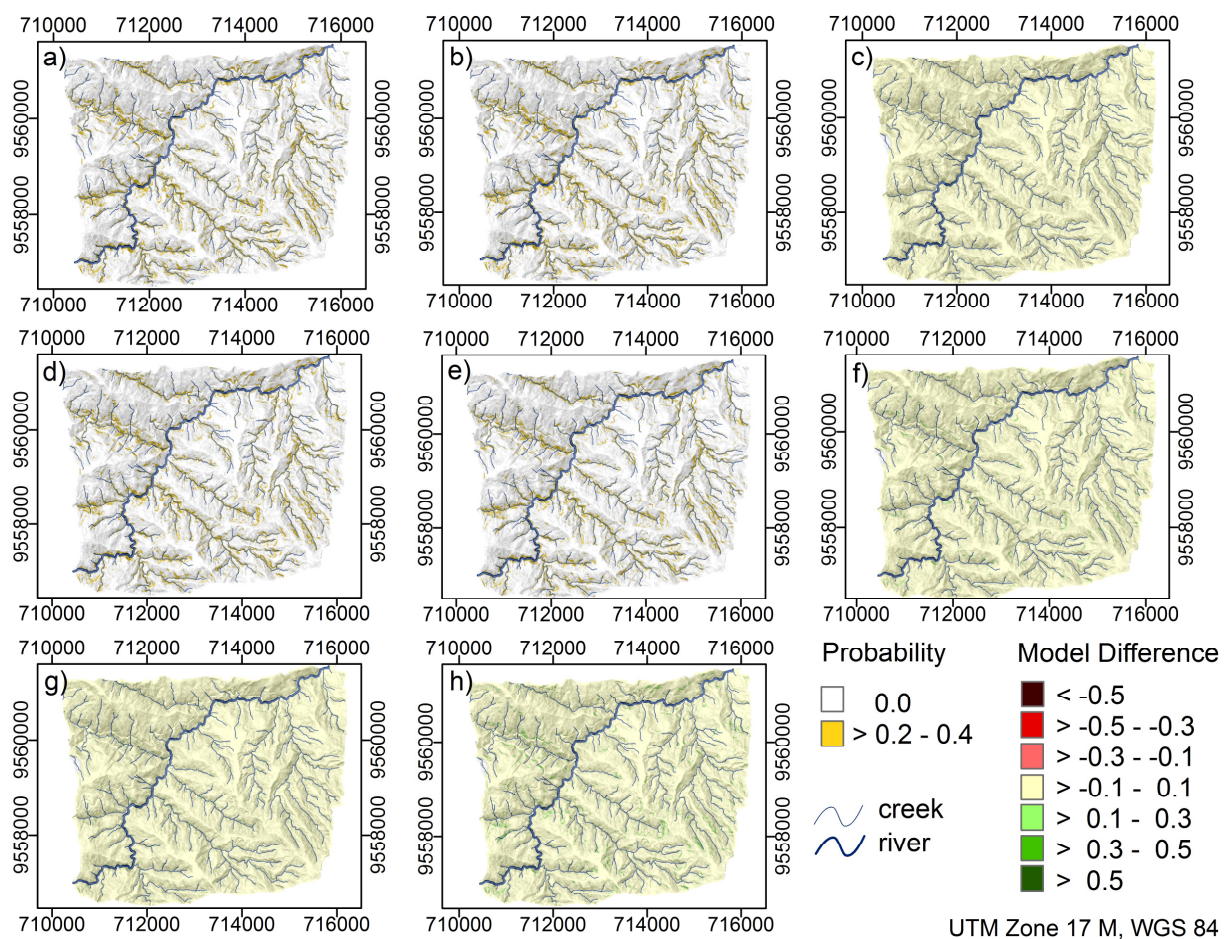
Figure 3.5: Maps of Leptosol occurrence probability (Overlaid hillshading with light source from north-east). Independent on WRB hierarchy: a) prediction by n. n. terrain values, b) prediction by mean terrain values and c) model difference. Dependent on WRB hierarchy: d) prediction by n. n. terrain values, e) prediction by mean terrain values and f) model difference. Difference between independent and WRB hierarchy dependent prediction: g) n. n. terrain values and h) mean terrain values.

Stagnosols are "soils exhibiting hydromorphic features for some time during the year in some part within 50 cm of the mineral soil surface and show a stagnic colour pattern and/ or an albic horizon in half or more of the soil volume" (FAO, IUSS Working Group WRB, 2007). Planosols are classified by similar diagnostic properties, but in addition display an abrupt textural change, which we could not confirm for the soils we sampled. Stagnosol probability is predicted throughout the research area with at least 0.25 (Figures 3.3c and 3.3f). The probability in both models depends on slope angle and altitude. It is higher on slopes < 40°. Above 2146 m a.s.l. for the prediction by n. n. and above 2135 m a.s.l. by mean terrain values, the probability increases even further. While curvature is of no importance for Stagnosol probability prediction by n. n. relief values, mean terrain values assign an even higher probability for concave plan curvature with 0.64. Landscape positions < 2146 m a.s.l. for

prediction by n. n. and < 2135 m a.s.l. by mean terrain values, and high slope angles account for the lowest probability of Stagnosols.

Model application to the research area is shown in Figure 3.6. Stagnosols reach higher probabilities by the mean terrain values model (Figure 3.6b) compared to the prediction from n. n. terrain values (Figure 3.6a). Figures 3.3c and 3.3f show that the difference between the probability prediction by n. n. and mean relief values (Figure 3.6c), + 0.1 – 0.3, is not due to this higher Stagnosol probability on high altitudes as predicted by mean terrain values on concave sites. This difference accounts for only 0.05. However, it is due to the reduced probability assigned to convex sites ≥ 2135 m a.s.l. (0.24 difference).
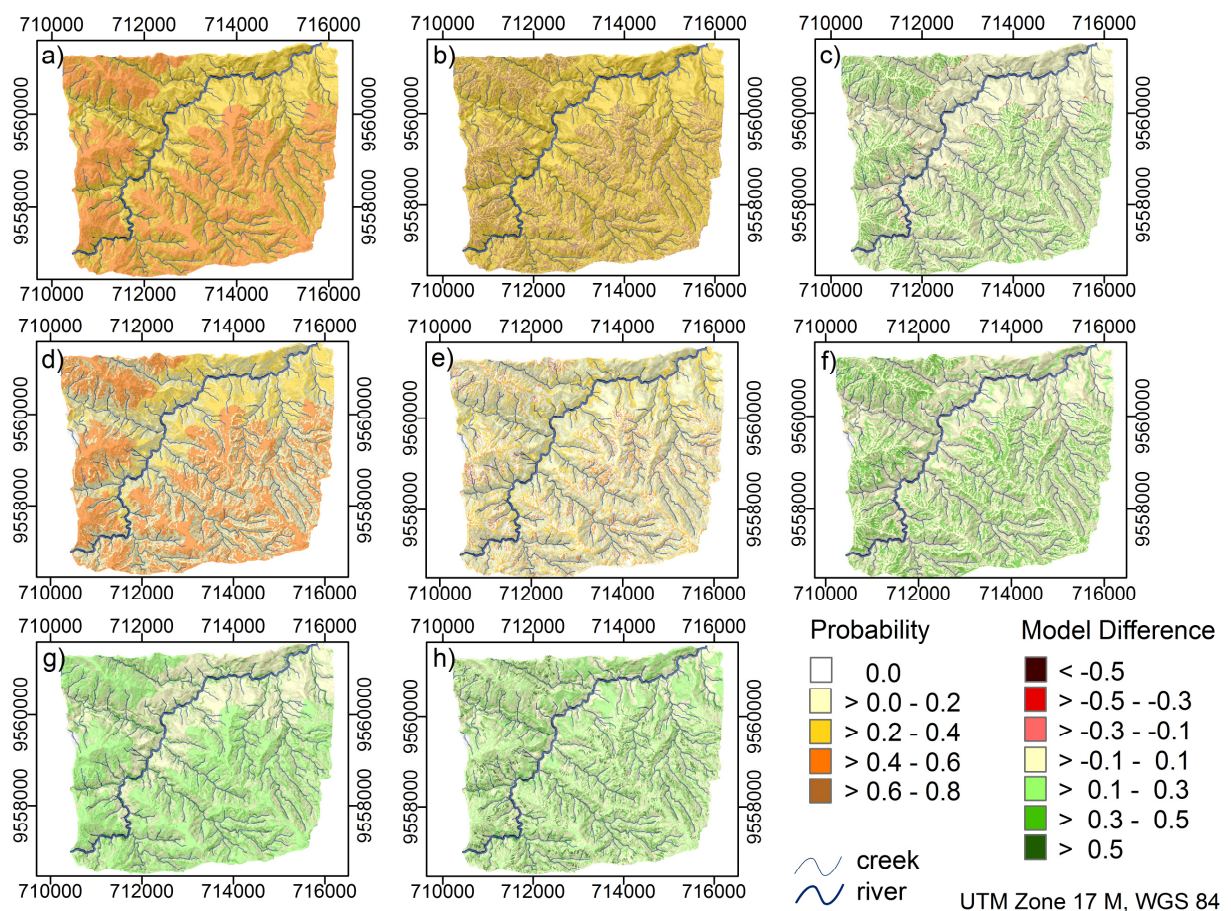
Figure 3.6: Maps of Stagnosol occurrence probability (Overlaid hillshading with light source from north-east). Independent on WRB hierarchy: a) prediction by n. n. terrain values, b) prediction by mean terrain values and c) model difference. Dependent on WRB hierarchy: d) prediction by n. n. terrain values, e) prediction by mean terrain values and f) model difference. Difference between independent and WRB hierarchy dependent prediction: g) n. n. terrain values and h) mean terrain values.

As a conclusion to this, the two models are quite similar, mainly differing by the dependence on curvature, which is not included in the model from n. n. relief values. Including WRB (FAO, IUSS Working Group WRB, 2007) hierarchy in the probability prediction, a site classified as Histosol or Leptosol cannot be classified as Stagnosol.

Accordingly, Histosol probability reduces Stagnosol probability to a perceptible extent (Figures 3.6d and 3.6e). Figures 3.6g and 3.6h show that these differences account for 0.1 to 0.3 for most of the research area with the prediction by n. n. terrain values (Figure 3.6g) still yielding less differences in the lower altitudes compared to the prediction by mean terrain values (Figure 3.6h). Differences between the two models are extended while including WRB hierarchy (Figure 3.6f), compared to that being independent of WRB hierarchy (Figure 3.6c).

We cannot provide any CTs for Umbrisols, Cambisols and Regosols. Umbrisol prediction was impossible, since the dataset we used contains only 7 Umbrisols among 367 sampled sites and is not enough to gain a clear prediction scheme. Furthermore, not all but some of the determined Umbrisols are situated within the accumulation zone of former landslides so that we would need an additional variable to predict their occurrence. Cambisols and Regosols, on the other hand, are rather unspecific RSGs which makes their prediction difficult. Cambisols need a cambic horizon, but apart from that they are rather determined by the absence of diagnostic criteria that would classify the soil for another RSG. Regosols are even worse, since they do not have any characteristic on their own, but refer to all soils that do not classify as another RSG.

3.3.2 Model performance and uncertainty

Overall CT model performance is limited (Table 3.1). Terrain attributes can likely only explain RSG distribution to a limited extent within this mountainous tropical landscape. Unfortunately, no information is available about parent material distribution, but we discovered rapid bedrock changes. The profound influence of landslides causes shifts in soil material and mixes it with rock material, leading to quite different soil properties. Although there has been a landslide inventory based on visible landslide scars on a time series of aerial photographs from 1962 to 1998 (Stoyan, 2000), most former landslides remain hidden under the regrown dense forest cover as we experienced during field work.

Table 3.1: Model quality of classification trees to predict Histosol and Stagnosol probability

RSG	Terrain Parameters	Model Pseudo R^2	CV Pseudo R^2
Histosol	nearest neighbour values	0.34	0.22
	mean values	0.35	0.21
Stagnosol	nearest neighbour values	0.22	0.19
	mean values	0.28	0.13

RSG = Reference Soil Group, CV = cross validation

CTs in general have certain disadvantages: (1) They are very dependent on the dataset used, i.e. some sample points more or less may lead to rather different models and (2) they predict abrupt values due to the grouping into end nodes. A continuous probability distribution of the RSGs in reality therefore is replaced by some probability classes according to Figure 3.3.

What makes WRB RSG prediction in general problematic is the character of the WRB itself. Assignment of some RSGs requires exceeding an absolute (Histosols) and for others a relative (Stagnosols) thickness value of a diagnostic horizon. If a soil has an organic layer ≥ 40 cm, it is classified as Histosol independent of its mineral properties. If the organic layer is 1 cm less, these mineral properties abruptly become important. Relating the extent of the stagnic horizon to soil depth obviously is not characteristic enough to allow for a good model relating the Stagnosol occurrence pattern to terrain parameters. This is probably the reason why we could not retrieve better models. As a consequence we do not consider the low R^2 as a problem, but as a natural phenomenon in predicting complex entities such as RSGs.

Furthermore, the calculated CT R^2 refers to a one value prediction. As was described earlier, a CT model usually assigns the category which forms the majority within each end node to the respective landscape position. It does not consider other categories assigned to that end node as classification possibility, but neglects them. Any soil map has a certain degree of uncertainty. Usually boundaries between soil units are drawn according to expert knowledge or GIS interpolations. However, the degree of uncertainty which is a logical phenomenon in any below ground investigation usually is not included within the soil map. The new generation of digital soil maps provides a new development in this area. Accordingly, our digital soil maps include this model uncertainty through assigning RSG occurrence probabilities instead of unique values. Other authors mainly used fuzzy-logic to include this uncertainty, e.g. McBratney and De Gruiter (1992), Hannemann (2010).

Another aspect to be considered, is that generally soil maps are gained on a much larger scale. Lagacherie and Holmes (1997) use a spatial resolution of 50 m, Moran and Bui (2002) use 250 m. Therefore, the small scale, 10 m resolution, in our soil maps might be another reason for the low R^2. The soils within the research area change within a few meters radius as typical for tropical soils. Accordingly, we used the highest possible resolution. This way low scale soil variability is included within the models, which would be neglected while working on a larger scale. We concluded

that the size of the dataset we applied is not enough to represent the investigated soil-landscape at this high precision.

3.3.3 Comparison with earlier soil map

A RSG probability prediction is also possible from a single CT which predicts all RSGs at once. Liess et al. (2009) established such a CT for the research area (Figure 3.7), but did not predict probabilities from it. We interpreted the percentage of the RSGs within each end node of this tree as occurrence probability for the RSGs according to the related landscape position and compared it to the findings from the various CTs of this study. The difference between RSG probability by the tree model from Liess et al. (2009) and our predictions is displayed in Figure 3.8. The first column maps the RSG probabilities according to Liess et al. (2009), the second column presents the differences between the latter and our prediction from n. n. relief values (WRB dependent), and the third column shows the differences regarding the prediction from mean relief values.

The model from Liess et al. (2009) (Figure 3.7) assigned a very high Histosol probability with 0.6 – 0.8 to about half of the research area. For some sites the predicted probability was even higher. In our new model, Histosol probability was less, 0.2 – 0.4 for most of the area (Figure 3.4b), but continuous on all sites with at least 0.2 (Figure 3.3a and 3.3d). We showed that Histosol probability is high within some landscape positions and for a VOFD from 54 – 175 m this is supported by a high number of sampled sites. In contrast to this, the end nodes in the tree model from Liess et al. (2009) mostly contain only a very limited number of sampling sites, e.g. the end nodes that predict particularly high Histosol probabilities (≥ 0.8) only contain 12 – 15 sampled sites. The node to which most sites were assigned and which is predicting Histosol probability with 0.78, refers to landscape positions in small catchments < 214 m HOFD, similar to our findings. The importance of the catchment size as first subdividing variable for model development was confirmed. For smaller catchment sizes, i.e. sites through which a smaller area discharges, Histosol occurrence is more likely.

We predicted Leptosols with low probability on steep slopes and close to the creeks (< 20/ < 19 m HOFD). The latter was confirmed by Liess et al. (2009) who predicted Leptosols < 21 m HOFD, but with a high probability of 0.71 (Figure 3.8d). 0.71 of 7 sampled sites that are contained within the respective end node no. 7 (Figure 3.7)

are 5 sampled sites. To use 5 sites to predict such a high probability is unreasonable.
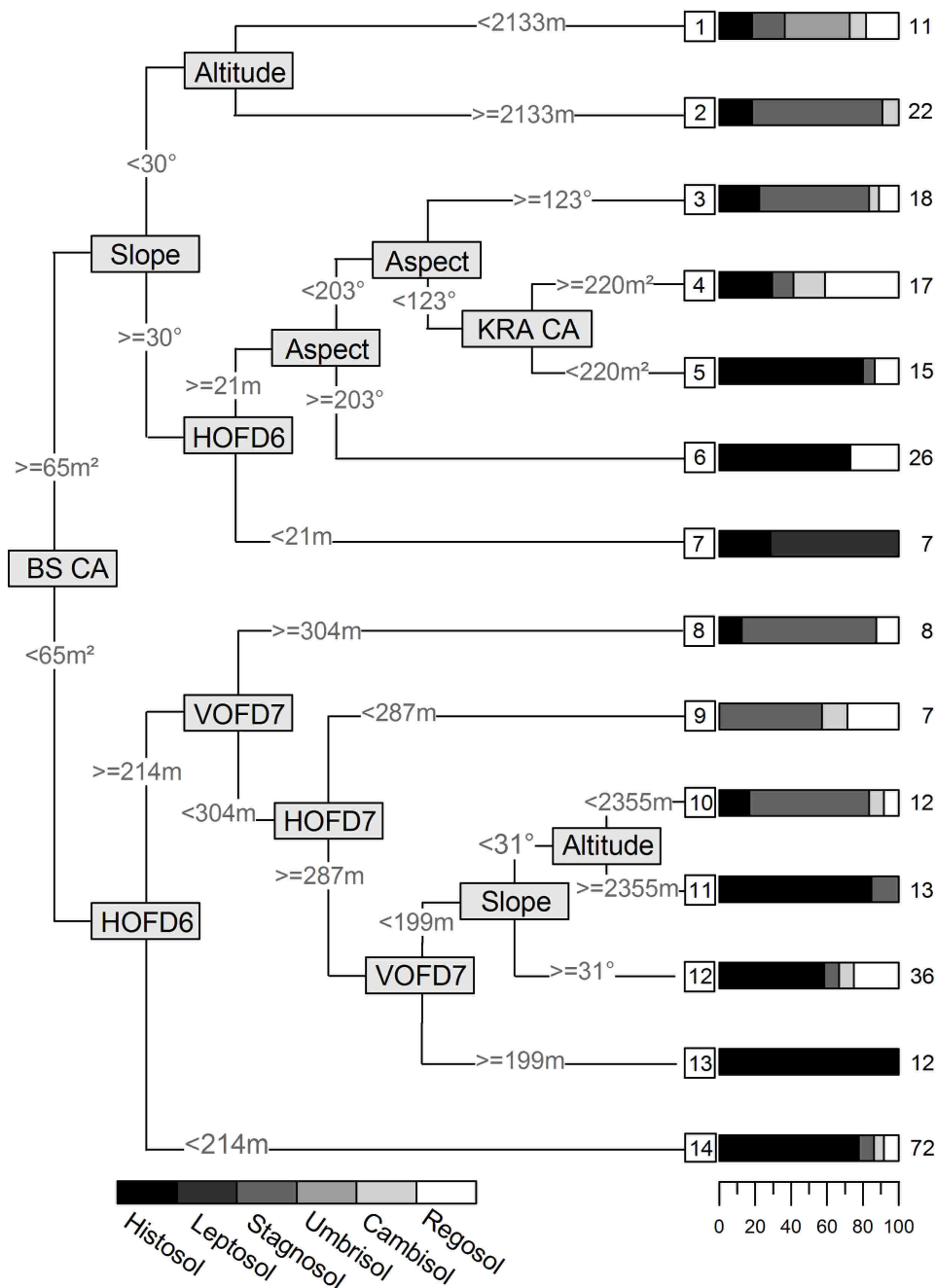
Figure 3.7: Classification tree model to predict RSG probability within the research area. Numbers before the boxplots indicate the node number, numbers behind the boxplots indicate the number of sample sites per end node. BS CA and KRA CA upslope contributing catchment area according to the Braunschweiger relief model and kinematic routing algorithm, HOFD horizontal and VOFD vertical overland flow distance, 6, 7 refer to different precision in channel network (adapted from Liess et al., 2009).

On steep slopes, especially in an area influenced by landslides, soils have less chance to develop. Hence, it is no surprise to find Leptosols in these landscape positions. Close to the creeks soil material is probably removed downslope within the channel system during times of high rainfall; through these sites a high amount of water discharges due to a high contributing catchment area. Here we discovered that

the organic layer on many sites directly overlies continuous rock.

Stagnosols were predicted with a higher probability by n. n. relief values compared to the model from Liess et al. (2009) (Figure 3.8h). This is due to the fact that we predicted Stagnosols as all soils that display sufficient stagnic properties, but neglected that some of them carry a sufficiently thick organic layer to qualify as Histosols. Stagnic properties and thick organic layers occur at the same landscape position: The WRB (FAO, IUSS Working Group WRB, 2007) describes Histosols as soils in "poorly drained basins and depressions" and "highland areas with a high precipitation–evapotranspiration ratio". Nevertheless, these two properties are seen as competing if it comes to soil classification by WRB. Two soils showing both a thick organic layer and stagnic properties are assigned to different RSGs even if they are different only by 1 cm in organic layer thickness. Prediction from mean relief values shows more similarities in Stagnosol probability to Liess et al. (2009) (Figure 3.8i) than prediction by n. n. terrain values. This is because Liess et al. (2009), who used a subset of our dataset, predicted the RSGs by mean relief values, too. Stagnosol probability increases above an altitude of 2146 m a.s.l. on slope angles < 40°. An increase in Stagnosol abundance with increasing altitude and decreasing slope angle was also described by Liess et al. (2009). Schrumpf et al. (2001) stated an increase in hydromorphic properties with increasing altitude and designated soils as Humaquepts (Soil Survey Staff, 2006). The increase with altitude can be attributed to the increasing rainfall (Rollenbeck, 2006). Lesser steep slope angles account for a slower discharge.

We assume the RSG probability predicted by various CTs, to better represent soil reality within the research area, since the dataset does not consist of all RSGs to an equal extent so that some are preferred over others during the tree subdivision process. Furthermore, the multiple CTs rather predict probabilities of soil diagnostic properties, which can occur simultaneously at one site within the soil profile. Accordingly, the model from Liess et al. (2009) overestimated Histosol probability for most sites as can be seen by the mainly green colours in Figure 3.8b and c. However, at the same time it underestimated Stagnosols in most of the area as can be deduced from the prevailing red colours in Figures 3.8h and i. In a similar way, Leptosols are overestimated by the model from Liess et al. (2009).
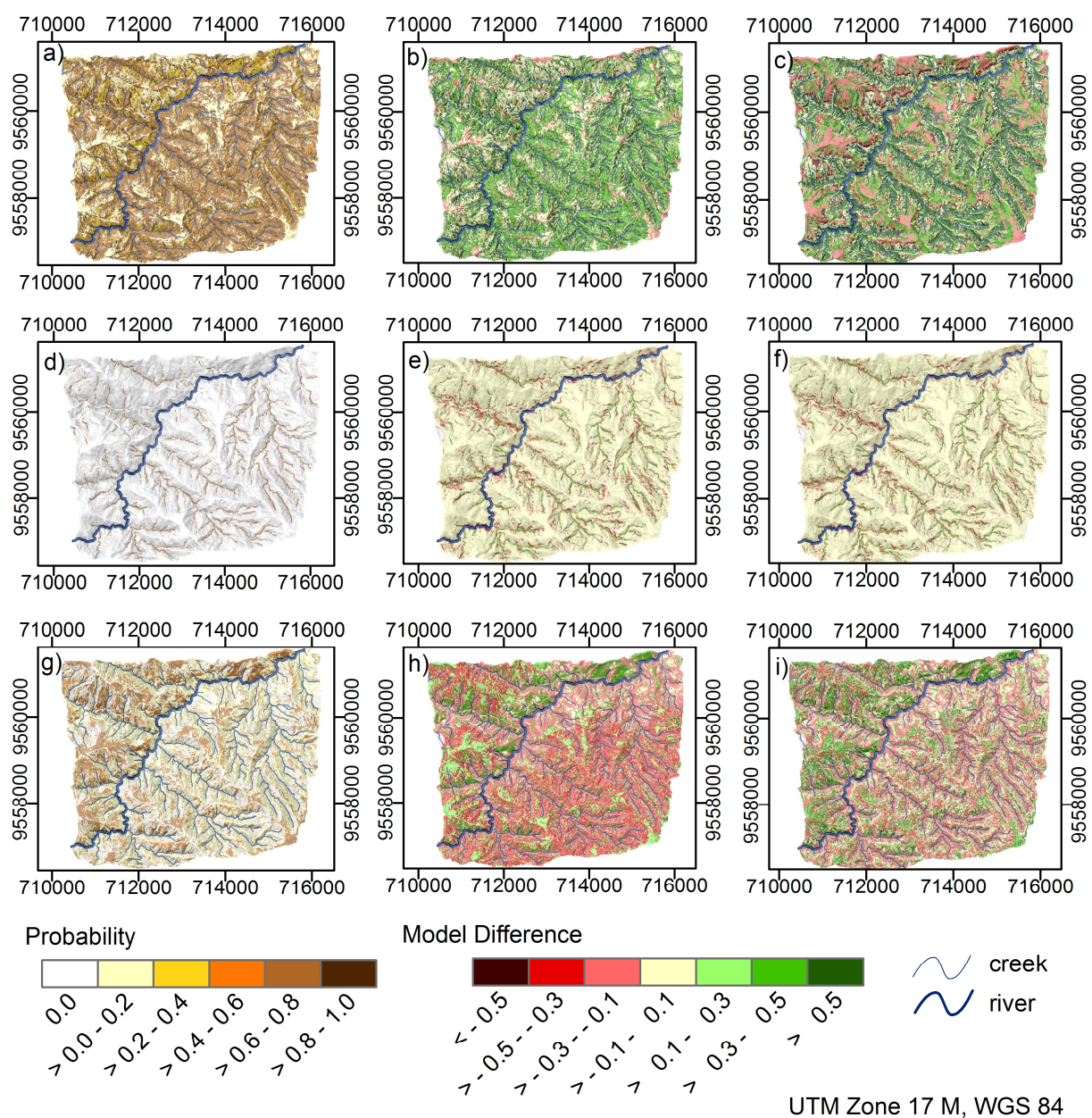
Figure 3.8: RSG probability prediction by the simple tree model from Liess et al. (2009) (column 1: a, d and g) and calculated difference in probability prediction between that model and the WRB dependent model from n. n. (column 2: b, e and h) and mean terrain values (column 3: c, f and i). Histosol (1st row), Leptosol (2nd row) and Stagnosol (3rd row). Overlaid hillshading with light source from north-east.

3.4 Conclusions

Differences between models adapted for n. n. compared to those adapted for mean terrain values showed only minor differences. We conclude that predicting all RSGs at once is not as good as predicting each RSG on its own by a CT. The dataset does not consist of all RSGs to an equal extent, so some RSGs are preferred over others during the tree subdivision process.

Model performance might be improved by choosing a lower resolution to exclude

small scale diversity, reducing model dependence on the dataset, applying a different statistical model or predicting soil properties instead of the complex RSG entities. However, further research is needed to prove these assumptions.

Model uncertainty in the digital soil maps is represented by the occurrence probabilities of the RSGs. Probabilities of various RSGs at the same landscape position can be understood as competing RSGs. But the probabilities of the various RSGs can also be interpreted as a soil composed of the various RSGs, i.e. various diagnostic horizons or various soil processes running simultaneously or successively as has been part of soil genesis theory for a long time (Simonson, 1959; Schelling, 1970). Thereby, this provides a good means to acknowledge inter-relations between the RSGs. An even better chance to acknowledge this would be the prediction of the diagnostic properties necessary for WRB classification by themselves. In accordance with McBratney and De Gruiter (1992), who thought to improve the existing soil classification systems via fuzzy sets, we would like to contribute the above-mentioned ideas to the development of a continuous soil systematisation system.

3.5   Acknowledgements

3.6   References

Bauer, J., Rohdenburg, H., Bork, H.-R., 1985. Ein digitales Reliefmodell als Vorraussetzung für ein deterministisches Modell der Wasser- und Stoff-Flüsse. In: Bork, H.- R., Rohdenburg, H. (Eds.). Landschaftsgenese und Landschaftsökologie H. 10, Parameteraufbereitung für deterministische Gebiets-Wassermodelle, Grundlagenarbeiten zur Analyse von Agrar-Ökosystemen, p. 1 – 15.

Behrens, T., 2003. Digitale Reliefanalyse als Basis von Boden-Landschafts-Modellen – Am Beispiel der Modellierung periglazialer Lagen im Ostharz. Boden und Landschaft 42. Gießen.

Böhner, J., McCloy, K. R., Strobl, J., 2006. SAGA – Analysis and Modelling Application. Göttinger Geographische Abhandlungen 115. Geographische sInstitut der Universität Göttingen.

Breimann, L., Friedmann, J. H., Olshen, R. A., Stone, C. J., 1984. Classification and regression trees, CRC press, Wadsworth.

Cimmery, V., 2007. User guide for SAGA, version 2.0), http://sourceforge.net/ projects/saga-gis/files/, 25.11.2009)

Crawley, M., 2007. The R Book. John Wiley & Sons Ltd, Chichester, England.

Dobos, E., Micheli, E., Baumgardner, M. F., Biehl, L., Helt, T., 2000. Use of combined digital elevation model and satellite radiometric data for regional soil mapping. Geoderma, 97: 367–391.

FAO, IUSS Working Group WRB, 2007. World Reference Base for Soil Resources, ISRIC, Rome.

Fries, A., Rollenbeck, R., Göttlicher, D., Nauss, T., Homeier, J., Peters, T., Bendix, J., 2009. Thermal structure of a megadiverse Andean mountain ecosystem in southern Ecuador, and its regionalization. Erdkunde, 63: 321–335.

Gessler, P., Moore, I., McKenzie, N., Ryan, P., 1995. Soil-landscape modelling and spatial prediction of soil attributes. International Journal of Geographical Information Systems, 9/ 4: 421– 432.

Hannemann, J., 2010. Die Berücksichtigung inhaltlicher und räumlicher Unschärfe bei der GIS-gestützten Erstellung von Bodenkarten. Dissertation Universität Bayreuth, Geowissenschaft. Shaker Verlag, Aachen 2010.

Hengl, T., Heuvelink, G.B.M., Stein, A., 2004. A generic framework for spatial prediction of soil variables based on regression-kriging. Geoderma, 120: 75–93.

Homeier, J., Dalitz, H., Breckle, S.-W., 2002. Waldstruktur und Baumartendiversität im montanen Regenwald der Estacón Cientíca San Franscisco. Südecuador. Ber. d. Reinh. Tüxen-Ges 14: 109–118.

Jenny, H., 1941. Factors of soil formation. A system of quantitative pedology, McGraw-Hill, New York.

Lagacherie, P., Holmes, S., 1997. Addressing geographical data errors in a classification tree soil unit predicton. International Journal of Geographic Information Science, 11: 183–198.

Lea, N. L., 1992. An aspect driven kinematic routing algorithm. In: Parsons, A. J. and Abrahams, A. D. (eds.) Overland Flow Hydraulics and Erosion Mechanics. London, 393 – 407.

Liess, M., Glaser, B., Huwe, B., 2009. Digital Soil Mapping in Southern Ecuador. Erdkunde, 63/ 4: 309–319.

Litherland, M., Aspen, J. A., Jemielita, R. A., 1994. The metamorphic belts of Ecuador. Overseas Mem. Br. Geol Surv 11: 1–147.

McBratney, A. B., DeGruiter, J. J., 1992. A continuum approach to soil classification by modified fuzzy k-means with extragrades. Journal of Soil Science, 43: 159–175.

Milne, G., 1935. Some Suggested Units of Classification and Mapping, Particularly for East African Soils. Soil Research, 4: 183–198.

Moran, C. J., Bui, E. N., 2002. Spatial data mining for enhanced soil map modelling. International Journal of Geographic Information Science, 16: 533–549.

Rollenbeck, R., 2006. Variability of precipitation in the Reserva Biólogica San Francisco / Southern Ecuador. Lyonia, A Journal of Ecology and Application, 9 (1): 43–51.

Schelling, J., 1970. Soil genesis, soil classification and soil survey. Geoderma, 4/3: 165–193.

Schrumpf, M., Guggenberger, G., Valarezo, C., Zech, W., 2001. Tropical montane rainforest soils. Development and nutrient status along an altitudinal gradient in the South Ecuadorian Andes. Die Erde, 132; 43–59.

Simonson, W. R., 1959. Outline of a Generalized Theory of Soil Genesis. Soil Science Society of America Journal, 23: 152–156.

Skidmore, A.K., Watford, F., Luckananurug, Ryan, P.J., 1996. An operational GIS expert system for mapping forest soils from a geographical information system. International Journal of Grographic Information Science, 5: 431–445.

Soil Survey Staff. 2006. Keys to Soil Taxonomy. 10th ed. United States Department of Agriculture, Natural Resources Conservation Service. http://soils.usda.gov/ technical/ classification/taxonomy/ (access: 22/10/2007)

Stoyan, R., 2000. Aktivität, Ursachen und Klassifikation der Rutschungen in San Francisco/ Südecuador. Diplomarbeit Universität Erlangen.

Strahler, A. N., 1957. Quantitative analysis of watershed geomorphology. Transactions of the American Geophysical Union, 38/ 6: 913–920.

Therneau, T. M., Atkinson, B., 2003. The rpart Package. http://cran.r-project.org/ web/packages/rpart/rpart.pdf (access: 28/02/2008)

Thomas, A. L., King, D., Dambrine, E., Couturies, A., Roque, A., 1999: Predicting soil classes with parameters derived from relief geologic materials in a sandstone region of the Vosges mountains (northeastern France). Geoderma, 90: 291–205.

Wilcke, W., Yasin, S., Valarezo, C., Zech, W., 2001. Change in water quality during the passage through a tropical montane rainforest in Ecuador. Biogeochemistry, 55: 45–72.

Wilcke, W. ,Yasin, S., Abramowski, U., Valarezo, C., Zech, W., 2002. Nutrient storage and turnover in organic layers under tropical montane rainforest in Ecuador. European Journal of Soil Science, 53: 15–27.

Wilcke, W., Valladarez, H., Stoyan, R., Yasin, S., Valarez, C., Zech, W., 2003. Soil properties on a chronosequence of landslides in montane rainforest, Ecuador. Catena, 53: 79–95.

Yasin, S., 2001. Water and Nutrient Dynamics in Microcatchments under Montane Forest in the South Ecuadorian Andes. Bayreuther Bodenkundliche Berichte, Band 73.

Zevenbergen L. W., Thorne C. R., 1987. Quantitative Analysis of Land Surface Topography. Earth Surface Processes Landforms 12: 47 – 56.

Chapter 4

Incomplete Soil Classification to Benefit the Soil Continuum

Prediction of Diagnostic Horizons of Andean Mountain Forest Soils

MAREIKE LIEß [a], BRUNO GLASER [b], BERND HUWE [a]

a University of Bayreuth, *Department of Geosciences, Soil Physics Group*
   Universitätsstrasse 30, 95447 Bayreuth, Germany

b *Martin-Luther University Halle-Wittenberg, Soil Biogeochemistry, von-Seckendorff-Platz 3, 06120 Halle, Germany*

Correspondence: Mareike Ließ, E-mail: mareike.liess@uni-bayreuth.de

Summary

The World Reference Base for Soil Resources (WRB) (FAO, IUSS Working Group WRB, 2007) at present does not acknowledge the soil continuum, but provides a sound basis to do so. We relate the WRB diagnostic horizons' thickness to the upper 100 soil centimetres and call it incomplete soil classification. Typical diagnostic horizon thickness and occurrence probability was predicted from terrain parameters by classification and regression trees (CART), throughout the research area in southern Ecuador. The two disadvantages of CART, abrupt prediction class boundaries and dependence on the dataset, were addressed by Jackknife partitions, and therefore hundredfold model runs of different data subsets, leading to a range of possible predictions. Accordingly, model performance was evaluated by means of hundredfold external cross validation. Terrain parameters were found to have a strong influence on topsoil properties, although no influence on the subsoil. Hence predicting horizon thickness and subsoil properties was sometimes difficult. Whether the first mineral soil horizon displays stagnic properties or not, might depend on physical soil properties in addition to terrain parameters. Incomplete soil classification resulted in histic and stagnic soil parts dominating the first 100 cm of the soil column for most of the research area.

Keywords: digital soil mapping, pedometrics, Jackknife, CART, incomplete soil classification

4.1 Introduction

Early methods in soil classification focused on genetic principles and emphasized the soil continuum. However, intensity of soil processes is difficult to measure and therefore the soil continuum was not represented by a continuous system. Contemporary approaches focus on measurable soil properties for soil classification, but still lack incorporation of the soil continuum.

The World Reference Base for Soil Resources (WRB) (FAO, IUSS Working Group WRB, 2007) uses diagnostic horizons for the assignment of Reference Soil Groups (RSGs). Usually a specific horizon thickness is needed to qualify for a particular RSG. A soil needs an organic layer thickness of at least 10 cm if this directly overlies

continuous rock or ≥ 40 cm to be classified as Histosol. On the other hand, many criteria are related to soil depth: Umbrisols need an umbric horizon of 10 cm if directly overlying continuous rock or of 20 – 25 cm depending on soil thickness. Stagnosols need a stagnic colour pattern or an albic horizon in half or more of the soil volume.

Liess et al. (2009) distinguished Histosols that are often associated with Stagnosols as the major reference soil group (RSG) in the research area. As we know from soil sampling, these two RSGs are very much interlinked and refer to very similar soils, which often only differ by one centimetre in organic layer thickness. What is the reason to group two soils into different RSGs only because the diagnostic horizon thickness differs in one centimetre, neglecting the fact that they are two very similar soils? This similarity should be acknowledged by the soil classification system. The term classification refers to the grouping of a continuous variable into various discrete classes. Within the WRB, values underneath the threshold that is needed to classify a soil into a particular RSG, are ignored or acknowledged only by prefixes. The soil continuum is therefore represented very poorly.

In this context, Albrecht et al. (2005) differentiated between the terms systematisation and classification: The scientific comprehension and expert based depiction of all information of an area of expertise that pays special tribute to the interrelations of the individual objects, is a systematisation. Nevertheless, in soil science it is often referred to as genetic classification. Classification in the literal meaning, refers to the target-oriented data based formation of units (classes) and therefore, makes grading of objects based on defined criteria possible. Consequently, for the WRB the term systematisation would be more adequate. The only other internationally applicable soil classification system, Soil Taxonomy (Soil Survey Staff, 2006), has rigid defined classes which are based on measurable soil properties, but makes soil classification labour-intensive and complex.

Minasny and McBratney (2007) developed a system based on the Australian Soil Classification to implicate the taxonomic distances and relationships between the various RSGs. McBratney and De Gruiter (1992) thought to improve the existing soil classification systems via fuzzy sets to acknowledge the soil continuum. This seems a good option, but would probably not be applicable for the general soil scientist during soil designation in the field. Ließ et al. (this issue) proposed to interpret RSGs which are predicted in the same landscape positions, not so much as competing

RSGs, but as soils composed of various diagnostic properties. In conclusion, they proposed to rather predict diagnostic properties instead of the RSGs. Supporting this proposal, we suggest using "incomplete soil classification" based on the WRB diagnostic horizons to acknowledge the soil continuum. It is easily applicable and implemented already within an overall accepted international soil "classification" system (WRB).

For most agricultural or silvicultural applications, the first 100 cm of the soil are sufficient (Blume et al., 2008; Fisher and Binkley, 2000). This is why we suggest relating soil classification to these first 100 cm and then calculate the diagnostic horizons' thickness as percentage of these 100 cm that also include the organic layer. The latter is necessary to integrate organic and mineral soils equally. In conclusion, a soil composed of 40 cm organic layer, 30 cm stagnic horizon and 30 cm cambic horizon should be classified as 40% histic, 30% stagnic and 30% cambic soil. A soil consisting of 35 cm organic layer, 50 cm stagnic horizon and 15 cm continuous rock could be referred to as 35% histic, 50 % stagnic and 15% leptic soil. These two soils are rather similar regarding the underlying soil genesis and occur next to one another. The WRB separates them into two different RSGs and describes their similarity merely by prefixes as is true for the Stagnosol (FAO, IUSS Working Group WRB, 2007). On the other hand, Histosol assignation according to the WRB does not make a difference in name between Histosols with stagnic properties and Histosols without stagnic properties.

We use relief parameters calculated from a digital elevation model, to predict soil diagnostic horizon thickness and occurrence probability on a landscape scale in the tropical mountain rainforest of southern Ecuador by classification and regression trees (CART). The results are continuous maps of diagnostic horizon thickness and occurrence probability, which are then used as example to show what we mean by incomplete soil classification.

Spatial prediction of soil properties from terrain attributes is a standard approach within digital soil mapping, e.g. Moore et al. (1993) and Odeh et al. (1994). Being at first an unwelcome nuisance that reduced map reliability, gradually soil variation and its unpredictability was seen as a key soil attribute by itself (Burrough et al., 1994). Hence, digital soil maps in contrast to traditional soil maps include prediction uncertainty.

4.2   Material and methods

The research area as well as the dataset and GIS methodology have been described in Ließ et al. (this issue). Values of terrain parameters are assigned by the nearest neighbour (n. n.) method and as mean of the area around the sampled location, buffered by GPS accuracy. Terrain parameters, calculated for each raster grid cell and used to predict soil diagnostic horizon thickness and probability, include altitude a.s.l., aspect, slope, profile and plan curvature (pr./ pl. curv), overland flow distance to the channel network (OFD) and upslope contributing catchment area, calculated by kinematic routing algorithm (KRA CA) (Lea, 1992) and Braunschweiger Digital Relief Model (BS CA) (Bauer et al., 1985).

4.2.1   Classification and regression trees

Classification and regression trees (CART) are applied to establish statistical models to relate soil properties, in this case the probability and thickness of the diagnostic horizons, to their position within the landscape, i.e. terrain parameters. CART methodology was first described by Breimann et al. (1984). The rpart library of the R-Project for Statistical Computing (Therneau and Atkinson, 2003) is used for its implementation.

According to CART, the dataset is subdivided always into two subgroups (nodes) until the data are too scarce, five by default in rpart. The splitting criterion used for this subdivision, includes one of the input parameters (e.g. slope angle) and the parameter value indicating the split location.

In classification trees, the subdivision is based on a categorical response variable, in this case, horizon presence or absence. The Gini index as a decision criterion determines which variable best separates the dataset in each group into two subsets. The percentage of the categorical value indicating horizon presence in each end node is referred to as occurrence probability of the horizon in the related landscape position (for further explanation see Ließ et al., this issue).

A regression tree is produced when the dataset is subdivided based on a continuous response variable, such as the thickness of a diagnostic horizon. The optimal split is chosen by minimising the mean square error R. R in any node t with the number of observations n and the predicted mean value $\bar{y}$ is calculated by:

$$R(t) = 1/n(t) \cdot \sum_{i=1}^{n} \left[y_i(t) - \bar{y}(t) \right]^2 \qquad (1)$$

The optimal split is found when the difference in R between the mother node and the left and right child node t_l and t_r

$$R(t) - \left[R(t_l) + R(t_r) \right] \qquad (2)$$

is maximised. A mean value is calculated for each end node of the tree; it is used for model prediction in the corresponding landscape positions.

CART has many advantages over other statistical modelling approaches. It is robust, as no presumption regarding the nature of the input data is made; categorical as well as continuous data can both be used. The same is true for the relationship between predictor and response variables; interactions and nonlinearities among variables are permitted. But there are also disadvantages in CART: (a) They assign several mean values to large areas with abrupt changes at their boundaries and hence, do not depict a very detailed prediction and (b) a small change in the quantity of sample points may lead to quite different tree structures.

To overcome these disadvantages, Jackknifing (Efron, 1982) was applied. 100 model runs constructed 100 trees of different random Jackknife subsamples (⅔ of the dataset). All 100 models were then applied to the research area and the predicted mean and standard deviation for each grid cell was calculated. Hence, the prediction uncertainty was estimated and the model dependence on one particular dataset was reduced. On the other hand, a more detailed prediction was established. The ⅓ of the dataset, which was unaccounted for during the tree construction, was then used to perform an external cross validation and evaluate model performance. For the limited storage capacities of the R software package, we had to reduce GIS grid accuracy to a grid cell size of 20 m.

4.2.2 Incomplete soil classification concept

The thickness of the diagnostic WRB horizons can be measured quite easily. For many horizons not even laboratory analysis is necessary. This brought us to the idea to use these horizons, which are already established in a well known and accepted "classification" system, to propose "continuous soil classification" via incomplete classification.

Within the WRB, many criteria, e.g. for the assignation of Stagnosols and Umbrisols

relate diagnostic horizon thickness to soil depth. However, relating the horizon thickness to soil depth is often difficult, especially if the complete soil depth cannot be reached by auguring or when excavating the soil profile. We decided to relate the WRB's diagnostic horizons to the upper 100 cm of the soil, starting not from the mineral soil surface, but including the organic layer also. The latter is necessary to integrate organic soils. Also, there are many criteria within the WRB classification (FAO, IUSS Working Group WRB, 2007) referring to these upper 100 cm. Figure 4.1 pronounces the diagnostic horizons referring to the RSGs we encountered within the research area.
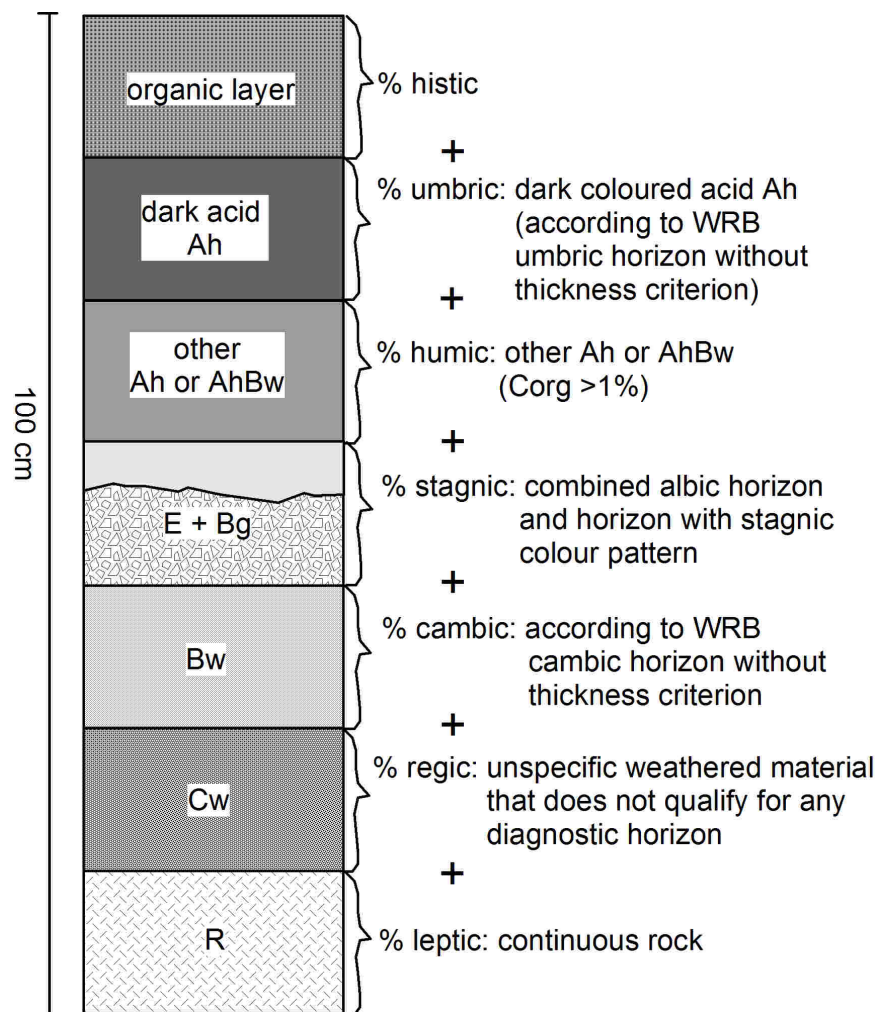
Figure 4.1: Assignation scheme for incomplete soil classification based on WRB (FAO, IUSS Working Group WRB, 2007) diagnostic horizons.

We favour this incomplete classification over the existing WRB systematic, because it acknowledges the soil continuum. In referring to the percentage each horizon is contributing to the upper 100 soil centimetres, no horizon is given dominance over another. To name the soil, the percentages are simply listed from top to bottom of the soil profile, facilitating the classification even further. Figure 4.1 so far only applies to

the soils we found within the research area. However, since it makes use of the well established WRB diagnostic horizons, it could easily be applied to other diagnostic soil horizons of the WRB.

4.3   Results and discussion

All relevant diagnostic horizons were predicted by CART models in their thickness and occurrence probability patterns. Probability prediction was only necessary for horizons absent in some soil profiles. Mean and standard deviation of the 100 applied models from Jackknife partitions refer to model prediction uncertainty of the digital soil maps. Horizon occurrence probability gives an additional measure of uncertainty. On sites with a low occurence probability, the soil will likely contain a thicker horizon than predicted by the horizon thickness model if it contains the horizon at all.

Typical soils within the study area could be simplified to a combination of four horizons: a histic horizon (organic layer), a dark-coloured topsoil horizon (humic/ umbric horizon), a horizon with albic and/ or stagnic properties (stagnic horizon) and a coloured subsurface horizon (cambic horizon).

4.3.1   Model performance to predict diagnostic horizons

Histograms of Pearson's r_{xy} from hundredfold external cross validation of the various tree models are presented in Figure 4.2. The probability model for the humic horizon refers to a dark coloured surface horizon (humic or umbric) and the model for the umbric horizon indicates the probability of this surface horizon to be umbric. Models from n. n. are always compared with those from mean terrain parameter values. The variability in r_{xy} from the various model runs indicates that Jackknifing the dataset is a good approach. Some parts of the data performed poorly in constructing a tree model ($r_{xy} \leq 0$), whereas others performed well ($r_{xy} = 0.5$). Hence, a single CART model depends very much on the data used in constructing it. Models to predict horizon thickness were best for the humic horizon, whereas horizon probability was best predicted for the stagnic horizon, when comparing the modes. However, whether models from nearest neighbour or mean terrain values performed better, was difficult to determine from the histograms. Therefore, the statistics displayed in Table 4.1 were calculated for the r_{xy} distributions.
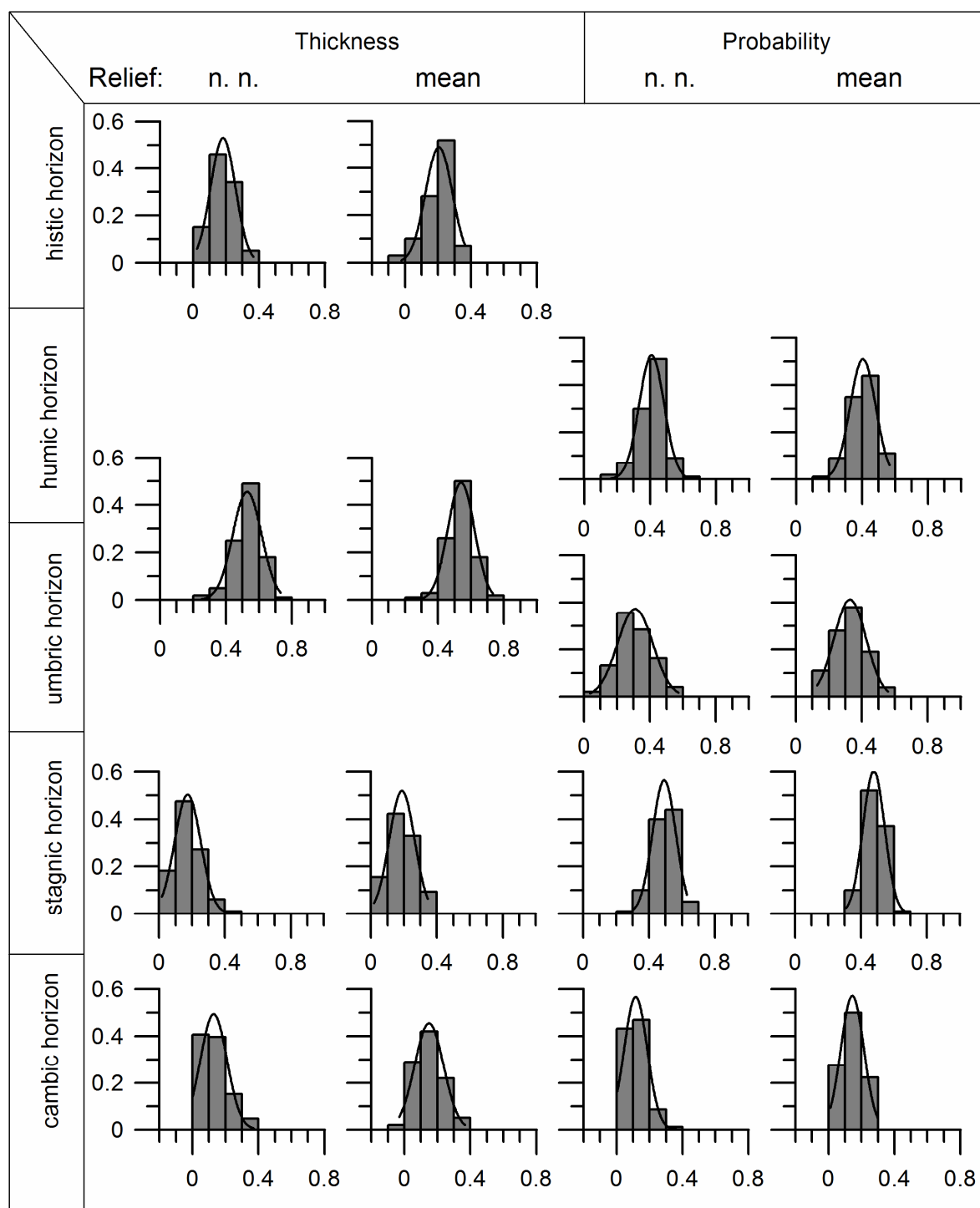
Figure 4.2: Histograms of Pearson's r_{xy} from hundredfold external cross validation for histic, humic, umbric, stagnic and cambic horizon thickness and occurrence probability. X = Pearson r_{xy}, Y= relative frequency (n. n./ mean = nearest neighbour/ mean terrain values).

Differences in mean and median between the two models (Table 4.1) are rather small. Regarding the umbric horizon prediction, the model from mean terrain parameter values appears to be better with a higher mean r_{xy} and a lower standard deviation.

Models to predict histic horizon thickness are rather poor with mean r_{xy} = 0.2 and maximum r_{xy} < 0.4. Probably, the organic layer thickness also depends on other

factors, not included in our model. Forest types mostly change with altitude or according to their position on the exposed ridges or protected side valleys (Homeier et al., 2002). Hence, vegetation is indirectly represented by altitude and OFD.

The model to predict humic horizon thickness performed much better as indicated by a mean r_{xy} of 0.5 and maximum r_{xy} of 0.7. However, mean r_{xy} to predict horizon probability was only 0.4 (Table 4.1). While model performance regarding the prediction of stagnic horizon thickness is rather poor (mean and median r_{xy} = 0.2), it is among the best for the prediction of the stagnic horizon probability (mean and median r_{xy} = 0.5) (Table 4.1). Hence, the occurrence of stagnic properties is obviously related to terrain parameters, whereas the extent of the stagnic horizon rather depends on other properties. This also explains why Ließ et al. (this issue) report poor model performance (R = 0.2) in Stagnosol probability prediction.

Table 4.1: Summary of Pearson's correlation coefficient distributions per horizon model

diagnostic horizon		terrain parameters	mean	std. dev.	min	25% quartile	median	75% quartile	max
histic	thickness	n. n.	0.18	0.08	0.02	0.14	0.18	0.23	0.37
		mean	0.21	0.08	-0.02	0.16	0.23	0.26	0.36
humic (umbric)	thickness	n. n.	0.53	0.09	0.25	0.47	0.53	0.59	0.73
		mean	0.54	0.08	0.27	0.49	0.55	0.59	0.73
	probability	n. n.	0.41	0.08	0.16	0.35	0.42	0.46	0.61
		mean	0.40	0.08	0.16	0.36	0.41	0.46	0.57
umbric	probability	n. n.	0.30	0.12	-0.09	0.24	0.30	0.38	0.57
		mean	0.33	0.10	0.13	0.26	0.33	0.40	0.56
stagnic	thickness	n. n.	0.17	0.08	-0.02	0.11	0.17	0.22	0.41
		mean	0.18	0.08	-0.02	0.13	0.18	0.24	0.35
	probability	n. n.	0.49	0.07	0.26	0.44	0.50	0.54	0.63
		mean	0.48	0.07	0.31	0.43	0.48	0.52	0.66
cambic	thickness	n. n.	0.10	0.10	-0.12	0.04	0.10	0.16	0.37
		mean	0.15	0.09	-0.03	0.09	0.15	0.20	0.37
	probability	n. n.	0.08	0.09	-0.15	0.03	0.09	0.15	0.36
		mean	0.13	0.08	-0.14	0.08	0.14	0.19	0.30

n. n.= nearest neighbour, std. dev. = standard deviation

Finally, the cambic horizon models had the worst overall model performance for both, horizon thickness and probability, with $r_{xy} \leq 0.10$ (n. n.). Models from mean terrain values performed only slightly better with $r_{xy} \leq 0.15$. Cambic horizon thickness and occurrence probability obviously cannot be predicted to a satisfying extent by terrain parameters. In contrast to the humic and stagnic horizon, the cambic horizon is a subsoil horizon. Its development is therefore less influenced by surface processes. Accordingly, Bauer et al. ([1]) limited downslope subsurface flow within the research

---

[1] The manuscript of this study was submitted to Journal of Hydrology.

area to the topsoil. Vanwalleghem et al. (2010) tried to predict spatial horizon variability from terrain parameters and yielded similar overall poor model efficiencies, ranging between 0.14 and 0.08. Park and Vlek (2002) modelled three-dimensional soil variability. They stated that soil attributes whose vertical distribution is strongly determined by vertical pedogenesis or unknown factors, were poorly modelled by environmental variables.

Altogether terrain parameters can only explain the occurrence of topsoil stagnic properties to a limited extent. As for horizon thickness their power is much less and terrain influence on subsoil has to be neglected. Other predictor variables that surely influence soil properties within the research area to a large extent, are parent material and landslide influence. Unfortunately, little is known regarding the spatial distribution of bedrock and landslides. However, the way in which terrain parameters influence the soil diagnostic horizons will be discussed.

4.3.2 Digital soil maps

Figure 4.3 shows the mean and standard deviation of the 100 model runs, applied to the research area for the models from n. n. (Figure 4.3a, b) and mean (Figure 4.3c, d) terrain values to predict histic horizon thickness. Values were grouped into classes in order to be mapped. Mean histic horizon thickness is predicted to be higher by models from n. n. compared to those from mean terrain values. However, few sites carry histic horizons ≥ 40 cm, what was rather common during sampling. Liess et al. (2009) described Histosols (organic layer ≥ 40 cm) to be the most common RSG. This can be explained by the rather poor model performance. Probably during tree construction, sites with thick histic horizons could not be clearly separated from others. High model variability, according to the different data subsets used in tree construction, is recognisable by the rather high standard deviation (c 20 – 30%).

Since we have 100 different tree models, grown from the different Jackknife partitions, the tree structure cannot be displayed. To describe the influence of the different variables, we calculated the mean and standard deviation of the terrain variables in the area covered by each of the mean thickness classes from Figure 4.3. Results are displayed in Table 4.2. The five classes are not represented equally within the research area, but the highest and lowest thickness class (5 and 1) are represented to a much lesser extent for the models from n. n. terrain parameter values.

Regarding the mean terrain values model, only class 5 is represented to this little extent, covering only 0.4% of the research area. Slope means indicate that the thickest histic horizons are found on the steepest slopes. Convex curvature leads to thicker histic horizons than concave curvature (exception class 5 model n. n. pl. curv). In addition, the thickest histic horizons are also found where the upslope contributing area is lowest. As for the influence of OFD, histic horizons are smallest close to the creeks, increase on the slopes with distance to the channel network and decrease again at even higher distances. Altitude and aspect do not show any simple influence.
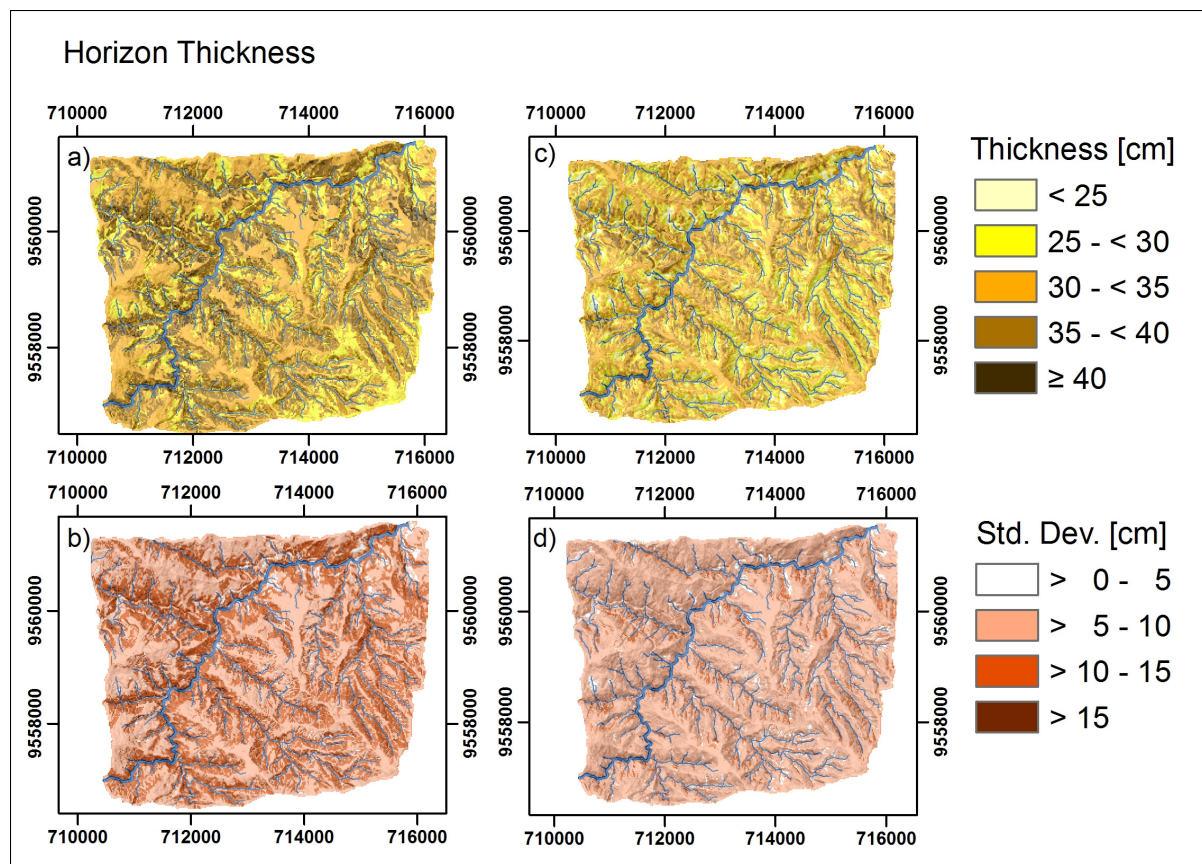
Figure 4.3: Maps of mean thickness and standard deviation of 100 models to predict histic horizon thickness applied to the research area (Overlaid hillshading with light source from north-east). a) Mean thickness and b) standard deviation predicted from n. n. terrain values, c) mean thickness and d) standard deviation predicted from mean terrain values.

Thick histic horizons are more likely on reduced moisture locations, hence on steep slopes, with small upslope contributing areas and on convex curvature. This is interesting, since the WRB describes Histosols as soils confined to poorly drained basins and depressions outside boreal, arctic and subarctic regions. Highland areas with a high precipitation/evapo-transpiration ratio are also mentioned as likely to bear Histosols. Nevertheless, it is likely that the wettest points in highland landscapes are

too wet to carry the thick histic horizons. However, considering the weak model performance, discussed above, this can only be understood as a minor tendency regarding the weak influence of terrain parameters.

Table 4.2: Mean and standard deviation of terrain parameters for histic horizon thickness classes from Figure 4.3a/ c

terrain parameters	class thickness [cm]	1 < 25	2 25 - <30	3 30 - <35	4 35 - < 40	5 ≥ 40
area [%]	n. n.	0.7	23.8	42.1	30.2	3.2
	mean	11.1	31.1	46.7	10.7	0.4
altitude [m]	n. n.	2221 ± 311	2258 ± 329	2295 ± 245	2222 ± 240	2128 ± 79
	mean	2180 ± 274	2272 ± 267	2280 ± 269	2210 ± 216	2106 ± 135
aspect [°]	n. n.	209 ± 76	203 ± 110	175 ± 113	188 ± 117	156 ± 139
	mean	220 ± 92	193 ± 106	187 ± 117	118 ± 125	176 ± 135
slope [°]	n. n.	21 ± 8	27 ± 8	31 ± 10	42 ± 5	42 ± 6
	mean	28 ± 9	34 ± 9	34 ± 11	35 ± 11	40 ± 5
pr. curv	n. n.	-0.0296 ± 0.0196	-0.0080 ± 0.0206	0.0023 ± 0.0129	0.0027 ± 0.0132	0.0031 ± 0.0123
	mean	-0.0166 ± 0.0228	-0.0017 ± 0.0154	0.0033 ± 0.0120	0.0054 ± 0.0121	0.0137 ± 0.0145
pl. curv	n. n.	-0.0502 ± 0.0196	-0.0082 ± 0.0219	0.0030 ± 0.0165	0.0042 ± 0.0134	-0.0007 ± 0.0117
	mean	-0.0190 ± 0.0209	-0.0034 ± 0.0174	0.0052 ± 0.0146	0.0084 ± 0.0147	0.0211 ± 0.0160
BS CA [m²]	n. n.	91454 ± 92888	18872 ± 46627	2833 ± 7979	2526 ± 5497	2521 ± 3201
	mean	36763 ± 63392	6940 ± 21094	1645 ±3054	1108 ± 854	740 ± 281
KRA CA [m²]	n. n.	1871287 ± 4501672	349014 ± 2141448	8779 ± 274347	3330 ± 19087	3340 ± 4895
	mean	777847 ± 3161036	40965 ± 649769	2021 ± 3203	1242 ± 753	451 ± 198
OFD [m]	n. n.	0 ± 3	153 ± 154	300 ± 195	211 ± 157	270 ± 156
	mean	66 ± 73	175 ± 135	288 ± 189	355 ± 182	213 ± 138

n. n.= nearest neighbour, pr./ pl. curv = profile/ plan curvature, BS/ KRA CA = contributing area, OFD = overland flow distance

The means of the hundredfold model runs to predict humic horizon thickness and probability applied to the research area are mapped in Figure 4.4. According to the applied model (Figure 4.4), humic horizon thickness is highest underneath c 2120 m a.s.l., it decreases between 2120 and 2420 m a.s.l. to ≤ 5 cm and increases again above 2420 m a.s.l. Humic horizon probability was also lowest at altitudes between 2120 and 2420 m a.s.l., and therefore the reason for the low predicted thickness. From field work we know, that most soils within these altitudes do not have a humic topsoil horizon, but start with a stagnic horizon directly at the mineral soil surface.

Few profiles include a humic horizon, which explains the relatively low mean value of 5. The occurrence pattern of the humic horizon can rather be explained by the absence of stagnic soil properties. The area with humic horizon thickness ≤ 5 cm or

horizon absence, respectively, covers 43% of the research area (Table 4.3).

UTM Zone 17 M, WGS 84
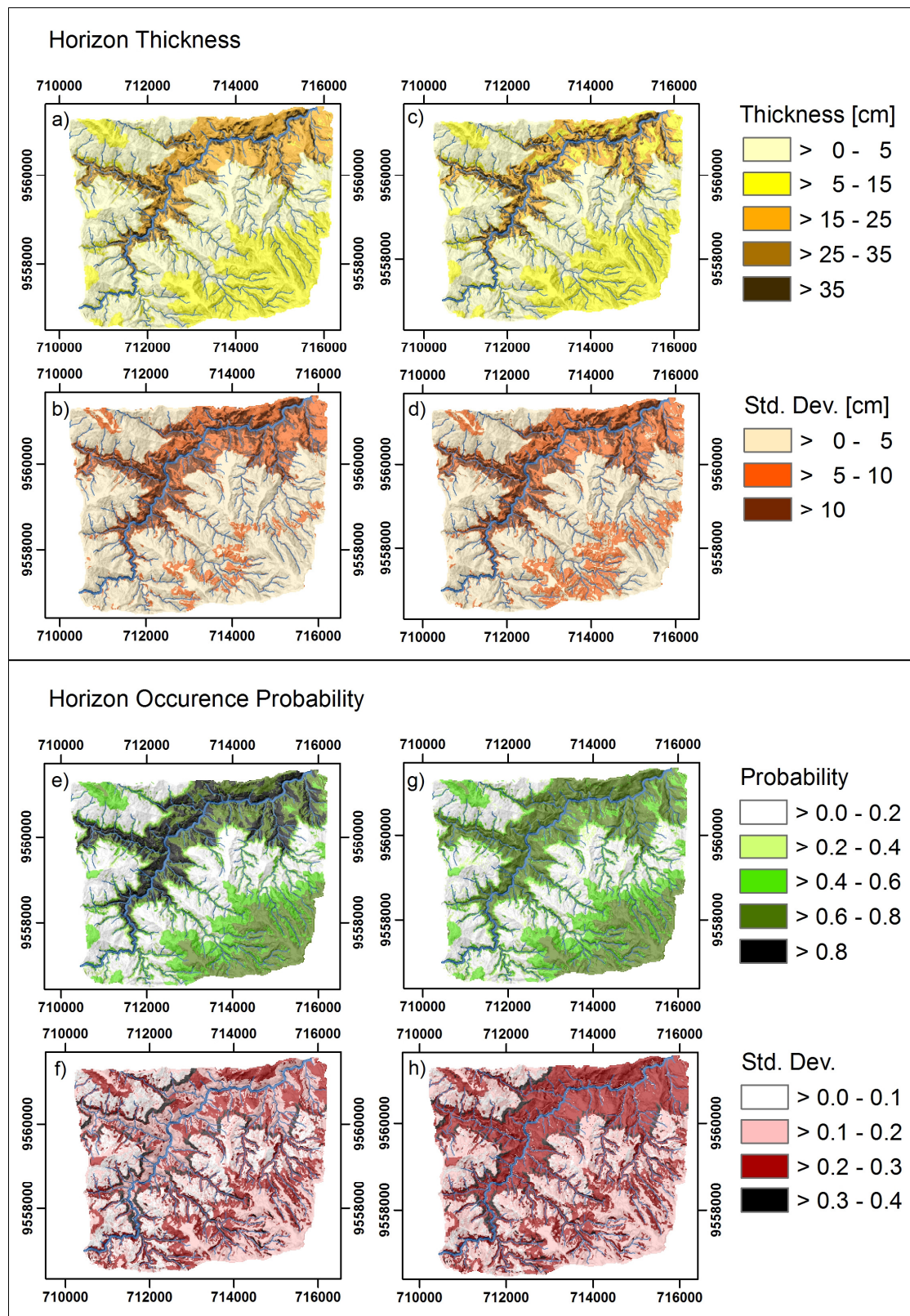
Figure 4.4: Maps of mean thickness and standard deviation of 100 models to predict humic horizon thickness and occurrence probability applied to the research area (Overlaid hillshading with light source from north-east). a) Mean thickness and b) standard deviation predicted from n. n. terrain values, c) mean thickness and d) standard deviation predicted from mean terrain values. e) Mean probability and f) standard deviation predicted from n. n. terrain values, g) mean probability and h) standard deviation predicted from mean terrain values.

Table 4.3: Mean and standard deviation of terrain parameters for the humic horizon thickness classes from Figure 4.4a/ c

terrain parameters	class thickness [cm]	1 0 - 5	2 May-15	3 15 - 25	4 25 - 35	5 > 35
area [%]	n. n.	43.1	29.8	16.2	7.8	3
	mean	43.1	33.7	14.9	5.5	2.8
altitude [m]	n. n.	2264 ± 91	2530 ± 237	1938 ± 97	1976 ± 96	1943 ± 102
	mean	2264 ± 91	2461 ± 291	1956 ± 129	1956 ± 99	1938 ± 102
aspect [°]	n. n.	179 ± 114	197 ± 119	191 ± 113	161 ± 107	182 ± 109
	mean	180 ± 113	198 ± 118	180 ± 112	166 ± 108	184 ± 110
slope [°]	n. n.	32 ± 9	34 ± 12	30 ± 8	39 ± 7	50 ± 3
	mean	32 ± 9	34 ± 11	30 ± 9	43 ± 3	50 ± 3
pr. curv	n. n.	0.0014 ± 0.0125	-0.0003 ± 0.0175	-0.0031 ± 0.0177	-0.0034 ± 0.0196	0.0002 ± 0.0206
	mean	0.0014 ± 0.0126	0.0001 ± 0.0166	-0.0050 ± 0.0201	-0.0020 ± 0.0180	0.0007 ± 0.0208
pl. curv	n. n.	0.0019 ± 0.0163	-0.0016 ± 0.0207	-0.0007 ± 0.0171	-0.0004 ± 0.0191	0.0006 ± 0.0187
	mean	0.0019 ± 0.0163	-0.0011 ± 0.0199	-0.0021 ± 0.0193	0.0008 ± 0.0175	0.0008 ± 0.0186
BS CA [m²]	n. n.	3537 ± 10063	9580 ± 33628	12099 ± 39404	8819 ± 27291	3083 ± 5941
	mean	3557 ± 10174	8464 ± 30922	16155 ± 45568	4538 ± 12099	3077 ± 5910
KRA CA [m²]	n. n.	4074 ± 7813	35414 ± 185238	502288 ± 2737024	79157 ± 720141	5261 ± 39546
	mean	4077 ± 7816	31426 ± 174432	574103 ± 2867708	39815 ± 658456	4692 ± 31758
OFD [m]	n. n.	259 ± 178	245 ± 203	235 ± 177	112 ± 89	111 ± 92
	mean	259 ± 178	264 ± 201	170 ± 155	115 ± 83	102 ± 74

n. n.= nearest neighbour, pr./ pl. curv = profile/ plan curvature, BS/ KRA CA = contributing area, OFD = overland flow distance

Differences between models from n. n. and mean terrain parameter values mainly refer to the lower sites close to the San Francisco River. Overall thickness and occurrence probability was higher for the former. In addition, mean standard deviation for probability values in this area was also lower for the n. n. models. This is why we would regard this model as better, although it was not indicated by the r_{xy} histograms in Table 4.1.

Surprisingly, the thickest humic horizons > 35 cm are to be found on mean slope angles 50 ± 3° and not as we would expect on lower inclinations (Table 4.3). Since there is no specific reason why very thick humic horizons should develop on steeper slopes, we attribute these thick humic (umbric) horizons to the accumulation zones of landslides that have been auger-sampled by chance. These accumulation zones due to the sampling scheme (Liess et al., 2009) were not sampled at higher altitude. Another reason might be that on less steep slopes we will rather find stagnic properties at the soil surface, due to a less rapid water flow. Ließ et al. (this issue)

also described a higher Stagnosol probability on lower slope angles. In conclusion, we assume altitude and slope to be the main terrain parameters determining humic horizon thickness.

Table 4.4: Mean and standard deviation of terrain parameters for probability classes of the humic horizon from Figure 4.4e/ g

terrain parameters	class probability	1 0 – 0.2	2 0.2 – 0.4	3 0.4 – 0.6	4 0.6 – 0.8	5 0.8 – 1.0
area [%]	n. n.	31.8	7.47	19.37	25.62	15.75
	mean	29.83	8.04	22.61	39.48	0.04
altitude [m]	n. n.	2283 ± 76	2244 ± 97	2407 ± 196	2303 ± 396	1961 ± 104
	mean	2283 ± 76	2259 ± 96	2337 ± 230	2195 ± 367	2354 ± 223
aspect [°]	n. n.	180 ± 112	176 ± 117	187 ± 120	204 ± 123	167 ± 91
	mean	179 ± 112	176 ± 120	192 ± 123	188 ± 111	234 ± 55
slope [°]	n. n.	31 ± 9	38 ± 10	36 ± 11	32 ± 11	36 ± 10
	mean	31 ± 8	34 ± 12	35 ± 11	34 ± 11	47 ± 2
pr. curv	n. n.	0.0026 ± 0.0108	-0.0006 ± 0.0151	-0.0012 ± 0.0180	-0.0021 ± 0.0182	-0.0016 ± 0.0178
	mean	0.0025 ± 0.0109	0.0011 ± 0.0135	-0.0020 ± 0.0183	-0.0015 ± 0.0178	-0.0286 ± 0.0204
pl. curv	n. n.	0.0025 ± 0.0160	0.0002 ± 0.0172	-0.0020 ± 0.0201	-0.0025 ± 0.0200	0.0029 ± 0.0162
	mean	0.0024 ± 0.0161	0.0009 ± 0.0170	-0.0027 ± 0.0201	0.0001 ± 0.0185	-0.0163 ± 0.0228
BS CA [m²]	n. n.	2769 ± 5414	4774 ± 12998	9563 ± 31605	10992 ± 38007	7755 ± 26077
	mean	2751 ± 5280	4138 ± 10637	10533 ± 34187	9086 ± 32293	11073 ± 11995
KRA CA [m²]	n. n.	3579 ± 6376	5055 ± 9624	37386 ± 197749	231832 ± 1750365	202880 ± 1771472
	mean	3593 ± 6406	4660 ± 9208	100254 ± 974648	192447 ± 1650526	25739 ± 31074
OFD [m]	n. n.	288 ±172	167 ± 156	231 ± 195	248 ± 201	145 ± 122
	mean	286 ± 170	211 ± 182	227 ± 192	207 ± 182	17 ± 13

n. n.= nearest neighbour, pr./ pl. curv = profile/ plan curvature, BS/ KRA CA = contributing area, OFD = overland flow distance

Table 4.4 summarises humic horizon probability class statistics from Figure 4.4e and g. While the models from n. n. terrain parameter values assigned a probability > 0.8 to 16% of the research area, the models from mean values assigned it to only 0.04%. Maps regarding the applied models of stagnic horizon thickness and probability are displayed in Figure 4.5. Stagnic horizon thickness increases above c 2140 m a.s.l. This is about the altitude where humic horizon thickness decreases. Stagnic horizon probability decreases above 2500 m a.s.l., while humic horizon probability increases. This comparison is interesting, since soil profiles within the research area either start with a humic or stagnic surface horizon underneath the organic layer. The two diagnostic horizons usually do not occur within the same soil profile.

The increase of stagnic horizon probability and thickness with altitude can be

attributed to increasing rainfall. According to Rollenbeck (2006), rainfall increases by 250 mm with 100 m altitude. At higher altitude, we assume that more water enters the soil than percolates to deeper soil layers. In accordance with this, Schrumpf et al. (2001) indicated an increase in hydromorphic properties with increasing altitude. On the other hand, increasing rainfall with altitude cannot explain the decreasing stagnic horizon probability above 2500 m a.s.l. However, the rainfall gradient that increases by 250 mm per 100 m altitude up to 2600 m a.s.l., decreases to 100 mm per 100 m altitude above (Rollenbeck, 2006). Furthermore, we assume that physical soil properties change above this altitude, so that wet soil hydraulic conductivity increases. The latter might also explain the abrupt decrease in probability underneath 2140 m a.s.l.

Table 4.5 and 4.6 indicate that thicker stagnic horizons are also more probable on lower slope angles. This seems reasonable and supports our assumptions for the thicker humic horizons on steeper slopes.

Table 4.5: Mean and standard deviation of terrain parameters for stagnic horizon thickness classes from Figure 4.5a/ c

terrain parameters	class thickness [cm]	1 < 15	2 15 - 30	3 30 - 45	4 45 - 60	5 > 60
area [%]	n. n.	25	24	11	34	7
	mean	22	30	11	31	6
altitude [m]	n. n.	1988 ± 137	2230 ± 265	2352 ± 172	2414 ± 205	2413 ± 219
	mean	2010 ± 170	2204 ± 258	2354 ± 185	2423 ± 208	2398 ± 197
aspect [°]	n. n.	192 ± 100	168 ± 125	148 ± 107	176 ± 109	325 ± 41
	mean	203 ± 103	158 ± 117	176 ± 113	177 ± 110	329 ± 38
slope [°]	n. n.	36 ± 11	39 ± 9	32 ± 9	28 ± 9	31 ± 7
	mean	36 ± 11	38 ± 9	32 ± 9	28 ± 9	30 ± 7
pr. curv	n. n.	-0.0037 ± 0.0202	0.0016 ± 0.0140	-0.0044 ± 0.0201	0.0021 ± 0.0119	0.0020 ± 0.0111
	mean	-0.0051 ± 0.0209	0.0003 ± 0.0156	-0.0019 ± 0.0173	0.0029 ± 0.0109	0.0020 ± 0.0113
pl. curv	n. n.	-0.0008 ± 0.0185	0.0007 ± 0.0166	-0.0047 ± 0.0233	0.0021 ± 0.0166	0.0011 ± 0.0186
	mean	-0.0016 ± 0.0192	0.0002 ± 0.0172	-0.0024 ± 0.0234	0.0026 ± 0.0160	-0.0006 ± 0.0178
BS CA [m²]	n. n.	11592 ± 37386	3522 ± 9337	17668 ± 46185	3642 ± 14146	3121 ± 8027
	mean	12920 ± 39669	5760 ± 20720	13749 ± 41318	2734 ± 7352	3059 ± 6244
KRA CA [m²]	n. n.	355135 ± 2244096	13758 ± 323928	58742 ± 235939	6696 ± 54980	4002 ± 9181
	mean	402875 ± 2386894	18271 ± 238830	43797 ± 199952	3600 ± 12093	4041 ± 7568
OFD [m]	n. n.	144 ± 139	238 ± 166	112 ± 118	316 ± 185	357 ± 190
	mean	123 ± 132	223 ± 164	158 ± 135	331 ± 184	355 ± 194

n. n.= nearest neighbour, pr./ pl. curv = profile/ plan curvature, BS/ KRA CA = contributing area, OFD = overland flow distance
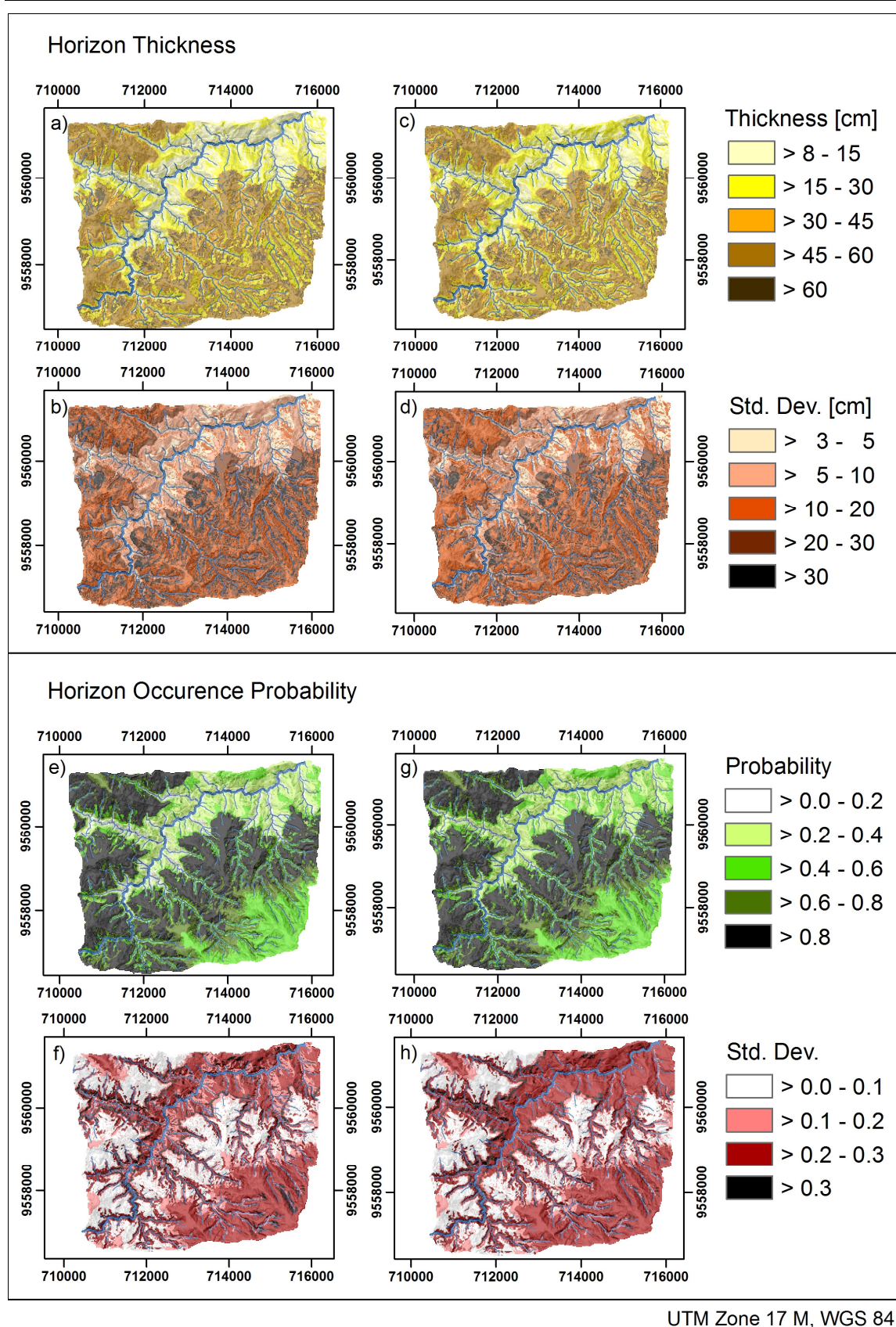
Figure 4.5: Maps of mean thickness and standard deviation of 100 models to predict stagnic horizon thickness and occurrence probability applied to the research area (Overlaid hillshading with light source from north-east). a) Mean thickness and b) standard deviation predicted from n. n. terrain values, c) mean thickness and d) standard deviation predicted from mean terrain values. e) Mean probability and f) standard deviation predicted from n. n. terrain values, g) mean probability and h) standard deviation predicted from mean terrain values.

Bauer et al. ([1]) investigated soil hydrological flow patterns within the research area and proved downslope subsurface flow within the stagnic soil layer. In conclusion, lower slope angles allow more water to enter the soil and would also lead to a decreased subsurface flow velocity within the stagnic layer. Unfortunately, other variables do not show such reasonable patterns.

Table 4.6: Mean and standard deviation of terrain parameters for occurrence probability classes of stagnic horizon from Figure 4.5e/ g

terrain parameters	class probability	1 0.0 - 0.2	2 0.2 – 0.4	3 0.4 – 0.6	4 0.6 – 0.8	5 0.8 – 1.0
area [%]	n. n.	6.2	18.5	21.9	14.3	39.1
	mean	1.9	20.4	24.3	15.1	38.3
altitude [m]	n. n.	1963 ± 113	1967 ± 143	2425 ± 346	2411 ± 173	2293 ± 109
	mean	2011 ± 130	1961 ± 140	2381 ± 355	2406 ± 177	2293 ± 108
aspect [°]	n. n.	192 ± 99	177 ± 115	190 ± 123	204 ± 112	179 ± 113
	mean	183 ± 104	185 ± 109	186 ± 124	201 ± 112	179 ± 113
slope [°]	n. n.	41 ± 9	34 ± 10	34 ± 11	40 ± 9	29 ± 8
	mean	47 ± 5	35 ± 10	34 ± 11	40 ± 9	29 ± 8
pr. curv	n. n.	-0.0078 ± 0.0244	-0.0023 ± 0.0181	-0.0029 ± 0.0183	0.0022 ± 0.0139	0.0026 ± 0.0110
	mean	-0.0132 ± 0.0227	-0.0032 ± 0.0199	-0.0023 ± 0.0182	0.0017 ± 0.0139	0.0026 ± 0.0109
pl. curv	n. n.	0.0028 ± 0.0184	-0.0001 ± 0.0180	-0.0044 ± 0.0214	0.0001 ± 0.0175	0.0026 ± 0.0159
	mean	0.0002 ± 0.0193	0.0003 ± 0.0183	-0.0037 ± 0.0212	0.0003 ± 0.0173	0.0026 ± 0.0158
BS CA [m²]	n. n.	11319 ± 34374	11299 ± 37765	12598 ± 38331	3162 ± 8773	2867 ± 5927
	mean	6376 ± 17035	12056 ± 38809	12157 ± 37638	3347 ± 9651	2842 ± 5853
KRA CA [m²]	n. n.	290588 ± 1917620	383196 ± 2370528	42475 ± 197452	3653 ± 6459	3717 ± 7214
	mean	28504 ± 246076	427293 ± 2485165	43294 ± 204194	3758 ± 6880	3691 ± 7116
OFD [m]	n. n.	57 ± 44	166 ± 123	253 ± 218	201 ± 162	299 ± 175
	mean	36 ± 11	131 ± 104	257 ± 213	197 ± 160	302 ± 175

n. n.= nearest neighbour, pr./pl.curv = profile/ plan curvature, BS/ KRA CA = contributing area, OFD = overland flow distance

The models from n. n. and mean terrain values, described so far, are similar. Though, this is not the case for the models concerning cambic horizon thickness (Figure 4.6). Figure 4.6a (n. n.) predicts decreasing cambic horizon thickness with altitude, while the model from mean terrain values shows a lower thickness along the ridges (≤ 10 cm) and most of the area with > 20 – 30 cm. This indicates that subsoil properties are not related to terrain parameters. Maps of cambic horizon thickness and probability have been included solely to present the incomplete soil classifications system.

---

[1] The manuscript of this study was submitted to Journal of Hydrology.

UTM Zone 17 M, WGS 84
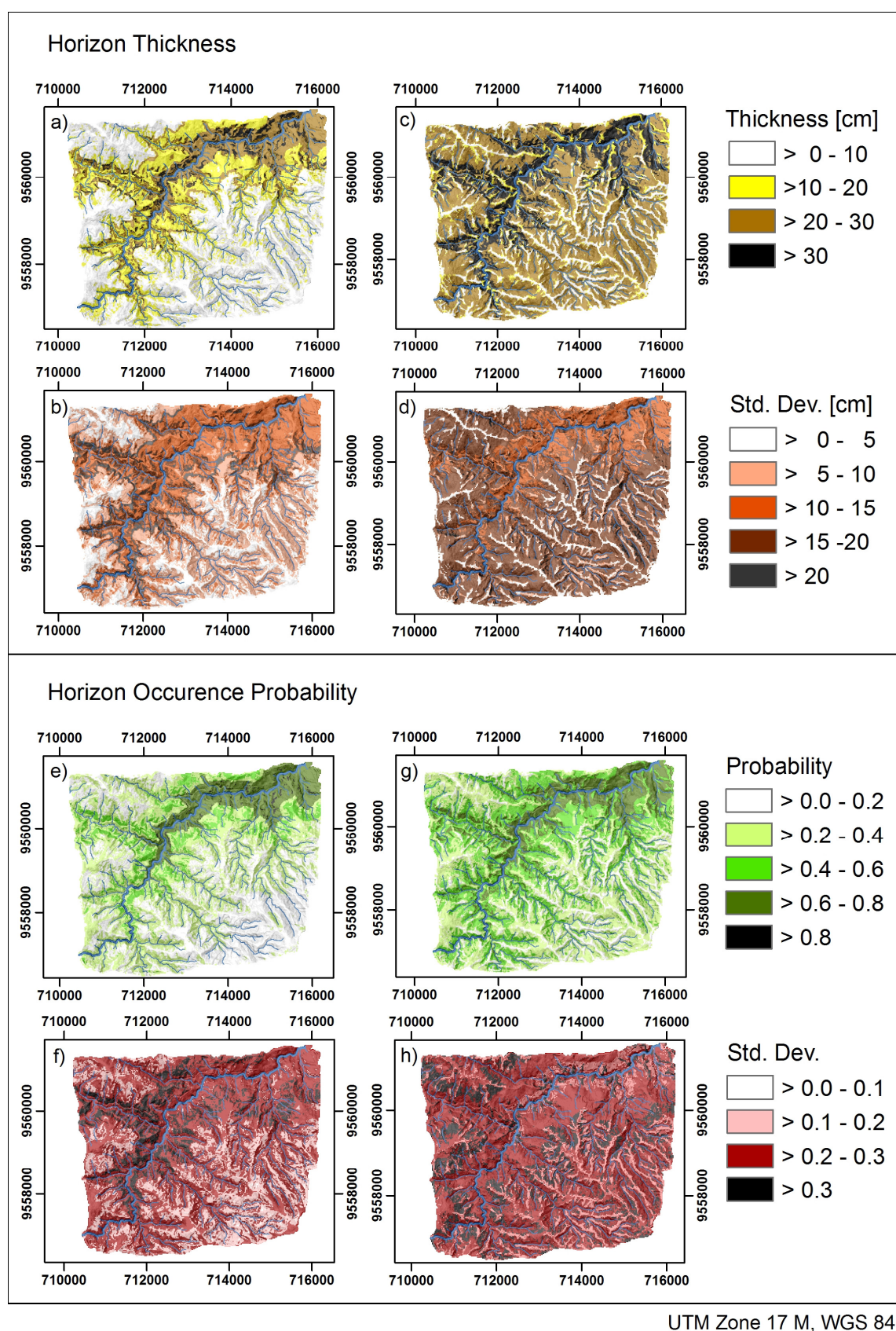
Figure 4.6: Maps of mean thickness and standard deviation of 100 models to predict cambic horizon thickness and occurrence probability applied to the research area (Overlaid hillshading with light source from north-east). a) Mean thickness and b) standard deviation predicted from n. n. terrain values, c) mean thickness and d) standard deviation predicted from mean terrain values. e) Mean probability and f) standard deviation predicted from n. n. terrain values, g) mean probability and h) standard deviation predicted from mean terrain values.

4.3.3 Incomplete soil classification

Liess et al. (2009; Ließ et al., this issue) described the occurence probability of the RSGs Histosol, Stagnosol and Leptosol within the research area, with Histosol and Stagnosol dominating. Our research supports this finding, i.e. thick histic horizons generally cover stagnic soils. We further assume non-stagnic soils at lower altitude as well as the decreasing probability of stagnic soils at higher altitude to be related to a change in soil texture and/ or bulk density. On the other hand, mean histic horizons ≥ 40 cm that would allow for a soil to be classified as Histosol (FAO, IUSS Working Group WRB, 2007) are predicted in ≤ 3% (Table 4.2) of the research area. However, sites predicted with a mean of 30 – 40 cm, would also have to be included due to the high standard deviation. The WRB classifies Histosols solely based on the thickness of the organic layer, regardless of its further characteristics. For a soil with only 39 cm organic layer, these mineral soil properties suddenly become important. Such a strict criterion is a problem in predicting mean horizon thickness as well as a problem to soil systematisation in general.
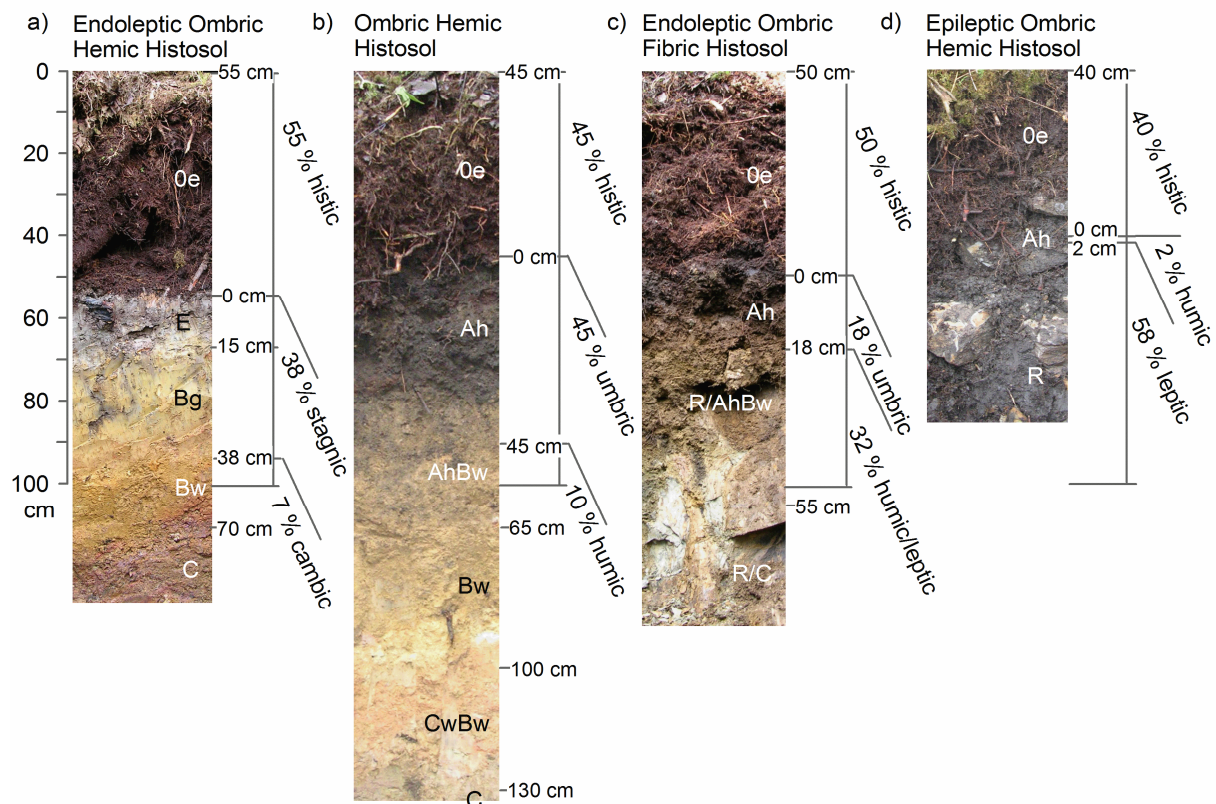
Figure 4.7: RSG Histosol classified according to the incomplete classification scheme. a) 55% histic, 38% stagnic, and 7% cambic soil. b) 45% histic, 45% umbric and 10% humic soil. c) 50% histic, 18% umbric and 32% humic/ leptic soil. d) 40% histic, 2% humic and 58% leptic soil.

Figure 4.7 shows various Histosols of the research area, classified according to the WRB and the incomplete classification scheme we proposed in Figure 4.1. It shows that a soil can have stagnic (Figure 4.7a), umbric (Figure 4.7b, c) or leptic (Figure 4.7c, d) properties underneath this thick organic layer. The intergrades to other RSGs in the WRB (FAO, IUSS Working Group WRB, 2007) are accounted for by prefixes, but we neither find stagnic nor umbric as a prefix for Histosols. Furthermore, nothing is said regarding the extent of those properties (a stagnic soil horizon could outrange a histic horizon).

To classify a soil as Stagnosol or stagnic, the stagnic soil layer again has to exceed a specific thickness, which in case of Stagnosols is not an absolute value, but related to soil depth. This shows some inconsequence within the "classification" system. Last but not least, the existing international soil "classification" system of the FAO, attributes very poorly to the gradual changes within the soil continuum. Figure 4.8 gives another example with the intimate linkage between the RSGs Histosol and Stagnosol.
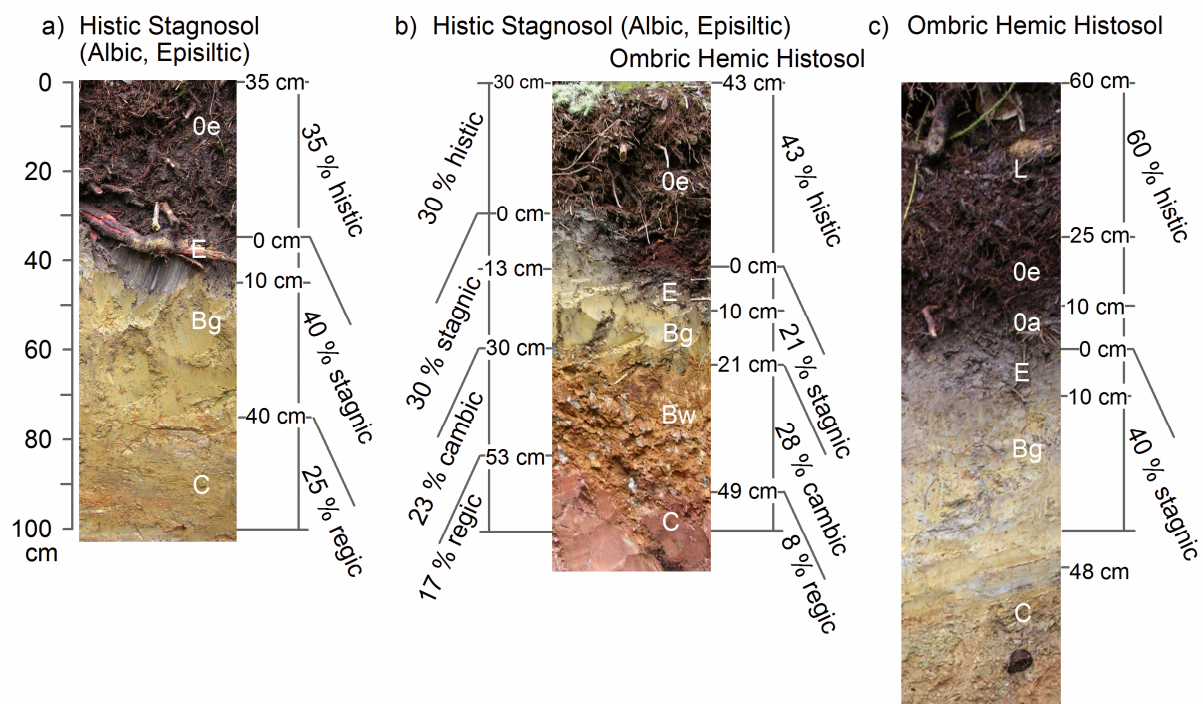
Figure 4.8: Continuous change between RSG Stagnosol and RSG Histosol.

It has to be questioned whether a soil with stagnic properties sufficiently pronounced to classify as Stagnosol, should be classified as Histosol only for the reason of an organic layer thickness of 40 cm instead of 39 cm. In addition, relating the diagnostic horizons to the upper 100 soil centimetres makes the prediction of the stagnic part

independent of the assignation of Histosol and Leptosol, which occur before Stagnosols within the WRB hierarchy. Therefore, the diagnostic properties would be treated equally without any hierarchy. Often even within one soil profile, the thickness of the organic layer or of the stagnic horizon changes significantly and would result in two RSG options for classifying the same soil profile. The profile in Figure 4.8b would classify as Stagnosol or Histosol depending whether we regard its left or right side. In this case, the proposed incomplete soil classification certainly provides the better concept. Accordingly, the soil in Figure 4.7a is described as 55% histic/ 38% stagnic/ 7% cambic soil; the soil in Figure 4.8b as 30 – 43% histic/ 30 – 21% stagnic/ 23 – 28% cambic/ 17 – 8% regic soil.

Figure 4.9 shows the incomplete soil classification scheme applied to the research area. Histic and humic/ umbric horizon together are always < 100 cm. In this way, the maps a, f, b and g in Figure 4.9 are equal to those presented in Figures 4.3 and 4.4, now representing percentages of the first 100 cm, except for the additional information of the probability of the humic horizon to be umbric. Following the typical horizon order histic, humic/ umbric, stagnic and cambic, the latter two on some sites are only partly included within these 100 cm, and therefore had to be recalculated. Recognisable from the dark colours in Figures 4.9a, c, f and h, the histic and stagnic components together account for the major part of the soil column (100 cm) throughout most of the research area. The regic/ leptic fraction in Figures 4.9e and k refer to the last part within the upper 100 cm, not specified as any diagnostic horizon. Since we sampled the soils until R or Cw horizon respectively, we could not differentiate between % leptic or regic, as we did for % humic or umbric within the Ah horizon. Figure 4.9e and k diagnose higher regic/ leptic soil parts close to the creeks and underneath 2140 m a.s.l. Expert knowledge gained during field work, provides us with the information that leptic soils occur on steep slopes and close to the creeks (Ließ et al., this issue).

The soil horizon maps in Figure 4.9 solely indicate the mean horizon thickness according to the 100 models based on different Jackknife partitions. They do, however, not include prediction uncertainty according to the earlier discussed digital soil maps displaying horizon occurrence probability and standard deviation.
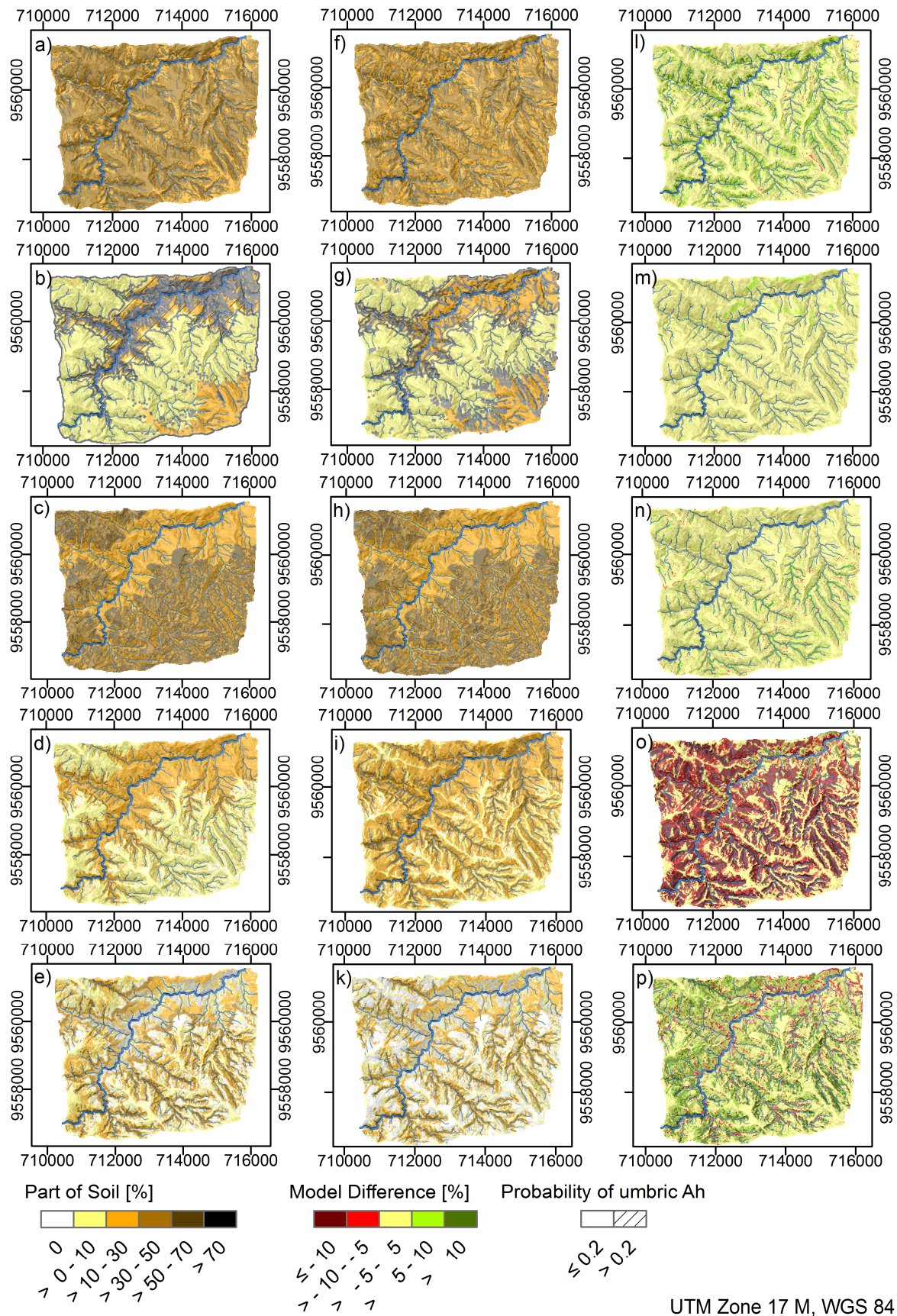
Figure 4.9: Incomplete soil classification according to Figure 4.1 (Overlaid hillshading with light source from north-east): % histic (a, f), % humic/ umbric (b, g), % stagnic (c, h), % cambic (d, i) and % regic/ leptic (e, k). The first column describes the prediction from nearest neighbour, the second column from mean terrain values. The third column shows the model differences.

4.4 Conclusions

Jackknifing is a good instrument to include prediction uncertainty in digital soil maps. Horizon occurrence probability prediction provides an effective second means to do so.

Terrain parameters were found to have a strong influence on topsoil properties, but rather no influence on the subsoil. However, even topsoil properties could not be explained completely by terrain parameters. We assume parent material and landslides have a strong influence on soil formation. To explain whether the first mineral soil horizon has stagnic properties or not, physical soil properties have to be considered in addition to terrain parameters. Further investigation is already in progress to prove this assumption.

Leaving soil classification incomplete, in order to acknowledge the soil continuum, seems a good alternative to combat the problems resulting from conventional soil classification. Accordingly, the characteristics and extent of diagnostic soil horizons make the results of soil genetic processes measurable. Horizons are given equal importance with each soil dominated by a different soil process, simply because it forms the major part of the first 100 soil centimetres. This has been part of soil genesis theory for a long time (Simonson, 1959; Schelling, 1970). Finally, this system can be easily applied to soils not represented within the research area, since it is based on the diagnostic horizons of a well established "soil classification" system.

4.5 Acknowledgements

4.6 References

Albrecht, C., Jahn, R., Huwe, B., 2005. Bodensystematik und Bodenklassifikation Teil 1: Grundbegriffe. Journal of Plant Nutrition and Soil Science, 168: 7-20

Bauer, F., Vinan, P., Balcazar, L., Bogner, C., Huwe, B., 2010a. Flow paths in soils of landslide affected and unaffected hillslopes in a montane rainforest of South Ecuador, part A. submitted to Journal of Hydrology

Bauer, F., Balcazar, L., Vinan, P., Bogner, C., Zeilinger, J., Huwe, B., 2010b. Flow paths in soils of landslide affected and unaffected hillslopes in a montane rainforest of South Ecuador, part B. submitted to Journal of Hydrology

Bauer, J., Rohdenburg, H., Bork, H.-R., 1985. Ein digitales Reliefmodell als Vorraussetzung für ein deterministisches Modell der Wasser- und Stoff-Flüsse. In: Bork, H.- R., Rohdenburg, H. (Eds.). Landschaftsgenese und Landschaftsökologie H. 10, Parameteraufbereitung für deterministische Gebiets-Wassermodelle, Grundlagenarbeiten zur Analyse von Agrar-Ökosystemen, p. 1 – 15.

Blume, H.-P., Brümmer, G. W., Schwertmann, U, Horn, R. Kögel-Knabner, I., Stahr, K., Auerswald,K. Beyer, L. Hartmann, A., Litz, N. Scheinost, A. Stanjek, H. Welp, G. Wilke, B.-M., 2008. Scheffer/ Schachtschabel Lehrbuch der Bodenkunde, 15th ed. Spektrum, Heidelberg.

Breimann, L., Friedmann, J. H., Olshen, R. A., Stone, C. J., 1984. Classification and regression trees, CRC press, Wadsworth.

Burrough, P. A., Bouma, J., Yates, S. R., 1994. The state of the art in pedometrics. Geoderma 62: 311 – 326.

Efron, B., 1982.The Jackknife, the Bootstrap and Other Resampling Plans.CBMS-NSF Regional Conference Series in Applied Mathematics. Society for Industrial and Applied Mathematics. J. W. Arrowsmith Ltd., Bristol, England.

FAO, IUSS Working Group WRB, 2007. World Reference Base for Soil Resources, ISRIC, Rome.

Fisher, R. F., Binkley, D.,2000. Ecology and Management of Forest Soils. 3rd Edition, John Wiley and Sons, New York.

Homeier, J., Dalitz, H., Breckle, S.-W., 2002. Waldstruktur und Baumartendiversität im montanen Regenwald der Estacón Cientíca San Franscisco. Südecuador. Ber. d. Reinh. Tüxen-Ges 14: 109-118.

Lea, N. L., 1992. An aspect driven kinematic routing algorithm. In: Parsons, A. J. and Abrahams, A. D. (eds.) Overland Flow Hydraulics and Erosion Mechanics. London, 393 – 407.

Liess, M., Glaser, B., Huwe, B., 2009. Digital Soil Mapping in Southern Ecuador. Erdkunde, 63/ 4: 309–319.

McBratney, A. B., DeGruiter, J. J., 1992. A continuum approach to soil classification by modified fuzzy k-means with extragrades. Journal of Soil Science, 43: 159-175.

Minasny, B., McBratney, A. B., 2007. Incorporating taxonomic distance into spatial prediction and digital mapping of soil classes. Geoderma, 142: 285-293.

Moore, I., Gessler, P., Nielsen, G., Peterson, G., 1993. Soil attribute prediction using terrain analysis. In: Soil Science Society of America Journal, 57/ 2: 443– 452.

Odeh, I., McBratney, A., Chittleborough, D., 1994. Spatial prediction of soil properties from landform attributes derived from a digital elevation model. Geoderma, 63/ 3– 4: 197– 214.

Park, S. J., Vlek, P. L. G., 2002. Environmental correlation of three-dimensional soil spatial variability: a comparison of three adaptive techniques. Geoderma 109: 117 – 140.

Rollenbeck, R., 2006. Variability of precipitation in the Reserva Biólogica San Francisco / Southern Ecuador. Lyonia, A Journal of Ecology and Application, 9 (1): 43-51.

Schelling, J., 1970. Soil genesis, soil classification and soil survey. Geoderma, 4/3: 165-193.

Schrumpf, M., Guggenberger, G., Valarezo, C., Zech, W., 2001. Tropical montane rainforest soils. Development and nutrient status along an altitudinal gradient in the South Ecuadorian Andes. Die Erde, 132; 43–59.

Simonson, W. R., 1959. Outline of a Generalized Theory of Soil Genesis. Soil Science Society of America Journal, 23: 152-156.

Soil Survey Staff. 2006. Keys to Soil Taxonomy. 10th ed. United States Department of Agriculture, Natural Resources Conservation Service. http://soils.usda.gov/ technical/ classification/taxonomy/ (access: 22/10/2007)

Vanwalleghem, T., Poesen, J., McBratney, A., Deckers, J., 2010. Spatial variability of soil horizon depth in natural loess-derived soils. Geoderma 157: 37 – 45.

Chapter 5

Uncertainty in the Spatial Prediction of Soil Texture

Comparison of Regression Tree and Random Forest Models

MAREIKE LIEß [a], BRUNO GLASER [b], BERND HUWE [a]

a University of Bayreuth, Department of Geosciences, Soil Physics Group
  Universitätsstrasse 30, 95447 Bayreuth, Germany
b Martin-Luther University Halle-Wittenberg, Soil Biogeochemistry, von-Seckendorff-
  Platz 3, 06120 Halle, Germany

Correspondence: Mareike Ließ, E-mail: mareike.liess@uni-bayreuth.de

Abstract

Within the southern Ecuadorian Andes, landslides have an impact on landscape development (Bussmann et al., 2008). The plan to apply pedotranfer functions to predict the saturated hydraulic conductivity for hydrological and landslide process models, made the regionalisation of soil texture an urgent matter. Statistical models were adapted to predict the spatial distribution of soil texture from terrain parameters. The performance of regression tree (RT) and Random Forest (RF) models was compared by 100 model runs on random Jackknife partitions. Digital soil maps of sand, silt and clay percentage mean and standard deviation indicate model variability and prediction uncertainty.

The area was investigated by 56 soil profiles and 315 auger points. Soil profiles were analysed horizon-wise by pipette, laser and field method (FAO, 2006). Results by pipette compared to laser method showed the expected shift to higher silt and lower clay contents. Linear regression equations were adapted. Field texture analysis did not provide satisfying results. It was therefore not possible to correct its results with the more precise laboratory data and use the bigger auger dataset, analysed by field method only, for soil texture regionalisation.

RF models performed better than RT models. All terrain factors considered in the analysis influenced soil texture of the surface horizon, but altitude a.s.l. was assigned the highest variable importance during model construction. Shallow subsurface flow is considered responsible for increasing sand/ clay ratios with increasing altitude, on steep slopes and with overland flow distance to the channel network by removing clay particles downslope. Deeper soil layers are not influenced by this process and therefore, did not show the same texture properties. However, the influence of parent material and landslides on the spatial distribution of soil texture cannot be neglected. Model performance, most probably, could be improved by a bigger dataset.

Key words: Regression tree, Random Forest, Jackknife, soil texture

5.1   Introduction

To establish digital soil maps, information from discrete sampling points can be interpolated when data distribution is sufficiently dense and terrain forms, parent

material and vegetation do not show abrupt changes between any two sampling points. Hence, there has to be spatial correlation between the observations to allow for interpolation (Goovaerts, 1999). In mapping big areas and particularly mountainous landscapes, data density is usually not enough. Furthermore, soil data is often collected along one-dimensional transects, whereas the application, a map, is two-dimensional. Hence, it is not sufficient to interpolate only along transects (Myers, 1994).

However, digital soil maps can also be developed by relating soils to terrain parameters by statistical models, a standard approach in soil-landscape modelling. Accordingly, McKenzie and Austin (1993) and De Bruin and Stein (1998) predicted topsoil clay content using terrain attributes. Brown et al. (2004) investigated potential terrain controls on surface texture for Ugandan soils. Furthermore, Zhao et al. (2009) regionalised soil texture from hydrographical parameters and Gobin et al. (2001) predicted spatial variability of soil texture in Nigeria.

Bishop and Minasny (2006) compared several statistical models that are often applied in digital soil mapping. Among the considered models, only ANNs were assigned a better predictive power than classification and regression trees (CART). Though, ANNs lack the ease of use, parsimony, interpretability and computational efficiency that applies for CART. Bagging trees and Random Forest (RF) according to Prasad et al. (2006) perform even better than regression trees (RTs), but lack the open model structure and therefore interpretable models RTs provides. We chose RTs and RF for their many advantages over other statistical modelling approaches.

Quite a number of recent publications used RF in ecological modelling. Peters et al. (2007) applied RF to predict the vegetation type occurrence of groundwater-dependent vegetation types. Polishchuk et al. (2009) adopted it to predict aquatic toxicity. On the other hand, applications of RF within soil science are still scarce. Soil organic carbon concentrations, clay content and pH were predicted with RF (Grimm et al., 2008; Viscarra Rossel and Behrens, 2010). RTs on the other hand are widely applied. McKenzie and Ryan (1999) used them to predict soil properties from terrain attributes and gamma radiometric survey. Tittonell et al. (2008) analysed the influence of soil and crop management on maize productivity. And Park and Vlek (2002) compared RTs to other methods in predicting the three-dimensional soil variability. Eventually, McBratney et al. (2000) included regression tree analysis in their overview of pedometric techniques in soil survey.

For hydrological modelling and landslide risk estimation, the three-dimensional distribution of soil texture is a necessary input parameter. Soil texture influences soil cohesion, water storage capacity and water flow velocity and therefore hydraulic conductivity. The research area is situated in the tropical mountain forest area of the southern Ecuadorian Andes. The domain is influenced by landslides, so that material is shifted from its original position. During field work, we discovered frequent changes of sandy, silty or clayey parent material. Accordingly, on Materialses, subsoil horizons probably did not form from the same parent material as surface horizons. No map concerning bedrock is available. Accessibility of the area is very limited. The aim of this study was to provide insight whether surface processes have an influence on soil texture distribution within the study area. Furthermore, we wanted to find out whether it is possible to spatially predict soil texture from terrain attributes, although we must assume a strong influence from parent material and landslides also.

5.2   Material and methods

5.2.1   Research area

The research area is located in the southern Ecuadorian Andes, between the provincial capitals Loja and Zamora, within the catchment of the San Francisco River and comprises an area of c 26 km² between 1720 and 3160 m a.s.l. (Figure 5.1). Average annual rainfall increases from 2050 mm at 1960 m a.s.l. to c 4400 mm at 3100 m a.s.l. (Rollenbeck, 2006); average air temperature decreases from 19.4 to 9.4 °C (Fries et al., 2009).

Situated within the Podocarpus – El Condor Biosphere Reserve, the area is covered by mountain rainforest as well as subpáramo vegetation above the tree line. It is located on a biodiversity hotspot and therefore exhibits high tree species diversity. Homeier et al. (2002) described different forest types according to altitude a.s.l. and their position on mountain ridges or within side valleys.

The area is part of the Chiguinda unit (Zamora Series). Parent material is mostly highly weathered. It comprises metasiltstones, siltstones and quartzites which are intermixed with layers of phyllite and clay schists (Litherland et al., 1994). However, a detailed map of the spatial occurrence is not available. Liess et al. (2009) provided a first soil map and described Histosols and Stagnosols as dominating Reference Soil Groups associated with Umbrisols, Cambisols, Leptosols and Regosols (FAO, IUSS

Working Group WRB, 2007). Stagnic properties and thick organic layers, according to Ließ et al.[1], occur at the same positions within the soil-landscape. Accordingly, the whole area has at least a minor Stagnosol and Histosol probability. While the former is highest on slopes < 40° above 2146 m a.s.l., the latter accounts for 0.2 – 0.4 for most of the area and depends on hydrological parameters ([1]). The research area is represented by a digital elevation model (DEM) of 2 m accuracy (Liess et al., 2009).
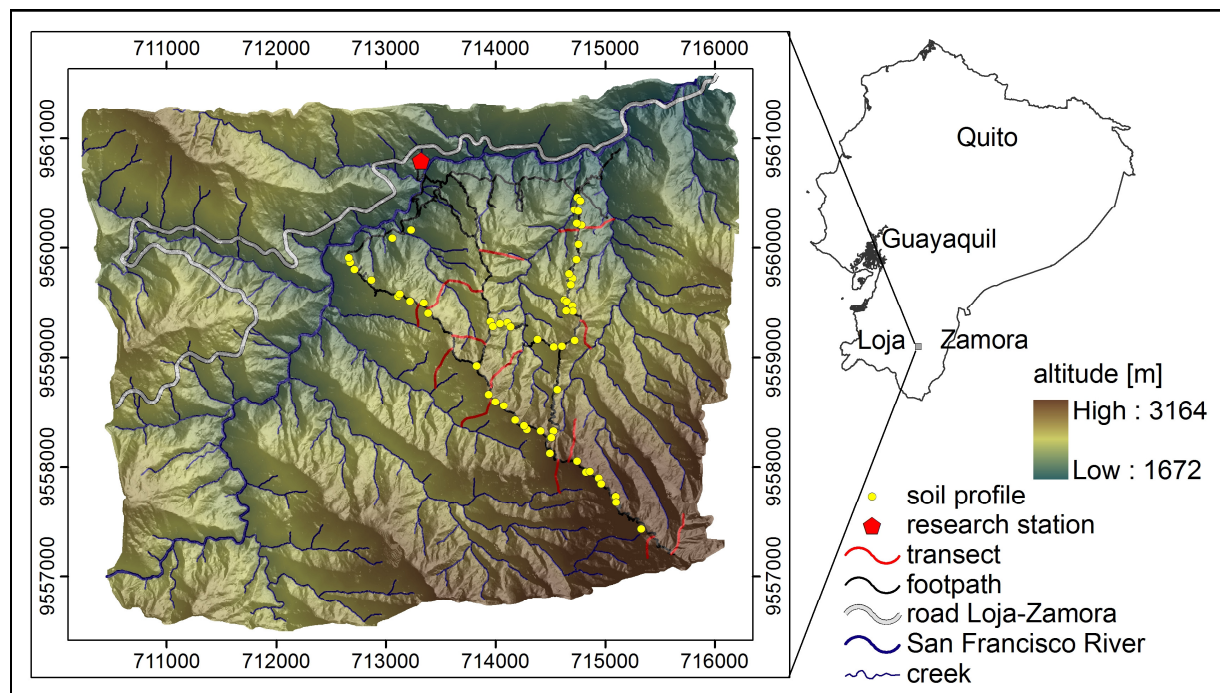
Figure 5.1: Research area. Position of soil profiles and auger sampling transects (adapted from Liess et al., 2009).

5.2.2 Soil dataset and positioning

Soil data was gained by 56 soil profiles (Figure 5.1) and 315 auger points until C horizon or bedrock. Sampling sites were selected according to a sampling design that includes 24 terrain classes formed by an overlay of 4 altitudinal, 3 slope and 2 aspect classes to guarantee a good cover and equal sampling extent throughout the landscape. Auger sampling was performed along transects (Figure 5.1) laid from mountain ridges towards side valley creeks. For a detailed description of the sampling design see Liess et al. (2009).

The dataset already carries some parameters describing its position, i.e. slope angle and aspect, whereas others have to be assigned from the GIS raster grids that were calculated from the DEM. The latter include altitude, profile and plan curvature, over-

---

[1] The occurrence probability of the WRB (FAO, IUSS Working Group WRB, 2007) Reference Soil Groups as well as the probability and thickness of the typical diagnostic horizons were predicted in earlier studies (European Journal of Soil Science, in review).

land flow distance to channel network (OFD) with Strahler order ≥ 5 as initiation threshold (Strahler, 1957) as well as the contributing area according to the Braunschweiger Digital Relief Model (BS CA) (Bauer et al., 1985) and the Kinematic Routing Algorithm (KRA CA) (Lea, 1992). Terrain parameters were assigned twofold to the sampling sites: (1) the nearest neighbour (n. n.) values and (2) the mean values within GPS accuracy radius. For a more detailed description of the GIS procedure and calculation algorithms see Liess et al. (2009).

5.2.3 Soil texture determination

Soil texture of the investigated soil profiles was determined by pipette, laser and field method. The precise laboratory analysis by pipette and laser was performed to include differences according to the method used for analysis. Soil texture particle size classes refer to 0 – 0.002 mm for clay, 0.002 – 0.063 mm for silt and 0.063 – 2 mm for sand.The much less precise determination in the field, according to the key to the soil textural classes from the Guidelines for Soil Description (FAO, 2006), was carried out in order to correct results from field analysis with laboratory data. In this way, soil texture could be regionalised based on the larger auger dataset which was analysed by field method only.

After sieving the oven dried samples (40°) to 2 mm, the sand fraction was gained by wet sieving after destroying organic matter and dispersion with sodium hexameta-phosphate. Silt and clay fractions were then analysed by pipette and laser method. The pipette method is a widely accepted sound technique in texture analysis. However, laser analysis is much faster, but depends on the instrument used for measurement. In order to make results from earlier investigations gained by laser analysis comparable to pipette measurement, we analysed with both methods. Furthermore, we investigated whether models adapted with laser texture as response variable, result better compared to those with pipette texture. Laser measurement was performed using a Master Sizer particle analyser from Malvern Instruments.

5.2.4 Regression tree and Random Forest

Regression trees (RTs) and Random Forest (RF) structure the above described dataset of terrain parameters and soil texture, to assign particular soil textures to typical landscape positions. Both models were implemented within the R-Project for

Statistical Computing software developed by Terry Therneau and Beth Atkinson (2003). RTs, first described by Breiman et al. (1984), were applied using the software package rpart; RF, based on Breiman and Cutler's Fortran code, was implemented by the package randomForest.

RTs subdivide the dataset most efficiently by a set of decision rules applied on the predictor variables to gain preferably homogeneous subgroups regarding the response variable. The rules are constructed by partitioning the dataset into successively smaller groups (nodes) with binary splits based on always one predictor variable. Tree splitting continues until the number of observations per end node is too small (less than 5 by default). Finally, the tree is pruned to avoid overfitting. Tenfold cross validation is applied by first separating the dataset into 10 subgroups, using 9 groups for tree construction and the 10th for error estimation. The optimal split is chosen in minimising the mean square error of the end nodes. This mean square error R in any node t with the number of observations n and the predicted mean value $\Box y$, is calculated by:

$$R(t) = 1/n(t) \cdot \sum_{i=1}^{n} \left[y_i(t) - \overline{y}(t) \right]^2 \tag{1}$$

The optimal split is found when the difference in R between the mother node and the left and right child node t_l and t_r

$$R(t) - \left[R(t_l) + R(t_r) \right] \tag{2}$$

is maximised. The mean of all data within a node is used for prediction purpose.

Random Forest (RF) is based on RT methodology. It differs, as it does not only grow a single tree, but a whole forest of trees. Furthermore, trees are grown without pruning (Breiman, 2001). However, tree diversity guarantees model stability. This is achieved by two means: (1) Choosing at random a subset of predictor variables to grow each tree and (2) growing each tree with a different random subsample and thereby varying the input dataset. Subsamples are drawn with replacement, i.e. bootstrapped (Efron, 1979). Trees are finally averaged for prediction purpose. Hence, the procedure involved in RF is called bootstrap aggregation (bagging).

One third of the cases is left out of the bootstrap sample and is not used in the construction of that particular tree. Other data are replicated to bring the sample to full size. The portion of the data drawn into the sample in a replication is known as the "in-bag" data. Correspondingly, the "Out-of-bag" data is used to estimate the generalization error. As forest size increases, this generalization error converges (Brei-

man, 2001). Consequently, while the number of trees is set sufficiently high (500), RFs do not overfit when more trees are added (Breiman, 2001, Peters et al. 2007). The size of the subset of variables – mtry – used to grow each tree, has to be selected by the user. It is a sensitive parameter determining model strength. By increasing mtry, the strength of each tree is growing, but at the same time correlation between trees increases also (Peters et al., 2007). Tree strength improves model performance, whereas correlation among trees weakens it. The optimal mtry can be determined by the function tuneRF, which is implemented within the R software package randomForest.

Although RF seems more of a "black box" approach compared to RT, since individual trees cannot be assessed, it still provides a means for interpretation, by giving measures for variable importance. The relative importance of the predictor variables is estimated based on how much worse the prediction would be if the data for that predictor were permuted randomly (Prasad et al., 2006).

Prasad et al. (2006) compared RTs and RF. Unfortunately, they based comparison on the training error and did not calculate it for an independent test dataset. To guarantee for a fair model comparison of RTs and RF, we compared 100 model runs with different Jackknife partitions of the data set by an external cross validation. Bishop and McBratney (2001) applied a similar approach to compare prediction methods. The known disadvantages of CART – (1) mean values are assigned to large areas with abrupt changes at their boundaries and (2) small changes in the dataset may lead to quite different tree structures – were overcome by applying the 100 models to the research area. Thus, model prediction is more differentiated and uncertainty in the prediction of soil texture's spatial distribution can be assessed by the mapped standard deviation of the prediction mean.

5.3   Results and discussion

5.3.1   Soil texture data

Figure 5.2 shows a ternary texture diagram displaying horizon data from 56 soil profiles analysed with pipette, laser and field method. Laser and pipette analyses assign most samples a texture of silt loam or loam and to a lesser extent of sandy loam. Texture results by Wilcke et al. (2003) and Bauer et al.[1] fall into the same range. In

---

[1] Personal communication. The manuscript was submitted to Journal of Hydrology.

contrast to this, field analysis determined samples nearly all as clay loam and therefore with higher clay and lesser silt content.
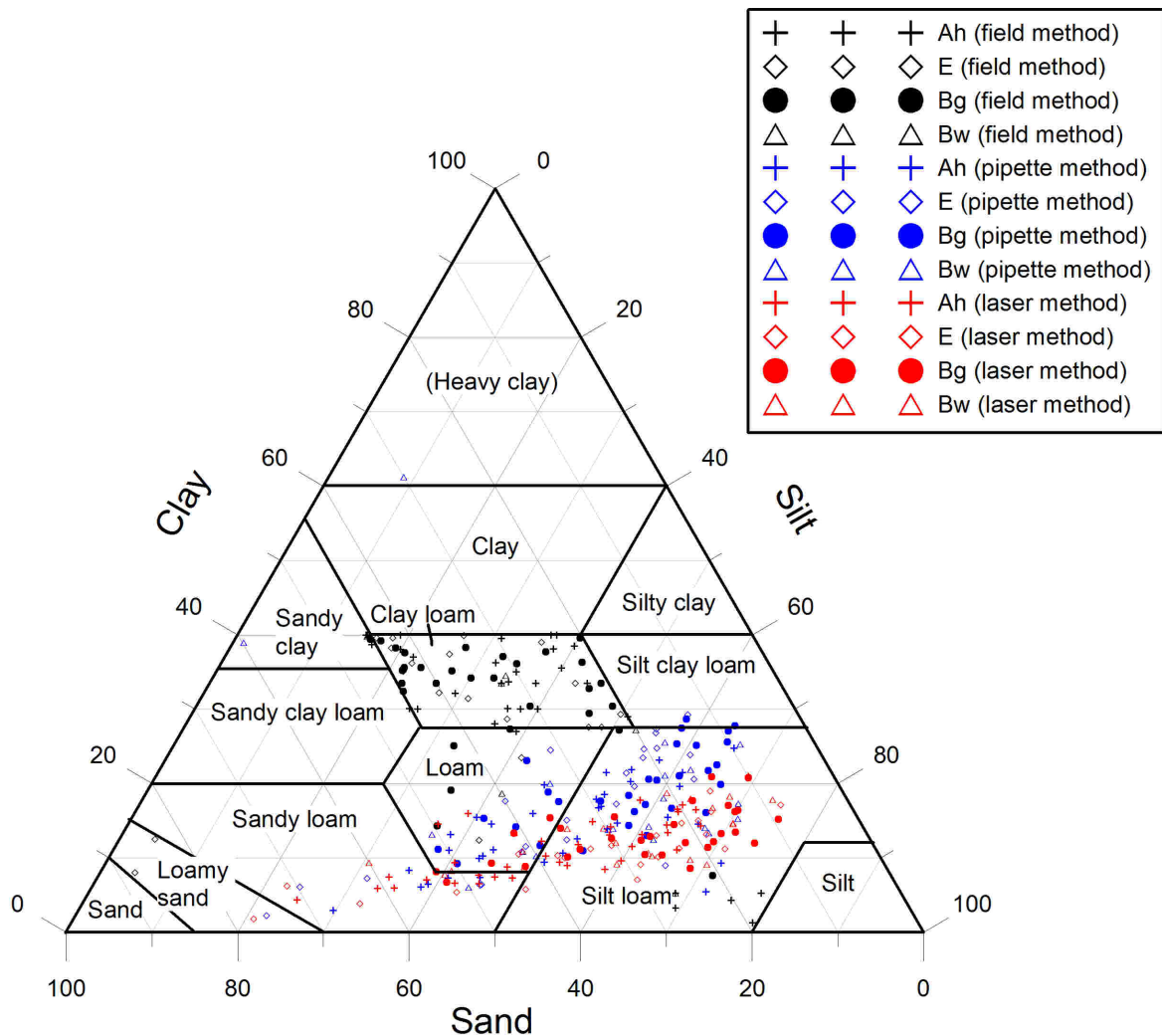
Figure 5.2: Soil texture ternary diagram. Texture determined by field, pipette and laser method. The data was grouped for the typical soil horizons.

The field method is based on the assumption that clay is cohesive, has a high plasticity and shows a shiny surface after squeezing between fingers (FAO, 2006). Silt in contrast is non-sticky and only weakly formable, has a rough and ripped surface and feels floury. However, the guidelines for soil description (FAO, 2006) state that the key for field soil texture class determination mainly works for soils having illite, chlorite and/or vermiculite composition. It therefore depends on mineralogical composition. Accordingly, soils containing smectite clays, may lead to an overestimation of clay content. We assume the latter to be the reason why we overestimated clay content in field determination of soil texture. Unfortunately, no data was available on clay mineral composition. However, clay contents, as determined by field method by other scientists working within the area (unpublished

results), were even higher and support this finding. As a consequence, we had to abstain from developing a transfer function and predict soil texture solely based on the smaller soil profile dataset.

Pipette and laser texture differed mainly in the lower clay and higher silt contents predicted by laser analysis (Figures 5.3). This is a well-known problem in texture analysis. Measurement of the clay size fraction by laser usually results in systematically lower percentages than those obtained by pipette method (Buurman et al., 2001). The difference itself mainly depends on the laser instrument used for analysis (Loizeau et al., 1994). But even if the same instrument is used, the relation among the two methods varies. Correlations depend on the material and the source areas. Furthermore, the relation may even change within one soil profile (Buurman et al., 2001). Hence, the establishment of a transfer function is not a trivial problem. Nevertheless, we adapted some simple linear regression equations to provide transfer relations for the research area, in order to make future results gained by laser method only comparable.
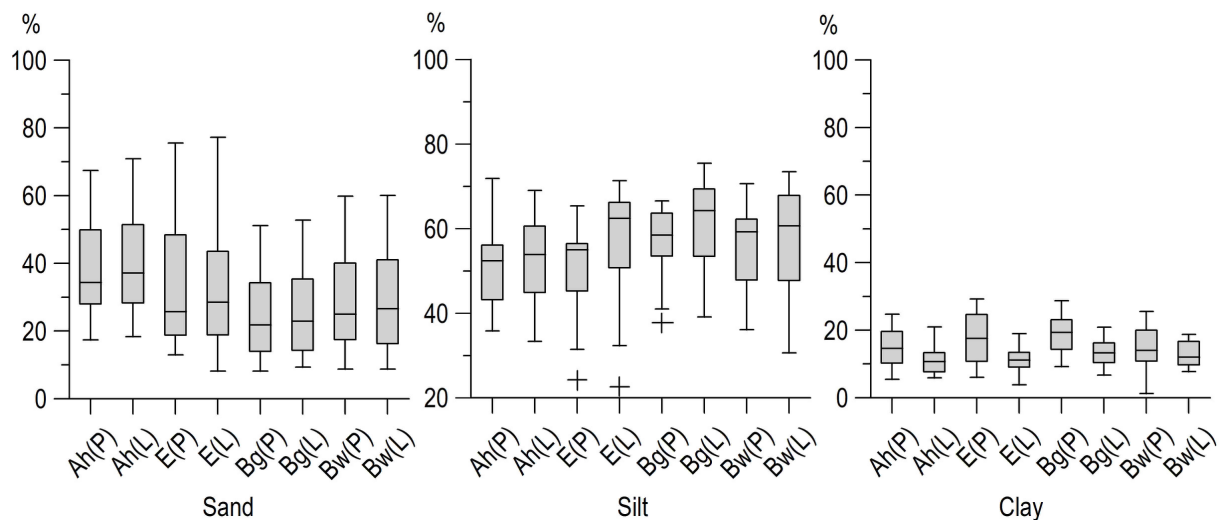
Figure 5.3: Comparison of horizon-wise soil texture, determined by pipette and laser method (P = pipette method, L = laser method).

Figure 5.4 shows the scatter plots with adapted linear regression equations and R^2. Sand contents determined by laser and pipette method differ only slightly, expressed by a very good R^2 of 0.98. Normally, sand contents should be exactly the same, since they are gathered by sieving before the remaining particles are measured by pipette or laser method. However, we realized that laser measurement assigned sand particle size to some additional percentage, what explains the difference. This is not surprising, since laser analysis on sand particles gives slightly coarser results compared to sieve analysis (Konert and Vandenberghe, 1997). Comparing silt results

from pipette and laser analysis, R^2 is still high with 0.8, but the adapted equation has a high intercept with 9.0%. Finally, R^2 of clay is the worst with only 0.44. This is due to the assumption of spherical particles by both methods. However, clay minerals are not spherical, but platy. Accordingly, clay minerals settle more slowly and therefore lead to an overestimation of clay by pipette method (Loveland and Whalley, 1991). On the other hand, laser method is known to underestimate clay content for the random orientation of the platy particles during measurement (Buurman et al., 1997). For the mentioned reasons, the transfer relations presented in Figure 5.4 have to be used with care.

$y = 0.96048x^{***} + 0.068$
$R^2 = 0.98$

$y = 0.80108x^{***} + 9.03518^{***}$
$R^2 = 0.80$

$y = 1.092x^{***} + 2.12$
$R^2 = 0.44$
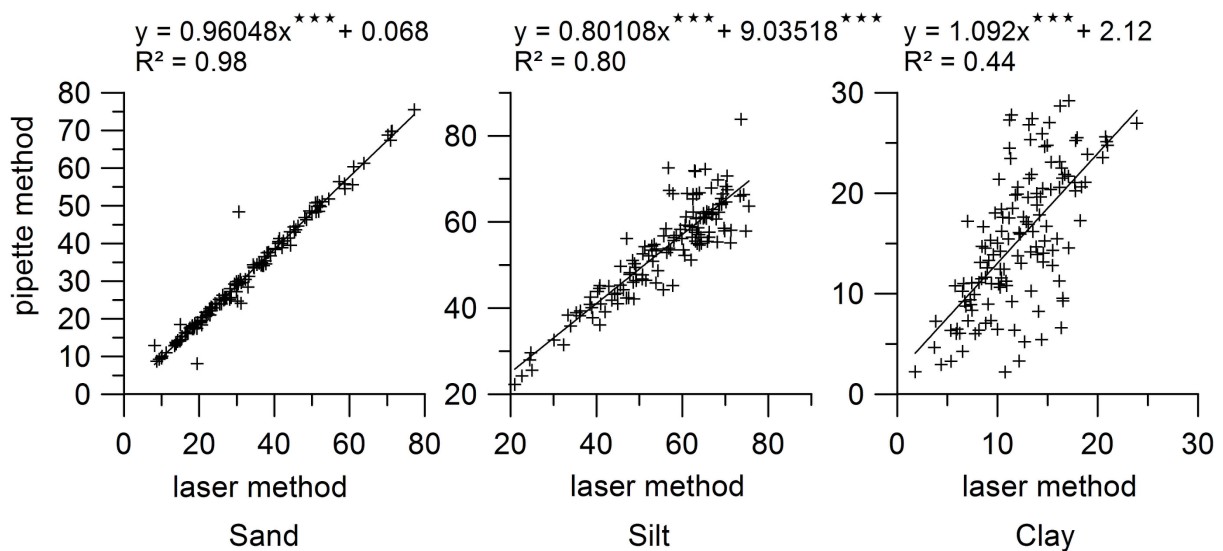
Sand

Silt

Clay

Significance codes: '★★★' 0.001, '★★' 0.01, '★' 0.05, '.' 0.1, ' ' 1

Figure 5.4: Linear relations between sand, silt and clay content from laser and pipette analysis.

In figure 5.3, the Ah horizon had the highest median for the sand and lowest for the silt fraction. For the sand fraction, differences in median are highest between Ah and Bg. While the data range for the silt fraction is rather equal between the horizons, it is much lower for Bg and Bw concerning the sand fraction. However, in general, differences between horizons are not sufficiently pronounced. Analysing soil horizon texture data with cluster analysis did not show any grouping by horizon. This is why we refrained from adapting models to predict soil texture in all typical horizons identified by Ließ et al.[1]. Instead, models were adapted to predict soil texture within the first and last soil horizon regardless of their characteristics, to investigate the hypothesis that soil texture within the research area is influenced by surface processes.

---

[1] The probability and thickness of the typical diagnostic horizons (FAO, IUSS Working Group WRB, 2007) were predicted in an earlier study (European Journal of Soil Science, in review).

5.3.2 Regression tree and Random Forest model performance

Eight models were constructed to predict sand, silt and clay content: The statistical models (a) RT and (b) RF were used to relate soil texture from (a) pipette and (b) laser analysis to (a) n. n. and (b) mean terrain values (2^3 models). To simplify, these models from now on are referred to as RT and RF pnn (pipette, n. n.), pm (pipette, mean), lnn (laser, n. n.) and lm (laser, mean) models.

Whenever a statistical model is constructed, model structure differs a bit. The RT subdivides the dataset each time differently for the calculation of the cross validation error which serves to choose the optimal tree. RF is influenced similarly by boot-strapping and selecting the subset of predictor variables for each tree of the forest. It is therefore difficult, to compare single model runs of RT with RF. Hence, we con-structed each model a hundred times with random Jackknife partitions, ⅔ of the dataset, and then performed an external cross validation with the rest. Pearson's correlation coefficient (r_{xy}) distributions were calculated as model quality estimate for each model. Their histograms are presented in Figure 5.5.

RF model performance was better than that of RTs. Though, considering the mode of the adapted Gaussian distribution curve, this picture was not so clear concerning models to predict clay content. On the one hand, Pnn and Pm RF models were better than their corresponding RT models. However, the opposite was true with respect to Lnn and Lm models. No clear decision could be obtained whether prediction from n. n. or mean terrain values was better. In order to better compare these results, we calculated some basic statistics of the r_{xy} distributions, which are displayed in Table 5.1. It makes a comparison of the r_{xy} distributions of the eight models, calculated to predict sand, silt and clay content each. Boxes in the table indicate the best of these eight models within the respective statistical category. RF Pm sand and clay models performed best considering the mean value of the r_{xy} distribution, whereas for silt, the RF model Lm performed best. Taking a look at the median and 75% quartile, RF Lm sand and silt models were best. Interestingly, from the clay models a RT model, Lm, performed better than the respective RF model. This model also stands out in reaching the overall best median, 0.47, among all models. However, in order to predict soil texture we need at least two texture classes. For this reason, we have to stick with choices where we have good models for at least two texture classes within the same model category Pm, Pnn, Lm or Lnn of RT or RF. This left us the choice between RF Pm and RF Lm. We chose Pm, the model with the highest mean r_{xy}.
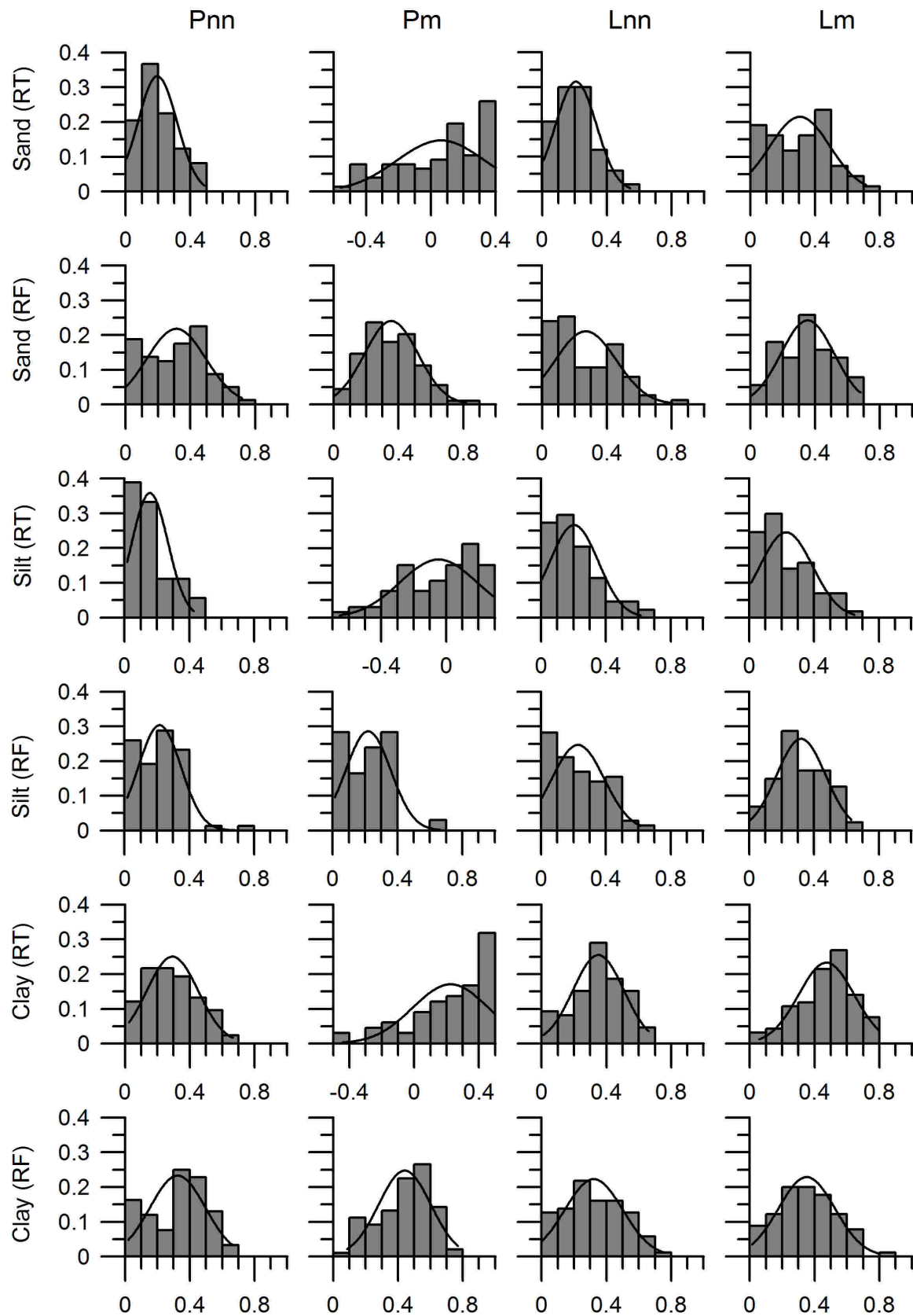
Figure 5.5: Histograms from Pearson's correlation coefficients gained from hundredfold external cross validation for RT and RF models to predict topsoil texture with adapted Gaussian distribution curves. X-value = Pearson's r_{xy}, Y-value = relative frequency.

Table 5.1: Summary of Pearson's r_{xy} distributions per soil texture model from Figure 5.5, 1st soil horizon

texture class	model	mean ± std. dev.	min	25% quartile	median	75% quartile	max
sand	RT Pnn	-0.012 ± 0.251	-0.733	-0.183	-0.005	0.171	0.485
	RF Pnn	0.229 ± 0.241	-0.526	0.037	0.240	0.431	0.719
	RT Pm	0.148 ± 0.298	-0.560	-0.070	0.198	0.390	0.634
	RF Pm	0.297 ± 0.229	-0.372	0.189	0.303	0.447	0.818
	RT Lnn	-0.003 ± 0.261	-0.711	-0.169	0.008	0.206	0.540
	RF Lnn	0.174 ± 0.236	-0.259	-0.001	0.144	0.330	0.803
	RT Lm	0.138 ± 0.305	-0.501	-0.093	0.144	0.405	0.714
	RF Lm	0.290 ± 0.245	-0.535	0.168	0.332	0.478	0.677
silt	RT Pnn	-0.059 ± 0.202	-0.527	-0.190	-0.086	0.080	0.424
	RF Pnn	0.110 ± 0.223	-0.564	-0.010	0.128	0.281	0.750
	RT Pm	0.111 ± 0.314	-0.659	-0.115	0.150	0.384	0.674
	RF Pm	0.090 ± 0.232	-0.544	-0.041	0.083	0.275	0.662
	RT Lnn	-0.027 ± 0.256	-0.730	-0.193	-0.052	0.132	0.612
	RF Lnn	0.112 ± 0.238	-0.468	-0.027	0.113	0.266	0.615
	RT Lm	0.075 ± 0.235	-0.424	-0.049	0.056	0.222	0.647
	RF Lm	0.264 ± 0.204	-0.323	0.150	0.267	0.408	0.630
clay	RT Pnn	0.219 ± 0.225	-0.409	0.086	0.241	0.384	0.664
	RF Pnn	0.292 ± 0.199	-0.183	0.110	0.323	0.437	0.658
	RT Pm	0.356 ± 0.271	-0.445	0.200	0.434	0.554	0.872
	RF Pm	0.431 ± 0.177	-0.180	0.323	0.469	0.558	0.771
	RT Lnn	0.280 ± 0.245	-0.560	0.160	0.344	0.452	0.658
	RF Lnn	0.266 ± 0.223	-0.320	0.107	0.277	0.441	0.756
	RT Lm	0.425 ± 0.252	-0.500	0.323	0.472	0.585	0.794
	RF Lm	0.302 ± 0.225	-0.320	0.170	0.331	0.445	0.802

std. dev. = standard deviation, RT = Regression tree, RF = Random Forest, P = pipette method, L = laser method, nn = nearest neighbour terrain values, m = mean terrain values

Models from mean terrain parameter values performed better than their counterparts from n. n. values with one exception, the RF silt models Pnn and Pm. However, regarding model performance it did not matter whether pipette or clay texture was used in model construction. Overall model performance was not bad considering maximum r_{xy} values of up to 0.87 (RT Pm) and above 0.6 for all RF models. Though, the wide range of r_{xy} showed that it is not enough to consider only one model run to really estimate model performance. Considering the mean and median of the model evaluated as best, RF Pm, sand reached an r_{xy} of 0.3 and clay 0.4 (median = 0.5). This is rather poor and standard deviation with 0.2 is high. Thompson et al. (2006) compared models to predict soil texture established for different areas and found r_{xy} ranging from 0.33 – 0.67, in dependence on the investigated area. Our models, explaining 30 – 40% of the variation in topsoil texture, are within the same performance range. In conclusion, dependence of topsoil texture on terrain attributes cannot be neglected. Though, the latter can explain the spatial texture distribution only in some respects.

To find out whether the relation between soil texture and terrain parameters can be attributed to soil surface processes like topsoil surface parallel water movement, and not only to parent material, a model to relate the soil texture in the last soil horizon to terrain parameters was also developed. Since profiles were excavated until bedrock or C horizon, this last soil horizon mostly refers to a C/B or C horizon. Figure 5.6 and Table 5.2 give a model performance overview.

The RT Pm model performance with a mode of the r_{xy} distribution ≤ 0 shows, that dependence of subsoil texture on terrain parameters can be neglected. However, the performance of the corresponding model for the 1st soil horizon was not much better. Nevertheless, the modes of the r_{xy} distribution for the last horizon are generally lower than those of the first horizon. Taking a look at the statistical summary in Table 5.2, this finding is even more pronounced by best r_{xy} mean and median values for sand and silt of 0.1. Clay model performance looked slightly better with r_{xy} = 0.2 (mean) and 0.25 (median) for the overall best model RF Lnn.

Table 5.2: Summary of Pearson's r_{xy} distributions per soil texture model from Figure 5.6, last soil horizon

texture class	model	mean ± std. dev.	min.	25% quartile	median	75% quartile	max.
sand	RT Pnn	0.006 ± 0.211	-0.578	-0.148	0.022	0.138	0.512
	RF Pnn	0.130 ± 0.183	-0.323	0.009	0.124	0.247	0.574
	RT Pm	-0.058 ± 0.226	-0.670	-0.202	-0.049	0.123	0.338
	RF Pm	-0.054 ± 0.226	-0.505	-0.223	-0.093	0.086	0.513
	RT Lnn	-0.013 ± 0.225	-0.554	-0.174	-0.009	0.140	0.442
	RF Lnn	0.080 ± 0.223	-0.433	-0.066	0.074	0.243	0.527
	RT Lm	-0.058 ± 0.204	-0.525	-0.187	-0.062	0.103	0.464
	RF Lm	-0.066 ± 0.199	-0.591	-0.213	-0.058	0.071	0.423
silt	RT Pnn	0.072 ± 0.277	-0.550	-0.142	0.128	0.272	0.602
	RF Pnn	0.067 ± 0.201	-0.358	-0.083	0.097	0.221	0.489
	RT Pm	0.052 ± 0.239	-0.620	-0.129	0.069	0.232	0.459
	RF Pm	-0.014 ± 0.208	-0.547	-0.145	0.005	0.120	0.450
	RT Lnn	-0.035 ± 0.236	-0.584	-0.196	-0.018	0.149	0.496
	RF Lnn	-0.005 ± 0.194	-0.474	-0.126	0.034	0.143	0.368
	RT Lm	-0.057 ± 0.253	-0.634	-0.202	-0.049	0.130	0.407
	RF Lm	-0.128 ± 0.200	-0.653	-0.249	-0.129	0.002	0.395
clay	RT Pnn	0.065 ± 0.219	-0.617	-0.082	0.082	0.227	0.559
	RF Pnn	0.012 ± 0.212	-0.509	-0.118	0.020	0.132	0.481
	RT Pm	-0.034 ± 0.234	-0.588	-0.211	0.002	0.146	0.496
	RF Pm	-0.122 ± 0.196	-0.489	-0.263	-0.118	0.037	0.299
	RT Lnn	0.024 ± 0.226	-0.520	-0.119	0.057	0.154	0.551
	RF Lnn	0.208 ± 0.229	-0.439	0.063	0.247	0.376	0.621
	RT Lm	0.030 ± 0.275	-0.600	-0.145	0.051	0.192	0.633
	RF Lm	0.090 ± 0.210	-0.410	-0.038	0.101	0.245	0.510

std. dev. = standard deviation, RT = regression tree, RF = Random Forest, P = pipette method, L = laser method, nn = nearest neighbour terrain values, m = mean terrain values
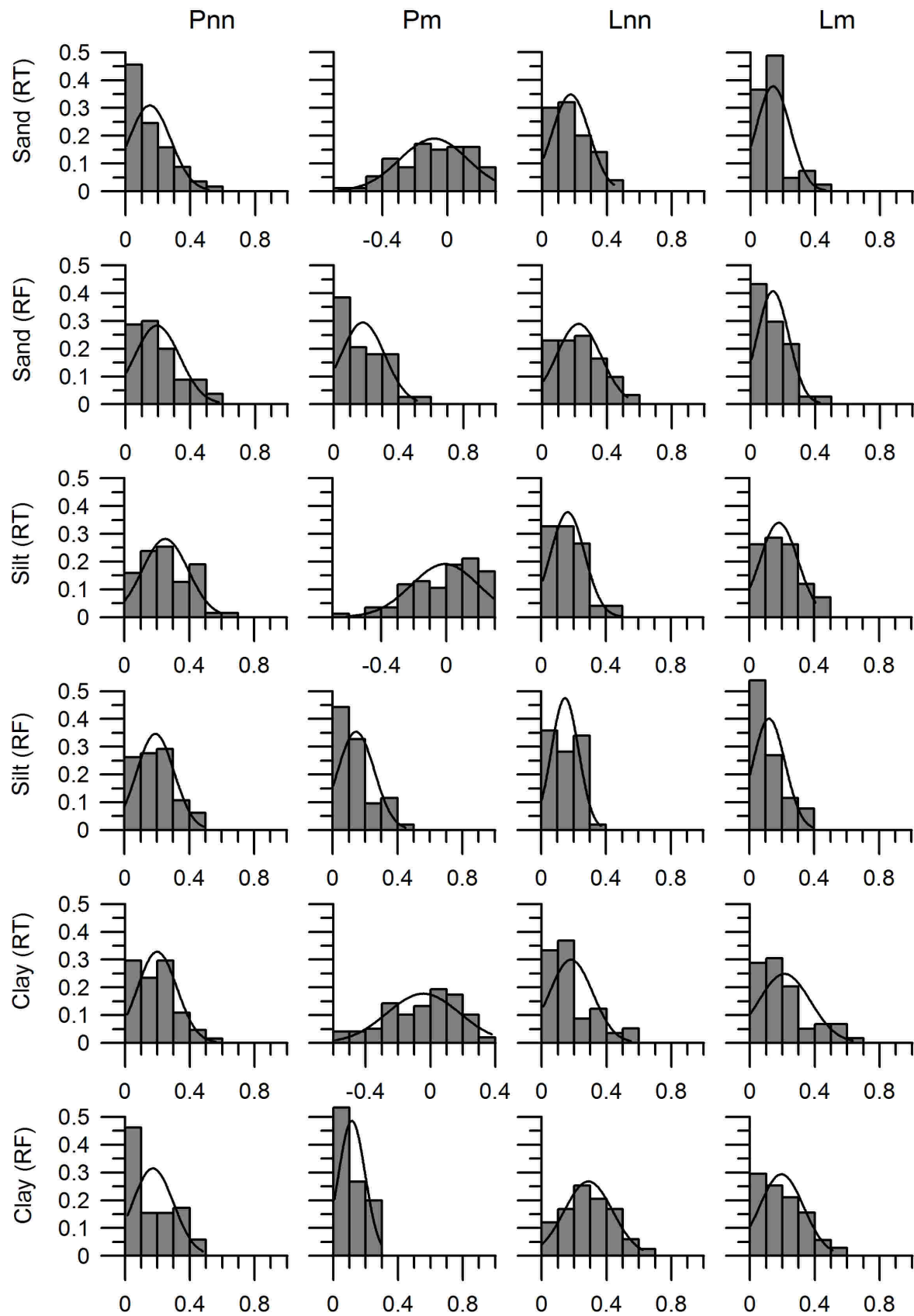
Figure 5.6: Histograms from Pearson's correlation coefficients gained from hundredfold external cross validation for RT and RF models to predict subsoil texture with adapted Gaussian distribution curves. X-value = Pearson's r_{xy}, Y-value = relative frequency.

Wilcke et al. (2008), who worked in a small subcatchment of the research area, did not find any systematic spatial change in subsoil texture either, but good correlations between topsoil texture and altitude. Henderson et al. (2005) predicted topsoil and subsoil clay content Australia-wide from terrain parameters by a decision-tree methodology similar to RTs, and equally reached a model performance of r_{xy} = 0.2 for subsoil and 0.4 for topsoil. Likewise, dependence of subsoil texture on terrain parameters was much less pronounced than for topsoil. This is not amazing since in general topsoil properties are better related to terrain parameters than subsoil properties (Park and Burt, 2002). Consequently, we assume that the better model performance regarding topsoil texture prediction can be attributed to surface processes.

As mentioned already, terrain parameters can explain the spatial distribution of soil texture only to a limited extend. Parent material has to be considered as an important predictor parameter. Therefore, material from the C and R horizon was cross-checked for its influence on soil texture which has to be neglected. However, we found strong evidence that most probably topsoil horizons did not form from the parent material underlying the soil profile. Bedrock changes within short distance and often within one soil profile. In addition, landslides are another important impact factor. They have a strong influence on soil-landscape formation in shifting soil and rock material.

Another reason for the poor model performance and the high standard deviation in particular has to be seen in the small dataset of only 56 soil profiles. This was not the initial plan, but unfortunately we could not make use of the larger auger data set. Nevertheless, so far no other statistical model was adapted to predict soil texture within this particular area and no other digital soil map is available. Therefore, we will still apply the best model to predict topsoil texture and discuss terrain influences.

5.3.3   Soil texture model and digital soil maps

Figure 5.7 gives an overview of the variable importance (VI) regarding the best model RF Pm, displaying the histograms of the VI of the 100 model runs. A VI of ≤ 0 indicates that a variable is of no importance in model construction. To get a better overview regarding the variables' importance, we rather refer to the statistical summary of the VI distribution in Table 5.3 (sand) and 5.4 (clay). Considering the mean and median, altitude had the highest overall VI for the sand and clay model.

Apart from this, aspect and plan curvature (pl.curv) were important as well. Aspect even had the highest 75% quartile and maximum after altitude. But since also all other variables reached maximum values of 4.6 to 8.8, we cannot neglect their influence. This also applies to the clay model. The latter's main difference is the higher importance of the OFD.
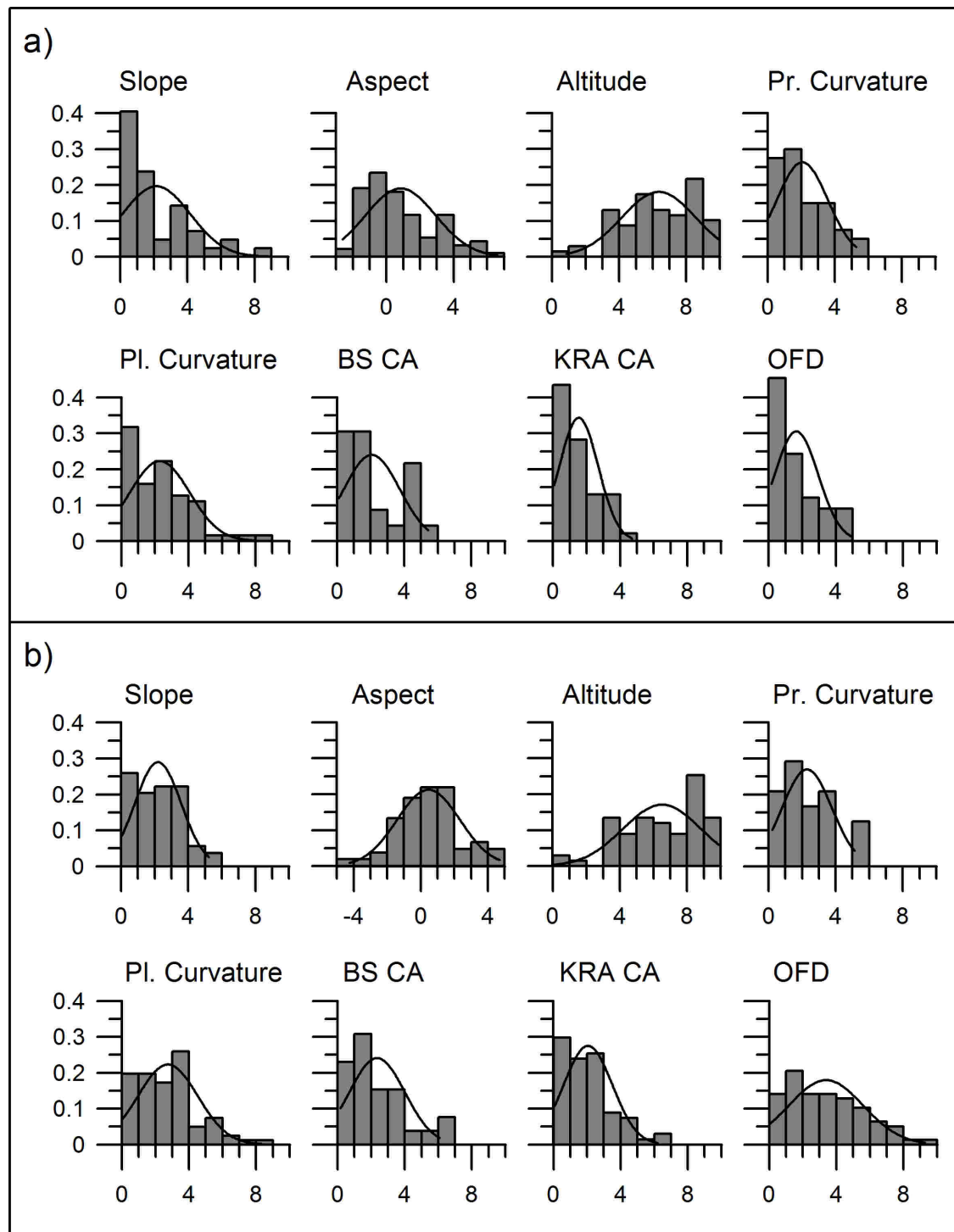

Figure 5.7: Variable importance histograms for the RF model Pm to predict topsoil texture. a) Model to predict sand content, b) model to predict clay content. Variable importance measure "% increase in mean square error" on X and relative frequency on Y axis (Pr. = Profile and Pl. = Plan).

Table 5.3: Variable importance statistics of histograms from Figure 5.7a, sand content

variable	mean ± std. dev.	minimum	25% quartile	median	75% quartile	maximum
slope	-0.008 ± 2.402	-6.065	-1.418	-0.721	0.971	8.765
aspect	1.279 ± 2.675	-2.626	-0.674	0.580	2.935	10.130
altitude	7.822 ± 3.449	-0.874	5.382	8.076	10.199	16.499
pr.curv	-0.666 ± 2.608	-4.771	-2.864	-1.165	1.242	5.245
pl.curv	0.871 ± 2.422	-4.638	-0.913	0.633	2.550	8.027
BS CA	-1.111 ± 2.203	-6.069	-2.642	-1.335	-0.171	5.437
KRA CA	0.075 ± 1.676	-3.208	-1.055	-0.050	1.065	4.696
OFD	-0.878 ± 2.146	-4.657	-2.437	-1.155	0.487	4.988

pr./ pl.curv=profile/ plan curvature, BS CA/ KRA CA = contributing area according to Braunschweiger Digital Relief Model/ kinematic routing algorithm, OFD = overland flow distance

Table 5.4: Variable importance statistics of histograms from Figure 5.7b, clay content

variable	mean ± std. dev.	minimum	25% quartile	median	75% quartile	maximum
slope	0.284 ± 2.294	-4.982	-1.158	-0.006	2.052	5.195
aspect	0.548 ± 1.927	-4.242	-0.640	0.464	1.438	5.878
altitude	8.857 ± 3.584	0.017	6.163	8.663	11.251	18.246
pr.curv	-1.238 ± 2.218	-5.761	-2.711	-1.688	-0.340	5.124
pl.curv	1.887 ± 2.595	-3.843	0.073	1.881	3.403	10.588
BS CA	-1.053 ± 2.295	-4.888	-2.515	-1.301	-0.034	6.070
KRA CA	0.816 ± 1.948	-3.241	-0.936	0.826	2.085	6.199
OFD	2.274 ± 3.021	-3.982	0.000	1.912	4.517	10.351

pr./ pl.curv=profile/ plan curvature, BS CA/ KRA CA = contributing area according to Braunschweiger Digital Relief Model/ kinematic routing algorithm, OFD = overland flow distance

Because of the excessive computation and limited R software memory size, DEM precision had to be reduced from 2 to 20 m cell size for model application. Surface horizon soil texture (sand and clay) was predicted by the best model RF Pm. Silt content was assigned as missing proportion to 100%. We already showed that model variability within each model run lead to a differing variable importance (Figure 5.7). Accordingly, not only one RF Pm model was applied to the research area, but the 100 models, which are each based on a different ⅔ subsample of the dataset. The maps of the sand, silt and clay contents in Figure 5.8 therefore display the mean of the 100 predictions as well as the standard deviation as prediction uncertainty. Figures 5.8b, d and f show the standard deviation of the sand (b), silt (d) and clay (f) contents. Regarding clay content it was mostly between 1 and 2% and in some parts even below 1%. In comparison to this, sand content standard deviation was mostly ≥ 2% and partly even ≥ 4%. However, comparing Figure 5.8a and b, it equally rises with sand content mean.
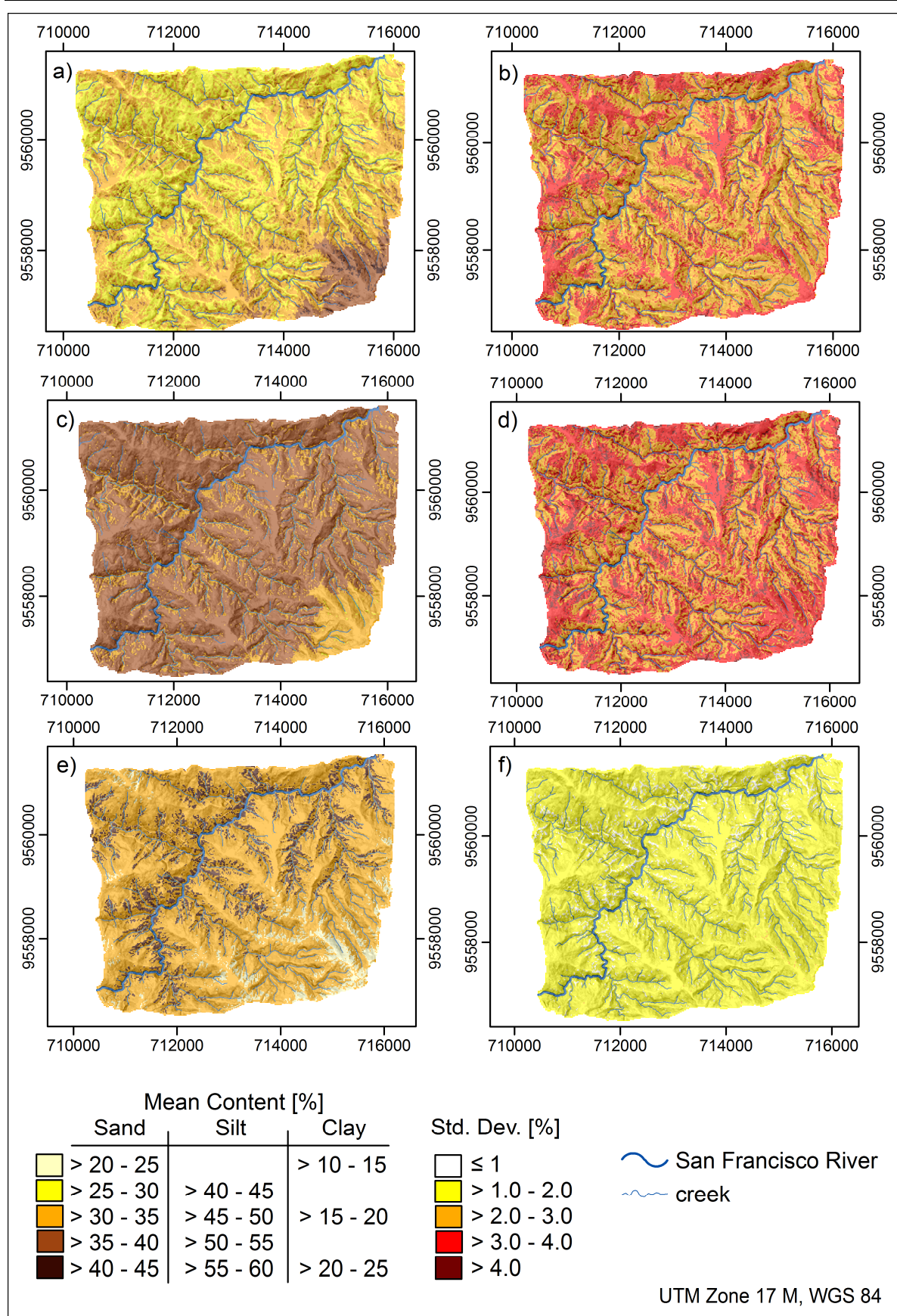
Figure 5.8: Soil texture maps of the research area gained by soil data extrapolation with statistical model Random Forest Pm: a) mean sand content, b) sand content standard deviation, c) mean silt content, d) silt content standard deviation, e) mean clay content, f) clay content standard deviation (Overlaid hillshading with light source from north-east).

The variables' importance in influencing soil texture was described in Figure 5.7. Altitude was distinguished as most important variable in predicting both, sand and clay contents. Nevertheless, we still do not know in which way terrain parameters influence soil texture. In order to understand why sand, silt and clay contents are higher or lower in specific areas, sand and clay content classes formed for map generalisation (Figure 5.8) were used to calculate the class mean and standard deviation regarding the model's input terrain parameters for the covered area. Silt was disregarded since its percentage was calculated from the other two. Of course, texture variation exists within these classes also, so that only a tendency can be described.

Sand content rises with mean altitude from class 1 to 5 (Table 5.5), whereas clay content decreases (Table 5.6). The higher sand content above c 2750 m a.s.l. is clearly visible in the south-eastern summit in Figure 5.8a. In conclusion, it is the reason for the lower silt content in the same area also (Figure 5.8c), 45 – 50% compared to 50 – 55% for most of the remaining area. Mean aspect for the lowest sand content class is significantly lower than for the other classes. However, in the map (Figure 5.8a) this influence is hardly visible because class 1 corresponds to only 0.028 km² (7 grid cells). Slope mean, 10 ± 5° compared to > 30°, and the mean contributing area (KRA CA) are also lower in sand content class 1 compared to the other classes. In general, sand content increases with slope and OFD, whereas curvature shows a tendency in that higher sand contents are to be found rather on concave curvature with the exception of class 1 considering profile curvature.

Table 5.5: Mean variable values and standard variation for sand content classes from Fig. 5.8

	Class 1	Class 2	Class 3	Class 4	Class 5
sand content [%]	20 - 25	25 - 30	30 - 35	35 - 40	40 - 45
area size [km²]	0.0028	11.51	12.12	2.20	0.14
altitude [m]	2001 ± 107	2175 ± 197	2262 ± 240	2636 ± 332	2890 ± 112
aspect [°]	116 ± 31	175 ± 97	193 ± 126	196 ± 130	189 ± 149
slope [°]	10 ± 5	31 ± 10	35 ±10	37 ± 10	40 ± 8
pr.curv	0.0008 ± 0.0023	0.0050 ± 0.0101	-0.0035 ± 0.0179	-0.0084 ± 0.0207	-0.0089 ± 0.0156
pl.curv	0.0081 ± 0.0018	0.0077 ± 0.0141	-0.0051 ± 0.0185	-0.0085 ± 0.0203	-0.0165 ± 0.0202
BS CA [m²]	2670 ± 3589	4655 ± 19285	9462 ± 31790	7262 ± 26833	7051 ± 18895
KRA CA [m²]	3429 ± 5379	58051 ± 952912	153834 ± 1372487	30862 ± 408074	10093 ± 23585
OFD [m]	138 ± 70	212 ± 151	246 ± 199	282 ± 224	422 ± 225

pr.curv = profile curvature, pl.curv = plan curvature, BS CA/ KRA CA = contributing area according to the Braunschweiger Digital Relief Model/ kinematic routing algorithm, OFD = overland flow distance

Table 5.6: Mean variable values and standard deviation for clay content classes from Fig. 5.8

	Class 1	Class 2	Class 3
clay content [%]	10 – 15	15 – 20	20 – 25
area size [km²]	1.32	21.67	2.97
altitude [m]	2695 ± 219	2257 ± 249	2078 ± 162
aspect [°]	185 ± 138	186 ± 116	180 ± 94
slope [°]	36 ± 10	34 ± 11	31 ± 7
pr.curv	-0.0013 ± 0.0132	-0.0008 ± 0.0166	0.0043 ± 0.0114
pl.curv	-0.0093 ± 0.0162	-0.0007 ± 0.0185	0.0113 ± 0.0101
BS CA [m²]	3234 ± 7813	7762 ± 28272	4267 ± 16790
KRA CA [m²]	4452 ± 9663	112667 ± 1196954	51736 ± 941869
OFD [m]	435 ± 191	238 ± 183	126 ± 70

pr.curv = profile curvature, pl.curv = plan curvature, BS CA/ KRA CA = contributing area according to the Braunschweiger Digital Relief Model/ kinematic routing algorithm, OFD = overland flow distance

Higher clay contents (Table 5.6) were found with decreasing altitude and on convex compared to concave curvature (pr.curv, pl.curv), on lower slope angle and closer to the channel network. The influences of altitude and OFD are also visible in Figure 5.8e. To summarize, sand content increases with increasing altitude, aspect, slope and OFD, displaying the highest sand contents on concave curvature, whereas clay content decreases with increasing altitude, slope and OFD, showing the highest clay contents on convex curvature.

Wilcke et al. (2008) already described a strong dependence of soil texture on altitude for the research area, expressed by a good positive correlation between altitude and sand content and negative regarding clay content. We found a VI of up to 10% for altitude in predicting soil texture and would not consider this strong. However, it has to be mentioned that the altitudinal transect Wilcke et al. (2008) investigated, comprises only a small subcatchment from 1880 to 2100 m a.s.l. Ziadat (2005) argued that the very small correlations of little significance between terrain factors and soil properties he found, could be attributed to the size of the research area. Consequently, he gained better results for smaller subcatchments of the same area. Gessler et al. (2000) explained the increase in sand content with altitude they discovered with the combination of down-profile and downslope removal of finer particles. This is rather logical and would explain not only higher sand/ clay ratios with altitude, but also with increasing slope angle and distance to the creeks. On the other hand, this would rather lead us to expect a higher sand/ clay ratio on convex and not on concave curvature, i.e. the contrary to our results regarding the dependence of soil texture on curvature. Hence, Gessler et al. (2000) and Pachepsky et al. (2001) in contrast to our findings described higher sand/ clay or sand/ silt ratios

on convex curvature. Accordingly, Martin and Timmer (2006) stated that in their investigation the largest spatial differences were those associated with the movement of water and soil particles from divergent shoulder positions to level or convergent landforms. Removal of finer particles from the more exposed convex positions would lead to their accumulation in concave positions. On the other hand, our results regarding the influence of terrain curvature on soil texture are not new. Brown et al. (2004) also predicted increasing sand contents in converging areas for poorly drained yellow grey soils in Uganda. Furthermore, they described this texture contrast to be reduced or even inverted on fine scale convexities. Hence, they proposed curvature influence on soil texture to be scale dependent. According to Liess et al. (2009,[1]), soils with a stagnic colour pattern are also of major importance within the research area, if not the most dominant soil types while neglecting organic layer thickness. Many scientists working within the area, assumed slope parallel subsurface flow in stagnic soils. Hydromorphic soil colours at the soil surface beneath a thick organic layer even on steep slopes ([1]), give further evidence for this argumentation. After all, Bauer et al.[2], who investigated soil hydrological flow paths within the research area, provided proof of a shallow subsurface flow within the E horizon (first horizon) of stagnic soils. Again, Stagnosol probability and stagnic horizon thickness increase with altitude ([1]). Removal of finer particles from > c 2750 m a.s.l. can be explained by the more exposed positions with shrub vegetation compared to forest at lower altitude, while at the same time the rainfall gradient increases (Rollenbeck, 2006). Fine scale convexities are obviously not influenced by this subsurface flow.

5.4   Conclusions and outlook

We found proof that all terrain factors considered in the analysis indeed influence soil texture of the surface horizon within the research area. Shallow subsurface flow as proposed by Bauer et al. ([2]), leads to increasing sand/ clay ratios with increasing altitude, on steep slopes and with overland flow distance to the channel network by removing finer particles downslope directly underneath the soil surface. The deeper soil layers, on the other hand, are not influenced by this shallow subsurface flow and

---

[1] The occurrence probability of the Word Reference Base (FAO, IUSS Working Group WRB, 2007) Reference Soil Groups and the probability and thickness of the typical diagnostic horizons were predicted in earlier studies (European Journal of Soil Science, in review).
[2] Flow paths in soils of landslide affected and unaffected hillslopes were investigated within our working group also. The manuscript was submitted to Journal of Hydrology.

therefore do not show the same texture properties. Curvature seemed to have the opposite effect on soil texture compared to that predicted by most other authors and cannot be explained by the shallow subsurface flow. Though, it might be attributed to the small scale curvature used in our calculations. Consequently, analysing the influence of terrain curvature, calculated on different scales, is part of future research plans.

The RF model that uses mean terrain parameter values and pipette texture performed best; it explained 30 – 40% of the variation in topsoil texture. Model performance might be related to the size of the study area as proposed by Ziadat (2005). Consequently, a more detailed dataset regarding each of the subcatchments might confirm this idea. We tried to provide such a dataset by sampling along transects (auger dataset), but unfortunately could not make use of it. However, the digital soil texture maps, that include prediction uncertainty through the standard deviation calculated from the 100 model runs, provide a sound basis for further modelling approaches.

Linear regression equations relating laser to pipette texture were established for the research area. Texture analysis by field method according to the guidelines for soil description (FAO, 2006) did not provide satisfying results. The field method would need adaptation in order to make its use in the research area reasonable. While this is not the case we recommend refraining from using it.

5.5 Acknowledgements

5.6 References

Bauer, F., Vinan, P., Balcazar, L., Bogner, C., Huwe, B., 2010a. Flow paths in soils of landslide affected and unaffected hillslopes in a montane rainforest of South Ecuador, part A. submitted to Journal of Hydrology

Bauer, F., Balcazar, L., Vinan, P., Bogner, C., Zeilinger, J., Huwe, B., 2010b. Flow paths in soils of landslide affected and unaffected hillslopes in a montane rainforest of South Ecuador, part B. submitted to Journal of Hydrology

Bauer, J., Rohdenburg, H., Bork, H.-R., 1985. Ein digitales Reliefmodell als Vorraussetzung für ein deterministisches Modell der Wasser- und Stoff-Flüsse. In: Bork, H.- R., Rohdenburg, H. (Eds.). Landschaftsgenese und Landschaftsökologie H. 10, Parameteraufbereitung für deterministische Gebiets-Wassermodelle, Grundlagenarbeiten zur Analyse von Agrar-Ökosystemen, p. 1 – 15.

Bishop, T. F. A., McBratney, A. B., 2001. A comparison of prediction methods for the creation of field-extent soil property maps. Geoderma 103: 149 – 160.

Bishop, T. F. A., Minasny, B., 2006. Digital Soil-Terrain Modeling: The Predictive Potential and Uncertainty. In: Grunwald, S. (Ed.) Environmental Soil-Landscape Modeling. CRC Press, Boca Raton.

Breimann, L., Friedmann, J. H., Olshen, R. A., Stone, C. J., 1984. Classification and regression trees, CRC press, Wadsworth.

Breiman, L., 2001. Technical Report for Version 3. http://oz.berkeley.edu/users/ breiman/randomforest2001.pdf (Access: 28/04/2010).

Brown, D. J., Clayton, M. K., McSweeney, K., 2004. Potential terrain controls on soil color, texture contrast and grain-size deposition for the original catena landscape in Uganda. Geoderma 122: 51 – 72.

Bussmann, R. W., Wilcke, W., Richter, M., 2008. Landslides as Important Disturbance Regimes – Causes and Regeneration. Beck, E., Bendic, J., Kottke, I., Makeschin, F. Mosandl, R. (Eds.). Gradients in a Tropical Mountain Ecosystem of Ecuador. Ecological Studies 198: 319 – 330.

Buurman, P, Pape, T., Muggler,C. C., 1997, Laser grain-size determination in soil genetic studies 1. Practical problems. Soil Science 162/ 3: 211 – 218

Buurman, P, Pape, T., Reijneveld, J. A., de Jong, F. van Gelder, E., 2001. Laser-diffraction and pipette-method grain sizing of Dutch sediments: correlations for fine

fractions of marine, fluvial, and loess samples. Netherlands Journal of Geosciences 80/ 2: 49 – 57.

Crawley, M. J., 2007. The R Book. John Wiley & Sons Ltd.

De Bruin, S., Stein, A., 1998. Soil-landscape modelling using fuzzy c-means clustering of attribute data derived from a Digital Elevation Model (DEM). Geoderma 83: 17 – 33.

Efron, B., 1979. Bootstrap Methods: Another Look at the Jackknife. In: The Annals of Statistics. 7, Nr. 1, S. 1 – 26.

FAO, 2006. Guidelines for soil description. Fourth Edition. Food and Acriculture Organization of the United Nations, Rome.

Fries, A., Rollenbeck, R., Göttlicher, D., Nauss, T., Homeier, J., Peters, T., Bendix, J., 2009. Thermal structure of a megadiverse Andean mountain ecosystem in southern Ecuador, and its regionalization. Erdkunde, 63: 321 – 335.

Gessler, P.E., Chadwick, O. A., Chamran, F., Althouse, L. and Holmes, K., 2000. Modeling Soil–Landscape and Ecosystem Properties Using Terrain Attributes. Soil Science Society of America Journal 64: 2046 – 2056

Gobin, A., Campling, P., Feyen, J., 2001. Soil-Landscape Modelling to Quantify Spatial Variability of Soil Texture. Physics and Chemistry of the Earth Part B: Hydrology, Oceans and Atmosphere 26/ 1: 41 – 45.

Goovaerts, P., 1999. Geostatistics in soil science: state-of-the-art and perspectives. Geoderma 89: 1 – 45.

Grimm, R., Behrens, T., Märker, M., Elsenbeer, H., 2008. Soil organic carbon concentrations and stocks on Barro Colorado Island — Digital soil mapping using Random Forests analysis. Geoderma 146: 102 – 113.

Henderson, B. L., Bui, E. N., Moran, C. J., Simon, D. A. P., 2005. Australia-wide predictions of soil properties using decision trees. Geoderma 124: 383 – 398.

Homeier, J., Dalitz, H., Breckle, S.-W., 2002. Waldstruktur und Baumartendiversität im montanen Regenwald der Estacón Cientíca San Franscisco. Südecuador. Ber. d. Reinh. Tüxen-Ges 14: 109 – 118.

Konert, M., Vandenberghe, J., 1997. Comparison of laser grain size analysis with pipette and sieve analysis: a solution for the underestimation of the clay fraction. Sedimentology 44: 523 – 535.

Lea, N. L., 1992. An aspect driven kinematic routing algorithm. In: Parsons, A. J. and Abrahams, A. D. (eds.) Overland Flow Hydraulics and Erosion Mechanics. London, 393 – 407.

Liess, M., Glaser, B., Huwe, B., 2009. Digital Soil Mapping in Southern Ecuador. Erdkunde 63/ 4: 309 – 319.

Ließ, M., Glaser, B. Huwe, B., 2010a. Incomplete Soil Classification to Benefit the Soil Continuum - Prediction of Diagnostic Properties of Andean Mountain Forest Soils. European Journal of Soil Science (in review).

Ließ, M., Glaser, B. Huwe, B., 2010b. Reference Soil Group Probability Prediction. European Journal of Soil Science (in review).

Litherland, M., Aspen, J. A., Jemielita, R. A., 1994. The metamorphic belts of Ecuador. Overseas Mem. Br. Geol Surv 11: 1–147.

Loizeau, J.L., Arbouille, D., Santiago, S. & Vernet, J.P., 1994. Evaluation of a wide-range laser diffraction grain-size analyser for use with sediments. Sedimentology 41: 353 – 361.

Loveland, P.G. & Whalley, W.R., 1991. Particle size analysis. In: Smith, K.A. and Mullins, C. E. (Ed.). Soil Analysis - Physical Methods. Marcel Dekker, New York. Pp 271 – 328.

Martin, W. K. E., Timmer, V. R., 2006. Capturing spatial variability of soil and litter properties in a forest stand by landform segmentation procedures. Geoderma 132: 169 – 181.

McBratney, A., Odeh , I. O. A., Bishop, T. F. A., Dunbar, M.S., Shatar, T.M., 2000. An overview of pedometric techniques for use in soil survey. Geoderma 97: 293 – 327.

McKenzie, N. J., Austin, M. P., 1993. A quantitative Australian approach to medium and small scale surveys based on soil stratigraphy and environmental correlation. Geoderma 57: 329 – 355.

McKenzie, N. J., Ryan, P. J., 1999. Spatial prediction of soil properties using environmental correlation. Geoderma 89: 67 – 94.

Meyers, D. E., 1994. Spatial interpolation: an overview. Geoderma 62: 17 – 28.

Pachepsky, Y.A., Timlin, D.J., Rawls, W.J., 2001. Soil water retention as related to topographic variables. Soil Science Society of America Journal 65: 1787 – 1795.

Park, S. J., Burt, T. P., 2002. Identification and Characterization of Pedomorphological Processes on a Hillslope. Soil Science Society of America Journal 66: 1897 – 1919.

Park, S. J., Vlek, P. L. G., 2002. Environmental correlation of three-dimensional soil spatial variability: a comparison of three adaptive techniques. Geoderma 109: 117 – 140.

Peters, J., de Baets, B., Verhoest, N. E. C., Samson, R., Degroeve, S., de Becker, P., Huybrechts, W., 2007. Random Forests as a tool for ecohydrological distribution modelling. Ecological Modelling 207: 304 – 318.

Prasad, A. M., Iverson, L.R., Liaw, A., 2006. Newer classification and regression tree techniques: Bagging and random forest for ecological prediction. Ecosystems 9: 181 – 199.

Rollenbeck, R., 2006. Variability of precipitation in the Reserva Biólogica San Francisco / Southern Ecuador. Lyonia, A Journal of Ecology and Application 9/ 1: 43-51.

Strahler, A. N., 1957. Quantitative analysis of watershed geomorphology. Transactions of the American Geophysical Union 38/ 6: 913–920.

Therneau, T. M., Atkinson, B., 2003. The rpart Package. http://cran.r-project.org/web/packages/rpart/rpart.pdf (access: 28/02/2008)

Thompson, J. A., Pena-Yewtukhiw, E. M., Grove, J. H., 2006. Soil–landscape modeling across a physiographic region: Topographic patterns and model transportability. Geoderma 133: 57 – 70.

Tittonell, P., Shepherd, K.D., Vanlauwe, B., Giller, K.E., 2008. Unravelling the effects of soil and crop management on maize productivity in smallholder agricultural systems of western Kenya—An application of classification and regression tree analysis. Agriculture, Ecosystems and Environment 123: 137 – 150.

Viscarra Rossel, R. A., Behrens, T., 2010. Using data mining to model and interpret soil diffuse reflectance spectra. Geoderma, in press.

Wilcke, W., Valladarez, H., Stoyan, R., Yasin, S., Valarez, C., Zech, W., 2003. Soil properties on a chronosequence of landslides in montane rainforest, Ecuador. Catena 53: 79 – 95.

Wilcke, W., Yasin, S., Schmitt, A., Valarezo, C., Zech, W., 2008. Soils along the Altitudinal Transect and in Catchments. Ecological studies 198, Gradients in a Tropical Mountain Ecosystem of Ecuador, Chapter 9. Springer, Berlin Heidelberg

Zhao, Z., Chow, T. L., Rees, H. W., Yang, Q., Xing, Z., Meng, F.-R., 2009. Predict soil texture distributions using an artificial neural network model. Computers and Electronics in Agriculture 65/ 1: 36 – 48.

Ziadat, F. M., 2005. Analyzing Digital Terrain Attributes to Predict Soil Attributes for a Relatively Large Area. Soil Science Society of America Journal 69: 1590 – 1599.

Chapter 6

Estimating Slope Stability in a Steep Andean Mountain Forest Region

Mareike Ließ [a], Bruno Glaser [b], Bernd Huwe [a]

a University of Bayreuth, Department of Geosciences, Soil Physics Group
Universitätsstrasse 30, 95447 Bayreuth, Germany
b Martin-Luther University Halle-Wittenberg, Soil Biogeochemistry, von-Seckendorff-Platz 3,06120 Halle, Germany

Correspondence: Mareike Ließ, E-mail: mareike.liess@uni-bayreuth.de

Abstract

Landslides are a common phenomenon within the Ecuadorian Andes and have an impact on soil-landscape formation. Within the research area, landslides are mainly composed of soil and mud slides, while rock slides occur to a much lesser extent (Bussmann et al., 2008).

Landslide susceptibility was determined in a steep mountain forest region in Southern Ecuador. Soil mechanical and hydrological properties in addition to terrain steepness were hypothesized to be the major factors in causing soil slides. Hence, the factor of safety (FS) was calculated as the soil shear ratio that is necessary to maintain the critical state equilibrium on a potential sliding surface. Regression tree (RT) and Random Forest (RF) models were compared in their predictive force to regionalise the depth of the failure plane and soil bulk density based on terrain parameters. The depth of the failure plane was assumed at the lower boundary of the stagnic soil layer or soil depth respectively, depending on soils being stagnic or non-stagnic.

Bulk density and the depth of the failure plane were regionalised with RF performing better than RT. The FS was determined in dependence of soil wetness referring to 0.001, 0.01, 0.1 and 3 mm/h net rainfall rate. Sites with a FS ≥ 1 at 3 mm/h (complete saturation) as unconditionally stable, sites with a FS < 1 at 0.001 mm/h were classified as unconditionally unstable. The latter coincide well with landslide scars from a recent aerial photograph.

Keywords: factor of safety, failure plane, Random Forest, regression tree, Jackknife

6.1 Introduction

In the Ecuadorian Andes, landslides are a common phenomenon. Naturally triggered landslides have an important landscape forming effect, and with their vegetation disturbance they are surmised to be one of the reasons for the high biodiversity within the Podocarpus – El Condor Biosphere Reserve where the research area is located (Bussmann et al., 2008). In affecting infrastructure, i.e. in particular the road connecting the regional capitals Loja and Zamora, landslides impose a considerable thread to human lives.

Within the research area (Figure 6.1), during 1962 – 1999 at least 8.5% of the area where affected by slide processes (Bussmann et al., 2008), at least 3.7% showed landslide scars in 2000 (Stoyan, 2000). This was concluded from aerial photographs since 1962. Nevertheless, the overall percentage affected by landslides is probably much higher. Distribution patterns vary considerably and so do size and shape. While the hillslopes are exposed to landslides for their steepness, the slides themselves are hypothesized to be mainly triggered by heavy rainfall (Bussmann et al., 2008). Furthermore, some landslides are single events while others show repeated mass movement or exhibit a continuing mass movement during times of high precipitation (Stoyan, 2000). Brenning (2005) calculated prediction errors for landslide susceptibility comparing different statistical modelling approaches based on a landslide inventory by Stoyan (2000). Unfortunately, his susceptibility maps lack an explanatory map legend so that in fact no information on the spatial distribution of landslide susceptibility within the research area is available.

Definitions of the factor of safety, the most important concept in slope stability analysis, are not unique (Zheng et al., 2006). The strength reserving definition (1) divides the shear strength of the soil by the shear stress that is necessary to bring the slope into the critical state equilibrium. The overloading definition (2) defines the factor of safety as the ratio of total resisting, i.e. stabilizing, to total driving, i.e. destabilizing, forces. While the first definition is based on soil mechanics, the latter includes much more factors, such as rock failure, earthquakes' influence and vegetation weight.

Geology is a complex field where information for the research area is lacking. However, a rock failure situation has to be considered completely different from a failure situation within the soil (Li, 2007). According to Bussmann et al. (2008), deeper reaching rock slides also occur within the area, but are rare in comparison to near surface soil slides. Seismic events are considered to help in triggering a landslide where the slope is unstable and soils are saturated with water. Vegetation is another factor that has to be considered. Although trees have often proved to act as stabilizing forces of mountain slopes (e.g. Riestenberg and Sovonick-Dunford, 1983; McIntosh et al., 2009), in the research area, vegetation is hypothesized to have more destabilizing than stabilizing impact. Forest vegetation weight is expected to support downslope forces, whereas the stabilizing impact of root cohesion can be neglected. During field work we confirmed that strong roots hardly penetrate the soil,

but stay within the organic layer, which rather forms a carpet on top of the mineral soil. Vanacker et al. (2003) investigated landslide patterns and their relation to land use in a man-made landscape close to Cuenca, Ecuador. According to their findings, forest biomass did not provoke decreasing slope stability. But forest in the area they investigated is only secondary or planted with exotic tree species. However, the impact of vegetation weight has to be postponed to later studies.

Soil mechanical and hydrological properties were hypothesized by Domínguez-Cuesta et al. (2007) to be the major factors in causing soil slides. Being interested in the influence of physical soil properties on landslides, we focussed on soil regionalisation and landform analysis to explain why landslides occurred on those locations where scars without vegetation are still visible within the landscape. After all, the primary objective was to estimate which sites are prone to future landsliding and under which net rainfall rate.

6.2 Material and methods

6.2.1 Slope failure concept for the research area

Within the research area, terrain form and slope steepness in particular provide the basic risk for slope failure. Whether a slope compartment fails depends on the weight burdening the failure plane. Thereby, the weight of the sliding soil compartment depends on its bulk density and the depth of the failure plane itself. Heavy or prolonged rain works in augmenting the sliding unit weight by increasing the soil wetness while at the same time it decreases the stabilizing effect of soil cohesion.

According to the earlier mentioned strength reserving definition, the factor of safety (FS) is defined as the ratio of the shear strength τ_f to the shear stress τ which is necessary to maintain the critical state equilibrium on a potential sliding surface (Fröhlich, 1955). The shear strength (kPa) of the soil according to Mohr-Coulomb is defined as

$$\tau_f = c' + (\sigma - \mu) \cdot \tan \varphi' \tag{1}$$

with c' the effective soil cohesion (kPa), σ the total normal stress (kPa), μ the pore water pressure and φ' the effective angle of soil internal friction. $\sigma - \mu$ can be expressed as

$$(\gamma_t - \gamma_w w) \cdot z \cdot \cos^2 \alpha \tag{2}$$

(Vanacker et al., 2003), the sliding unit weight component (excluding water content) acting perpendicular to the inclination and therefore stabilizing, with γ_t the total unit weight of the sliding material (kN/m³), γ_w the unit weight of water (9.81 kN/m³), w the equilibrium soil saturation, $z \cdot \cos \alpha$ the depth of the failure plane (m) perpendicular to the inclination and α the slope angle (°).

The shear stress, i.e. the downslope component of the sliding unit weight, can be expressed as

$$\tau = \gamma_t \cdot z \cdot \cos \alpha \cdot \sin \alpha \qquad (3)$$

Equation 4 results from Equations 1 – 3.

$$FS = \frac{c' + (\gamma_t - \gamma_w w) \cdot z \cdot \cos^2 \alpha \cdot \tan \varphi'}{\gamma_t \cdot z \cdot \cos \alpha \cdot \sin \alpha} \qquad (4)$$

For shallow subsurface runoff parallel to the ground surface (Bauer et al.[1]), the soil saturation, w, is computed by Equation 5 (O'Loughlin, 1986; Montgomery and Dietrich, 1994) based on the upslope contributing area A (m²), the local slope angle α (°), the net rainfall rate q (m/s), the saturated soil transmissivity T (m²/s) and b the grid cell size (m).

$$w = \left(\frac{q \cdot A}{b \cdot T \cdot \sin \alpha} \right) \qquad (5)$$

The upslope contributing area for each grid cell was determined using the flow tracing kinematic routing algorithm (Lea, 1992). Soil transmissivity was calculated by

$$T = K_{sat} \cdot z \cdot \cos \alpha \qquad (6)$$

with K_{sat} the saturated hydraulic conductivity and z the saturated soil depth and hence the depth of the failure plane. The soil is completely saturated at $w = 1.0$, the maximal soil wetness in Equation (4). When the calculated wetness according to Equation (5) exceeds 1.0, overland flow is the consequence.

Earlier investigations within the research area discovered that soils with a stagnic colour pattern, covered by huge organic layers (20 – 90 cm) are dominating the soil-landscape (Liess et al., 2009; [2]). Rainfall is high, ranging between 2050 mm at 1960 m and 4400 mm at 3200 m a.s.l. (Rollenbeck, 2006) and the low soil hydraulic conductivity leads to the formation of stagnic soil layers. The investigation of soil hydrological flow patterns (Bauer et al.[1]) proved that water entering the soil causes

[1] Personal communication, manuscript submitted to Journal of Hydrology
[2] The occurrence probability of the Word Reference Base (FAO, IUSS Working Group WRB, 2007) Reference Soil Groups and the probability and thickness of the typical diagnostic horizons were predicted in earlier studies (European Journal of Soil Science, in review).

shallow, slope parallel subsurface flow only within the stagnic horizon and does not proceed any further down the soil profile. According to these findings, we assume the failure plane at the lower boundary of the stagnic horizon regarding initial landslide triggering.

On slopes already affected by landslides, preferential water flow down the soil profile and probably until bedrock is helped by the high rock content (Bogner et al., 2008; Bauer et al.[1]). The water opens gaps in the slope (observed during soil sampling), which are widened until another landslide is triggered. This increases the probability of landslides occurring on slopes already affected by landslides and explains also why some slopes show repeated mass movement. As a consequence, the depth of the failure plane was considered at complete soil thickness on these deep percolation sites.

A failure situation even deeper within the weathered bedrock cannot be neglected, but considering only soil mechanics for the stability concept, we assume soil depth as maximum depth of the failure plane. For a rock failure situation, a different concept would have to be applied (Li, 2007). Since we cannot say for sure whether a site was affected by a landslide or not unless forest vegetation did not regrow and the landslide scar is still visible in an aerial photograph or from ground check, we considered two possible depths of the failure plane: (1) at the lower boundary of the stagnic horizon and (2) at soil depth.

6.2.2 Soil and terrain data

In order to calculate landslide susceptibility, continuous information on soil properties such as bulk density, soil cohesion, angle of internal friction and soil depth is needed. Therefore, digital soil maps have to be established from discrete observation points. The investigated soil data comprises 56 soil profiles and 315 auger points. They were positioned within the steep mountain forest landscape according to a sampling design comprising 24 terrain classes (Liess et al., 2009) and along transects from ridges to side valley creeks (Figure 6.1). Soil bulk density and cohesion were determined horizon-wise by core samples (100 cm³) and a field vane within the soil profiles, while stagnic horizon thickness and soil depth were measured within the auger samples also.

---

[1] Flow paths in soils of landslide affected and unaffected hillslopes were investigated within our working group also. The manuscript was submitted to Journal of Hydrology.
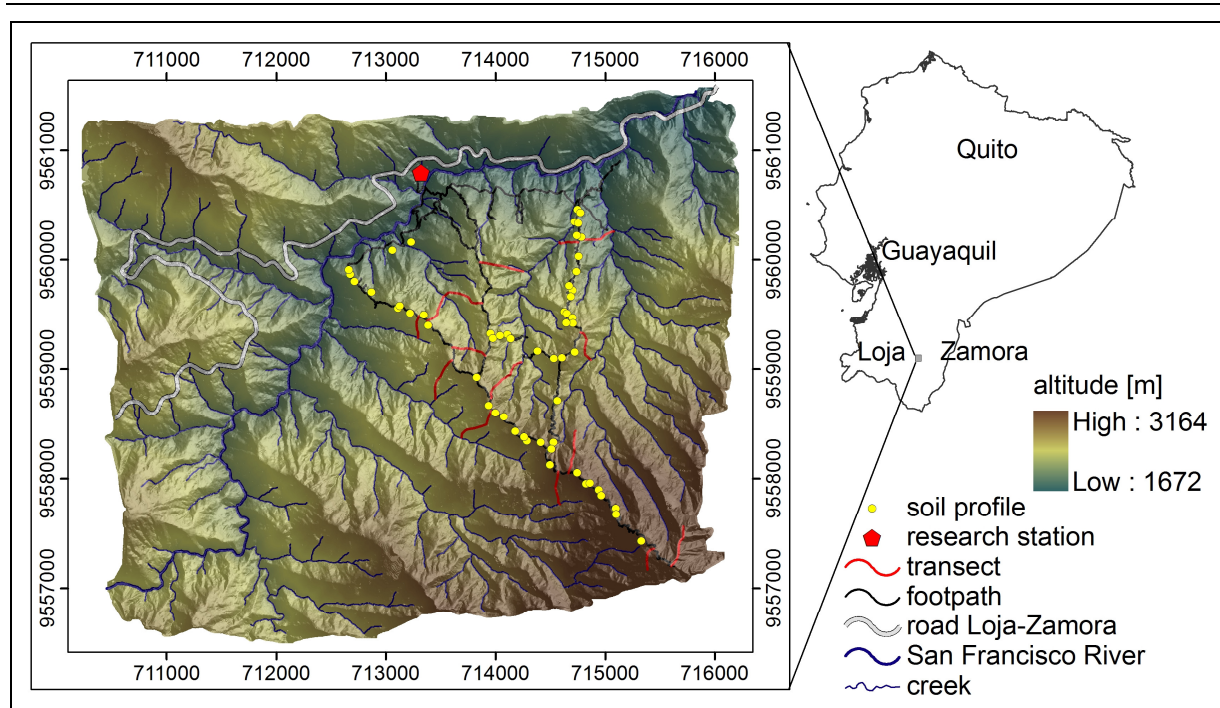
Figure 6.1: Soil dataset with auger points along transects and soil profiles. Overlaid hillshading with light source from north-east (adapted from Liess et al., 2009).

Finally, statistical models were applied to relate the soil information to terrain parameters. This approach is based on the theory that landscape morphology determines soil development in general and soil surface properties in particular. According to Jenny's (Jenny, 1941) concept, the soil is seen as intimately linked with its position in the landscape. Material translocation and the area's hydrology also have a considerable impact.

GIS raster grids of the terrain parameters that were calculated from a 2 m DEM (Liess et al. 2009) include altitude, slope, aspect, profile and plan terrain curvature (pr.curv/ pl.curv), upslope contributing catchment area and overland flow distance to the channel network (OFD). Some terrain parameters were also assessed during sampling, i.e. slope and aspect and used in model development. All others had to be assigned to the soil data set from the GIS raster grids. They were assigned twofold: (1) by assigning the nearest neighbour (n. n.) terrain values and (2) by buffering the location with GPS accuracy and assigning the mean terrain values. GPS accuracy was high on the exposed mountain ridges (3 m) and gradually decreased when moving down into the side valleys due to limited reachability for satellite signal. This introduced a spatially dependent variable smoothing into the analysis. The continuous raster grids were used for prediction purpose.

Slope, aspect and curvature were calculated by the 2nd Degree Polynom from Zevenbergen and Thorne (1987). The channel network was allocated using the

Strahler Stream Order ≥ 5 (Strahler, 1957) as initiation threshold based on expert knowledge of the research area.

Two principle flow mechanisms are available for calculating the upslope contributing catchment area, i.e. the area contributing flow to each grid cell: (1) flow is permitted to move between grid cell centres only and (2) flow moves freely. The latter is referred to as flow tracing mechanism. In both mechanisms, linear and flow distribution with divergence is possible and therefore, single or multiple flow direction. From mechanism (1) we chose the Braunschweiger Digital Relief Model (BS CA) (Bauer et al. 1985), a multiple flow mechanism and from (2) we chose the Kinematic Routing Algorithm (KRA CA) (Lea 1992), a one-dimensional flow tracing algorithm. Terrain analysis as well as the calculation of soil wetness and the FS was carried out in SAGA, free open source GIS software developed by Geosystem Analysis (Böhner et al., 2006).

6.2.3 Regression tree and Random Forest

Regression tree (RT) and Random Forest (RF) statistical models were used to predict soil properties from terrain attributes. RT was applied because of its "white box"-character indicating the complete model structure. Random Forest lacks this open structure, but for being composed of many "non-correlated" regression trees was expected to result in better model performance. It still provides means for interpretation in giving measures for variable importance. Both statistical models were performed within the open-source data analysis environment R (version 2.10.1; R Development Core Team, 2010). RTs, first described by Breiman et al. (1984), were implemented with the software package rpart; RF, based on Breiman and Cutler's Fortran code, was implemented with the package randomForest.

RTs subdivide the dataset by a set of decision rules applied on the predictor variables to gain preferably homogeneous subgroups regarding the response variable. The rules are laid through partitioning the dataset into successively smaller groups (nodes) with binary splits based on a single predictor variable. The optimal split among all predictor variables is chosen in minimising the mean square error of the response variable. The various subdivision rules result in a tree diagram. The mean of all data within one node is used for prediction purpose.

RF is based on RT methodology. It differs in that it grows a whole forest of RTs, grown without pruning (Breiman, 2001). Tree diversity guarantees model stability.

This is achieved by two means: (1) Choosing at random a subset of predictor variables (mtry) to grow each tree and (2) sampling with replacement (bootstrapping) and thereby varying the input dataset. As forest size increases, the generalization error converges (Breiman, 2001). The number of trees therefore needs to be set sufficiently high to allow for this convergence. Consequently, RFs do not overfit when more trees are added, but produce a limited generalization error (Breiman, 2001; Prasad et al., 2006; Peters et al., 2007).

The size of mtry has to be selected by the user. It is a sensitive parameter determining model strength for it defines the strength of each individual tree and the correlation between any two trees in the forest. With mtry the strength of each tree and the correlation among trees increases (Peters et al., 2007). Tree strength improves model performance, whereas correlation among trees weakens it. The optimal mtry can be determined by the function tuneRF of the R software package randomForest.

RT and RF model performance were compared by hundredfold model runs on random ⅔ Jackknife subsamples of the dataset, while the remaining ⅓ of the dataset was used for cross validation with Pearson's r_{xy}.

6.3 Results and discussion

6.3.1 Depth of the failure plane

The failure plane was assumed at the lower boundary of the stagnic soil layer or complete soil depth. The former required the prediction of the thickness of the stagnic horizon and overlying Ah horizon, the latter the prediction of mineral soil depth. Within the research area, Ah and stagnic horizon usually do not occur within the same soil profile. Though, model generalization by calculated tree node means, made the prediction of both, Ah and stagnic horizon, necessary. Soil depth was measured as depth until Cw or R horizon.

RT and RF model performance with terrain parameter values assigned as n. n. (RTnn and RFnn) or mean values (RTm and RFm) to predict soil depth as well as Ah and stagnic horizon thickness was compared via hundredfold external cross validation. Histograms of the 100 Pearson r_{xy} are displayed in Figure 6.2. RF models were established with the optimal mtry = 2 and 500 trees. They performed better than RT models considering the r_{xy} distribution mean. However, their performance to

predict soil depth and stagnic horizon thickness was poor with mean r_{xy} = 0.24 and 0.22. On the other hand, mean r_{xy} to predict Ah horizon thickness was much better with mean r_{xy} = 0.6 for the best model (RFm).
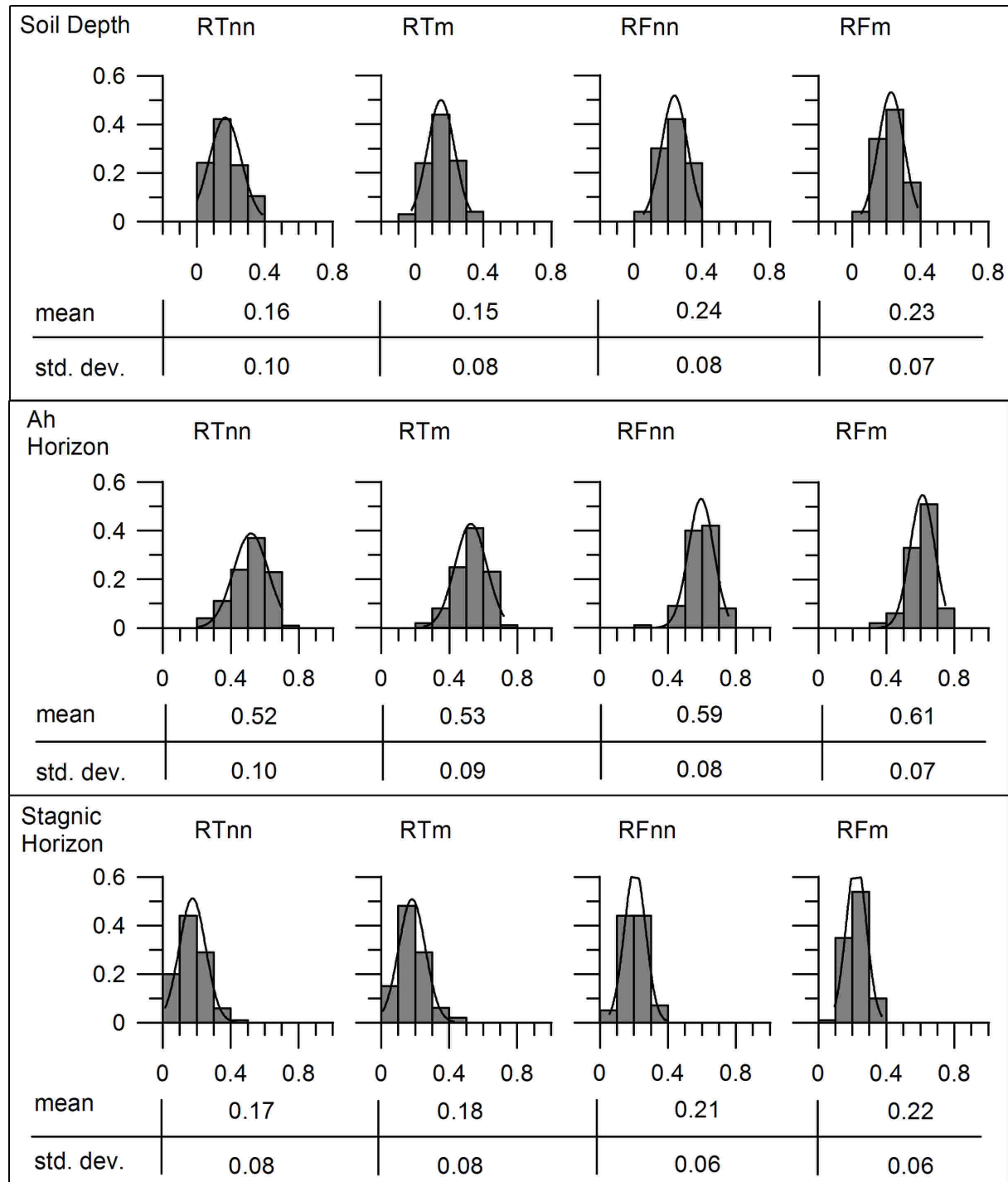

Figure 6.2: Histograms, mean and standard deviation (std. dev.) of hundredfold Pearson r_{xy} cross validation of models to predict soil depth as well as Ah and stagnic horizon thickness. Prediction by Random Forest (RF) and regression tree (RT) using terrain values assigned as nearest neighbour (nn) or mean (m) values. X-value = Person's r_{xy}, Y-value = relative frequency.

Terrain attributes can likely only explain horizon thickness and particularly soil depth to a limited extent. The vertical development of the soil profile is less influenced by surface processes. Bauer et al. ([1]) limited downslope subsurface flow within the research area to the topsoil. Ließ et al. ([2]) related the occurrence of stagnic properties to terrain parameters, whereas the extent of the stagnic horizon could not be explained. Park and Vlek (2002) reported that soil attributes whose vertical distribution is strongly determined by vertical pedogenesis or unknown factors are poorly modelled by environmental variables.

Another aspect to be considered is the spatial map resolution. The soils within the research area change within a few meters radius as typical for tropical soils. Accordingly, we used the highest possible DEM resolution. This way, small scale soil variability was included within the models, which would be neglected while working on a larger scale. We conclude that the size of the dataset we applied was not enough to represent the investigated soil-landscape at this high precision. However, for lack of any better option, we still applied the overall best model to predict the depth of the failure plane and discuss the influence of terrain parameters, keeping in mind that they can only explain it partially.

The overall best model was used to predict soil depth (RFnn), Ah (RFm) and stagnic (RFm) horizon thickness. Figure 6.3a displays the terrain variable importance in constructing the RFnn model to predict soil depth, Figure 6.3b shows it regarding the RFm models to predict Ah and stagnic horizon thickness. The variable importance measure indicates by how much the mean square error (MSE) would increase if the respective predictor would be suspended from the model (Prasad et al., 2006).

For the construction of the soil depth and Ah horizon model, all predictor variables were of importance, whereas the stagnic horizon model excluded aspect and profile curvature (pr.curv). This is interesting, since we expected the westerly and easterly exposed slopes to carry thicker stagnic layers. According to Rollenbeck (2006) the main wind directions, east and west, receive heavy convective rainfall on western slopes from September to April and on eastern slopes from May to September. Accordingly, concave sites were expected to have thicker stagnic layers for the reason of higher water accumulation and wetness. That this process was not included in the model might be due to the small scale curvature (4 m) used in our

---

[1] The manuscript of this study was submitted to Journal of Hydrology.
[2] The occurrence probability of the WRB (FAO, IUSS Working Group WRB, 2007) Reference Soil Groups as well as the probability and thickness of the typical diagnostic horizons were predicted in earlier studies (European Journal of Soil Science, in review).

analysis. Altitude was the most important predictor in all three models.

Figure 6.3c maps the depth of the failure plane, regionalised by the soil depth model. In its prediction as well as the prediction of other soil properties it was necessary to reduce DEM precision to 10 m to abate calculation time. Correspondingly, further calculations regarding soil wetness and the FS were based on 10 m precision also.

It is clearly visible that mineral soil depth decreases with altitude (compare Figure 6.1). This was expected since lower temperature with increasing altitude usually leads to lower chemical weathering rates. The air temperature within the study area decreases with altitude from 19.4 °C to 9.4 °C (Fries et al., 2009). On the contrary, Figure 6.3d indicates an increasing depth of the failure plane with altitude as considered at the lower boundary of the stagnic horizon (combined Ah and stagnic horizon thickness). As a consequence, Figure 6.3e, which shows the difference of the two predictions (Fig. 3c - 3d), displays positive values in the lower and negative values in the upper part of the research area. Schrumpf et al. (2001) also stated an
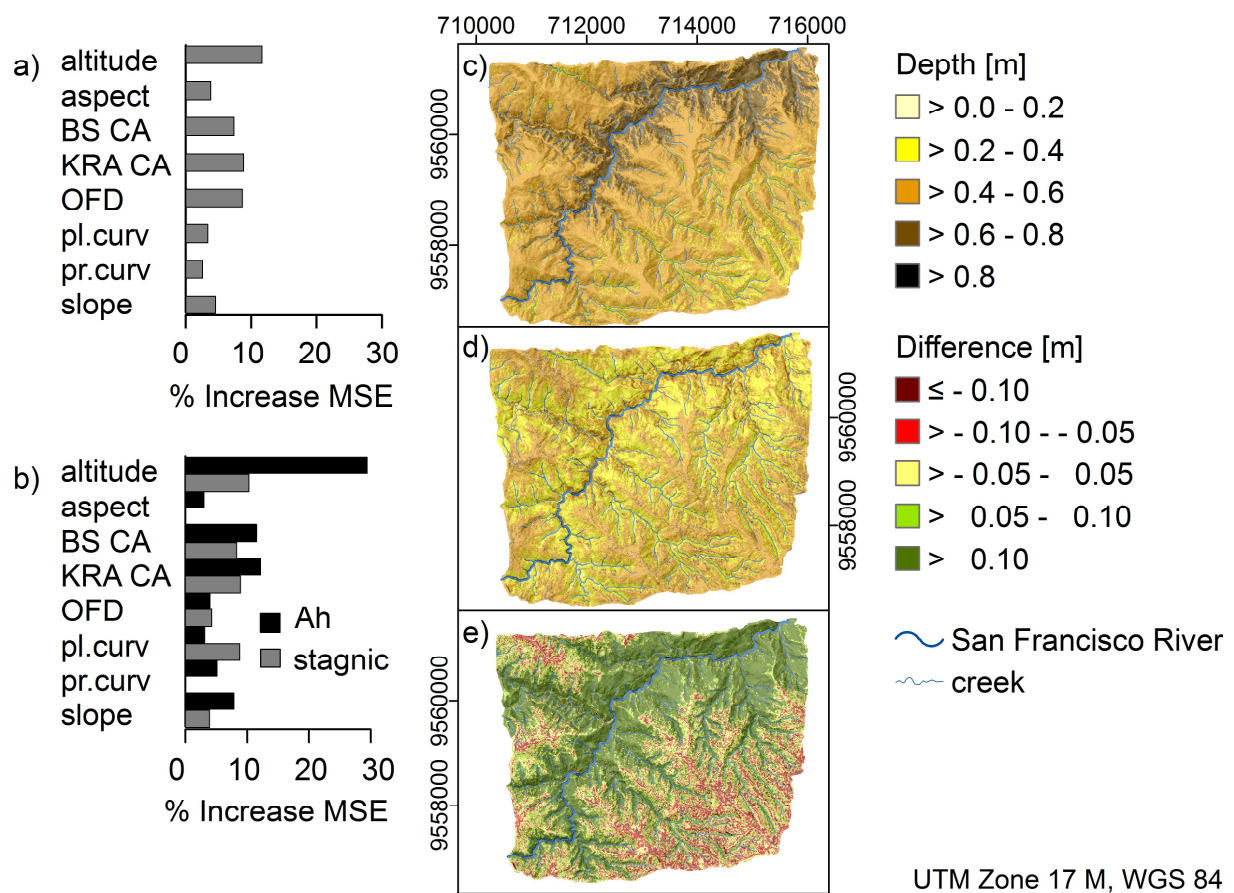

Figure 6.3: Variable importance measures of the models to predict the depth of the failure plane: a) at soil depth, b) at the combined Ah and stagnic horizon thickness, and the models applied to the research area: c) predicted soil depth, d) predicted lower boundary of the stagnic horizon and e) difference between the two predictions c) – d) (Hillshading with light source from north-east).

increase in hydromorphic properties with increasing altitude. This goes along with an increasing average total annual rainfall from 2050 mm at 1960 m a.s.l. to c 4400 mm at 3100 m a.s.l. (Rollenbeck, 2006).

6.3.2 Sliding unit weight

Dry bulk density was needed to calculate the dry sliding unit weight. To obtain the total sliding unit weight at critical state equilibrium (Eq. 4), the weight of water was then added according to the soil wetness (Eq. 5). Figure 6.4 gives an overview of the bulk density per soil horizon. Bulk density in the stagnic soil layer (E and Bg horizon) is higher than in the Ah and Bw horizon as can be deduced from data between quartiles as well as from mean and median.


Horizon	Mean	Median
H1	1.1 ± 0.2	1.1
Ah	1.0 ± 0.2	1.1
E	1.2 ± 0.2	1.2
Bg	1.2 ± 0.2	1.2
Bw	1.1 ± 0.2	1.0
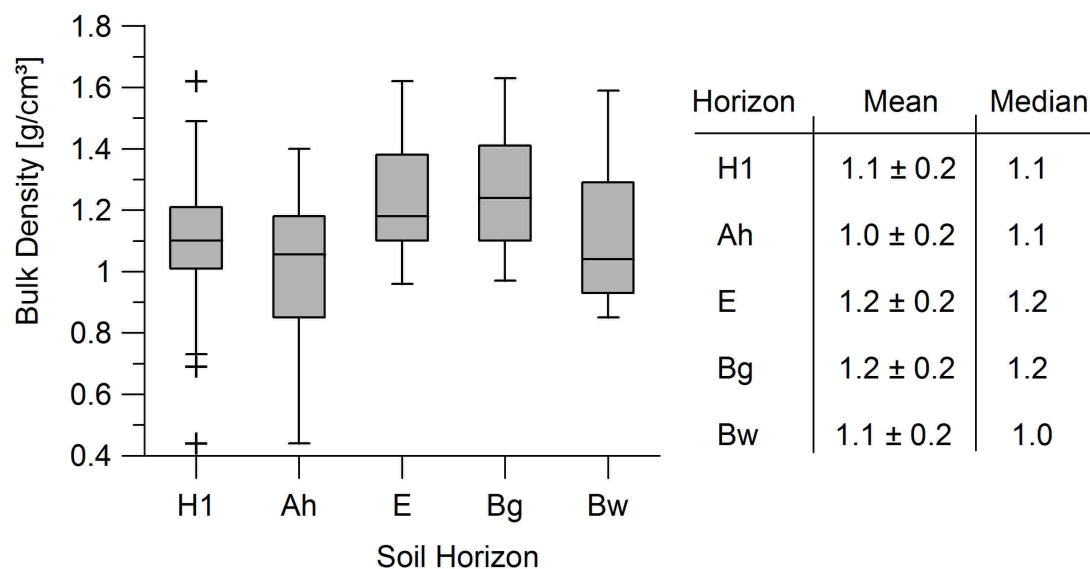
Figure 6.4: Bulk density of the horizons H1, Ah, E, Bg and Bw. H1 refers to the first soil horizon regardless of its characteristic.

Bauer et al.[1] reported similar findings. On the one hand, they described values between 1.0 ± 0.1 and 1.4 ± 0.5 g/cm³ for the topsoil of Stagnosols. On the other hand, their investigation of the topsoil horizons of landslides showed values of only 0.9 ± 0.1 to 1.2 ± 0.2 g/cm³. We assume that Ah horizons within the study area rather developed on accumulated landslide material, whereas soils developing on in-situ material include a stagnic soil layer, which is usually found at the soil surface.

Horizon-wise model development to predict bulk density from terrain parameters was not possible. We therefore predicted the bulk density within the first soil horizon (H1) regardless of its characteristic, expecting topsoil bulk density to be much more dependent on surface morphology. On the other hand, we had to consider subsoil

---

[1] Personal communication. The manuscript of this study was submitted to Journal of Hydrology.

bulk density also. From Figure 6.4 it can be observed that Bw mean bulk density is the same as in H1 and a bit higher than that of Ah. Though, Bw median is the lowest of all horizons. Correspondingly, we used the predicted H1 bulk density also for the subsoil.

Figure 6.5 shows the histograms of the 100 Pearson's r_{xy} from external cross validation to compare RT and RF models to predict bulk density from n. n. (RTnn and RFnn) and mean terrain values (RTm and RFm). RF models where again constructed with the optimal mtry = 2 and 500 trees. According to the r_{xy} distribution mean, RFnn was the best model with mean r_{xy} = 0.3 and maximum r_{xy} = 0.7. Reasons for the poor performance of some parts of the dataset are similar to those discussed for the depth of the failure plane models. Though, in addition we now also encountered a high r_{xy} standard deviation (0.2) which is probably due to the small dataset. Bulk density was only measured in 56 soil profiles. Using a smaller test dataset, e.g. 5%, to leave the major part of the data for model development, might improve r_{xy}. However, splitting of the datset was only done to compare model performance. Spatial prediction was based on the complete datset.

|	RTnn	RTm	RFnn	RFm
mean	0.16	0.18	0.28	0.25
std. dev.	0.27	0.24	0.21	0.17
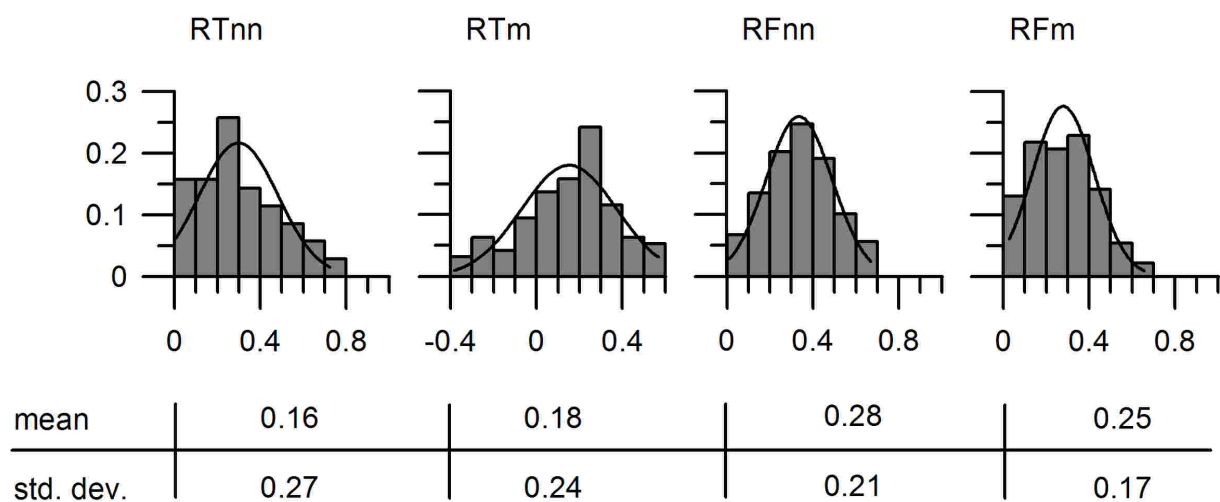
Figue 6.5: Histograms, mean and standard deviation (std. dev.) of Pearson's r_{xy} of 100 models to predict bulk density. Prediction by Random Forest (RF) and regression tree (RT) models using terrain values assigned as nearest neighbour (nn) or mean (m) values.

Figure 6.6a shows the terrain parameter influence on model construction (RFnn). Figure 6.6b maps the predicted bulk density within the research area. Sites < 2000 m a.s.l. display a lower bulk density compared to those above. Further research is needed to decide whether this is a construct (poor model performance). Some of the investigated soil profiles at low altitude showed evidence of former landslide influence, having most probably formed in the accumulation zone of landslides.

These soils had a lower topsoil bulk density. However, Ließ et al.[1] predicted stagnic soils with a probability ≥ 0.5 above 2090 m a.s.l. and assumed that the development of a stagnic topsoil layer might depend on physical soil properties. We assume that the development of stagnic soils might be related to the higher bulk density above 2000 m a.s.l.

We hypothesize that the occurrence of non-stagnic soils within the research area is due to landslide impact. Apart from stagnic soils with huge organic layers, Leptosols, Regosols, Cambisols and Umbrisols (FAO, IUSS Working Group WRB, 2007) also occur within the landscape under study (Liess et al., 2009). We relate their existence to landslide occurrence as was already proposed by Liess et al. (2009) for Cambisols only. Wilcke et al. (2003), Bussmann et al. (2008) and Bauer et al.[2], who investigated soils on landslides within the research area, described them as Cambisols or Regosols. We suppose Cambisols and Umbrisols to form on landslide material on the foot slope, whereas Leptosols remain where soil material was removed from the
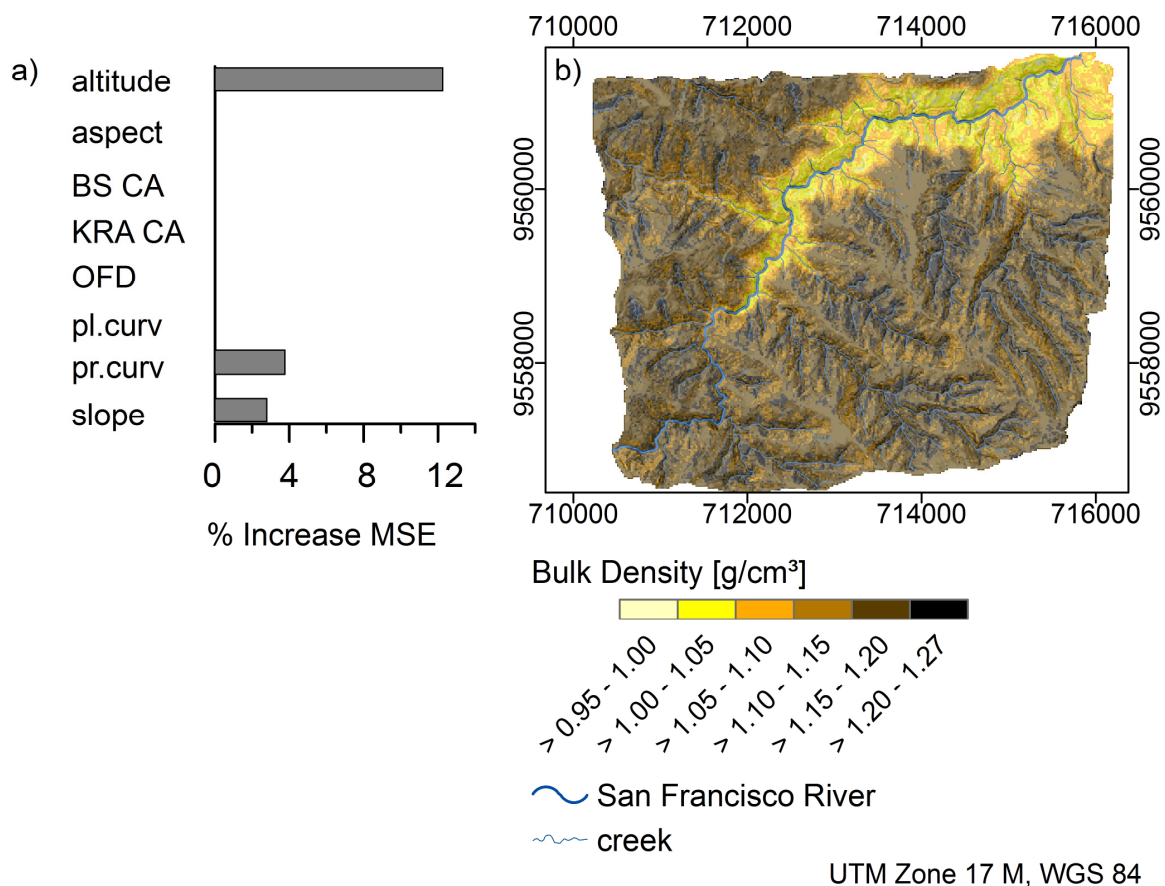

Figure 6.6: Variable importance measure of the RFnn model to predict bulk density (a) and regionalised bulk density (b) (Hillshading with light source from north-east).

---

[1] The occurrence probability of the stagnic soil layer was predicted with $r_{xy} = 0.5$ in an earlier study (European Journal of Soil Science, in review).

[2] Personal communication. The manuscript of this study was submitted to Journal of Hydrology.

source area, due to the very steep position not allowing for soil development. Regosols occur where weathered material has not been removed until bedrock or on relocated material with high rock content. According to this, without the influence of landslides the whole area would be covered by stagnic soils. However, further studies are necessary to prove this hypothesis and improve the prediction of bulk density. For now, we use the regionalised bulk density for the calculation of the FS.

6.3.3 Soil wetness

Soil wetness was calculated according to Equation 5. Apart from slope angle and upslope contributing catchment area, which were already used to predict soil depth and bulk density, K_{sat} was needed to calculate soil transmissivity (Eq. 6). A well known characteristic of K_{sat} measurements is that values vary over several orders of magnitude. Bauer et al.[1] measured K_{sat} within a subcatchment of the research area, 1900 – 2100 m a.s.l., which is dominated by non-stagnic soils in the lower and stagnic soils in its upper part (Kreutzer and Martini, 2002), and reported values ranging between $5.1 * 10^{-7}$ and $3.0 * 10^{-4}$ m/s within the first mineral soil horizon. On the other hand, Bauer et al.[1] differentiated K_{sat} in stagnic soils from that in landslide-affected soils. The topsoil of the accumulation zone of an old landslide showed rather high K_{sat} values of $5.1 * 10^{-5} \pm 2.9 * 10^{-5}$ m/s (median = $4.9 * 10^{-5}$ m/s), which according to Bauer et al.[1] can be explained by a preferential flow path network. K_{sat} in the topsoil of stagnic soils was determined with $6 * 10^{-7} \pm 7 * 10^{-7}$ m/s (median = $3.2 * 10^{-7}$ m/s), two orders of magnitude lower. These differences in K_{sat} might be attributed to the higher bulk density in stagnic soils.

K_{sat} changes in space and with depth. Its measurement is time consuming and the values range over several orders of magnitude. We simplified it according to the findings from Bauer et al. ([1]) and used only two values: $4.9 * 10^{-5}$ m/s were assigned to soils without stagnic properties and $3.2 * 10^{-7}$ m/s to soils with stagnic properties. Categories stagnic and non-stagnic were defined according to the occurrence probability of a stagnic soil layer ≥ and < 0.5 ([2]). This basically assigned stagnic soils > 2090 m a.s.l. and non-stagnic soils beneath. In reducing K_{sat} to these two values, we simplified reality neglecting that K_{sat} changes with space and soil depth.

---

[1] Personal communication. The manuscript of this study was submitted to Journal of Hydrology.
[2] The occurrence probability of the stagnic soil layer was predicted with $r_{xy} = 0.5$ in an earlier study (European Journal of Soil Science, in review).

The calculation of soil transmissivity (Eq. 6) includes the depth of the failure plane. Following earlier assumptions, soil wetness was calculated assuming (a) the complete soil volume and (b) the soil until the lower boundary of the stagnic soil layer as water conducting layer. Soil wetness according to (a) and (b) for net rainfall rates 0.001, 0.01, 0.1 and 3 mm/h is displayed in Figure 6.7.
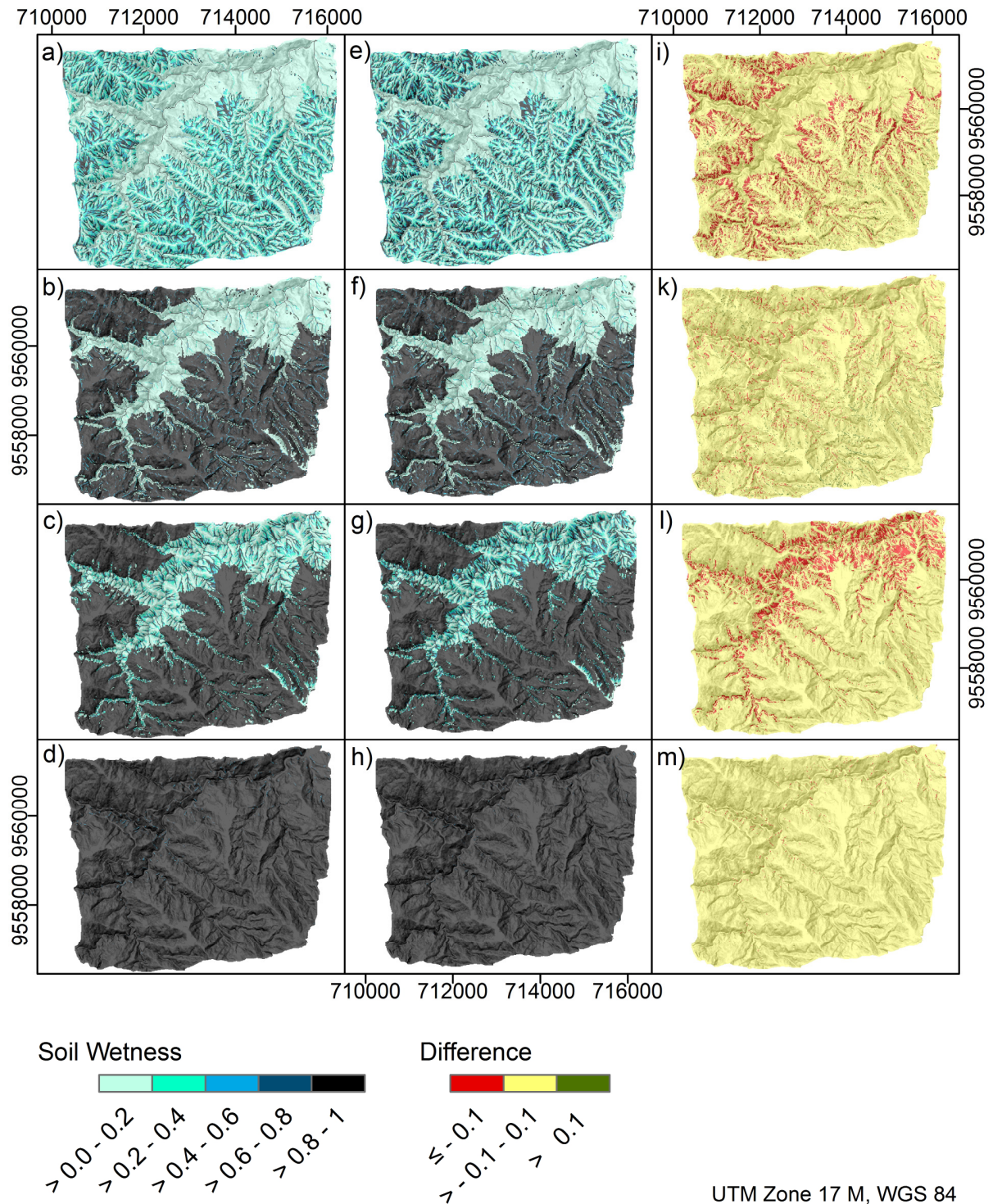

Figure 6.7: Soil wetness for the net rainfall rates 0.001 (1st row), 0.01 (2nd row), 0.1 (3rd row) and 3 (4th row) mm/h. Transmissivity was calculated with complete soil depth (1st column) and depth until the lower boundary of the stagnic horizon (2nd column). Wetness differences (1st - 2nd column) are displayed in the 3rd column (Hillshading with light source from north-east).

We considered the soil wetness at 0.001 mm/h as usual minimum saturation rate of the soils (Figures 6.7a and 6.7e), since the soils within the investigation area are sometimes found at low wetness, but never completely dry. On the other hand, a net rainfall rate of 3 mm/h leads to rather complete saturation within the area (Figures 6.7d and 6.7h). While at q = 0.01 mm/h rather all sites with a stagnic horizon probability ≥ 0.5 ([1]) are saturated (Figures 6.7b and 6.7f), an increase to q = 0.1 mm/h leads to a wetness increase on sites < 0.5 stagnic horizon probability (Figures 6.7c and 6.7g). While in Figure 6.7i the wetness difference refers to stagnic soils, q = 0.1 (Figure 6.7l) leads to an increase of soil wetness in non-stagnic soils.

Prolonged rainfall or rainstorm events are considered responsible for the triggering of landslides. Climate and precipitation in particular have been widely studied within the research area. Emck (2007) reported rainstorm events ≥ 20 mm/h (5.6 * 10^{-6} m/s); Rollenbeck (personal communication) even measured maximum precipitation rates from 26 mm/h (7.2 * 10^{-6} m/s) at about 1940 m a.s.l to 30 mm/h (8.3 * 10^{-6} m/s) at about 3000 m a.s.l.

Transpiration and forest canopy interception within the research area were investigated by Motzer (2003), Fleischbein et al. (2006) and Oesker et al. (2007). While Motzer (2003) and Fleischbein et al. (2006) investigated only small plots between 1900 and 2150 m a.s.l., Oesker et al. (2007) measured precipitation throughfall in different forest types at different altitudes. Still, unfortunately only forests up to 2210 m a.s.l. were considered, with the highest having the lowest canopy height of only 10 – 15 m and therefore reaching the highest throughfall of 92%, whereas the valley forest at 1960 – 2070 m a.s.l. displayed the lowest throughfall with 71% according to its canopy height of 25 – 30 m.

Water loss to deeper rock layers was neglected unless on sites already affected by landslides as was discussed earlier. However, after prolonged rainfall or rainstorm events soils within the whole area are saturated with water.

6.3.4 Soil cohesion

Soil cohesion was measured horizon-wise in 56 soil profiles. The lowest cohesion, 3 kPa, was detected in soils completely saturated with water. Model adaptation depends on many factors and is rather complex. Therefore, we assumed a minimal

---

[1] The occurrence probability of the stagnic soil layer was predicted with r_{xy} = 0.5 in an earlier study (European Journal of Soil Science, in review).

cohesion of 3 kPa at critical state equilibrium all over the area. Wu and Sidle (1995) used 2.5 kPa within their slope stability model for steep forested basins what is rather similar. Figure 6.8a shows the impact of soil cohesion ranging between 0 and 3 kPa on the FS.

6.3.5 Factor of safety

To calculate the factor of safety (FS) with equation (4) several input parameters are required. Slope angle was obtained from the DEM and soil cohesion was assumed to be 3 kPa for the failure situation. Total unit sliding weight γ_T was calculated from dry soil bulk density ρ, gravitational acceleration g and soil wetness w by

$$\gamma_T = \rho \cdot g + 1 \cdot g \cdot w \qquad (7)$$

The depth of the failure plane was considered to be at the lower boundary of the stagnic horizon or soil depth. Though, we lack information on the internal friction angle φ. Vanacker et al. (2003), who also investigated slope failure in Ecuador, assumed φ = 22° (tan φ = 0.4), but references stated by Mayne and Swanson (1981) would propose a higher φ (35°, tan φ = 0.7), based on studies from different areas for siltic soils, which dominate the research area ([1]).

We analysed the change of the FS in dependence on φ, soil cohesion, soil depth and bulk density. Since the FS is determined by many different parameters, we displayed its dependence on wetness (x) and slope angle (y) while all other variables were held constant (Figure 6.8). In inserting various such constant values for only one parameter, cohesion, soil depth, bulk density or φ, we could display the change of the curve describing FS = 1 in dependence on this parameter. The results in Figure 6.8 were expected in that a higher soil cohesion, lower soil depth, lower bulk density and higher φ lead to a higher FS.

Figure 6.9 shows the calculated FS categories at different soil wetness stages with the depth of the failure plane at soil depth (Figures 6.9a and 6.9b) and at the lower boundary of the stagnic horizon (Figures 6.9d and 6.9e). φ = 22° (Figures 6.9a and 6.9d) and 35° (Figures 6.9b and 6.9e) were applied to include the possible range. We will refer to the calculated stability classes resulting from the four combinations as sd_22 and sd_35 (failure plane at soil depth with φ = 22° and 35°) and stag_22 and stag_35 (failure plane at the lower boundary of the stagnic layer with φ = 22° and 35°).

[1] earlier study on soil texture distribution within the research area, submitted to Geoderma.
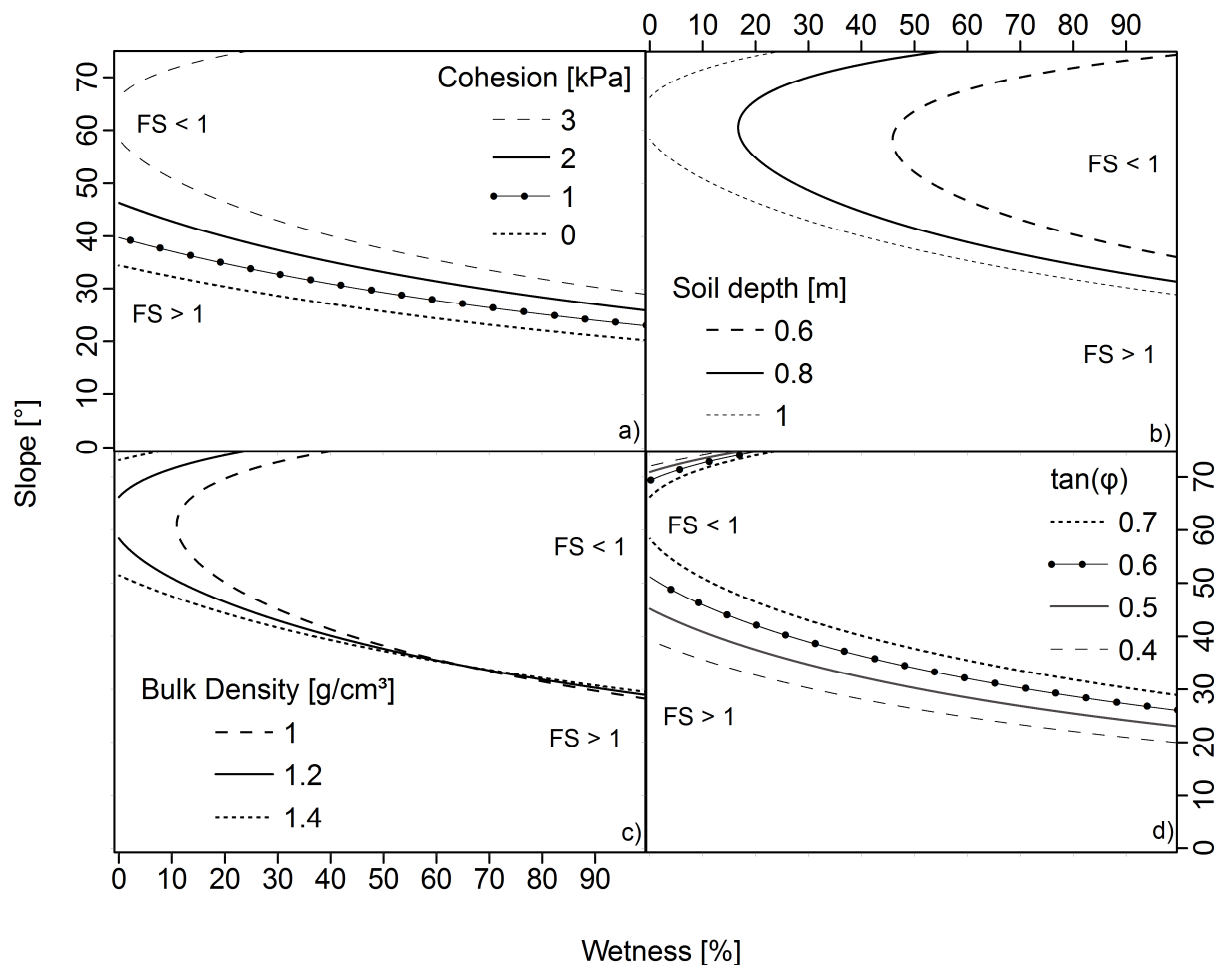
Figure 6.8: Factor of Safety (FS) as function of wetness and slope angle. The curves indicate FS = 1, value ranges outside the curves indicate FS > 1 and ranges inside the curves FS < 1: a) cohesion varied, b) soil depth varied, c) bulk density varied and d) the angle of internal friction (φ) varied. Unless stated otherwise, cohesion = 3 kPa, tan (φ) = 0.7, bulk density = 1.2 g/cm³.

We followed Montgomery and Dietrich (1994) that unconditionally unstable sites are those even unstable when dry and unconditionally stable sites are those predicted as stable when completely saturated, with the minor change that we refrain from considering the area as completely dry at any time. Steady observation has shown that soils within the research area under thick organic layers ([1]) and mountain rainforest vegetation never dry out completely. Therefore, we consider the sites with a FS < 1 at 0.001 mm/h net rainfall rate as unconditionally unstable and those with a FS ≥ 1 at complete saturation (3 mm/h) as unconditionally stable. The three categories in between display instability (FS < 1) at rainfall rates 0.01, 0.1 and 3 mm/h.

As expected from Figure 6.8, the highest area percentage displaying instability of any kind is assigned considering sd_22 (Figure 6.9a), whereas the lowest percentage is found for stag_35 (Figure 6.9e). Unconditionally unstable sites account for 6.5 % of

---

[1] The occurrence probability of the Word Reference Base (FAO, IUSS Working Group WRB, 2007) Reference Soil Groups and the probability and thickness of the typical diagnostic horizons were predicted in earlier studies (European Journal of Soil Science, in review).

the research area for the former and 0.5% for the latter; unconditionally stable sites for 39.7% and 92.6% respectively (Table 6.1). While comparison of the two maps which refer to the same depth of the failure plane mostly lead to a general increase in stability with φ = 35° compared to φ = 22° (Figures 6.9c and 6.9f), considering a different depth of the failure plane leads to different unstable sites and not simply a general increase or decrease in stability (Figures 6.9g and 6.9h).

Ranges of slope angle within the stability classes (Table 6.1) indicate that all sites < 31°/ 30° are unconditionally stable for sd_35 and stag_35, whereas decreasing φ reduces unconditionally stable sites to slope angles < 23°/ 22°. However, high slope angles alone do not lead to higher instability. Slope ranges within the various instability classes are about the same. Variables that influence soil wetness (KRA CA and K$_{sat}$) show similar findings. Ranges vary between stability classes, but minimum values are rather equal. This also applies for bulk density where the lowest densities are included in the two highest stability classes. Like low inclination, an extremely shallow depth of the failure plane, < 0.4 m/ 0.34 m, leads to stable sites. However, stable sites are also found considering a high depth of the failure plane. We assume
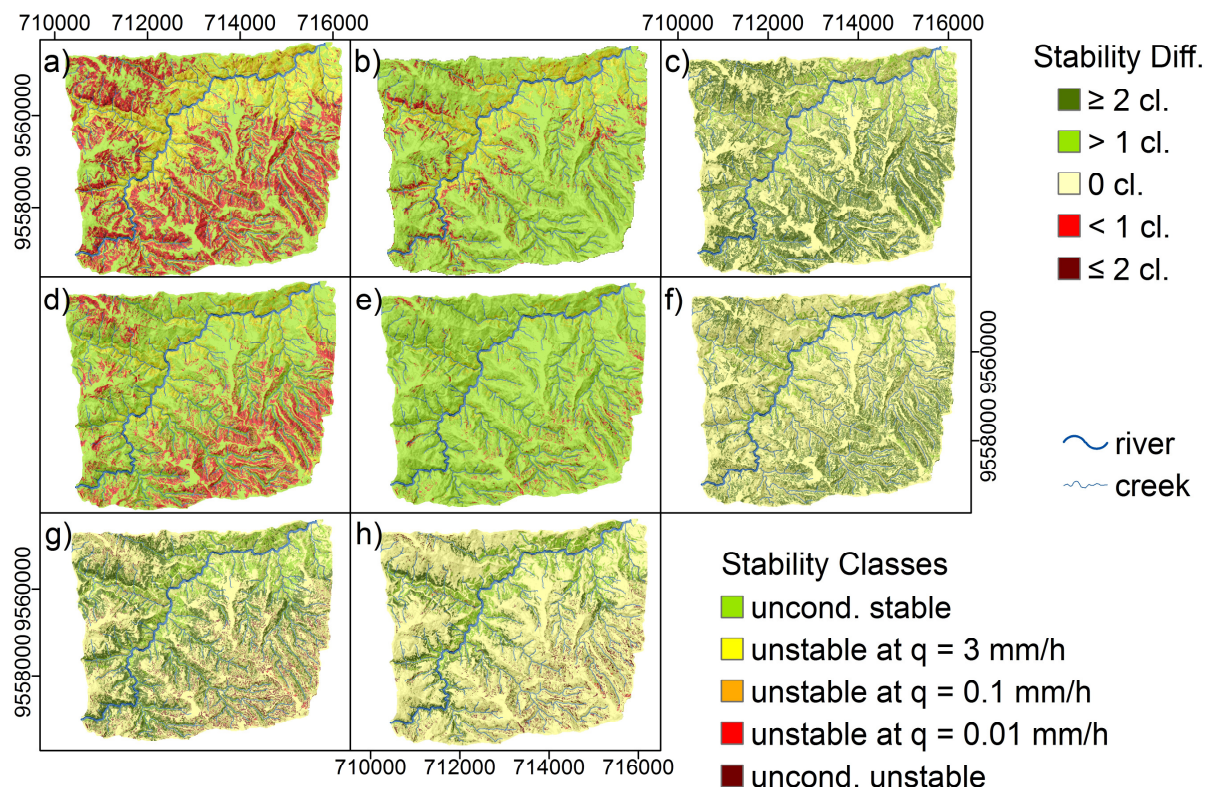
Figure 6.9: Slope stability classes in dependence on net rainfall rate (cl. = classes, Diff. = Difference). Depth of the failure plane at soil depth: a) φ = 22°, b) φ = 35°, depth of the failure plane at the lower boundary of the stagnic horizon: d) φ = 22°, e) φ = 35°, and prediction differences: c) = a) – b), f) = d) – e), g) = a) – d) and h) = b) – e) (Hillshading with light source from north-east).

Table 6.1: The FS influencing parameter ranges within the stability classes

failure plane	φ	variable	Stability Class				
			uncond. stable	unstable at 3 mm/h	unstable at 0.1 mm/h	unstable at 0.01 mm/h	uncond. unstable
soil depth	35	area [%]	78.1	13.3	1.9	5.7	1.0
	22		39.7	19.7	6.1	28.0	6.5
stagnic horizon	35		92.6	3.1	1.1	2.7	0.5
	22		67.1	8.9	2.8	17.8	3.4
soil depth	35	slope [°]	0 - 76	32 - 69	31 - 68	33 - 68	34 - 65
	22		0 - 76	24 - 70	23 - 68	24 - 68	24 - 67
stagnic horizon	35		0 - 76	34 - 71	30 - 67	32 - 72	32 - 70
	22		0 - 76	27 - 72	22 - 66	23 - 72	24 - 70
soil depth	35	KRA CA [m²]	100 - 25143800	100 - 5700	100 - 56000	200 - 396800	1800 - 17722100
	22		100 - 25143800	100 - 4600	100 - 42900	100 - 391300	700 - 19717300
stagnic horizon	35		100 - 25143800	100 - 4000	100 - 41600	200 - 381000	1700 - 3284200
	22		100 - 25143800	100 - 6100	100 - 37200	100 - 321200	300 - 17056300
soil depth	35	K$_{sat}$ [mm/h]	1.15, 176.40	176.4	1.15, 176.40	1.15, 176.40	1.15, 176.40
	22		1.15, 176.40	176.4	1.15, 176.40	1.15, 176.40	1.15, 176.40
stagnic horizon	35		1.15, 176.40	176.4	1.15, 176.40	1.15, 176.40	1.15, 176.40
	22		1.15, 176.40	176.4	1.15, 176.40	1.15, 176.40	1.15, 176.40
soil depth	35	bulk density [g/cm³]	0.81 - 1.33	0.80 - 1.29	0.89 - 1.27	0.90 - 1.29	0.97 - 1.28
	22		0.82 - 1.33	0.80 - 1.32	0.89 - 1.31	0.90 - 1.32	0.97 - 1.33
stagnic horizon	35		0.81 - 1.33	0.80 - 1.25	0.88 - 1.28	0.90 - 1.29	0.99 - 1.29
	22		0.81 - 1.33	0.80 - 1.31	0.88 - 1.31	0.89 - 1.32	0.97 - 1.32
soil depth	35	depth of failure plane [m]	0.24 - 0.86	0.40 - 0.86	0.41 - 0.89	0.40 - 0.87	0.41 - 0.81
	22		0.24 - 0.80	0.34 - 0.84	0.35 - 0.86	0.34 - 0.89	0.34 - 0.86
stagnic horizon	35		0.10 - 1.04	0.40 - 0.92	0.41 - 1.08	0.40 - 1.17	0.41 - 0.91
	22		0.10 - 1.04	0.34 - 0.92	0.34 - 0.99	0.34 - 1.08	0.34 - 1.17
soil depth	35	wetness at 0.001 mm/h net rainfall	0.00 - 1.00	0.00 - 0.01	0.00 - 0.10	0.04 - 0.99	0.48 - 1.00
	22		0.00 - 1.00	0.00 - 0.01	0.00 - 0.10	0.01 - 0.99	0.03 - 1.00
stagnic horizon	35		0.00 - 1.00	0.00 - 0.01	0.01 - 0.10	0.05 - 0.98	0.56 - 1.00
	22		0.00 - 1.00	0.00 - 0.02	0.00 - 0.10	0.02 - 0.99	0.05 - 1.00
soil depth	35	wetness at 0.01 mm/h net rainfall	0.00 - 1.00	0.00 - 0.10	0.04 - 1.00	0.36 - 1.00	1
	22		0.00 - 1.00	0.00 - 0.10	0.01 - 1.00	0.07 - 1.00	0.28 - 1.00
stagnic horizon	35		0.00 - 1.00	0.00 - 0.10	0.06 - 1.00	0.46 - 1.00	1
	22		0.00 - 1.00	0.00 - 0.17	0.01 - 0.99	0.23 - 1.00	0.46 - 1.00
soil depth	35	wetness at 0.1 mm/h net rainfall	0.02 - 1.00	0.02 - 0.99	0.39 - 1.00	1	1
	22		0.02 - 1.00	0.02 - 0.99	0.10 - 1.00	0.65 - 1.00	1
stagnic horizon	35		0.02 -1.00	0.02 - 0.96	0.58 -1.00	1	1
	22		0.02 -1.00	0.02 -1.00	0.06 -1.00	1	1
soil depth	35	wetness at 5 mm/h net rainfall	0.46 - 1.00	0.58 - 1.00	1	1	1
	22		0.53 -1.00	0.46 - 1.00	1	1	1
stagnic horizon	35		0.46 -1.00	0.68 - 1.00	1	1	1
	22		0.53 -1.00	0.46 - 1.00	1	1	1

KRA CA = upslope contributing area, K$_{sat}$ = saturated hydraulic conductivity

that it is the combination of slope angle and sliding unit weight with the latter being determined by bulk density, depth of the failure plane and wetness that determine whether a site is stable or unstable.

According to the concept for the depth of the failure plane, i. e. water percolation until the lower boundary of the stagnic soil layer or until bedrock, we would not decide which of the maps in Figure 6.9 represents reality best. We assume that reality might be found in some combination of the maps. Regarding the distribution of stagnic soils in the research area ([1]), we conclude that Figure 9a and 9b better represent the area < 2090 m a.s.l. and 9d and 9e above.

As we considered soil mechanics and hence the total sliding unit weight of soil only, we diregarded that these soils carry thick organic layers ([1]) with a huge water storing capacity (Leutner et al., personal communication) and natural forest as considerable vegetation weight. Including both would lead to further destabilisation and hence might make $\varphi = 35°$ a more reasonable choice than $\varphi = 22°$, as well as a shallower depth of the failure plane compared to that at soil depth. In conclusion, we consider Figure 6.9 as a first estimation of slope stability within the research area.

Unconditionally unstable sites are independent of soil wetness and therefore also of any water storing capacity of the organic layer and vegetation. In order to further evaluate our prediction of the FS, we overlaid an aerial photograph of the research area (AG Jordan, 2005) with those sites predicted as unconditionally unstable (Figure 6.10). While maps IIa and IIc calculated with $\varphi = 22°$ cover most landslide scars, the other two ($\varphi = 35°$) cover only few, so that we regard $\varphi = 22°$ the better choice.

The selected subarea, map II (Figure 6.10), shows a good concordance between landslide scars and sites predicted as unconditionally unstable. Surely rainfall has an impact on landslide triggering, but many of today's open landslide scars are the consequence of unconditionally unstable slopes. Intense rainfall provides the small driving force necessary to cause these instable sites to collapse. Although most of the landslide scars are situated on unconditionally unstable sites, our investigation has shown that other sites also become unstable with increasing soil water saturation. Single event landslides that once occurred on these sites are probably again covered by dense forest and therefore not recognisable in the aerial photograph. Soil investigation proved their existence.

---

[1] The occurrence probability and thickness of the typical diagnostic horizons were predicted in an earlier study (European Journal of Soil Science, in review).
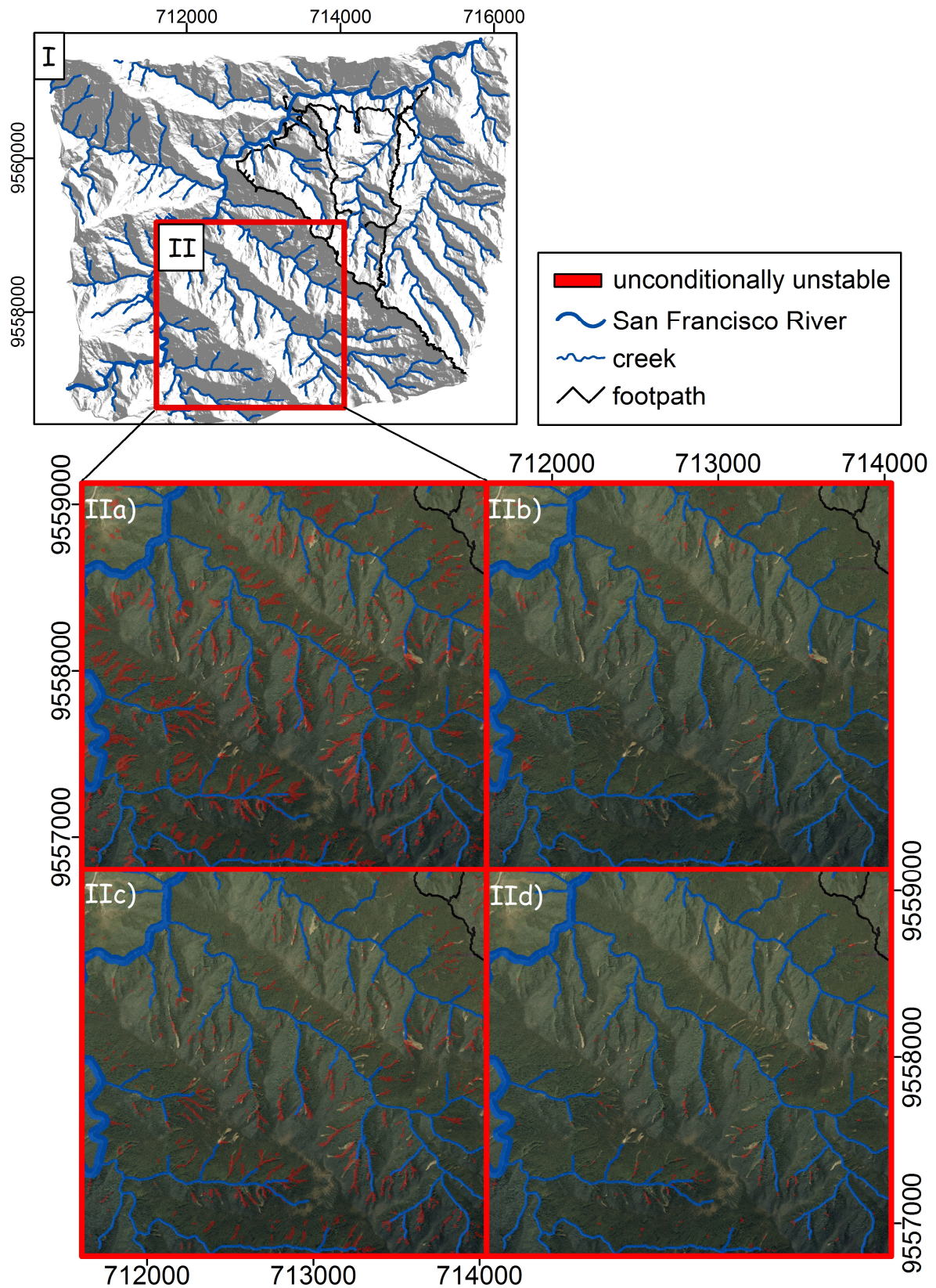
UTM Zone 17 M, WGS 84

Figure 6.10: Aerial photograph 2005 (AG Jordan) with landslide scars and unconditionally unstable sites. FS calculated with the failure plane at soil depth: φ = 22° (IIa) and 35° (IIb). FS calculated with the failure plane at the lower boundary of the stagnic horizon: φ = 22° (IIc) and 35° (IId) (Hillshading with light source from north-east).

6.4   Conclusions and outlook

We hypothesize that the complete research area would be covered by stagnic soils without the influence of landslides that lead to lower bulk densities in their accumulation zones.

The lower boundary of the stagnic soil layer and soil depth were regionalised and proved to be a good estimation of the depth of the failure plane. However, terrain parameters explained the spatial distribution of soil bulk density and the depth of the failure plane only to a relatively small extent. Nevertheless, their prediction uncertainty still allowed for a reasonable prediction of unconditionally unstable sites. A first estimation of landslide susceptibility was provided and approved by comparison with landslide scars on a recent aerial photograph.

For the prediction of the FS, φ and the depth of the failure plane seemed to be more important than a precise prediction of bulk density. Setting bulk density at random within the detected ranges might still predict landslide scars as unconditionally unstable sites. This assumption as well as the influence of soil cohesion needs further investigation. Future research will include vegetation weight and the water storing capacity of the organic layer in the calculation of the FS.

6.5   Acknowledgements

6.6   References

Bauer, F., Vinan, P., Balcazar, L., Bogner, C., Huwe, B., 2010a. Flow paths in soils of landslide affected and unaffected hillslopes in a montane rainforest of South Ecuador, part A. submitted to Journal of Hydrology

Bauer, F., Balcazar, L., Vinan, P., Bogner, C., Zeilinger, J., Huwe, B., 2010b. Flow paths in soils of landslide affected and unaffected hillslopes in a montane rainforest of South Ecuador, part B. submitted to Journal of Hydrology

Bauer, J., Rohdenburg, H., Bork, H.-R., 1985. Ein digitales Reliefmodell als Vorraussetzung für ein deterministisches Modell der Wasser- und Stoff-Flüsse. In: Bork, H.- R., Rohdenburg, H. (Eds.). Landschaftsgenese und Landschaftsökologie H. 10, Parameteraufbereitung für deterministische Gebiets-Wassermodelle, Grundlagenarbeiten zur Analyse von Agrar-Ökosystemen, p. 1 – 15.

Beven, K. J., Kirkby, M. J., Schofield, N., Tagg, A. F., 1984. Testing a physically-based flood forecasting model (TOPMODEL) for three U. K. catchments. Journal of Hydrology 69: 119-143.

Bogner, C., Engelhardt, S., Zeilinger, J., Huwe, B., 2008. Visualization and Analysis of Flow Patterns and Water Flow Simulations in Disturbed and Undisturbed Tropical Soils. Beck, E., Bendic, J., Kottke, I., Makeschin, F. Mosandl, R. (Eds.). Gradients in a Tropical Mountain Ecosystem of Ecuador. Ecological Studies 198: 387 – 396.

Böhner, J., McCloy, K. R., Strobl, J., 2006. SAGA – Analysis and Modelling Application. Göttinger Geographische Abhandlungen 115. Geographische sInstitut der Universität Göttingen.

Breimann, L., Friedmann, J. H., Olshen, R. A., Stone, C. J., 1984. Classification and regression trees, CRC press, Wadsworth.

Breiman, L., 2001. Technical Report for Version 3. http://oz.berkeley.edu/users/ breiman/randomforest2001.pdf (Access: 28/04/2010).

Brenning, A., 2005. Spatial prediction models for landslide hazards: review, comparison and evaluation. Natural Hazards and Earth System Sciences 5, 853 – 862

Bussmann, R. W., Wilcke, W., Richter, M., 2008. Landslides as Important Disturbance Regimes – Causes and Regeneration. Beck, E., Bendic, J., Kottke, I., Makeschin, F. Mosandl, R. (Eds.). Gradients in a Tropical Mountain Ecosystem of Ecuador. Ecological Studies 198: 319 – 330.

Domínguez-Cuesta, M. J., Jiménez-Sánchez, M., Berrezueta, E., 2007. Landslides in the Central Coalfield (Cantabrian Mountains, NW Spain): Geomorphological features, conditioning factors and methodological implications in susceptibility assessment. Geomorphology 89: 358 – 369.

Emck, P. 2007. A Climatology of South Ecuador - With special focus on the Major Andean Ridge as Atlantic-Pacific Climate Divide. PhD-thesis, Naturwissenschaftliche Fakultäten der Friedrich-Alexander-Universität Erlangen Nürnberg.

FAO, IUSS Working Group WRB, 2007. World Reference Base for Soil Resources, ISRIC, Rome.

Fleischbein, K., Wilcke, W., Valarezo, C., Zech, W., Knoblich, K., 2006. Water budgets of three small catchments under montane forest in Ecuador: experimental and modelling approach. Hydrological Processes 20: 2491–2507.

Fries, A., Rollenbeck, R., Göttlicher, D., Nauss, T., Homeier, J., Peters, T., Bendix, J., 2009. Thermal structure of a megadiverse Andean mountain ecosystem in southern Ecuador, and its regionalization. Erdkunde, 63: 321–335.

Fröhlich, O. K., 1955. General Theory of Stability of Slopes. Géotechnique 5/1: 37 – 44.

Jenny, H., 1941. Factors of soil formation. A system of quantitative pedology. New York.

Kreutzer, D., Martini, J., 2002. Bestimmung und Regionalisierung der gesättigten hydraulischen Leitfähigkeiten in Böden unter tropischem Bergregenwald in Ecuador mit verschiedenen Methoden. Diplomarbeit, Gießen.

Lea, N. L., 1992. An aspect driven kinematic routing algorithm. In: Parsons, A. J. and Abrahams, A. D. (eds.) Overland Flow Hydraulics and Erosion Mechanics. London, 393 – 407.

Leutner, B. F., Bauer, F., Huwe, B., 2010. Water flow in the organic layer of a tropical mountane rainforest in southern Ecuador - an inverse modelling study. Manuscript in preparation.

Li, X., 2007. Finite element analysis of slope stability using a nonlinear failure criterion. Computers and Geotechnics 34: 127 – 136.

Liess, M., Glaser, B., Huwe, B., 2009. Digital Soil Mapping in Southern Ecuador. Erdkunde 63/ 4: 309 – 319.

Ließ, M., Glaser, B. Huwe, B., 2010a. Incomplete Soil Classification to Benefit the Soil Continuum - Prediction of Diagnostic Properties of Andean Mountain Forest Soils. European Journal of Soil Science (in review).

Ließ, M., Glaser, B. Huwe, B., 2010b. Reference Soil Group Probability Prediction. European Journal of Soil Science (in review).

Mayne, P. W., Swanson, P. G., 1987. The Critical-State Pore Pressure Parameter from Consolidated-Undrained Shear Tests. In: Laboratory Shear Strength of Soil. ASTM STP 740, Yong, R. N., Townsend, F. S. (Eds.). American Society for Testing Materials, pp. 410 – 430.

McIntosh, P.D., Price, D.M., Eberhardt, R., Slee, A.J., 2009. Late Quaternary erosion events in lowland and mid-altitude Tasmania in relation to climate change and first human arrival. Quaternary Science Reviews 28: 850 – 872.

Montgomery, D. R., Dietrich, W.E., 1994. A physically based model fort he topographic control on shallow landsliding. Water Resources Research 30/ 4: 1153-1171

Motzer, T. M., 2003. Bestandesklima, Energiehaushalt und Evapotranspiration eines tropischen Bergregenwaldes (Süd-Ecuador). Dissertation zur Erlangung des Doktorgrades (Dr. phil.) im Fachbereich Geographie der Fakultät für Volkswirtschaftslehre der Universität Mannheim

Oesker, M., Homeier, J., Dalitz, H., 2007. Spatial Heterogeneity of Canopy Throughfall Quantity and Quality in a Tropical Montane Forest in South Ecuador. in: L.A. Bruijnzeel et al. (eds.) 2006/07 Mountains in the Mist: Science for Conserving and Managing Tropical Montane Cloud Forest. University of Haawaii Publishers. Honolulu. Hawaii

O'Loughlin, E.M., 1986. Prediction of surface saturation zones in natural catchments by topographic analysis. Water Resources Research 22/ 5: 794 – 804.

Park, S. J. and Vlek, L. G. (2002): Prediction of three-dimensional soil spatial variability: a comparison of three environmental correlation techniques. In: Geoderma 109, 117–140. Doi:10.1016/S0016-7061(02)00146-5

Peters, J., de Baets, B., Verhoest, N. E. C., Samson, R., Degroeve, S., de Becker, P., Huybrechts, W., 2007. Random Forests as a tool for ecohydrological distribution modelling. Ecological Modelling 207: 304 – 318.

Prasad, A. M., Iverson, L.R., Liaw, A., 2006. Newer classification and regression tree techniques: Bagging and random forest for ecological prediction. Ecosystems 9: 181 – 199.

Riestenberg, M. M., Sovonick-Dunford, S., 1983. The role of woody vegetation in stabilizing slopes in the Cincinnati area, Ohio. Geological Society of America Bulletin 94: 506 – 518.

Rollenbeck, R., 2006. Variability of precipitation in the Reserva Biólogica San Francisco / Southern Ecuador. Lyonia a journal of ecology and application 9/ 1: 43 – 51.

Schrumpf, M., Guggenberger, G., Valarezo, C., Zech, W., 2001. Tropical montane rainforest soils. Development and nutrient status along an altitudinal gradient in the South Ecuadorian Andes. Die Erde, 132; 43–59.

Strahler, A. N., 1957. Quantitative analysis of watershed geomorphology. In: Transactions of the American Geophysical Union 38 (6), 913–920.

Stoyan, R., 2000. Aktivität, Ursachen und Klassifikation der Rutschungen in San Francisco/ Südecuador. Diplomarbeit Universität Erlangen.

Vanacker, V., Vanderschaeghe, M., Govers, G., Willems, E., Poesen, ., Deckers, J., De Bievre, B., 2003. Linking hydrological, infinite slope stability and land-use change models through GIS for assessing the impact of deforestation on slope stability in high Andean watersheds. Geomorphology 52: 299 – 315.

Wilcke, W., Valladarez, H., Stoyan, R., Yasin, S., Valarezo, C., Zech, W., 2003. Soil properties on a chronosequence of landslides in montane rainforest, Ecuador. Catena 53: 79 – 95.

Wu, W., Sidle, R. C., 1995. A distributed slope stability model for steep forested basins. Water Resources Research 31/ 8: 2097 – 2110.

Zevenbergen, L. W., Thorne, C. R., 1987. Quantitative analysis of land surface topography. Earth Surface Processes and Landforms 12: 47 – 56.

Zheng, H., Tham, L.G., Liu, D., 2006. On two definitions of the factor of safety commonly used in the finite element slope stability analysis. Computers and Geotechnics 33: 188 – 195.

Acknowledgements

Declaration of Authenticity

To the best of my knowledge and belief, this thesis contains no material previously published or written by another person, except where due reference has been made. This thesis contains no material which has been accepted or definitely rejected for the award of any other doctoral degree in any university.

Ehrenerklärung

Hiermit erkläre ich, dass ich diese Arbeit selbständig verfasst und keine anderen als die von mir angegebenen Quellen und Hilfsmittel benutzt habe.

Ferner erkläre ich, dass ich anderweitig mit oder ohne Erfolg nicht versucht habe, diese Dissertation einzureichen. Ich habe keine gleichartige Doktorprüfung an einer anderen Hochschule endgültig nicht bestanden.

_____

Bayreuth, den 12. November 2010